Diss. ETH NO. 26965

Assessment and optimization of geological carbon storage and energy production from deep natural gas reservoirs

A thesis submitted to attain the degree of

DOCTOR OF SCIENCES of ETH ZURICH

(Dr. sc. ETH Zurich)

presented by

EZEKIEL, JUSTIN CHIMA

M.Sc. in Oil and Gas Field Development Engineering,
China University of Petroleum (East China), China

born on 02.06.1986
citizen of Nigeria

accepted on the recommendation of

Prof. Dr. Martin O. Saar   ETH Zurich
Prof. Dr. Anozie Ebigbo   Helmut Schmidt University, Hamburg
Prof. Dr. David Bruhn   TU Delft and GFZ Potsdam

2020

Abstract

_____

Geothermal energy development has been regarded as one of the promising renewable energy options that contributes in the reduction of the global dependence on fossil-fuel, non-renewable, energy sources. It has also been proposed that using supercritical carbon dioxide ($scCO_2$), in place of the traditional water, as the heat-transmission working fluid to develop geothermal energy comes with added benefits. Sedimentary geothermal reservoirs have been identified as more favorable potential sites for CO_2-based geothermal energy development and CO_2 storage because of their abundant geothermal reserves, massive CO_2 storage capacity and larger heat exchange pore area. The utilization of $scCO_2$ as a working fluid for heat extraction from sedimentary reservoirs, referred to as CO_2-plume geothermal (CPG) systems, has thus far focused its application mostly on the aquifer system. However, hot natural gas reservoirs have shown to contain not only natural gas resources but significant geothermal energy reserves, and these energies can be simultaneously recovered during the conventional primary drive till uneconomic depletion. Afterwards, CO_2 can serve as a working fluid for the dual purpose of enhancing gas recovery (EGR) and geothermal energy extraction, while being simultaneously stored in the natural gas reservoir. Thus, this approach is referred to, in this thesis, as a combined CO_2-EGR–CPG system and constitutes a CO_2 capture double-utilization and storage (CCUUS) system. In this thesis, we carry out critical researches to assess the feasibility and performance of this novel combined dual-energy extraction technology that will further improve the CO_2-based geothermal methodology and take it to a new technology readiness level (TRL).

First, we introduce the concept and the potential synergies (or benefits) associated with the combined CO_2-EGR–CPG system. To optimize the power output of the combined system, we integrate the reservoir, wellbore and surface power-generation processes. We then present a numerical simulation study to assess the technical feasibility of the proposed system in co-producing natural gas and geothermal energy for power generation. The results confirm that the proposed conceptual and implementation strategies enhance the gas field's overall energy production, enable CO_2 sequestration, and extend the useful lifetime of the gas field. This indicates that deep natural gas reservoirs can constitute ideal sites for the deployment of not only EGR and geologic CO_2 storage but also CPG.

Second, we carry out an optimization study on the most important parameters for the design of the CPG-component of the combined system, which is the CO_2 mass flowrate. Numerical analyses show that the flowrate does not only influence the power generated at the turbine, but also has a significant effect on the pressure drawdown in the reservoir, which can potentially lead to water flowing into the production well. The increase in water flow in the wellbore can eventually affect

the production performance and the overall efficiency of the CPG system. An integrated numerical modeling approach is employed to investigate the effects of operational and reservoir parameters on the two-phase flow regime achieved in the production well and on the power generation of a CPG system. Our results show, for all parameters considered, the minimum flowrate and superficial CO_2 velocity required to ensure an annular flow in the CPG vertical production well, while maximizing the power generated. Furthermore, we provide a useful insight that low CO_2 flowrate and velocity is one of the reasons why the first CO_2 thermosiphon experiment test, at the Cranfield site, was unsuccessful. Therefore, in future CPG-related projects (including the combined CO_2-EGR–CPG system), it is important to consider the potential influence of water entering the production well for flowrate optimization.

Applying the lessons learnt from the results of the first two studies, we carry out reservoir simulations to evaluate the sensitivity of different key reservoir and operational parameters on the natural gas recovery, extractable geothermal-energy and CO_2-storage performance of the combined CO_2-EGR–CPG system. These parameters include reservoir permeability, permeability anisotropy, reservoir temperature, relative permeability, mean ambient surface temperature, and well pipe diameter. Using depleted and partially depleted natural gas reservoir examples, we also investigate the performance of the combined system, with/without the CO_2-plume establishment stage, and its capability to achieve the required minimum superficial CO_2 velocity at the base-case production mass flowrate used. The simulation results show that partially depleted reservoirs, with CO_2 plume establishment stage, achieve the best overall performance and the quickest transition time to the CPG stage. Reservoir temperature is determined to be the most significant reservoir parameter that influences the total energy-recovery and CO_2-storage performance of the combined CO_2-EGR–CPG system.

The overall results of the thesis show that the combined system can pave the way for future practical cost-effective implementation and commercialization of the CO_2-based geothermal system to generate more energy. At the same time, the combined system enables CO_2 storage and the energy produced can compensate for the cost of CO_2 storage. Further power-generation optimization studies, using real natural gas field cases, to improve our understanding of the usefulness of combining CO_2-EGR and CPG projects, and considering the techno-economic implication, are recommended.

Zusammenfassung

_____

Die Förderung geothermischer Energie wird als eine der vielversprechenden Optionen für erneuerbare Energien angesehen, die zur Verringerung der globalen Abhängigkeit von fossilen, nicht erneuerbaren Energiequellen beiträgt. Es wurde bereits festgestellt, dass die Verwendung von überkritischem Kohlendioxid ($scCO_2$) anstelle von Wasser als wärmeübertragendes Arbeitsmedium für die Entwicklung der geothermischen Energie mit zusätzlichen Vorteilen verbunden sein könnte. Sedimentäre geothermische Reservoire sind aufgrund ihrer hohen geothermischen Potentialen, ihrer massiven CO_2-Speicherkapazität und ihrer grossen Porenfläche für CO_2-basierte Geothermie gut geeignet. Die Nutzung von $scCO_2$ als Arbeitsfluid für die Wärmegewinnung aus sedimentären Reservoiren wird als CO_2-Plume-Geothermie (CPG) bezeichnet. Die Forschungsarbeit in diesem Bereich konzentrierte sich bisher vor allem auf salinäre Aquifere. Es hat sich jedoch gezeigt, dass heisse Erdgasreservoire nicht nur Erdgasressourcen, sondern auch bedeutende geothermische Energie enthalten und dass diese Ressourcen gleichzeitig während der konventionellen Gas-Förderung gewonnen werden können. Danach kann CO_2 als Arbeitsfluid sowohl für die Erdgasgewinnung (EGR) als auch für die Förderung der geothermischen Energie dienen und gleichzeitig in der Erdgaslagerstätte gespeichert werden. Daher wird der Ansatz in dieser Arbeit als ein kombiniertes CO_2-EGR-CPG-System bezeichnet und stellt ein System der CO_2-Abscheidung mit doppelter Nutzung und Speicherung (CCUUS) dar. In dieser Arbeit führen wir kritische Untersuchungen durch, um die Durchführbarkeit und Leistung dieser neuartigen kombinierten Energiegewinnungstechnologie zu bewerten, die die CO_2-basierte Geothermie weiter verbessern und sie auf ein höheres Technologiebereitschaftsniveau (TRL) bringen soll.

Zunächst stellen wir das Konzept und die potenziellen Synergien (oder Vorteile) vor, die mit dem kombinierten CO_2-EGR-CPG-System verbunden sind. Um die Leistung des kombinierten Systems zu optimieren, integrieren wir die Prozesse der Reservoir-, Bohrloch- und Oberflächenenergieerzeugung. Dann stellen wir eine numerische Simulationsstudie vor, um die technische Machbarkeit des vorgeschlagenen Systems bei der Koproduktion von Erdgas und geothermischer Energie für die Stromerzeugung zu bewerten. Die Ergebnisse bestätigen, dass die vorgeschlagenen Konzept- und Implementierungsstrategien die Gesamtenergieproduktion des Gasfeldes verbessern, die CO_2-Sequestrierung ermöglichen und die Nutzungsdauer des Gasfeldes verlängern können. Dies deutet darauf hin, dass tiefe (teilweise erschöpfte) Erdgaslagerstätten ideale Standorte für den Einsatz nicht nur von EGR und geologischer CO_2-Speicherung, sondern auch von CPG darstellen.

Zweitens führen wir eine Optimierungsstudie der wichtigsten Parameter für das Design der CPG-Komponente des kombinierten Systems durch, nämlich die CO_2-Massenstrom. Numerische Analysen zeigen, dass die Durchflussmenge nicht nur die an der Turbine erzeugte Leistung beeinflusst, sondern auch einen signifikanten Einfluss auf den Druckabfall im Reservoir hat, was dazu führen kann, dass Wasser in das Förderbohrloch fliesst. Die Zunahme von Wasser im Bohrloch kann sich letztendlich

auf die Förderleistung und die Gesamteffizienz des CPG-Systems auswirken. Ein integrierter numerischer Modellierungsansatz wird verwendet, um die Auswirkungen von Betriebs- und Reservoirparametern auf das im Produktionsbohrloch erreichte Strömungszustände und auf die Stromerzeugung eines CPG-Systems zu untersuchen. Unsere Ergebnisse zeigen für alle betrachteten Parameter den minimalen CO_2-Durchsatz, der erforderlich ist, um eine Ringströmung in der vertikalen CPG-Förderbohrung zu gewährleisten und gleichzeitig die erzeugte Energie zu maximieren. Darüber deuten unsere Ergebnisse darauf hin, dass die niedrige CO_2-Fliessgeschwindigkeit bzw -Durchflussrate einer der Gründe ist, warum der erste CO_2-Thermosiphon-Feldversuch am Standort Cranfield nicht erfolgreich war. Daher ist es bei zukünftigen CPG-bezogenen Projekten (einschliesslich des kombinierten CO_2-EGR-CPG-Systems) wichtig, den potenziellen Einfluss von Wasser, das in das Förderbohrloch eintritt, zur Optimierung der Durchflussrate zu berücksichtigen.

Unter Berücksichtigung der Ergebnisse aus den ersten beiden Studien führen wir Reservoirsimulationen durch, um die Sensitivität verschiedener Parameter in Bezug auf die Erdgasgewinnung, die extrahierbare geothermische Energie und die CO_2-Speicherleistung des kombinierten CO_2-EGR-CPG-Systems zu bewerten. Zu diesen Parametern gehören die Permeabilität, die Permeabilitätsanisotropie, die Temperatur des Reservoirs, die relative Permeabilität, die durchschnittliche Umgebungstemperatur an der Oberfläche und der Bohrlochdurchmesser. Anhand von Beispielen für erschöpfte und teilweise erschöpfte Erdgasreservoies untersuchen wir auch die Leistung des kombinierten Systems (mit/ohne Anlaufphase – d. h., eine Phase, in der CO_2 in das Reservoir injiziert wird, um eine Mindestgrösse der CO_2-Ansammlung zu erreichen) und seine Fähigkeit, den erforderlichen minimalen CO_2-Durchsatz im Bohrloch zu erreichen. Die Simulationsergebnisse zeigen, dass teilweise erschöpfte Reservoire mit einer Anlaufphase die höchste Gesamtleistung und die schnellste Übergangszeit zum CPG-Stadium erreichen. Die Temperatur des Reservoirs ist der wichtigste Parameter, der die gesamte Energiegewinnungs- und CO_2-Speicherleistung des kombinierten CO_2-EGR-CPG-Systems beeinflusst.

Die Gesamtergebnisse der Dissertation zeigen, dass das kombinierte System den Weg für eine zukünftig praktische, kosteneffiziente Umsetzung und Kommerzialisierung des CO_2-basierten geothermischen Systems zur Erzeugung von mehr Energie ebnen. Gleichzeitig ermöglicht es die CO_2-Speicherung und kann die Kosten der CO_2-Speicherung kompensieren. Wir empfehlen weitere Studien zur Optimierung der Stromerzeugung unter Verwendung realer Erdgasfelder und unter Berücksichtigung der technisch-wirtschaftlichen Auswirkungen, welche zur Verbesserung unseres Verständnisses der Nützlichkeit der Kombination von CO_2-EGR- und CPG-Projekten beitragen können.

If I have seen further, it is by standing on the shoulders of Giants.

— Sir Isaac Newton (1676)

Acknowledgement

_____

First, I thank the *Almighty God*, who is my maker, protector and sustainer.

Thank you so much *Martin*, for supporting my coming to ETH Zurich, providing good working conditions, and diligently supervising my work. Research-wise, you always provide me with useful and important input, and give big-picture feedback, which greatly improves my work.

Anozie, I am thankful for the supervision, advices and training I received from you these 4 years. I am grateful for your relentless contributions, feedback and pushing me to be, and do, better. I learnt so much from the millions of "scientific" discussions (oral and via email) we had.

I thank *David* for being the external examiner of my thesis. I still remember our brief, but impactful, discussion in Strasbourg (France) at EGW 2018.

Special thanks to *Tim* for being the chairperson of my PhD defence, and I am also grateful for all the professional assistance you accorded me during a difficult period. Further thanks go to *Greg* who was an excellent mediator during the difficult period.

I am grateful *to Ben*, who taught me many engineering concepts and calculations, which helped to improve my work. Thanks to *Nagasree* for her help with many TOUGH2-related issues.

My sincere thanks to *Antonio* for selflessly assisting me before and during my PhD program. I would also thank *Dominik* for assisting me with various numerical computation issues.

I am thankful to *Dominique* and *Sigrid* for their support in many administrative matters. Thanks to *Isamu* who supported me in many IT matters. Thanks to *Diya* for working with me.

I am grateful to *Anniina* and *Mehrdad*, for being there for me during the difficult period.

I would like to thank my office colleagues and all the GEG group (past and present) members. I enjoyed the cakes, conversations and jokes we shared within and outside Room F55.

Special thanks to the *Swiss Federal scholarship department, and the coordinators,* for the award of the scholarship that partly funded my PhD program. I am always grateful to *Sandra* and *Stefan* who stood by me and made sure I had a successful PhD program.

I am very grateful to the *Pastors and brethren* of RCCG SOP Wallisellen (Zurich), with whom I spent much of my time outside work. Your selfless acts of kindness will always be remembered.

I am thankful to my parents *Victor and Joy*, my siblings *Chigozie, Chidinma, and Favor*, who have supported, encouraged and being there for me in good and difficult times.

Finally, to my darling wife, *Irene,* and my son (my carbon-copy) *Ikechukwu MJ*, I am so thankful to God that I have you in my life, and I am very grateful for all you do for me. I love you!

Contents

List of Figures

List of Tables

1

Introduction

In the following, introductions to the topics of Carbon Capture and Storage (CCS), CO_2-based Enhanced Gas Recovery (EGR), CO_2 Plume Geothermal (CPG), and the concept of their mutual combination for energy recovery and CO_2 storage in natural gas reservoirs are given. The motivation, objectives and structure of the thesis are also presented.

1.1 Carbon capture and storage (CCS) technology

The effects of global warming on the environment (including sea level rise, extreme weather conditions, etc.) is on the rise due to anthropogenic emissions of greenhouse gases, mostly carbon dioxide (CO_2). The development and the use of clean, green, low-carbon, more energy-efficient and renewable energy sources are ways of reducing emissions. However, the paths to achieving the widespread and economical accessibility to these alternative clean energy sources are quite complicated and slow. An intermediate solution is required to reduce the greenhouse gas emissions. Hence, the technology, known as CCS, which features the capture of CO_2 from flue gases of power plants (and other large CO_2-emitting industrial plants) and stored in suitable, carefully selected geological formations, has been developed and applied worldwide. CCS is widely considered as part of the technologies needed to achieve net-zero emissions (Bert et al., 2005; Global CCS Institute, 2019; Townsend et al., 2020).

CCS operations on its own is very expensive, however, with its versatile applications and the urgency of the climate crisis, the cost of CCS will vary across industries and power-generation applications (Beck and Temple-Smith, 2020). For example, the deployment of CCS offers the oil and gas industry a practical way of reducing their carbon footprint and it also serves as an enabler to meeting the industry's clean growth and decarbonization goals (Global CCS Institute, 2019). CCS is considered to have numerous synergies to the operations of oil and gas industry. Several areas of application of CCS in the oil and gas

industry include (Guloren, 2020): (i) reinjecting separated CO_2 from natural gas (after gas processing) before the natural gas can be transported; (ii) CCS is planned to be incorporated in the commercialization of stranded high CO_2 gas fields (with CO_2 concentration rates as high as 50%). An example is the CO_2 gas fields in Malaysia; (iii) plans are underway to develop post-combustion natural-gas-fired power plant coupled with CCS (in the Net Zero Teesside project in the UK.); (iv) coupling CCS with Steam Methane Reformers (SMR) of natural gas used to produce low-carbon hydrogen (e.g. Shell's Quest facility); etc.

Other varied CCS applications include – CO_2 capture, from the flue gas of Boundary Dam's coal-fired power plant (operated by Saskpower, Canada), and storage in the close by Aquistore site; steel; cement; fertilizer industries, etc.

The coupling of CCS to industrial utilization of the captured CO_2, termed "Carbon Capture, Utilization and Storage (CCUS)" can reduce its costs. CCUS is expected to contribute 9% of the cumulative emissions reduction before 2050 (Figure 1.1), to meet the goal of limiting temperature rises to 1.5 °C. Hence, the widespread use and deployment of CCUS technology is even more important now (Global CCS Institute, 2019). Carbon taxes and credit policies, if implemented by governments, has also been identified to be favorable to the widespread application of CCUS (Beck and Temple-Smith, 2020).
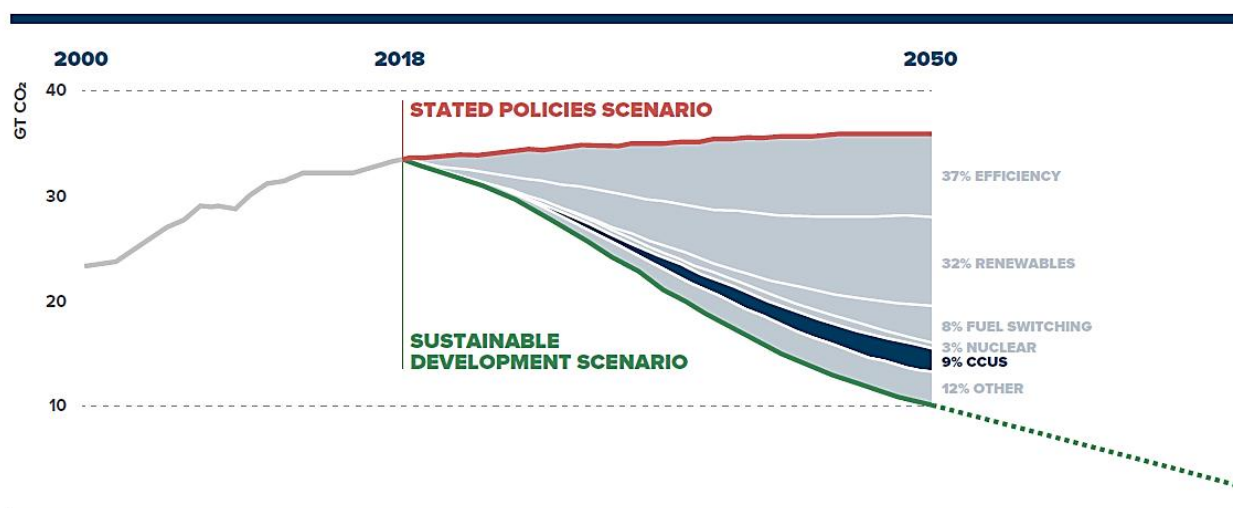
Figure 1.1: International Energy Agency (IEA)'s sustainable development scenario for CO_2 emission reduction. (Source: International Energy Agency, 2018; Global CCS Institute, 2019).

Figure 1.2 shows some the location of CO_2 storage sites (planned and under way) in the world. Suitable captured CO_2 storage sites include saline aquifers, depleted oil and gas fields, deep unmineable coal seams, etc. Depleted oil and gas reservoirs are considered

prime candidates for the storage of CO_2 due to the integrity and safety benefits that such sites provide. The depleted fields, having originally contained oil and gas, will not be adversely affected by the injected CO_2. The CO_2 injection for storage may be optimized for enhanced oil or gas recovery in fields that are still in production (or depleted reservoirs that still have remaining (economic-viable) oil or gas reserves in place), which are typical examples of utilizing the capture CO_2 and simultaneously storing some of it in these reservoirs. Examples include the CO_2 injection demonstration site in Netherlands, where CO_2 is injected for enhanced gas recovery (EGR) and storage in the K12-B gas reservoir; and the enhanced oil recovery (EOR) example of Weyburn oil field in Canada (Bert et al., 2005; International Energy Agency, 2018).
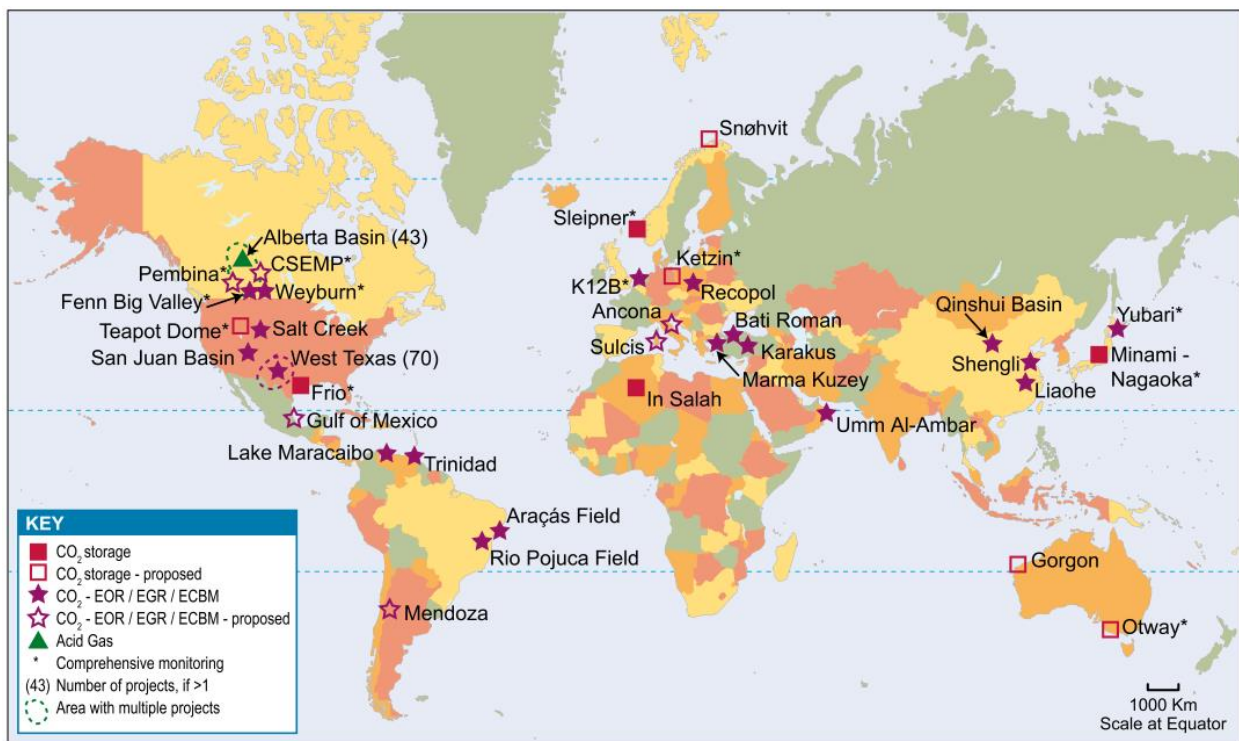
Figure 1.2: Location of sites where activities relevant to CO_2 storage are planned or under way (Source: Bert et al., 2005).

Furthermore, a database of 155 geological provinces was used to evaluate the worldwide CO_2 storage potential in disused oil and gas fields (IEAGHG R&D Programme, 2000). Based on the assumption that about 75% of the pore space, left after the extraction of the hydrocarbons, is filled with CO_2, the study (IEAGHG R&D Programme, 2000) concluded that the global capacity of CO_2 storage in depleted gas fields is about 797 gigatons (Gt), which is about 86% of the total global CO_2 storage capacity in proven hydrocarbon (oil and gas) reservoirs. However, this value reduces to 651 Gt if associated gas reservoirs are

excluded and could further reduce if we consider practical issues such as that some field sizes are too small to be economically viable, the long period of time before giant fields become available for injecting CO_2, and accessibility problems associated with some giant gas fields. Including all these constraints, the report by IEA (IEAGHG R&D Programme, 2009) gives CO_2 storage capacity estimates of 33 Gt in 2020 and 158 Gt in 2050.

1.2 Combining CO₂-EGR and CPG in deep natural gas reservoirs

In order to provide an overview of the combining CO_2-EGR and CPG technologies, it is useful to describe the CO_2-EGR and CPG systems individually, before detailing the aspects relevant to combining the two technologies.

1.2.1 CO₂-EGR

One of the several applications of utilizing, and storing, captured or separated CO_2 is by using it as a pressure enhancing source to displace remaining natural gas in the reservoir to the production well and thus recover them (IEAGHG R&D Programme, 2009).

CO_2 injection into natural gas reservoirs has been studied for CO_2 storage and EGR (e.g., Oldenburg et al., 2001, 2004b; Polak and Grimstad, 2009; Leeuwenburgh et al., 2014). Published studies on the injection of CO_2 into depleted gas reservoirs with the purpose of improving gas recovery and storing CO_2 go as far back as the early 1990s (Koide et al., 1993; van der Burgt et al., 1992). Numerical simulations and laboratory experiments have been carried out using geological data from gas fields in different countries, including USA (e.g., Oldenburg et al., 2001; Oldenburg and Benson, 2002; Oldenburg, 2003; Jikich et al., 2003), Italy (e.g., Procesi et al., 2013), Australia (Khan et al., 2013; Regan, 2010), Austria (e.g.,Clemens et al., 2010; Polak et al., 2006; Polak and Grimstad, 2009), Netherlands (e.g.,Van Der Meer et al., 2005; Meer et al., 2009; Leeuwenburgh et al., 2014), Germany (e.g., Rückheim et al., 2005; Denney, 2006; Kühn et al., 2011, 2012; Gou et al., 2014) and China (e.g., Xie et al., 2014; Shi et al., 2017), to study the feasibility of carrying out CO_2-EGR in the natural gas reservoirs in these countries. Some examples of the published pilot projects of CO_2 injection into depleted natural gas reservoirs include:

- the CO_2-EGR project in the Budafa Szinfelleti field of Hungary(Papay, 1999a, 1999b);

- the CO_2-EGR and CO_2 storage project in K12-B depleted gas field in the Netherlands (Van Der Meer et al., 2005; Meer et al., 2009);

- the CLEAN project in the Altmark gas field, Germany (Rückheim et al., 2005; Denney, 2006; Kühn et al., 2012, 2011).

Results from various studies has shown that significant amounts of additional natural gas can be recovered through CO_2-EGR (e.g., Oldenburg et al., 2001; Regan, 2010; Leeuwenburgh et al., 2014; Gou et al., 2014). The results also show that the efficiency of CO_2-EGR depends on the reservoir type, the temperature and pressure conditions, the reservoir anisotropy and heterogeneity, the injection and production strategies, the fluid-rock interactions and other factors (Jikich et al., 2003; Hou et al., 2012; Gou et al., 2016). Technically, issues, caused by mixing of CO_2 and natural gas and by early breakthrough of CO_2 at the production well, are believed to be some of the reasons why CO_2-EGR has received far less attention than CO_2-EOR (Bachu, 2003; Oldenburg, 2003; Khan et al., 2013). However, at reservoir conditions, CO_2 is denser and more viscous than methane. These favorable properties tend to minimize mixing and can yield stable methane displacement by CO_2 (Oldenburg et al., 2001; Oldenburg and Benson, 2002). Injecting CO_2 at the bottom of the reservoir and extracting methane from the top ensures that the denser CO_2 remains below the methane (Oldenburg and Benson, 2002; Polak and Grimstad, 2009; Feather and Archer, 2010), thereby minimizing CO_2 upconing at the production well. Zhang et al. (in Zhang et al., 2017) pointed out that a high ratio of CO_2 injection to fluid production rate is advantageous for extracting more natural gas from (partially) depleted reservoirs, because it minimizes the diffusive mixing of CO_2 and natural gas. If a mixed gas is produced at the surface, CO_2 can be separated with amine solvents or membranes to recover almost 97% pure methane (Brunetti et al., 2010; Dutcher et al., 2015). The separated CO_2 can be reinjected into the reservoir.

1.2.2 Geothermal potential of deep natural gas reservoirs

Natural gas represents an important fraction of the world's energy resources. In 2017, the world's proven natural gas reserves were about 193.5 trillion cubic meters and annual natural gas production reached about 3.68 trillion cubic meters, which is equivalent to approximately 3.16 billion tons of oil (BP, 2018). The combustion of natural gas emits about 30% less CO_2 than that of oil and roughly 45% less CO_2 than that of coal, per power generated through combustion (Spath and Mann, 2000), thereby contributing much less to global climate change than oil or coal do. Hence, natural gas can serve as a complementary fuel as society transitions from an almost sole reliance on fossil fuels to a widespread, or even sole, utilization of renewable energy resources. Furthermore, natural

gas provides a temporary solution to the problem that solar and wind energy are only intermittently available (Logan et al., 2013; Geoscience Australia and Bureau of Resources and Energy Economics (BREE), 2014; Loutan, 2015).

Natural gas occurs in suitable subsurface geological formations, bounded by an impermeable caprock above the reservoir formation. Subsurface temperatures and pressures increase with depth. At moderate depths, typically 2–3 km, more oil is generated relative to natural gas (Tissot and Welte, 1984; Bjørlykke, 1989). The temperature interval at which this happens is commonly referred to as the 'oil window'. At greater depths (and higher temperatures), however, oil is converted to natural gas, and the hydrocarbon-bearing reservoirs usually contain primarily natural gas (mostly methane).

These reservoirs are commonly referred to as non-associated natural gas reservoirs. Such 'non-associated' or 'dry' natural gas reservoirs typically occur at temperatures above 100 °C and at depths of ~3–5 km (see Table 1.1). Zhang et al. (Zhang et al., 2017) estimate geothermal potentials ranging from approximately 40–8800 Petajoules (PJ), which is equivalent to approximately 1.5–300 million tons of standard coal, for some examples of high-temperature natural gas reservoirs. Common geological controls for the location of some of these high-enthalpy reservoirs include the convection-dominated geothermal play systems of the extensional domain geothermal type and the conduction-dominated geothermal play systems (hydrothermal inter-cratonic basin and orogenic belt geothermal type) (Moeck, 2014).

High temperature (HT) natural gas reservoirs can generate both natural gas resources and considerable geothermal energy (Zhang et al., 2017; Ezekiel et al., 2020). In general, these reservoirs are found at depths of more than 3000 m. The reservoir temperature is usually higher than 100⁰C, and the original reservoir pressure tends to be greater than 30 MPa. We present in Table 1, six examples of onshore, deep, HT natural gas reservoirs in the world. The reservoir temperature and pressure of these natural gas reservoirs varies within a range of 100 – 204 °C and 35 – 100 MPa respectively. The current state of these natural gas reservoirs is outlined in the table. Table 1 also provides a guideline to select example reservoir lithologies and properties, which we use in our example numerical model (presented in the subsequent chapters of this thesis). Some other examples of HT natural gas reservoirs, particularly for gas fields in China, have been provided by Zhang et al. (in Zhang et al., 2017).

Table 1.1: An overview of the geologic characterization and geothermal potential of some of the world's high-temperature natural gas reservoirs. Note that the dashes (–) denote missing information.

Gas reservoir	Khuff, Dukhan field, Qatar	Altensalzwedel sub-field in Altmark gas field, Germany	Groningen giant gas field, Netherlands	Judge Digby, Onshore Gulf of Mexico, USA	Rousse, Lacq Basin, France	Arun giant gas field, Indonesia
Lithology	Carbonate (dolomite)	Fluviatile siltstones and sandstones	Slochteren sandstone and the Ten Boer claystone	Carbonate	Fractured dolomites and dolomite breccias	Carbonate (limestone)
Reservoir type	Non-associated gas	Non-associated gas	Primarily non-associated gas	Primarily non-associated gas	Depleted gas	Non-associated gas and condensate
Geological structure	Anticlinal trapping	Closed block, bound by faults	Anticlinal structures that are bounded by faults.	Fluvial-deltaic complex, with faulted closures	Isolated faulted horst limited by ESE-WNW and NNW-SSE normal faults.	North-south trending feature
Seal	Lime mudstones and shale	Thick Zechstein (salt) caprock	Anhydrite Zechstein (salt) Formation	–	Cretaceous mudstones (top and lateral seal)	–
Depth, m	2989 (top)	3400	3000	5400 – 7000	4500	2867 – 3200
Thickness, m	518	–	70 – 240	365	> 120	330 (thickest zone)
Area, km²	324	14	900	–	–	92.5
Reservoir volume, 10^9 m³	167.8	–	63 – 216	–	–	30.5
Porosity, fraction	0.05 (average)	–	0.1 – 0.25 (average 0.17)	0.20 (average)	0.03 (average)	0.16
Permeability, 10^{-15} m²	30 (average)	–	0.1 – 3000 (average 260)	1000 (average)	< 1 (pores), 5 (fractures)	1466
Temperature, °C	174	125 (average)	102.2 (average)	204	150	178
Initial pressure, MPa	42.6 (at 3050m)	42.5	34.7 (at 2875 m)	100	48.5	48.9
GIIP*, 10^9 Sm³	104	270	2900	–	–	457
Start of production	1978	2003	1963	1977	–	1971
Well diameter**, m	<0.25	–	0.12 - 0.15	–	–	0.17 – 0.24
Current status	Buffer store for excess gas from the North Field. Production still ongoing	Almost depleted, about 96% GIIP already produced. Planned for EGR and CO2 storage operations.	Production still ongoing, though at a reduced rate to reduce the occurrence of production-induced seismicity. Some parts in the North are being used for natural gas storage.	Gas production is still going on.	Site of a completed CO2 storage pilot project.	Gas production is still going on
References	(Abi-Aad Naji, 1998; Al-Siddiqi and Dawe, 1999; Brindley et al., 1984; Qatar, 1991)	(Denney, 2006; Hannis et al., 2017; IEAGHG, 2017; Kühn et al., 2012, 2011; Rückheim et al., 2005)	(De Ruiter, J., van der Laan, G., & Udink, 1967; van Beek and Troost, 1979; Vos, 2003; Dijksman and Steenbrink, 2009)	(Burke, 2011, 2010, 2009; Carlo and Martin, 1979)	(Sahuquet and Ferrier, 1982; Garcia et al., 2012)	(Pathak et al., 2004)

* GIIP – Gas initially in place (at standard cubic meter).

** Most oil and gas wells typically appear to have a diameter of 5 inches (~12 cm) or 7 inches (~17 cm) at the target interval.

1.2.3 **The CPG system**

Geothermal energy is an important renewable energy resource as it is, aside from bio energy and small-scale hydropower, the only renewable energy resource that can provide both baseload and dispatchable power and that, in contrast to bio energy, does not compete as an agricultural resource. Quite the opposite, geothermal energy can help with growing agricultural products (in greenhouses) and thus with feeding a growing world population (Adaro et al., 1999; Bakos et al., 1999). It has also been proposed that geothermally heated water can be used to enhance oil recovery by reducing the viscosity of the oil (Ziabakhsh-Ganji et al., 2018). However, geothermal energy is heavily underutilized as few locations on Earth exhibit sufficiently high subsurface temperatures at relatively shallow depths (of 2–3 km) to enable the efficient use of geothermal heat and/or electricity.

The use of CO_2 as a subsurface working fluid for extracting geothermal energy has been studied by different scholars (e.g., Brown, 2000; Pruess, 2006; Randolph and Saar, 2011a). The technology is not restricted to petrothermal (i.e. enhanced geothermal system, EGS, or hot dry rock, HDR) resources but can also be applied in naturally porous and permeable formations that typically do not require hydraulic stimulation, such as saline formations as well as oil and gas reservoirs (Randolph and Saar, 2011a; Zhang et al., 2014, 2017). These naturally porous and permeable formations, of course, have the added benefit that substantial amounts of CO_2 can be permanently stored in them, which cannot be said for petrothermal systems. In other words, in highly porous and permeable formations, an actual, large-scale CO_2-plume can form, which, in turn, enables the CO_2-based extraction of substantial amounts of geothermal energy (Randolph and Saar, 2011a, 2011b; Zhang et al., 2014; Xu et al., 2016).

When using supercritical CO_2 as the subsurface energy-extraction fluid, the efficiency of electricity generation approximately doubles compared to using traditional groundwater/brine for geothermal energy extraction and conversion (Adams et al., 2015). CO_2 possesses favorable heat-extraction properties (high thermal expansivity and low kinematic viscosity) compared to water, such that low- and medium-enthalpy geothermal reservoirs can be utilized more efficiently when employing supercritical CO_2 as the subsurface working fluid than when traditional groundwater or brine is used. The low kinematic viscosity leads to high injectivity. The high thermal expansivity of supercritical CO_2 results in substantial differences in CO_2 density between the injection and the production wells, which induces a buoyancy-driven thermosiphon and minimizes or eliminates parasitic pumping requirements of the CO_2-based geothermal energy system (Brown, 2000; Atrens et al., 2009; Randolph and Saar, 2011a; Adams et al., 2015).

For CO_2-plume geothermal (CPG) systems, a permeable sedimentary formation overlain by a low-permeability formation (caprock), providing structural or stratigraphic CO_2 trapping, is required. As the injected CO_2 circulates in the reservoir, it is geothermally heated in the subsurface. Part of the heated CO_2 is produced at the surface and can be used for electric power generation in a direct CPG power plant. Alternatively, the heat can be extracted from the fluid and used for geothermal heating or for electricity generation via an ORC power plant. The cooled CO_2 is reinjected into the reservoir so that 100% of the initially injected CO_2 is still permanently stored and the CO_2 plume grows over time. Then, more CO_2 production (and injection) wells may be installed, so that both the geologic CO_2 storage and the CPG system grow over time (Figure 1.3).
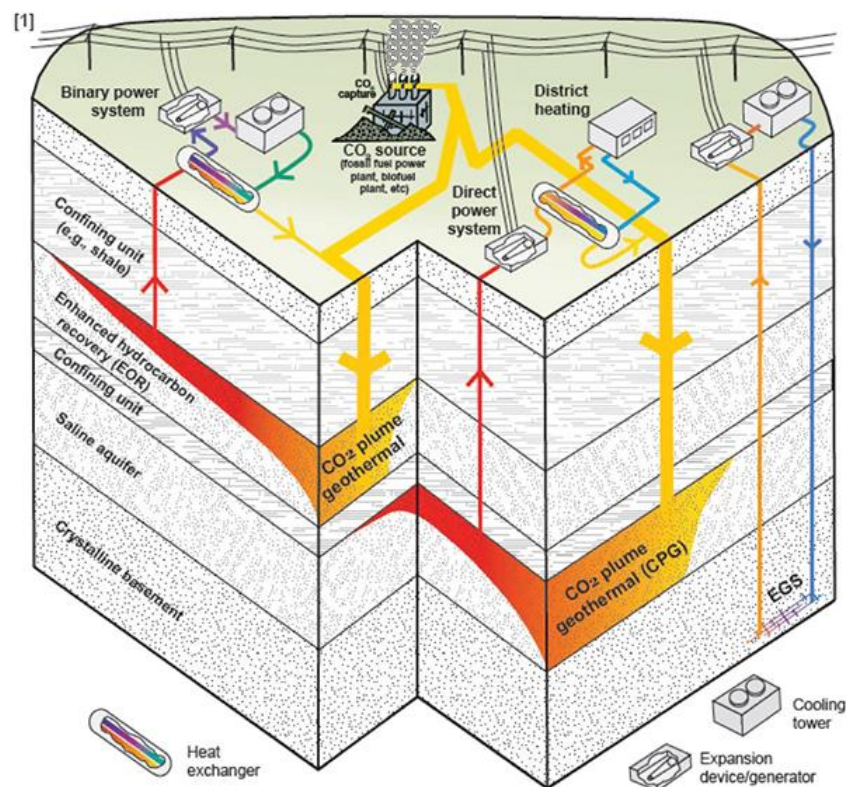
Figure 1.3: Schematic of the CPG system (Source: Randolph and Saar, 2011a)

To understand the geothermal heat extraction capabilities of the CPG system, Randolph and Saar (Randolph and Saar, 2011a), using a flowrate of 300 kg/s and a reservoir temperature and a pressure of 100 °C and 25 MPa, respectively, showed numerically that a CPG system, compared to conventional water-based and engineered geothermal systems (EGS), can generate up to 2.9 and 5 times, respectively, higher geothermal heat-mining rates. Janke and Kuehn (Janke and Kuehn, 2011) showed that, at a constant flowrate of 70 kg/s, reservoir temperature and pressure of 100°C and 25 MPa, and depth of 2.5 km, about 2 – 8 times more power can be generated in a direct CPG power cycle than in a binary ORC power plant. Adams et al. (Adams et al., 2015) compared electric power output for a CPG and a brine-based geothermal power plant at varying reservoir conditions. Generally, their simulation

results show that for both cases of CO_2 pump-based and CO_2 thermosiphon-based power systems, CO_2 direct systems typically generate more net power than indirect (ORC) power systems. For example, their base-case simulation results show that, at a depth of 2.5 km, a well diameter of 0.27 m, and reservoir permeabilities varying from $5 \times 10^{-14}\,m^2$ to $1 \times 10^{-12}\,m^2$, the net power generated by the direct thermosiphon-based CPG system is about a factor of 2.5 – 8 times greater than the net power generated by the indirect CO_2 thermosiphon-based system with R245fa as the secondary Rankine fluid. For a multi-layered CPG system, Garapati et al. (in Garapati et al., 2014) numerically showed that the produced mass fraction of CO_2, the heat-mining rate, and the pore-pressure drop in the reservoir are influenced by the permeability of the layers and their stratigraphic position within the reservoir. Numerical simulations also show that the minimum amount of CO_2 needed for CPG increases with permeability, reservoir depth, and well spacing (Garapati et al., 2015a).

CO_2 injection (into porous and permeable formations) for geothermal energy development (CPG) is also associated with carbon sequestration during and after the heat-mining process. A significant part of the injected CO_2 will not only be stored by stratigraphic trapping as a CO_2 plume underneath the caprock but can eventually also by stored by capillary/residual, dissolution, and long-term mineral trapping.

1.2.4 The combined CO2-EGR–CPG system

Integrating the different processes of CO_2-EGR and CPG, which have been described above, is a promising technology, as the natural gas reservoir can be used for 1) natural gas recovery (Utilization 1), 2) highly efficient geothermal energy utilization (Utilization 2), and 3) large-scale CO_2 storage (Storage) underneath a caprock that has served for millions of years as a safe sealing unit for natural gas. Including CO_2 capture in the nomenclature, the system constitutes a CO_2 capture double-utilization and storage (CCUUS) system, as outlined above.

The general implementation process of the combined CO_2-EGR–CPG system for power generation is shown in Figure 1.4. Prior to CO_2 injection, the produced hot natural gas can be combusted in a gas turbine to generate electricity onsite or transported away for offsite use. If the natural gas is transported away, it is likely beneficial to extract heat from the natural gas to facilitate the compression of the natural gas for transport in a pipeline. The extracted heat can then be used for electric power generation via an indirect system. In an indirect system, the hot natural gas passes through a heat exchanger (evaporator) that drives a secondary Rankine cycle, as shown in Figure 1.4. Typically, indirect systems have smaller overall system thermal efficiency compared to the direct systems (Adams et al., 2015).
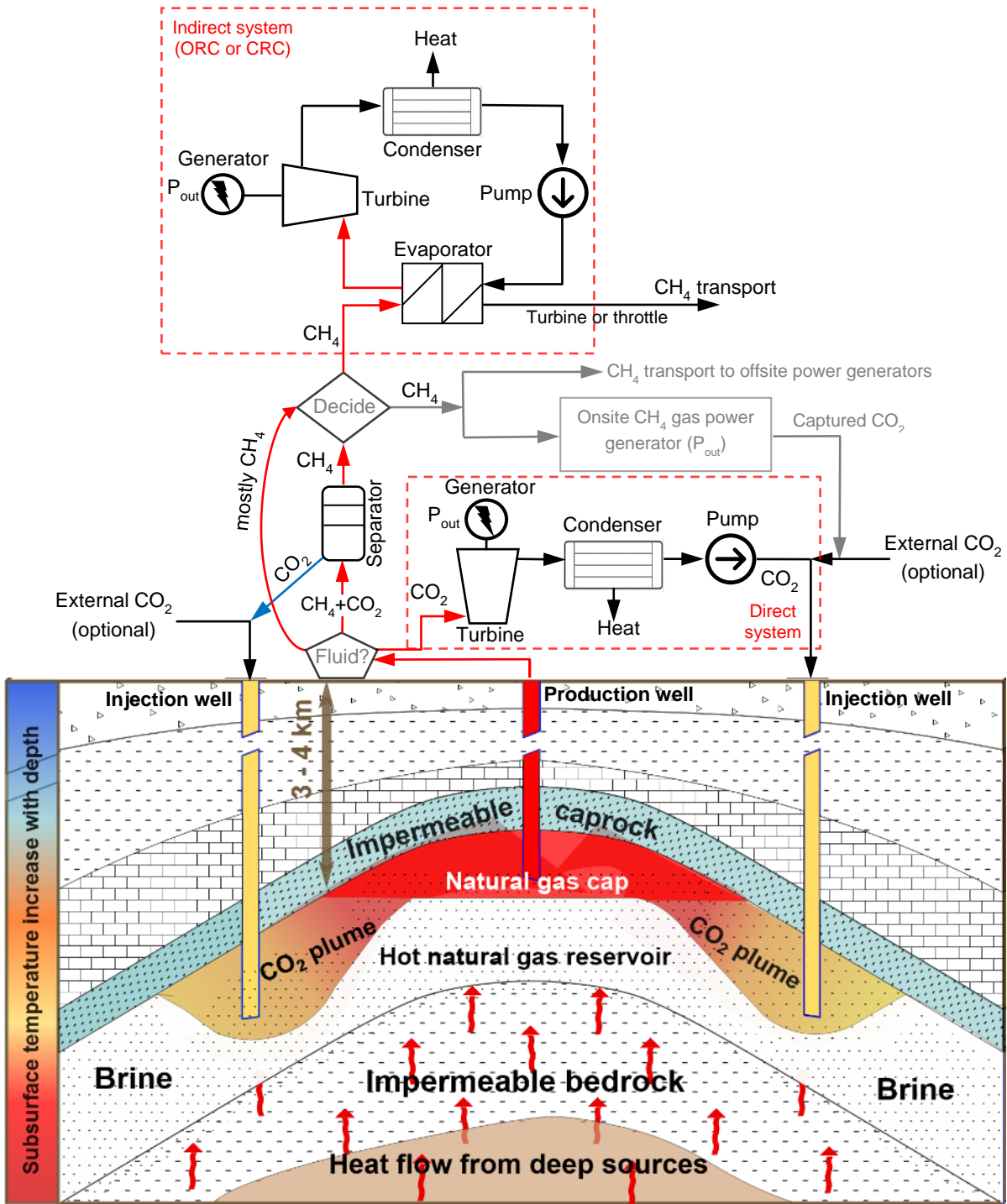
Figure 1.4: Illustration of the reservoir and surface components of the CO₂ injection into a deep, hot natural gas reservoir for co-production of natural gas, CO₂ and heat, i.e. a combined CO₂-EGR–CPG system.

When CO_2 injection has started (due to uneconomical primary-drive natural gas production), the remaining natural gas is produced in mixture with CO_2, requiring separation upon production at the surface. The geothermal energy contained in the separated methane can be extracted from the methane and converted to power using an ORC or a CRC. Meanwhile, the separated CO_2 stream is reinjected into the natural gas reservoir (as shown with the blue arrow in Figure 1.4). When the produced fluid's CO_2 mass

fraction (in the gas phase) reaches at least 96%, the produced fluid can be sent directly to the CO_2 gas turbine expansion system without requiring prior separation, as the CO_2 turbine can be designed to handle such relatively low fractions of methane. Once the (mostly) CO_2 has passed through the turbine, it is cooled and condensed to the liquid phase, using a cooler/condenser (Figure 1.4). This reduces and typically eliminates pumping/compressing power requirements (Adams et al., 2014). Then the cooled CO_2 is reinjected into the reservoir to continue the extraction of geothermal energy from the natural gas reservoir.

1.2.5 Potential benefits of the combined system

By combining CO_2-EGR and CPG systems, there are clear synergy effects that have potential benefits and can increase the overall system's efficiency. They include:

1. The combined system, if efficiently managed, can lead to an increase in the total amount of producible energy (chemical natural gas energy and geothermal energy). This additional geothermal energy (in the form of direct heat or converted to electricity), or the revenue that can be generated from the additional geothermal energy produced, can be used to compensate for the costs of gas-field operations and/or carbon (capture and) storage operations (Rubin and Zhai, 2012; Zhai and Rubin, 2013); hence, enhancing carbon capture, utilization, and storage (CCUS).

2. Natural gas reservoirs have proven traps and sealing caprocks that prevent lateral and upward escape of the gas in place, which led to the long-term accumulation of the natural gas in the reservoirs. This indicates that the CO_2, injected into these reservoirs will very likely also remain trapped for a long period of time. However, leaky abandoned wells could pose a threat to the CO_2 storage security (Nogues et al., 2011; Jung et al., 2013), although it has also been suggested that, even if leakage through a deep caprock occurs, multiple intervening caprocks at (somewhat) shallower depths will reduce the leakage rate towards the land surface to very small, or even zero, quantities (Bielicki et al., 2015)

3. In a conventional CPG operation, formation brine needs to be displaced by the injected CO_2 in order to establish a CO_2 plume (Garapati et al., 2015a; Zhang et al., 2016). In a gas reservoir, however, the establishment of the CO_2 plume constitutes the CO_2-EGR process, which is an important synergy effect. In addition, a reduced water content in the reservoir reduces the potential for interactions between acidic CO_2-rich water with the host rock, the well, and the surface equipment (Cui et al., 2016; Zhang et al., 2017).

4. The technology to screen reservoirs for technical feasibility and to design, operate and monitor CO_2 injection into natural gas reservoirs for enhanced gas recovery and CO_2 storage is already in place, as it has been developed by the gas industry. These technologies can be adapted to work efficiently in the proposed combined system. The utilization of a natural gas reservoir has usually already resulted in the production of

extensive and often expensive multidisciplinary datasets, such as (3D) seismic, magnetotelluric, reservoir, and fluid production information that were acquired, processed, and interpreted during field exploration and often also during subsequent fluid production from the reservoir (Figure 1.4). This significantly reduces investment costs for CCS and CPG, needed to acquire these datasets. Using an existing natural gas reservoir would imply that the reservoir exploration and development stages (reservoir engineering, drilling wells, etc.) have already been completed and that many of the associated costs have already been paid for by the natural gas field operator before the combined system begins. Some existing infrastructure (surface facilities, wells, etc.) at the gas fields may be adapted for the combined system for carrying out CPG operations. This is favorable because it reduces the investment costs of carrying out CPG in such a "brownfield" setting. For the purpose of electricity generation and supply, combining the two systems could also have some positive effects on the levelized cost of electricity (LCOE), since more energy is obtained with a small increase in the investment costs by producing the additional, geothermal energy. In addition, if the natural gas field is close to gas-fired power plants, the CO_2 captured from these plants does not need to be transported a long distance to the natural gas field for injection.

5. Oil/gas companies can delay (perhaps for some decades) most of the expensive clean-up and abandonment stages of a field while implementing the proposed combined system. For example, a natural gas field, that would otherwise be shut down after natural gas production or EGR ceases, may recover otherwise stranded assets such as wells, offshore platforms, etc., prolonging the useful lifetime of these assets (Figure 1.4). For the case of compartmentalized natural gas reservoirs, injecting CO_2 for EGR and CPG purposes will also lead to the recovery of the depleted reservoir pressures, thus reducing or preventing production-induced hazards (Gurevich and Chilingarian, 1993; Suckale, 2009; Bazyrov et al., 2017).

1.3 Research motivation and objectives

1.3.1 Research motivation

In Section 1.2.5 above, we have presented the potential synergic benefits associated with the combined CO_2-EGR–CPG combined system. There are a number of open questions which arise.

i. Using a scalable reservoir example, can the above benefits of the combined system be shown to be achievable?

ii. Is the combined system feasible and can the proposed implementation concept be easily transferred/adapted for a real-field application?

iii. What is the effect of liquid-phase entering the production well on the performance of the gas production well, its controlling factor(s), and implication to power generation?

iv. Can the performance of the combined system be optimized, with respect to natural gas recovery, geothermal-energy extraction and CO_2 storage?

v. What are the reservoir and operational parameters that can influence the energy recovery (for power generation) and CO_2 storage capabilities of the combined CO_2-EGR–CPG system?

1.3.2 Research objectives

To attempt to answer the questions posed above, the aim of this work is to develop a coupled numerical (reservoir, wellbore and power plant) model, using realistic reservoir parameters, and carry out numerical simulations which could aid in accomplishing the objectives of this research. The specific objectives of this thesis include:

a. To assess the feasibility of the combined system, using the proposed implementation process described in Section 1.2.4, and identify/validate the potential benefits associated with the combined system.

b. To assess the potential natural gas recovery and power-generation performance, at the different stages, of the combined system.

c. To develop design criteria for the CPG production well system, indicating the reservoir conditions and operational strategies, which are important to improving the fluid-and-heat productivity performance of the CPG-component of the combined system.

d. To perform parameter-space optimization studies to investigate the effects of both controllable factors (i.e. operational parameters) and uncontrollable factors (i.e. reservoir properties) on the fluid-productivity, energy-recovery (for power generation) and CO_2-storage performance of the combined CO_2-EGR–CPG system.

1.4 Thesis structure

A brief overview of the structure and organization of this thesis is given as follow.

Chapter 2 presents an overview (including the different operational stages) of the combined system. The reservoir model coupled with wellbore and surface-power-plant models, developed to conduct numerical simulations to study the feasibility of the combined system, is described in detail. The simulation results for the natural gas recovery, geothermal-energy extraction and conversion to power, and CO_2 storage are presented. Discussions on optimizing the power-generation potential of the combined system are also reported in this chapter.

In Chapter 3, a method to determine the two-phase flow regime in the CPG production well is described. A coupled reservoir-wellbore-power model is used to study the effect of varying reservoir and operational parameters on water entering the production well and their influences on the power generation potential of the CPG-component of the combined system. A general method to determine the minimum superficial gas (or bulk) velocity for designing a CPG system is proposed and then applied to provide insight to explain one of the reasons the first CO_2 thermosiphon experiment (in Cranfield, USA) failed.

Chapter 4 presents a preliminary parameter-sensitivity study of the combined system, which focuses on the effect of a selection of key reservoir and operational (non-reservoir) parameters and conditions on the natural gas recovery, geothermal-energy extraction and CO_2-storage performance, for the different operational stages, of the combined system.

Chapter 5 provides a detailed summary of the research conducted in this thesis and presents recommendation for future work.

2

Combining natural gas recovery and CO₂-based geothermal energy extraction for electric power generation

_____

Justin Ezekiel[a], Anozie Ebigbo[a], Benjamin M. Adams[a], Martin O. Saar[a,b]

[a]Geothermal Energy and Geofluids Group, Department of Earth Sciences, ETH-Zürich, Sonneggstrasse 5, 8092 Zürich, Switzerland

[b]Department of Earth and Environmental Sciences, University of Minnesota, Minneapolis, USA

---

[*] Some sections of this published article have been moved to the Introduction chapter of this thesis.

Abstract

We investigate the potential for extracting heat from produced natural gas and utilizing supercritical carbon dioxide (CO_2) as a working fluid for the dual purpose of enhancing gas recovery (EGR) and extracting geothermal energy (CO_2-Plume Geothermal – CPG) from deep natural gas reservoirs for electric power generation, while ultimately storing all of the subsurface-injected CO_2. Thus, the approach constitutes a CO_2 capture double-utilization and storage (CCUUS) system. The synergies achieved by the above combinations include shared infrastructure and subsurface working fluid. We integrate the reservoir processes with the wellbore and surface power-generation systems such that the combined system's power output can be optimized. Using the subsurface fluid flow and heat transport simulation code TOUGH2, coupled to a wellbore heat-transfer model, we set up an anticlinal natural gas reservoir model and assess the technical feasibility of the proposed system. The simulations show that the injection of CO_2 for natural gas recovery and for the establishment of a CO_2 plume (necessary for CPG) can be conveniently combined. During the CPG stage, following EGR, a CO_2-circulation mass flowrate of 110 kg/s results in a maximum net power output of 2 MW_e for this initial, conceptual, small system, which is scalable. After a decade, the net power decreases when thermal breakthrough occurs at the production wells. The results confirm that the combined system can improve the gas field's overall energy production, enable CO_2 sequestration, and extend the useful lifetime of the gas field. Hence, deep (partially depleted) natural gas reservoirs appear to constitute ideal sites for the deployment of not only geologic CO_2 storage but also CPG.

Keywords: Deep natural gas reservoirs, geothermal energy, enhanced gas recovery, CO_2-plume geothermal, reservoir simulation, power generation.

2.1 Introduction

One of the greatest scientific, technological, economic, and thus ultimately societal challenges of this century is how to provide energy to a growing global population, while mitigating global climate change, caused by carbon dioxide (CO_2) emissions to the atmosphere. Geothermal energy is typically regarded as a promising renewable and clean energy source that can make a significant contribution to solving the above challenge if it is more extensively deployed and efficiently utilized (Axelsson et al., 2005; Lund and Boyd, 2016; Rybach, 2003). Carbon capture and geologic storage (CCS) can also play a significant role in reducing anthropogenic CO_2 emissions while still using conventional fossil fuels to generate electricity (Bert et al., 2005).

An approach that combines geothermal energy utilization and geologic carbon storage is the concept of a CO_2-Plume Geothermal (CPG) system, proposed by Randolph and Saar (Randolph and Saar, 2011a, 2011b). This concept involves the injection of (supercritical) CO_2

into existing, naturally porous and permeable geologic formations (reservoirs) for geothermal energy recovery and eventually geologic storage of all the injected CO_2. Suitable formations can be deep saline aquifers, geopressured reservoirs, or (partially depleted) oil and natural gas reservoirs. This technology treats the captured CO_2 as a resource to extract and utilize geothermal energy, and not simply as a waste product. During this approach, a portion of the subsurface-injected and geothermally heated CO_2 is temporarily produced at the surface, providing energy for electricity generation or direct heat utilization, and then reinjected into the reservoir, so that all the injected CO_2 is ultimately stored. As the CO_2 is both utilized and eventually permanently stored underground, CPG constitutes an actual carbon, or CO_2, capture utilization and storage (CCUS) system or, to stay within the theme of this special issue, a CO_2 capture, valorization and storage system.

The utilization of supercritical CO_2 as the energy transmission fluid during geothermal energy extraction has several advantages over conventional water injection and circulation. At typical reservoir conditions, supercritical CO_2 has a lower kinematic viscosity (i.e. higher mobility) and a higher thermal expansivity coefficient than water. The low kinematic viscosity leads to larger fluid injectivities and fluid flowrates through the reservoir (Adams et al., 2015, 2014). The high thermal expansivity of supercritical CO_2 results in substantial differences in CO_2 density between the injection and the production wells, which induces a buoyancy-driven thermosiphon and minimizes or eliminates parasitic pumping power requirements of the CO_2-based geothermal energy system (Adams et al., 2014; Atrens et al., 2009). These properties of supercritical CO_2 result in a favorable geothermal heat-extraction performance (and thus roughly double the electricity-generation efficiency) for supercritical CO_2, compared to water or brine (Adams et al., 2015). However, the CO_2-water-rock interaction in the geothermal reservoirs can be complicated. Salt precipitation (caused by backflow of water and water evaporation) around the injection well can lead to reservoir damage (reduction in porosity and permeability) and limit the CO_2 heat-extraction performance (Cui et al., 2017a; Pruess, 2006; Zhang et al., 2016).

CO_2 injection into natural gas reservoirs has been studied for enhanced gas recovery (EGR) and geologic CO_2 storage (Al-Hasami et al., 2005; Oldenburg, 2003; Oldenburg et al., 2001). Results from numerical simulations and the information contained in the publications related to pilot projects indicate that significant amounts of additional natural gas can be recovered through CO_2-based EGR (CO_2-EGR) (Gou et al., 2014; Leeuwenburgh et al., 2014; Oldenburg et al., 2001). CO_2-EGR may be economically feasible if there (i) are low supply costs to obtain CO_2 (or subsidies), (ii) is little CO_2 breakthrough and a slow mixing rate of CO_2 and CH_4, and (iii) is a significant amount of remaining CH_4 to be recovered from the reservoir (Oldenburg et al., 2004). One of the main concerns regarding CO_2-EGR is that of potential degradation of the natural gas resource through mixing with CO_2. However,

numerical simulation studies show that, at typical reservoir conditions, the physical properties of CO_2 and natural gas, such as the dynamic viscosity, the density, and the solubility, are favorable for reservoir re-pressurization without extensive mixing, if appropriate reservoir-management and production-control procedures are followed (Khan et al., 2013; Oldenburg et al., 2001; Patel et al., 2016). If a mixed gas is produced at the surface, CO_2 can be separated with amine solvents or membranes (Brunetti et al., 2010; Dutcher et al., 2015). After the CO_2-EGR process, the depleted natural gas reservoirs are considered suitable locations for CO_2 storage. Such reservoirs have held natural gas for very long times, which suggests that they can safely store CO_2 over very long time scales as well (Bert et al., 2005; IEAGHG R&D Programme, 2009).

There has been little attention to, and research on, CO_2-based geothermal energy exploitation from deep natural gas reservoirs. This may be due to uncertain CO_2 markets, the low price of natural gas, corrosion issues and the disparity between the oil and gas industry on the one hand and the emerging geothermal energy industry on the other hand, regarding their different geoenergy extraction and utilization interests. In any case, most reports on CO_2-based geothermal exploitation focus on saline aquifers (in both sandstone and carbonate reservoirs) (Ganjdanesh et al., 2015; Garapati et al., 2015a; Randolph and Saar, 2011b; Romero et al., 2015; Zhang et al., 2014) and geo-pressured reservoirs (Ganjdanesh et al., 2014, 2013). Zhang et al. (Zhang et al., 2017) and Cui et al. (Cui et al., 2016) appear to be the only studies thus far that investigate the feasibility of heat mining and associated CO_2 storage in high-temperature depleted gas reservoirs. They suggest that the injection of CO_2 to extract geothermal energy in depleted, high-temperature gas reservoirs is more attractive than the CO_2-based geothermal system in deep saline aquifers. This is mainly the case because the pore-water content (leading to salt precipitation), which reduces the heat-mining performance of CO_2, is generally lower in gas reservoirs than in saline aquifers. These previous studies on CO_2 injection for EGR and geothermal exploitation only consider the heat mining and natural gas enhanced recovery from the reservoir perspective, and the associated salt-precipitation problems. In this study, we extend these existing studies by considering thermodynamic wellbore processes as well as heat extraction and heat-to-power conversion at the surface.

For the system proposed here, we consider the potential of extracting heat from produced hot natural gas (during primary recovery) for electric power generation via a suitable indirect power generation system. Subsequently (i.e. post-methane-depletion), we investigate ways of adding value to CO_2 (otherwise a waste greenhouse gas) storage. We valorize CO_2 two-fold by utilizing the CO_2 as a working fluid both for enhancing natural gas recovery and for extracting geothermal energy, from the same deep natural gas reservoir, for electricity generation via a direct power system, while still ultimately storing

all of the CO_2, so that this constitutes as CO_2 capture double-utilization and storage (CCUUS) system. To calculate the electric power generation of the proposed CO_2-based geothermal energy system, we couple the wellbore processes (considering heat transfer) to the geologic reservoir processes. This coupling enables us to obtain the thermophysical properties of the produced fluid at the surface in order to calculate the power output for both the direct and the indirect power generation system. In summary, we propose a technology that involves combining the three processes:

(i) conventional natural gas production and CO_2-EGR,

(ii) CO_2-based geothermal energy utilization, and

(iii) geological CO_2 storage, ultimately of all the originally injected CO_2.

The last two processes are collectively referred to as a CO_2-Plume Geothermal (CPG) system. We, therefore, refer to this integrated system as a combined CO_2-EGR–CPG system. We are, in a chronological fashion, classifying the combined system into five operational stages (Figure 2.1).
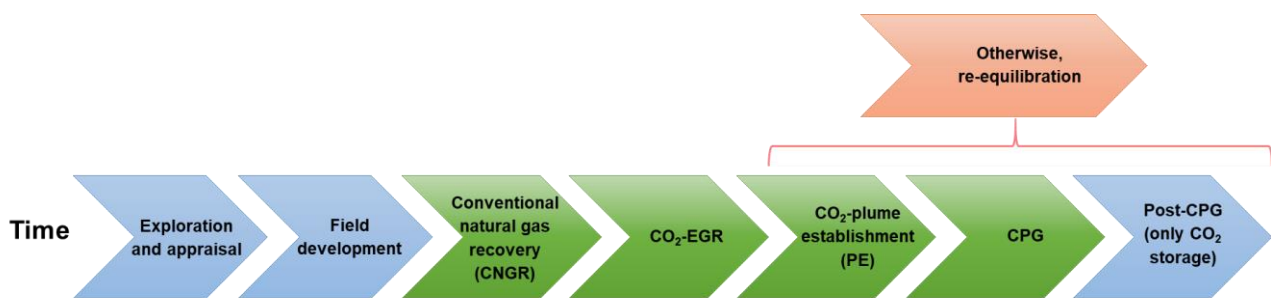
Figure 2.1: The proposed operational stages of the combined CO_2-EGR–CPG system. The stages represented by the green-colored boxes are discussed in this paper. If there are no further activities after the CO_2-EGR stage, the re-equilibration stage (red-colored box) follows, which does not generate revenue and, in the long run (field abandonment), requires money to plug the wells and clean up the field. Therefore, adding CO_2-Plume Geothermal (CPG) and CO_2 storage after the CO_2-EGR stage provides a use, and thus a revenue source, for otherwise stranded assets. The PE stage may come before or after the CO_2-EGR stage, depending on the operational strategy (Zhang et al., 2017).

CNGR Stage: The conventional natural gas recovery (CNGR) stage involves the production of natural gas during primary recovery (water/gas drive) until it is depleted, or the reservoir pressure is depleted (in the case of a compartmentalized reservoir), and it becomes uneconomical to produce more natural gas. Heat is extracted from the geothermally heated natural gas using a heat exchanger after the natural gas is produced and before it is sent to a processing plant or a power plant. The extracted heat can be converted to power using an indirect power system, such as an Organic Rankine Cycle (ORC) power plant or a CO_2-based Rankine Cycle (CRC), installed close to the production well.

CO_2-*EGR Stage:* The CO_2-EGR stage starts with the injection of CO_2 into the natural gas reservoir, while natural gas production continues. The CO_2 can come from a facility that captures the CO_2 that results from combusting the methane (CH_4) that is produced from the natural gas reservoir itself and/or from any other CO_2 source. For economical combustion of methane, coupled with carbon capture, an oxy-combustion carbon capture technology (with high-purity oxygen) is better-suited than a post-combustion carbon capture technology, because of the former's high net power generation and high CO_2 capture rate (Ahn et al., 2019). Since CO_2 is commonly denser than methane under typical reservoir conditions, injecting the CO_2 at the bottom and producing gas at the topmost part of the reservoir can help minimize mixing between the CO_2 and the methane (Oldenburg et al., 2004; Oldenburg et al., 2001). As more CO_2 is injected into the reservoir, a gas mixture of CO_2 and CH_4 is produced, where the CO_2 fraction increases and the CH_4 fraction decreases with time. It is necessary to separate the fluids in order to get high-quality CH_4 and pure CO_2, making the separated CO_2 suitable for re-injection. Thus, the mixed fluids are separated in a suitable separator (in this case a membrane that is cost-effective and has high separation efficiency) at the surface. However, the separation process leads to a pressure reduction in the CO_2 stream, with a magnitude that depends on the process design, for which CH_4 loss, cost, membrane surface area, and pressure reduction have to be optimized. A discussion of this optimization procedure is beyond the scope of this study. We thus assume here that, due to this CO_2 pressure reduction, no geothermal power is generated from the CO_2 that has been separated from the CH_4. Thus, the separated CO_2 is here simply reinjected into the geologic reservoir without utilization during the (brief) CO_2-EGR stage. However, we do assume heat extraction from the separated CH_4 by a heat exchanger for either direct use or conversion to electric power in an indirect power system, such as an ORC or a CRC.

PE Stage: The CO_2-plume establishment (PE) stage recovers the reservoir pressure to the original level, especially in a compartmentalized reservoir, by shutting-in the production well, while continuing with CO_2 injection. Another goal here is to charge the reservoir with CO_2 and establish a CO_2 plume between the injection and the production wells. Hence, the PE stage may come before (as is the case in the simulations shown later) or after the CO_2-EGR stage, depending on the operational strategy.

CPG Stage: The CPG stage is reached when the mass fraction of CO_2 in the produced fluid reaches a certain value (here we choose 96%). During this stage, geothermally heated CO_2, and initially some methane, are produced from the established CO_2 plume and used to generate electricity directly (i.e. no heat exchanger and secondary cycle are used), employing a CO_2 turbine expansion system (that can handle minor amounts of methane) and electricity generator at the surface. The CO_2 stream, leaving the outlet of the turbine, is then condensed (cooled) and reinjected into the reservoir.

Post-CPG Stage: The post-CPG stage (only CO_2 storage) starts when the reservoir heat has been depleted to an uneconomical degree, fluid production from the reservoir is stopped, and the reservoir is converted to a pure CO_2 storage site.

In this paper, we present an overview and assess the potential of the proposed technology. Using a generic anticlinal natural gas reservoir model, coupled with the numerical wellbore and surface-power-plant models, we conduct numerical simulations to study the feasibility of extracting heat from produced natural gas, and of using CO_2 as a working fluid for the dual purpose of enhancing natural gas recovery and extracting geothermal energy from deep natural gas reservoirs for electric power generation, while still simultaneously, and eventually permanently, storing the subsurface-injected CO_2, i.e. a CCUUS system.

2.1 Numerical modeling and simulation

To assess the feasibility of the proposed system from a technical point of view, a numerical model of an anticlinal, non-compartmentalized natural gas reservoir is set up. In Section 1, we broadly introduced five operational stages (Figure 2.1) that can be generally considered for the combined system. They are: 1) the conventional natural gas recovery (CNGR) stage, 2) the CO_2-EGR stage, 3) the CO_2-plume establishment (PE) stage, 4) the CPG stage, and 5) the post-CPG (only CO_2 storage) stage. In this section, we apply the first four stages in carrying out the numerical modeling of natural gas recovery and geothermal energy extraction for the combined CO_2-EGR–CPG system. We also present a wellbore model that is coupled to the reservoir model. The wellbore model is applied to obtain the final temperature and pressure of the produced fluid at the wellhead (land surface). With this production-wellhead information, we also model the power-conversion processes via the surface power plants for the different stages considered in this study (Figure 1.3).

2.1.1 **Reservoir modeling**

2.1.1.1 *Model description*

Using some of the reservoir properties of the examples of the hot natural gas fields given in Table 1, we set up a generic, small-scale model of a natural gas reservoir with an anticlinal structure. The model is scalable to account for actual gas reservoir sizes, gas extraction schemes, and CPG potentials. The reservoir is assumed to be a sandstone reservoir overlain by a caprock and underlain by a bedrock, both having a very low permeability of 10^{-19} m^2. The size of the full model is 4.5×3.0 km^2, with a reservoir thickness of 100 m. The full model (Figure 2.2 left) has 4 injection (blue) and 4 production (red) wells, where the injection wells are located 550 m from the dome center, and the production wells are 100 m from each other. By using this well arrangement, the modeling domain can be reduced to one-quarter of the

full model (Figure 2.2 right) due to symmetry. Hence, the computational cost is reduced. The injected CO_2 can accumulate at the crest of the dome, near which the production wells are located. The four identical, symmetrically located, production wells enable together four times the fluid production flowrate of a single producer. Note that the dome slopes more steeply in the y-direction than in the x-direction. The grids are refined near the production and injection wells and are coarser at the lateral boundaries. Hence, grid-cell sizes range from $10 \times 10 \times 20$ m^3 to $40 \times 40 \times 20$ m^3.
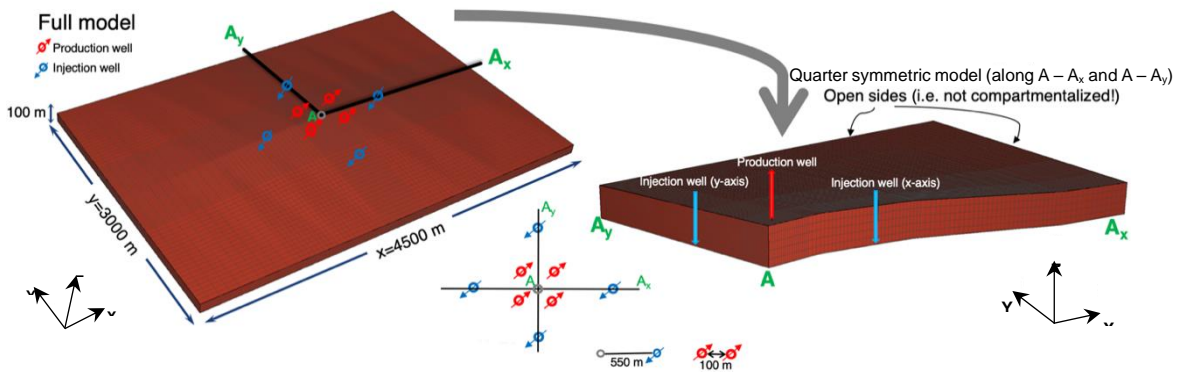
Figure 2.2: The full model (left) and the symmetric quarter model (right), showing the location of the production and injection wells. The overlying, impermeable caprock is not shown. The reservoir is not compartmentalized (i.e. no lateral reservoir boundaries exist).

For numerical modeling, we use PetraSim (RockWare, 2017; Yamamoto, 2008) and the TOUGH2-EOS7C module (Oldenburg et al., 2004) for simulating gas (methane and CO_2) and water flow as well as heat transport in the natural gas reservoir. TOUGH2 solves the fluid flow and heat transport equations, using the integral finite difference method for space discretization and the first-order, fully implicit finite differences method in time (Pruess et al., 2012). The modeled system includes two-phase flow and three components, i.e. water, CO_2, and methane.

The initial distribution of gas saturation (see Figure 2.4a below) is achieved by running an initialization simulation (simulating 100,000 years) in which the natural gas is allowed to accumulate under the caprock until steady state is reached. Dirichlet boundary conditions are set for the lateral boundaries of the reservoir, which implies that there can be lateral water/brine and heat influx into the reservoir from the far-field sides of the reservoir-bearing formation. There is no fluid flow and no heat flux set for the vertical boundaries of the reservoir. The van Genuchten-Mualem relative permeability and van Genuchten capillary pressure models are used to calculate the relative permeability and capillary pressure, respectively (Genuchten, 1980; Mualem, 1976). The saturation of the fluid entering the production well from the formation grid-cell containing the production well depends on the

Table 2.1: Parameters of the reservoir simulation model.

Parameter	Value
Reservoir size (km³)	4.5 x 3.0 x 0.1
Depth (km)	3
Porosity (-)	0.2
Horizontal permeability, kh (m²)	10^{-13}
Permeability anisotropy, kh/kv (-)	10
Thickness (m)	100
Reservoir initial pressure	Hydrostatic (30 MPa at the base)
Reservoir initial temperature (°C)	150
Initial gas saturation	As shown in Figure 2.4a
Residual gas saturation (-)	0.01
Residual water saturation (-)	0.25
van Genuchten parameters, α (Pa), m	3x10³, 0.77
Mol. diffusivity in gas; in water (m²/s)	10^{-5}, 10^{-10}
Rock grain density (kg/m³)	2650
Thermal conductivity, λ_{wet}, λ_{dry} (W/m°C) *	2.51, 1.60
Rock specific heat capacity (J/kg°C)	1000
Rock compressibility (1/Pa)	10^{-10}
Natural gas composition (mass fraction)	0.99 methane, 0.01 natural CO_2
CO_2 injection enthalpy (J/kg)	2.8x10⁵†
Lateral boundary conditions of the reservoir	Hydrostatic pressure; 150 °C (Dirichlet boundary condition).
Top and bottom boundary conditions of the reservoir	No fluid flow and no heat flux

* λ_{wet} and λ_{dry} are formation heat conductivity under fully water-saturated and fully gas-saturated conditions, respectively. Sommerton's (Somerton, 1992) interpolation formula for heat conductivity, λ, as a function of water saturation (S_l) is used, i.e. Equation (2.1): $\lambda(S_l) = \lambda_{dry} + (S_l^{0.5}[\lambda_{wet} - \lambda_{dry}])$ (Pruess et al., 2012).

† Given the average pressure and temperature of CO_2 at the injection wellhead, determined from the power-plant model in Section 2.1.1.1 (22 °C, 6 MPa), the CO_2 enthalpy at the bottom-hole is estimated using the wellbore model described in Section 2.2.

relative mobilities of the gas and water phases (Buckley and Leverett, 1942; Pruess et al., 2012), i.e.,

$$S_l^{well} = M_l/(M_l + M_g); \text{ water saturation in the well} \tag{2.2}$$

and

$$S_g^{well} = 1 - S_l^{well}; \text{ gas saturation in the well,} \tag{2.3}$$

where

$$M_\alpha = k_{r\alpha}/\mu_\alpha$$

Here, M_α, $k_{r\alpha}$, and μ_α are the mobility, relative permeability, and dynamic viscosity, respectively, of the phase (gas, subscript g, and liquid, subscript l), denoted by alpha (α), in the formation grid-cell containing the production well.

The relevant simulation parameters, including rock and fluid properties, are summarized in Table 2.1.

2.1.2 Reservoir simulations

Table 2.2 shows the duration and the injection and production rates for each operational stage (Figure 2.1). During the conventional natural gas recovery (CNGR) stage, only natural gas (assumed here: 99% methane, 1% natural CO_2) is produced at a constant production rate of 2.5 kg/s/well for 26 years via the vertical production wells, located close to the crest of the reservoir (Figure 2.2, left). We set a production interval of 20 m from the top of the reservoir for the production wells. The CNGR stage is set to end when the water saturation at the production wells starts increasing.

For the CO_2 injection stages, four vertical injection wells are introduced (Figure 2.2, left). CO_2 is injected via the four vertical injection wells across the entire reservoir thickness (100 m). To quickly charge the depleted natural gas reservoir with CO_2 and to minimize water upconing at the production well, a period of 1.5 years for the PE stage is observed immediately after the CNGR stage. During this time, the production wells are shut in and CO_2 is injected at a rate of 27.5 kg/s/well.

Table 2.2: Injection/production rates and simulation time for the operational stages of the combined system. Stages: CNGR=Conventional Natural Gas Recovery, PE=CO_2-Plume Establishment, EGR=Enhanced Gas Recovery, CPG=CO_2-Plume Geothermal. Note that, in the simulations, the PE stage comes before the EGR stage (which is shown in reverse order in Figure 2.1) and the Post-CPG stage is not considered.

Stage	CNGR	PE	EGR	CPG
Duration (years)	26.0	1.5	1.5	35.0
Start →End (years)	0→26.0	26.0→27.5	27.5→29.0	29.0→64.0
Total production rates for the 4 production wells (kg/s) *	10	–	24	110
Total CO_2 injection rates for the 4 injection wells (kg/s) **	–	110	110	110

* The mass production flowrates, used for the different stages, can be converted to volumetric flowrates (here in standard m^3 per day), using the standard state conditions of 25 °C and 0.1 MPa, resulting in: 1.33×10^6 m^3/d for the CNGR stage; 1.77×10^6 m^3/d for the CO_2-EGR stage (at equal mass fractions of CO_2 and CH_4); 5.33×10^6 m^3/d for the CO_2-Plume Geothermal (CPG) stage, which is also equal to the volumetric injection flowrates**.

The CO_2-EGR stage starts when the production wells are reopened to resume production of the fluids. For the CO_2-EGR stage, the CO_2 injection rate is set to be about 4.5 times larger than the fluid production rate (6 kg/s/well). This is to prevent water upconing at the production wells, to quickly establish a gas connection between the injection and the production wells, and to ultimately establish a largely CO_2-filled reservoir (Zhang et al., 2017). During this stage, CO_2 breakthrough occurs at the production well, and the CO_2 mass fraction in the produced fluid continuously increases. The CO_2-methane mixture has to be

separated at the surface, and the separated CO_2 is reinjected. Hence, a decreasing amount of external CO_2 is needed for the CO_2 injection. However, most of the injected CO_2 has to be external. We (arbitrarily) define the end of this CO_2-EGR stage as the moment when the CO_2 mass fraction in the produced gas reaches 96%, i.e. after 1.5 years.

During the CPG stage, the injected CO_2 is practically all previously produced CO_2. Any liquid water (typically a small amount) is removed from the produced fluid. After electricity generation and cooling, the pure CO_2 is reinjected into the reservoir. The total CO_2 injection and production flowrates are both set to be equal to 110 kg/s for the 4 production well and injection well pairs (Table 2.2). This mass flowrate is chosen to guarantee that we achieve an expected relatively high power output, as described in the power-mass flowrate analysis presented in Appendix A.1. For this example, the CPG stage is (arbitrarily) set to end when the reservoir temperature at the production wells decreases by 50 °C (which occurs, in our example case, 35 years after the CO_2-EGR stage). At this time, we consider the geothermal reservoir to be too thermally depleted to generate power at competitive costs. The reservoir may still be used for CO_2 storage if it has remaining CO_2 storage capacity. This final CO_2 storage stage is not simulated here. Hence, the total simulation time considered in this base-case example, including the four stages (CNGR, PE, EGR, and CPG), is 64 years.

2.1.3 Reservoir simulation results

2.1.3.1 *CNGR stage*

The initial reservoir fluid pressure near the top of the anticlinal structure, where the production wells are located, is 29.75 MPa. During the 26 years of simulated conventional natural gas recovery, the reservoir fluid pressure around the inlets of the production wells slightly decreases by ~2 MPa (Figure 2.3a). Water influx from the boundaries of the non-compartmentalized reservoir prevents a stronger reduction in fluid pressure. During the same 26 years of natural gas production, the reservoir temperature around the inlets of the production wells reduces by only 0.35 °C (Figure 2.3b).

The water versus natural gas saturation distribution in the reservoir pore space at the start and at the end of the CNGR stage are shown in Figure 2.4a and b, respectively. As natural gas is produced by the production wells at the crest of the reservoir, water from the far-field moves towards the center of the reservoir to replace the produced volume of natural gas, which originally occupied the pore spaces. After 26 years of natural gas production, most reservoir pores are filled with water and the natural gas cap has diminished, leaving a small natural gas volume at the top of the reservoir (Figure 2.4b). The CNGR (left) section of Figure 2.3c shows the time series of the in-situ total (natural gas) saturation around the production well inlet (i.e. in the computational grid-cell that contains the production well) during the 26 years of the CNGR stage. We observe that, as the natural gas is being produced, the

natural gas saturation in the pore space around the production well inlet slightly increases from 0.75 to 0.80. This results from the continuous evaporation of residual water into the mobile gas phase.

2.1.3.2 *CO_2 injection and fluid production stages (PE, CO_2-EGR and CPG stages)*

During the CO_2-plume establishment stage, only CO_2 injection and no gas production occurs. During this stage, the reservoir fluid pressure increases (Figure 2.3a) to values as high as 31.01 MPa and 30.14 MPa around the injection and production wells, respectively. During CO_2 injection, the occurrence of formation water backflow towards the CO_2 injection well, caused by rapid evaporation of formation water and the resulting high capillary-pressure gradient, can lead to salt precipitation and reduced permeability (formation clogging) in the area close to the injection well (Cui et al., 2016; Zhang et al., 2016). A pressure build-up around the injection well can be observed in the case of a potential permeability reduction, which may lead to requiring a pump to inject the CO_2 (Kim et al., 2012).

Figure 2.3a shows that immediately after the CO_2-EGR stage starts (from Year 27.5 onwards), the reservoir fluid pressures around the production wells decline sharply due to the increase in fluid production rate (from 10 to 24 kg/s). However, within a very short time, the pressure pulse, derived from the CO_2 injection, leads to a slight recovery of the reservoir fluid pressure around the production well (Figure 2.3a). The reservoir fluid pressure then decreases again during the start of the CPG stage, caused by the increase in the gas production rate (from 24 kg/s to 110 kg/s). Finally, once the production mass fraction of CO_2 approaches unity (i.e. mostly CO_2 is both injected and produced), the reservoir fluid production pressure gradually increases towards a steady-state value of ~26.7 MPa towards the end of the CPG stage.

Figure 2.3a also shows that the reservoir (hydrostatic) fluid pressure in the injection well region and along the x-axis of the model is less than that along the y-axis of the model. This is due to the difference in elevation between the two axes of the model. The region along the x-axis is shallower than the region along the y-axis of the model (Figure 2.2).

The reservoir temperature at the inlet of the production wells remains constant during the PE stage (Figure 2.3b). During the EGR and the subsequent CPG stage, Figure 2.3b shows that the reservoir temperature at the inlet of the production wells declines from ~149.7 °C to ~100 °C (i.e. by ~50 °C) in 36.5 years. This temperature decline is caused by the gradual cooling of the reservoir due to the steady injection of cold CO_2 at the injection wells during that time period. Figure 2.5 shows the temperature distribution in the reservoir at the end of the CPG stage. The cool CO_2 front has just arrived at the location of the production well, after 35 years in the CPG stage in this example simulation.
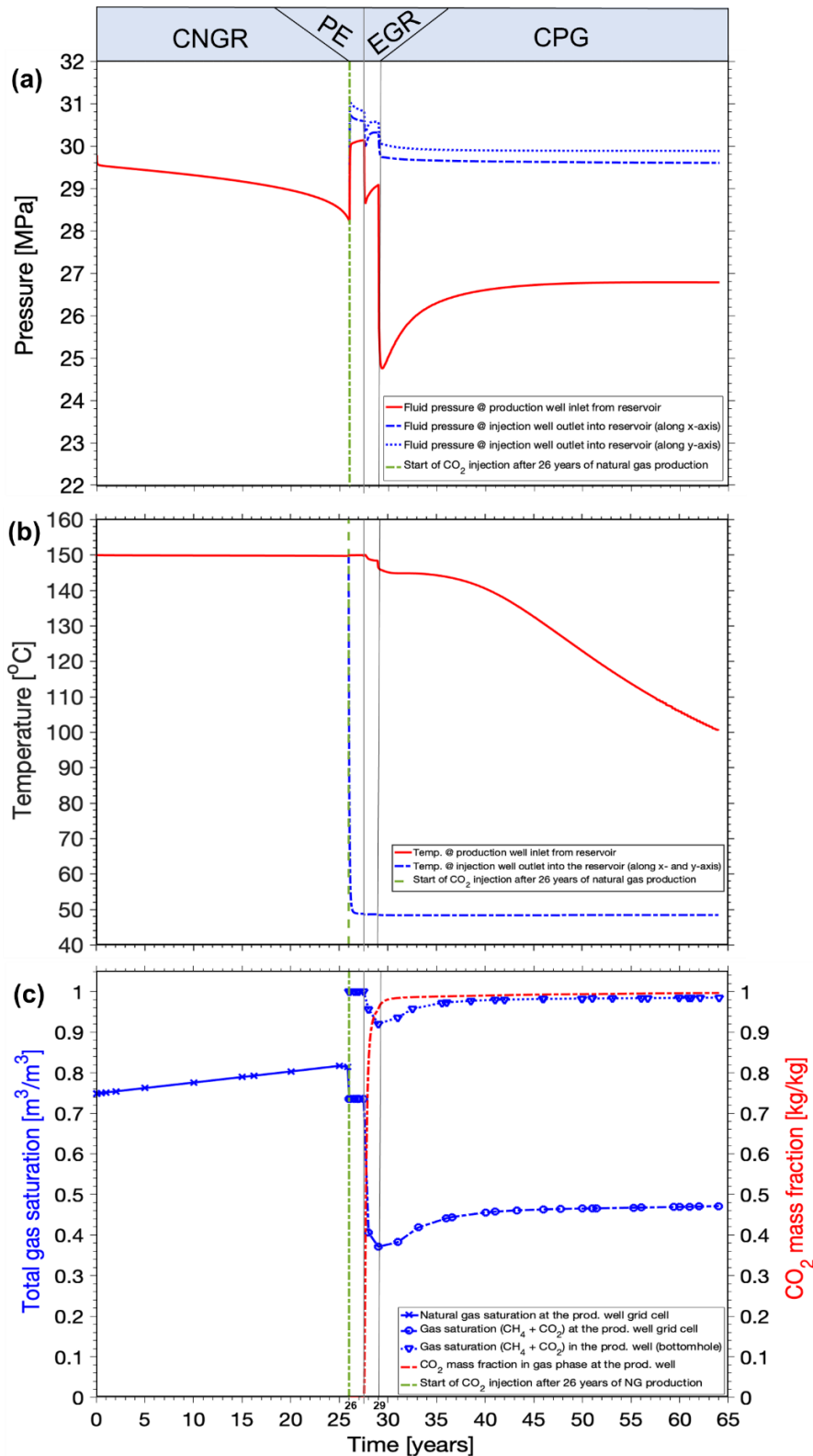
Figure 2.3: Time series of (a) bottom-hole pore-fluid (gas-phase) pressure and (b) fluid temperature in the reservoir around the production wells and around the injection wells. (c) Time series of the gas saturation around the production well grid cell and in the production well (i.e. the saturation of natural gas during the CNGR stage and the total gas (methane and CO_2) saturation during the other 3 stages) as well as the CO_2 mass fraction (in the gas phase) around the production well grid cell and in the production well. The vertical dashed green line at 26 years marks the onset of CO_2 injection into the reservoir.
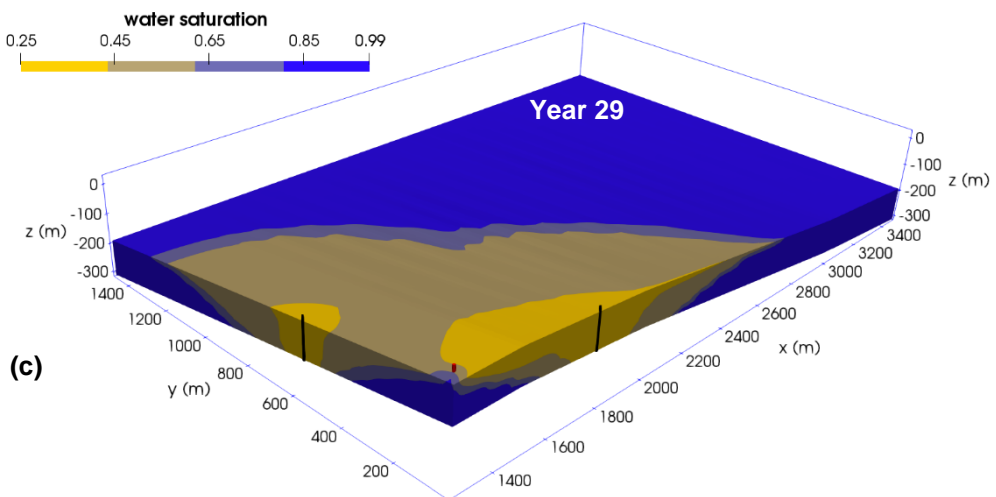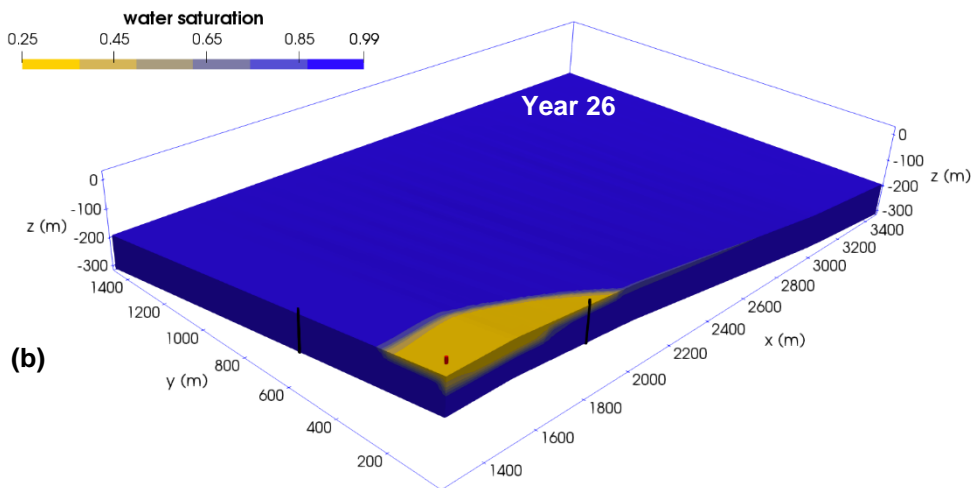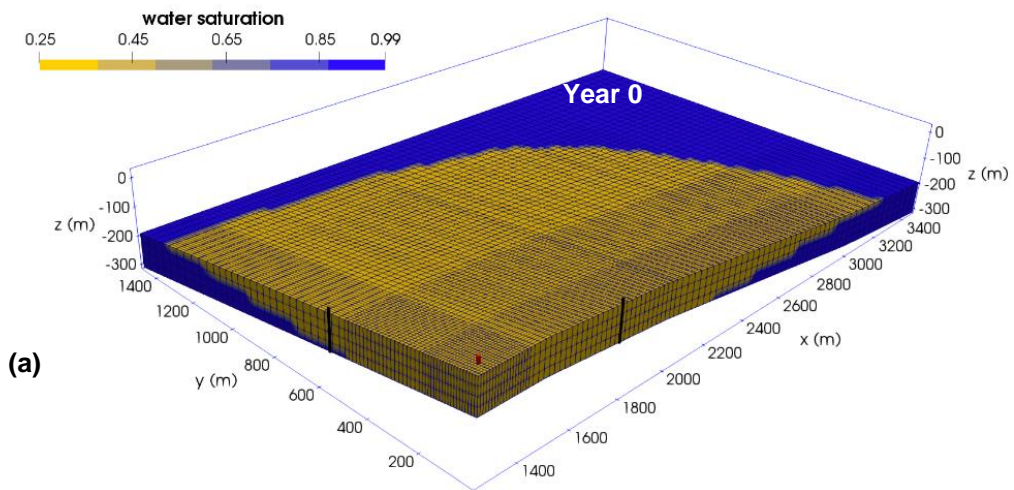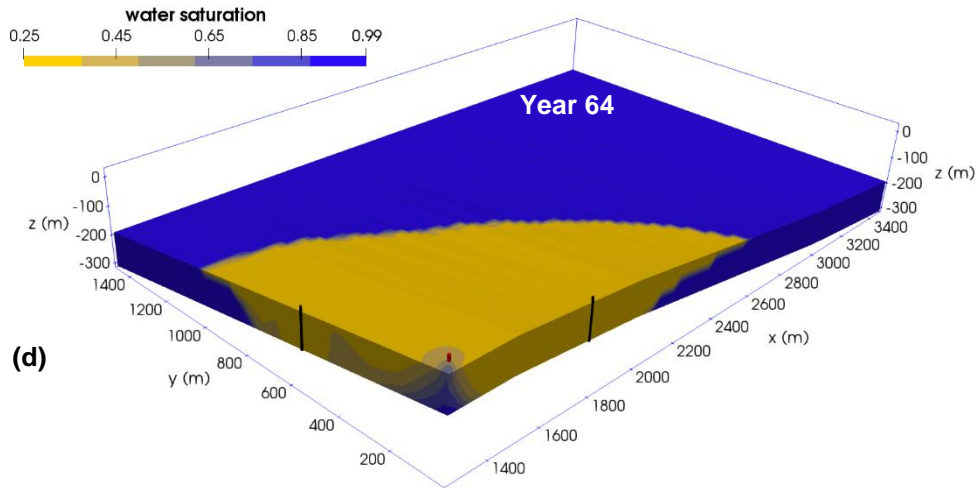
Figure 2.4: Quarter model showing the water saturation and the locations of the injection wells in black and the production well near the crest of the anticline in red (a) before natural gas production starts (Year 0), also showing the grid-cells of the reservoir model, (b) at the end of natural gas production (Year 26), showing the remaining natural gas at the crest of the anticline (c) after 3 years of injection of external CO_2 during the CO_2-EGR stage (Year 29), and (d) at the end of CO_2 circulation during the CPG stage (Year 64), which lasted for 35 years. Note, the color bar starts from the residual water saturation S_{wr} (0.25) and ends with the highest water saturation value, i.e. the water saturation at the residual gas saturation (S_{gr}) (which is $1 - 0.01 = 0.99$); z-axis is exaggerated by a factor of 1.5.
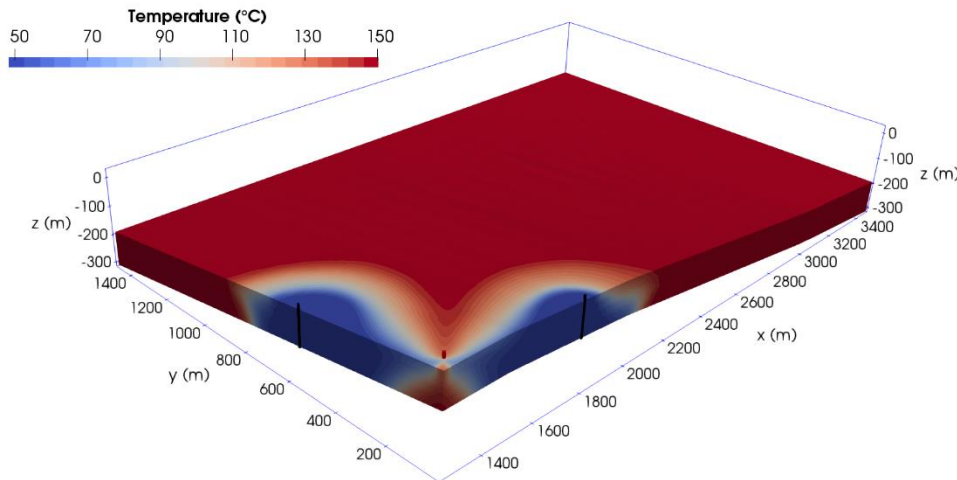
Figure 2.5: Quarter model showing the temperature distribution in the reservoir at the end of the 35-year CPG stage (64 years). The cool CO_2 front has just arrived at the location of the production well.

The 3D model of the water-saturation distribution at the end of the 1.5-year CO_2-EGR stage (at Year 29) and at the end of the CPG stage (at Year 64) are shown in Figure 2.4c and 2.4d respectively. Figure 2.3c shows the time series of total (methane and CO_2) gas saturation around the production well inlet during the PE, CO_2-EGR, and the CPG stages. During the PE stage (no production), the total gas saturation slightly decreases from 0.80 to 0.74, indicating that the water around the production well is slightly increasing. At the start of the EGR, the 3D model, presented in Figure 2.6, shows the mixing of CO_2 with methane approaching the production well location. The red line shown in Figure 2.3c indicates that the mass fraction (amount of mixing) of the two gases (natural gas and CO_2) at the

production well inlet increases from 0.01 (almost natural gas) at the start of EGR and quickly reaches 0.96 (almost all CO_2) at the end of the CO_2-EGR stage. Hence, during the CO_2-EGR stage, mixed gas can be produced at the surface, requiring separation, using a suitable high CH_4/CO_2 selectivity membrane. Figure 2.3c also shows that, as the CO_2-EGR stage starts (production well is opened), the increase in production rate leads to upconing of water into the production well. The water upconing leads to a drop in the total gas saturation, around the production well inlet, from 0.74 to about 0.38 at the end of the CO_2-EGR stage. However, we observe that the calculated saturation of the gas entering the well, which is calculated using Equations (2.2) and (2.3), is 1 (i.e. no water) at the PE stage, and it starts to drop as the CO_2-EGR stage starts, due to the water upconing effect around the production well. At the end of the CO_2-EGR stage, when the reservoir gas saturation is at its lowest value (i.e. 0.38), the calculated gas saturation of the fluid flowing into the production well is about 0.92 (Figure 2.3c). This shows that even at low (mixed) gas saturations in the reservoir around the production well, the mixed gas is preferentially drawn into the production well, instead of water. This results from the mixed gas having a significantly higher mobility than water, under the given pressure and temperature conditions (Buckley and Leverett, 1942; Pruess et al., 2012).
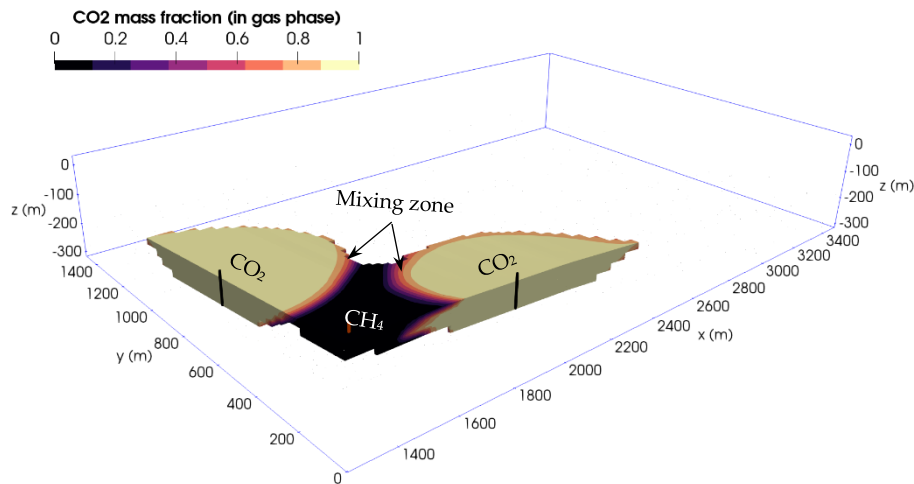
Figure 2.6: Quarter model showing the mixing of CO_2 and methane at the beginning of the CO_2-EGR stage. The part of the model with no gas phase saturation has been blanked.

At the end of the CO_2-EGR stage, Figure 2.4c shows that the CO_2 saturation in the reservoir increases as CO_2 injection goes on. Figure 2.3c shows that the CO_2 mass fraction in the gas phase (at the production well inlet) increases from 96% at the end of the CO_2-EGR stage (beginning of CPG stage) and reaches 99% only 2.5 years into the CPG stage, due to produced methane (and minor amounts of liquid water) being removed and replaced by external CO_2, while produced CO_2 is reinjected into the natural gas reservoir. At the beginning of the CPG stage, a significant amount of CO_2 begins to reach the production well

grid cell in the model and displaces the water around the production well, reducing the water upconing effect that occurred during the previous (CO_2-EGR) stage (Figure 2.3c). Continuous injection and production of CO_2 causes the reservoir gas saturation to increase and the aqueous fluids, initially present in the geothermal reservoir, to quickly be removed by dissolution (evaporation) into the flowing CO_2 stream. Hence, the gas (mostly CO_2) saturation, in the reservoir, surrounding the production-well inlet, keeps increasing during the CPG stage, approaching a steady-state value of ~0.49 (Figure 2.3c). Due to the above-mentioned mobility effect (Buckley and Leverett, 1942), the calculated gas saturation entering the production well also increases rapidly at the beginning of the CPG stage and is above 0.98 throughout almost the entire CPG stage. Figure 2.4d shows that at the end of the CPG stage, the CO_2 saturation reaches 0.70 in most parts of the reservoir, as the injected CO_2 has pushed the invading water out of the reservoir model domain.

At the time of relatively high water saturations in the well (during the CO_2-EGR stage and early during the CPG stage), the aqueous solutions of the produced fluid, containing CO_2 (carbonic acid), can be quite corrosive, and can attack the steel liners and casings in the production well (Pruess, 2006). However, as shown in Figure 2.3c , the gas saturation in the well quickly increases (after the CO_2-EGR stage), replacing the fluids containing small amounts of water initially present in the well. It is thus expected that the dry CO_2 stream then produced lowers the risk of corrosion in the production wells.

All the CO_2 initially injected underground is eventually permanently stored in the reservoir after the total 38 years of CO_2 injection. In other words, the 1.5-year CO_2 plume establishment (PE) stage, the 1.5-year CO_2-EGR stage and the 35-year CPG stage (Table 2.2) are all CO_2 storage stages, during which external CO_2 is continuously added to the reservoir and eventually permanently stored in the reservoir. Additionally, the CPG stage, terminated when the reservoir temperature has been reduced to a value that is uneconomical for further heat extraction and usage, may be followed by a pure CO_2 storage stage (Figure 2.1), depending on the remaining CO_2 storage capacity of the reservoir.

2.2 Wellbore model

A simple, one-dimensional wellbore model (incorporating heat transfer) is used in this study to determine the influence of the different fluid components (CO_2 and methane) on the final temperature and pressure of the produced fluid at the surface (production wellhead). For the vertical production well considered, the initial conditions are defined as the reservoir (bottom-hole) pressure and temperature (Figure 2.3a and b) at any given time during the three stages that are associated with fluid production (i.e. CNGR, EGR and CPG). The high compressibility of CO_2 leads to significant pressure drops as the CO_2 rises through

the production well. This, in turn, causes a temperature decrease. Hence, it is important to study the thermophysical processes in play during the flow of CO_2 in the production wells.

To set up the wellbore model, the vertical production well (3000 m long) is divided into 100 equal elements. Conservation of mass equations, as presented in (Adams et al., 2015; Atrens et al., 2009), are used to numerically calculate the fluid state in the production well across each 30 m-long vertical well segment, as the fluid flows up along the wellbore (Figure 2.7). The friction factor used in the wellbore model is calculated using the Moody Chart and is dependent on the inner diameter of the well, well surface roughness and the velocity of the fluid (i.e. the Reynolds number) (Moody, 1944). We assume that the gas production well is made of stainless steel pipes, such as Bare CR13 well piping (used in corrosive environments), with a surface roughness of 55×10^{-6} m (Adams et al., 2015; Farshad and Rieke, 2006). The wellbore diameter, D_w, considered here is 0.14 m. It is chosen to be close to the typical average diameter of wells used in oil and gas fields (Adams et al., 2015). We develop the model in MATLAB, using the CoolProp-MATLAB wrapper (Bell et al., 2014) for the iterative calculation of the thermodynamic properties of the different fluid components using the standard equations of state; (Bell and Jäger, 2016).
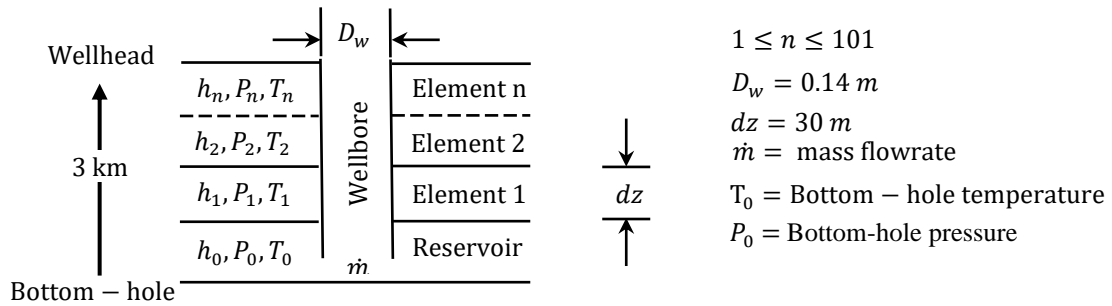
Figure 2.7: Illustration of the one-dimensional wellbore model (not to scale). h, P, T, and D_w are the enthalpy, pressure, temperature, and wellbore diameter, respectively, at each of the 30 m-long wellbore elements.

Heat loss from the wellbore to the surrounding rocks is significant in the production wells because of the high temperature of the produced fluids. Hence, we also carry out numerical calculations for convective and conductive heat transfer to/from the rock surrounding the production well as the fluid rises through the wellbore. The conductive heat exchange between the formation and fluids in the wellbore is calculated using the time-convolution method of discretizing the wellbore and using semi-analytical solutions of radial conductive heat flow, as proposed by Zhang et al. (Zhang et al., 2011). To keep the wellbore calculations simple, we are making the same assumptions as done by Zhang et al. (Zhang et al., 2011), for instance, (i) negligible vertical conductive heat flow within the formation and (ii) no thermal resistance between the cased well and the formation.

The convective heat transfer function for each well element is determined using the Nusselt number, which is calculated from the Reynolds and Prandtl numbers (Randolph et al., 2012). Convective heat transfer occurring outside the wellbore is assumed to be negligible because

of the relatively low-permeability, overlying caprocks (Adams et al., 2015; Randolph et al., 2012). We assume a homogeneous lithological unit for the overburden formations with a constant thermal conductivity of 2.1 W/m°C, which is divided into 100 equal elements to account for the changes in the thermophysical properties of the produced fluid. A heterogenous overburden unit will require complex heat transfer coefficient calculations that vary with each unit, especially when heat advection by groundwater is included in permeable overburden units.

To account for the decrease in energy as the fluid rises, the energy conservation equation is also applied in the wellbore model. The wellbore model yields approximate temperature, pressure and mass flow values of the produced fluid as it reaches the wellhead, which also serves as input for calculating the produced fluid enthalpy required for determining the electric power generation. The wellbore model parameters considered in this study are presented in Table 2.3. In Appendix A.2 (Figure A.2), we show an example of production wellhead temperature and pressure for different mass fractions of CO_2, ranging from 0 to 1 (i.e. from all methane to all CO_2). The results from the wellbore model show that, as the fluid rises in the production well, the fluid temperature and pressure decrease more strongly with increasing CO_2 mass fraction in the produced fluids.

Table 2.3: Parameters for wellbore and power plant models

Parameters	Values
Well length (m)	3000
Well diameter (m)	0.14
Geothermal gradient (°C/km)	45
Ambient mean annual temperature at surface (°C)	15
Fluid components	CO_2 and CH_4
Mean formation thermal conductivity (W/m°C)	2.1
Mean formation density (kg/m³)	2650
Mean formation specific heat capacity (J/kg °C)	1000
Well pipe material and surface roughness, m	Bare CR13; 55 x 10^{-6} (Adams et al., 2015; Farshad and Rieke, 2006)
Power systems	Direct CO_2 system – no pumping requirement; fluid – >90% CO_2 Indirect system; fluid – 1,1,1,3,3-Pentafluoropropane (R245fa) (Adams et al., 2015)
Direct turbine isentropic efficiency, η_{ie}	0.78
ORC turbine efficiency	0.80
Condensing or cooling tower approach temperature (°C)	7
CO_2 injection temperature at surface (°C)	22

The increase in the CO_2 mass fraction in the produced fluid increases the fluid density, causing an increase in the fluid pressure loss and invariably a decrease in the temperature of the fluid as it rises buoyantly to the surface. Also, an increase in the production well

diameter, at a constant fluid mass flowrate, increases the heat transfer to the surrounding rocks, which leads to a drop in the wellhead temperature (and negligible increase in pressure), as shown in Figure A.3.

In order to estimate the enthalpy of the CO_2 at the bottom of the injection well (i.e. the injection point in the reservoir), we use a simple injection wellbore model (similar to the one for the production wellbore model) in which the injection borehole is discretized into 30 m-long segments. The temperature and pressure responses of the injected CO_2 in the injection wellbore are solved numerically along each well segment. The temperature of the CO_2 increases with depth as the fluid pressure increases (due to the gas compression effect) (Lindeberg, 2011). However, in the injection wellbore model, we neglect the transfer of heat from the surrounding rock to the relatively cool CO_2 in the wellbore. This is a conservative assumption, as the temperature of the CO_2 at the point of injection into the reservoir is lower (cooling the reservoir more significantly) than what it would be without this assumption. The boundary conditions for this model include the pressure and temperature at the injection wellhead (obtained from the power-plant model) and the pressure at bottom-hole (obtained from the reservoir simulation).

2.3 Coupling reservoir and wellbore models

The wellbore model is coupled with the reservoir simulations (Section 2.1.2) to obtain the wellhead pressure (Figure 2.8a) and the wellhead temperature (Figure 2.8b) of the produced fluid as a function of time. For Figure 2.8b, we consider the change in fluid temperature due to pressure loss and wellbore heat loss as the fluid rises through the production well. We observe that the wellhead temperature at the start of the CNGR stage (early times) shows a large drop. This results from the cooling of the fluid due to heat transfer to the surrounding rocks, as the fluid rises to the Earth surface during early times. However, after a very short duration, a thermal equilibrium is reached between the fluid in the wellbore and the wall of the wellbore, so that the fluid is produced at a constant temperature of ~110 °C. During the CNGR stage, the temperature of the produced fluid reduces by ~39 °C as the fluid moves from the reservoir to the surface (wellhead). This large heat loss to the surrounding rocks and associated temperature drop results from the small well diameter (0.14 m) and the low fluid production rates (2.5 kg/s/well) employed during the CNGR stage.

We note that there is no fluid production during the CO_2-plume establishment stage (between 26 and 27.5 years). At the start of the first year of EGR, when the production flowrate is increased from 2.5 to 6 kg/s/well, heat loss in the production wellbore to the surrounding rock reduces, so that the production wellhead temperature increases from ~110 °C to ~125 °C. Thereafter, as the produced gas composition changes from mostly methane to mostly CO_2, the temperature of the produced fluid at the wellhead declines.
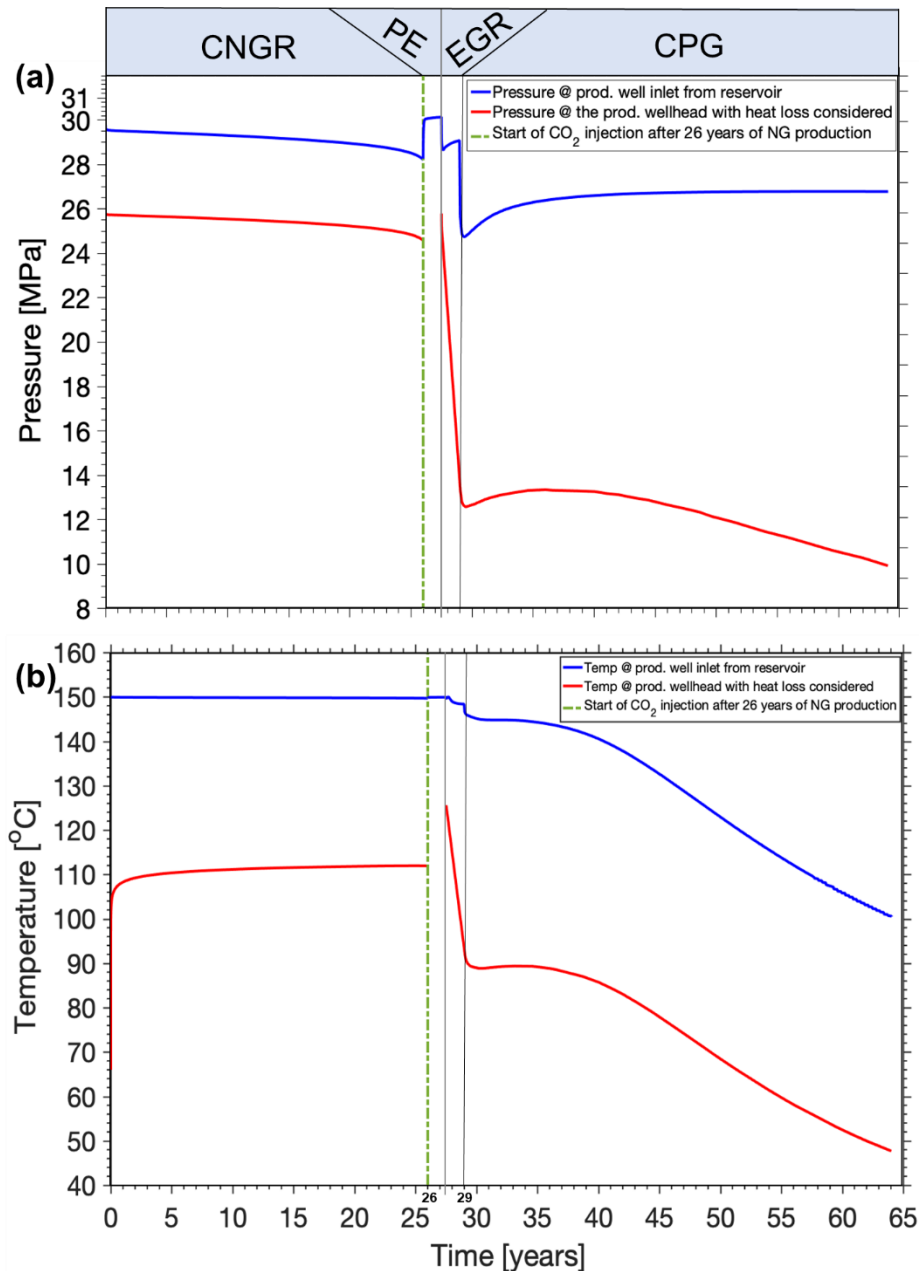
Figure 2.8: Time series of (a) pressure and (b) temperature inside the production well at the bottom of the well (blue) and at the wellhead (red), with frictional and heat losses from the production well considered. The vertical dashed green line at 26 years marks the onset of CO_2 injection into the reservoir.

During the first third of the CPG stage (between Year 30 and Year 40), the production wellhead CO_2 temperature is approximately constant at around 88 °C. After Year 40, the reservoir cools significantly, decreasing the wellhead CO_2 temperature. The curves for the bottom-hole and the wellhead temperature in the production well (Figure 2.8b) are offset by ~55 °C. For larger well diameters and higher flowrates, there would be less heat loss to the surrounding rock (Ramey Jr., 1962) and the drop in the wellhead temperature of the produced CO_2 would only come from the expansion of the CO_2 and not from heat loss to the surrounding rock during fluid ascent in the production well. Hence, larger well diameters greatly improve the CO_2-based geothermal power generation performance.

Figure 2.9a shows the reservoir fluid pressure at the bottom and at the wellhead of the production well. During the CNGR stage (Years 0 to 26), the production wellhead pressure is about 4 MPa lower than the reservoir (bottom-hole) production pressure. During the CO_2-EGR stage, the wellhead pressure decreases sharply, due to the arrival of CO_2 at the production well, which drives the produced gas composition towards larger CO_2 fractions (i.e. higher density). After Year 29.5 (during the CPG stage), the production wellhead pressure increases as the reservoir production pressure (i.e. the fluid pressure at the bottom of the production well) increases, but declines gradually after Year 40 due to decreasing reservoir production temperatures caused by the above-mentioned cooling of the reservoir around the production well (bottom-hole).

The results obtained for the wellhead temperature and pressure, after considering wellbore fluid-pressure and heat losses, are used in Section 2.4 to calculate the geothermal power generated over the production lifetime of the reservoir (a total of 62.5 years in our example case).

2.4 Energy production and CO2 storage analyses

Table 2.4 shows the summarized energy-analysis results for the small-scale combined-system example. The results include: the amount of natural gas that can be recovered; the time to establish a CO_2 plume in the natural gas reservoir; the amount of heat and electric power that can be produced; and the amount of CO_2 that can be stored during the number of years considered in this example study.

2.4.1 Power-plant models

The amount of natural gas produced during the various stages is presented in this section. As described in Section 1.2.4, the thermal energy in the produced natural gas during the CNGR stage and the thermal energy in the produced or separated natural gas during the CO_2-EGR stage can be extracted and used for power generation in an indirect (ORC) system. Also, the hot CO_2 stream produced during the CPG stage can be used to generate power by sending it to a direct CO_2 turbine expansion system (Figure 1.4).

In this study, the ambient heat rejection average annual surface temperature, T_{sur}, is assumed to be 15 °C (Table 2.3). R245fa (1,1,1,3,3-Pentafluoropropane) and the produced CO_2 are used as the working fluids for the indirect (ORC) and direct CPG systems, respectively. R245fa, as a refrigerant, is a representative working fluid for the ORC system due to its good thermodynamic performance and environmental advantages, such as low global-warming and ozone-depletion potentials (Surindra et al., 2019). An R245fa-based ORC model has been developed by Adams et al. (Adams et al., 2015). Hence, for the power generation calculation of the indirect system, we employ the same calculations as those

performed for the R245fa-based ORC model described in detail in the supplementary information provided by Adams et al. (in Adams et al., 2015). After the working fluids have been used to generate electricity, they pass through a heat-rejection system to cool and condense before reuse in the case of R245fa (indirect system) or reinjection into the natural gas reservoir in the case of CO_2 (direct system). The variables and constants used are described in the nomenclature table.

Table 2.4: Simulation results for the different stages, showing the energy produced (electric power generated) and final amount of CO_2 stored.

Stages	Open BC simulation	Results	Energy (GW$_e$h)
CNGR (26 years)	Natural gas recovery factor, %	81.9	
	Average thermal energy extractable from the produced methane over 26 years, MW$_{th}$h	387	
	Average net electric power generated from the heat extracted from the produced methane for 26 years, MW$_e$	0.08	18.22
CO$_2$-EGR (1.5 years)	Additional natural gas recovery factor, %	2.7	
	Average thermal energy extracted from the produced/separated methane, over 1.5 years, MW$_{th}$h	54	
	Average net power generated from the heat extracted from the produced/separated methane in an indirect power plant system, over 1.5 years, MW$_e$	0.19	2.43
CPG (35 years)	Average net power generated from the produced CO$_2$, in a direct power plant system, over 35 years, MW$_e$	1.58	484.43
SUMMARY			
Net power generated	Total average net power generated from the: indirect system (over 27.5 years), MW$_e$ and direct system (over 36.5 years), MW$_e$	0.09 1.58	21.68 484.43
	Total average net power generated from the produced Fluids during the project's life (64 years), MW$_e$	0.91	506.11
CO$_2$ stored	Total amount of CO$_2$ stored over 1.5 years of external CO$_2$ injection, Million tons	16.54	
Other	CO$_2$ mass fraction (XCO$_2$) at the end of the CO$_2$-EGR stage	0.96	
	CO$_2$-charging time to reach 90%, 99% XCO$_2$ at the production well, years	2.25, 5.50	
	Bottom-hole fluid pressure after 38 years of CO$_2$ injection and circulation for: injection well outlet, MPa, and Production well inlet, MPa	29.6 – 29.9 26.7	

The amount of heat extracted, Q_{ex}, and power generated, $P_{t,ind}$, by the indirect system can be calculated using Equations (2.4) and (2.5), respectively (Adams et al., 2015),

$$Q_{ex} = X_{CH4} \cdot \dot{m} \cdot (h_{in\_ind} - h_{out\_ind}), \tag{2.4}$$

where

$$h_{in\_ind} = f(P_{wh}, T_{wh}),$$

$$h_{out\_ind} = f(P_{wh}, T_{out}),$$

and

$$P_{t,ind} = \eta_{th} \cdot Q_{ex}. \tag{2.5}$$

Here, X_{CH4} is the produced methane mass fraction, P_{wh} and T_{wh} are the wellhead pressure and temperature of the produced fluid, respectively, h_{in_ind} and h_{out_ind} are the enthalpies of R245fa entering the turbine and leaving the turbine, respectively (for the indirect system), T_{out} is the outlet temperature of the primary fluid, methane, as it leaves the ORC. η_{th} is the thermal efficiency of an R245fa cycle, i.e. the ratio of the net power generated and the thermal power available. Here, we can find the thermal efficiency of the R245fa Rankine cycle and the outlet temperature of the primary fluid from two correlation plots, presented in Appendix A.3 (Figure A.5 and Figure A.6, respectively), which finds η_{th} and T_{out}, using the prevailing inlet temperature of the primary fluid and the surface ambient temperature. Hence, these plots show that the thermal efficiency of our example system ranges from 0.042 to 0.047, and the outlet temperature, T_{out}, is approximately in the range of $56 - 58$ °C.

For the direct-CO2-system, the turbine (gross) power, $P_{t,dir}$, generated is calculated using Equation (2.6). This shows that the power output of the turbine is the product of the CO2 mass flowrate, $\dot{m}$, and the difference between the turbine inlet and exit enthalpies, which is calculated using the isentropic turbine efficiency, η_{ie},

$$P_{t,dir} = X_{CO2} \cdot \dot{m} \cdot (h_{in} - h_{out}), \tag{2.6}$$

where

$$h_{out} = h_{in} - \left[\eta_{ie} \cdot (h_{in} - h_{out,s}) \right],$$

$$h_{out,s} = f(P_{cond}, S_{in}),$$

$$h_{in}, S_{in} = f(P_{wh}, T_{wh}),$$

$$P_{cond} = f(T_{out\_cond}, Q = 0)$$

Here, X_{CO2} is the produced mass fraction of CO2, h_{out} is the outlet enthalpy of CO2, considering the given turbine's isentropic efficiency, $h_{out,s}$ is the outlet enthalpy of CO2 leaving the condenser, considering a perfect turbine (i.e. isentropic expansion, $\eta_{ie} = 1$), h_{in} and S_{in} are the enthalpy and entropy, respectively, of the fluid at the inlet of the turbine, P_{cond} is the pressure of the fluid leaving the condenser, Q is the mass vapor quality at the prevailing temperature and pressure, (0 = liquid phase), and T_{out_cond} is the temperature of the cooled and condensed CO2 leaving the condenser. It is set to be the addition of the ambient surface temperature and the condenser approach temperature, i.e. 15 °C + 7 °C = 22 °C). 7 °C, the condenser approach temperature, used in this study, has been calculated elsewhere as the optimal approach temperature that yields the maximum net power output (Adams et al., 2015, 2014). See the Supplemental Information provided by Adams et al. (in

Adams et al., 2015) for details regarding how the values for the condenser approach temperatures were calculated and 7 °C chosen as the optimal temperature.

For a CO_2 direct thermosiphon system (without the use of a throttle valve or pump), the pressure of the fluid leaving the condenser, P_{cond}, to the injection wellhead, is set to be equal to the fluid pressure at the outlet of the turbine. However, when a throttle valve is introduced between the condenser and the injection wellhead, the mass flowrate of the system could be less, resulting in a decrease of the pressure losses in the production well and in the reservoir. In turn, an increase in the fluid temperature at the production wellhead can occur. This would lead to an increase in the power generated by the turbine due to the decrease in the CO_2 density in the turbine (Adams et al., 2015, 2014).

The net power, P_{net}, generated by the direct system is then defined by Equation (2.7). For the direct CO_2 thermosiphon system, P_{net} varies as a function of mass flowrate,

$$P_{net} = P_{t,dir} - P_{co} - P_{pump}, \tag{2.7}$$

where P_{co} and P_{pump} are the parasitic cooling/condensing power and pump power, respectively, required to operate the power plant. For a breakdown of the parasitic power losses, refer to Section 2.3 in Adams et al (Adams et al., 2015). The pump power, P_{pump}, is equal to zero in our study (because of the thermosiphon effect) (Adams et al., 2014). The heat-extraction rates of the cooling and condensing towers are equal to the products of the CO_2 mass flowrate and the difference between the enthalpies of the turbine inlet, $h_{in,c}$, and outlet, $h_{out,c}$. To calculate the parasitic power requirements of the cooling and condensing towers, we use the product of the heat-extraction rate and the parasitic load fraction, λ_p, which is the ratio of parasitic energy load (kW$_e$) to heat-rejection energy (kW$_{th}$). We set λ_p to be equal to 0.03 (see detailed description of the parasitic load fraction in Section 2 of the Supplemental Information, provided by Adams et al. (Adams et al., 2015)). In general, the parasitic power requirements of the cooling and condensing towers can be defined as

$$P_{co} = X_{CO2} \cdot \dot{m} \cdot \left(h_{in,c} - h_{out,c}\right) \cdot \lambda_p. \tag{2.8}$$

Therefore, the calculated temperature and pressure of the cooled and condensed CO_2 (leaving the cooler/condenser) at the CO_2 reinjection wellhead fall within the ranges 22 – 26 °C and 6.0 – 6.7 MPa, respectively (accounted for only in the direct CPG system as only that system requires coupling the CO_2 injection wells to the power plant system on the land surface). This implies that the CO_2 is injected in its liquid form, which reduces or eliminates the pumping-power requirement. This is the case, as the flow depends on the density difference between the injection (high-density CO_2) and the production wells (low-density CO_2) (Adams et al., 2014). However, the injected CO_2 reaches the target natural gas reservoir, located at a depth of 3 km in this example, as a supercritical fluid. We can see in Figure 2.3a and b that the injected CO_2 reaches the natural gas reservoir at a prevailing average reservoir

pressure of 29.65 MPa and a temperature of 48 °C. Based on the wellhead pressure and temperature and on the bottom-hole pressure of the injection well, the injection wellbore model is used to determine the specific enthalpy of the CO_2 at the bottom-hole, yielding 2.8×10^{-5} J/kg.

2.4.2 Energy production and conversion during the different combined CO₂-EGR–CPG system stages

As stated before, different forms of energy may be produced, and if desired converted, by the combined CO₂-EGR–CPG system during several of its stages (Figure 2.1). The natural gas itself constitutes chemical energy (neglected hereafter), but it also carries with it, upon production, heat (and technically pressure) energy, as it has been geothermally heated to the reservoir temperature during natural gas storage in the reservoir over geologic times. Similarly, CO₂ injected into the reservoir is geothermally heated, so that the production of that CO₂ extracts that geothermal heat and pressure energy (enthalpy) from the reservoir.
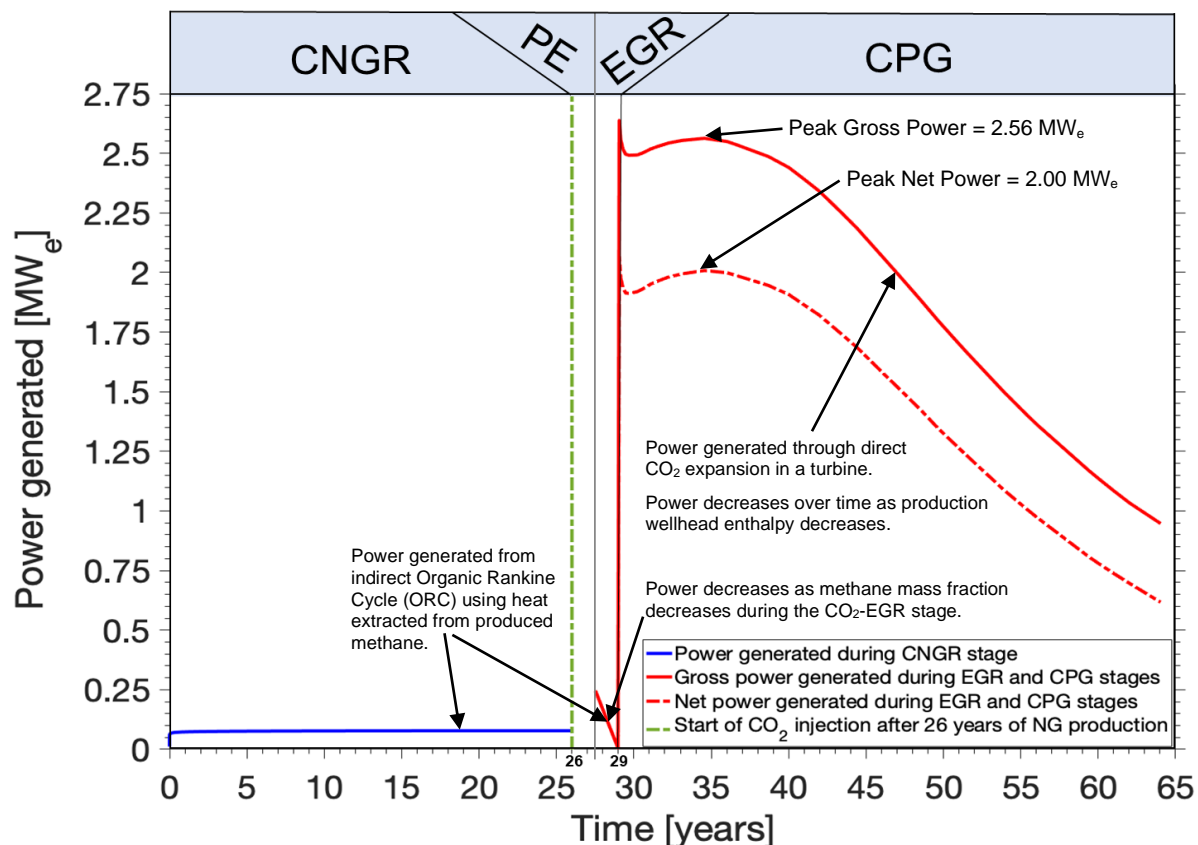
Figure 2.9: Time series of the geothermal electricity generated from all 4 production wells over 64 years. Calculations are made based on the concept that power is generated from the heat extracted from the produced methane via a Rankine cycle (indirect system), and power is generated from the produced CO₂ via CO₂ expansion in a direct CO₂ turbine (i.e. a direct CPG system as described by Adams et al. (in Adams et al., 2015)).

The wellhead information (temperature, pressure) obtained from the reservoir and wellbore model, and the information about fluid production rate (and/or circulation rate during CPG) and CO_2 mass fraction in the produced fluid, are used to calculate the electric power generated from the heat energy (and the pressure energy in case of CPG), employing the two power plant (heat engine) systems described above, during the different stages. The CNGR and CO_2-EGR stages require only the indirect system. The CPG stage requires only the direct CPG system for power generation.

The extractable heat energy and power generated during the different stages are calculated (Table 2.4 and Figure 2.9) and discussed below. Table 2.4 shows the summarized energy analysis results for the different stages. Figure 2.9 shows the time-series of the total geothermal power (gross and net) generated from all 4 production wells, using the indirect and direct systems.

2.4.2.1 *CNGR stage*

The energy produced during this stage includes both the chemical energy of the natural gas itself, which can be converted through combustion in pure oxygen, and the geothermal energy extracted from the reservoir by the natural gas, which can be converted to power via, for example, an ORC system. The former is outside the scope of our study here. The initial mass of the methane in our example reservoir, before the CNGR stage commences, is calculated to be 9.6×10^9 kg. When converted to its volume equivalency, the original gas in place (OGIP) is about 14.31 billion standard cubic meters (Bscu.m) (International Standards Organization, 1996). This OGIP is only about 13.8%, 0.5%, and 3.1% of the OGIP in the Khuff, Groningen, and Arun gas reservoirs, respectively (Table 2.1). Approximately 81.9% of the OGIP (Table 2.4) is recovered during the CNGR stage.

The thermal energy and power generated are summarized in Table 2.4. For the CNGR stage, the results show that an average of 0.39 $TW_{th}h$ thermal energy can be extracted (Q_{ex}) from the produced natural gas over the 26-year CNGR period. The average electric power generated from the extracted thermal energy with the indirect system, calculated using Equation (2.4), is approximately 0.08 MW_e (i.e. 18.22 GW_eh of electricity over a 26-year period) in this small-scale example case, which is highly scalable.

2.4.2.2 *CO2-EGR stage*

The mass of the additional/enhanced natural gas recovery, during the CO_2-EGR stage, is 2.6×10^8 kg. Therefore, approximately 2.7% of the original gas in place (OGIP) is additionally recovered during the 1.5-year CO_2-EGR stage. During this stage, the mass fraction of the additionally produced methane (in the gas phase) decreases with time, leading to a decline in the extractable heat (and thus generated electric power) from the methane (Figure 2.9).

However, the average thermal energy that can be extracted from this additional/enhanced natural gas recovery is 54 $GW_{th}h$, which can be converted to ~0.19 MW_e of electricity (i.e. ~2.43 GW_eh over the 1.5 years of the CO_2-EGR stage) with the indirect ORC system. During this stage, the wellhead pressure of the mixed fluid produced at the land surface, would partly be lost across the separation membrane and would thus no longer be available in the CO_2 stream. Hence, the separated pure CO_2 leaves the separator at a lower pressure (Chu and He, 2018), and is then reinjected into the reservoir without power generation.

2.4.2.3 *CPG stage*

For the direct CPG system, the average net power generated by passing the produced CO_2 stream directly through a CO_2 turbine expansion system is about 1.58 MW_e (0.48 TW_eh over the 35 years of the CPG stage). The average gross power generated is 2.06 MW_e, and an average of 0.48 MW_e is lost as parasitic power needed by the cooler/condenser. It should be noted that off-shore systems would likely employ direct ocean-water cooling systems, thereby significantly reducing the cooling/condensing parasitic power losses. An average peak net electric power of ~2.00 MW_e is achieved (between Year 30 and Year 40) during the CPG stage. After Year 40, the net power decreases as a result of reservoir cooling (thermal breakthrough occurring at the production wells). We again emphasize that this is only a small-scale example system, which is highly scalable.

During the CPG stage, assuming that the geothermal energy contained in the produced CO_2, is converted to power via the indirect (ORC) system, the average net power that can be generated is about ¼ of the calculated average net power generated by passing CO_2 through the direct CPG system in our example case here.

2.5 Discussion

2.5.1 **Power generation and some other benefits identified from our example models**

We are presenting here an overview and a modeling example to show that deep (and thus hot) natural gas reservoirs (depleted or partially depleted) can conveniently combine natural gas recovery and CO_2-Plume Geothermal (CPG) implementations. Our simulations yield a total natural gas recovery factor of 84.6% (i.e. 81.9% and 2.7% during the CNGR and the CO_2-EGR stages, respectively), where 2.7% of OGIP during 1.5 years of CO_2-EGR appears fair given that an average of 3.1% OGIP is produced per year during the CNGR stage. In our simulations, 21.68 GW_eh geothermal net electricity is generated over a period of 27.5 years (26 years of CNGR and 1.5 years of CO_2-EGR), via an ORC-based indirect system, using the heat extracted (441.20 $GW_{th}h$) from the produced methane. While this extracted thermal energy value is only a small fraction (about 1/295th) of the thermal energy

that can be obtained when the same amount of produced natural gas (from both stages) is combusted over a period of 27.5 years, it is still a significant contribution to the total amount of producible energy.

Chu and He (2018) (Chu and He, 2018) achieve natural gas-processing (i.e. CO_2-separation, using a carbon membrane) at costs as low as 1.12×10^{-2} $/(STP)m^3 for sweet natural gas at a feed pressure of 9 MPa. Considering the global average price estimate for electric power, generated from natural gas, 0.11 $/(STP)m^3 in 2019 (U.S. Energy Information Administration, 2020), the separation process is worthwhile. However, these authors also estimate a 1.26 MW power demand for the same separation case mentioned above, which includes the power required for the compression of the gases. The power demand in our case will be lower because the gases are already pressurized when they exit the borehole and also when they reach the production wellhead, as presented in Figure 2.8a. However, the power (average of 0.19 MW$_e$) obtained from the heat extracted from the separated methane during the CO_2-EGR stage is probably less than the power needed for the separation, which means that for this stage, external power could be required. In this case, the objective of the CO_2-EGR stage is to obtain high-quality (i.e. low-CO_2-content) natural gas for sale/combustion and to recapture and reinject the CO_2 in the gas stream. Detailed economic and energy-balance analyses are needed especially for the CO_2-EGR stage in order to optimize the power-generation potential of this stage and the combined system in general.

In addition, during the CPG stage, a higher value of electric energy (485 GW$_e$h) is generated from the produced CO_2 via a direct CO_2 turbine expansion system (i.e. a CPG system). In our calculations, the value of the net power output is reduced to a quarter when an ORC (R245fa-based) power system is used instead of the direct CO_2 turbomachinery. This corroborates the findings of Adams et al. (Adams et al., 2015), where they estimated, for a reservoir permeability of 10^{-13} m^2 and well diameters of 0.27 m, a factor of 6 times more net power generation by a direct CO_2 (thermosiphon) power system than by an indirect CO_2 (thermosiphon) power system. This result is a consequence of indirect systems having overall much smaller thermal efficiencies than direct systems. This reduced thermal efficiency of indirect systems could be caused by the so-called "pinch point" problem, associated with the R245fa-based Rankine cycle, where the thermal energy extracted from the primary fluid is not efficiently recovered, so that useful thermal energy is left in the primary fluid leaving the ORC (Adams et al., 2015). Note that this pinch-point problem is eliminated when CO_2 is used as the secondary working fluid, which may then be termed a CO_2 Rankine Cycle (CRC). In all, we show that the combined system favors the co-production of natural gas and geothermal energy for power generation in an Organic Rankine Cycle (ORC), as well as using supercritical CO_2 as a heat-transmission working

fluid for the dual purpose of enhancing gas recovery and extracting geothermal energy for power generation via a direct CO_2 turbomachinery (i.e. CPG system).

2.5.2 Optimizing the power generation potential of the combined system

Our small-scale example system includes only one well cluster with 4 injection and 4 production wells. Actual natural gas reservoirs or entire fields will likely contain many wells that could be converted to the described combined CO_2-EGR–CPG system. More net electric power can be generated when the dimensions of the natural gas production system are upscaled (number of wells, well placement, production rates). The exact value of the geothermal power that can be generated with more wells depends on the well configuration and operation strategy. Some additional large-diameter well drilling may also be required if significantly more power output is desired, as even small increases in well diameter cause a significant reduction in fluid pressure losses during fluid flow in wells, as pressure losses are inversely proportional to the fifth power of the well diameter (Adams et al., 2015). Consequently, significantly more geothermal electricity would be generated if larger well diameters were employed. Nonetheless, in our example here, we chose a well diameter of only 0.14 m as that is a typical well diameter for existing gas well fields. If new wells are to be drilled, the high costs of drilling new (large-diameter) wells may be compensated by the reduction in the overall brownfield CPG development costs, compared to establishing CPG in a greenfield situation (as brownfield CPG development can make use of previous, often expensive reservoir characterizations, existing surface infrastructures, etc.).

Furthermore, electric power output from the system increases if reservoir temperatures and permeabilities are higher or heat-sink temperatures are lower (Adams et al., 2015; Garapati et al., 2015a). Reservoir heterogeneities will likely impact (reduce) the power output (and energy extraction) performance of the system. They may lead to more mixing of the CO_2 and the CH_4. Fingering caused by the presence of heterogeneities could prevent the establishment of a continuous, compact CO_2 plume in the reservoir. However, of more importance is a sufficiently permeable connection between the injection wells and the production wells (Garapati et al., 2014). Maximizing the net electric power generation requires optimizing the fluid mass flowrate, as larger fluid mass flowrates also increase pressure losses. Hence, running the CPG stage at the optimum CO_2 mass flowrate, which is higher than during the earlier fluid production stage (Table 3), results in maximized electric power generation rates and, potentially, reduced investment costs (Ezekiel et al., 2019).

The heat-depletion rate, and associated reservoir lifespans, of the natural gas reservoir are important factors to take into consideration when planning the operation strategy of the combined CO_2-EGR–CPG system. For example, the lifespan of the geothermal power plant component of the system can be increased by operating the combined system in such a way

that it depletes the geothermal reservoir heat more slowly. Similarly, operating the combined system with optimum well spacings between the injectors and producers (in a greenfield situation, where well placements have not yet been determined) and CO_2 circulation rates can lead to reduced heat-depletion rates in the reservoir and a reduction in water upconing near production well inlets and/or reduced water intake at production wells. This is also the case for our study here, as we could further optimize our arrangement of wells and CO_2 circulation rates 1) to reduce the small amount of water upconing that we see in our simulations at the beginning of the CO_2-EGR stage, 2) to increase the time it takes for thermal breakthrough to occur at the production wells (i.e. decrease heat-depletion rates) and 3) to optimize the thermosiphon-driven power generation. However, such a parameter-space optimization study is beyond the scope of the present preliminary assessment study. The example system, while based on actual deep natural gas reservoirs (Table 1.1), is still rather generic and mainly serves to demonstrate, at a first-order level, what characteristic electric power generation capacities to expect from the here-introduced combined CO_2-EGR–CPG system.

As the proposed system is a geologic CO_2-sequestration-based approach, all risks associated with geologic CO_2 storage are also potential risks associated with the proposed combined system. For example, CO_2 may leak to the surface or to a freshwater aquifer through faults or abandoned wells (Jewell and Senior, n.d.; Jung et al., 2013). However, all potential benefits of geologic CO_2 Capture and Storage (CCS), such as reducing global climate change (Bert et al., 2005), are also part of the proposed combined CO_2-EGR–CPG system, a CO_2 capture double-utilization and storage (CCUUS) system, where the electric power output of the combined system can offset or surpass the electric power penalty of performing CCS, while ultimately still storing 100% of the injected CO_2.

2.6 Conclusions

This study highlights the technical feasibility of a technology with the potential to contribute to the valorization of CO_2. The proposed system uses CO_2 to enable (briefly, over 1.5 years) Enhanced Gas Recovery (EGR) and (predominantly, over 35 years) CO_2-based geothermal power generation and subsequent geologic storage of the CO_2 in deep natural gas reservoirs. The proposed system is thus a Carbon Capture double-Utilization and Storage (CCUUS) system, where 100% of the underground-injected CO_2 is ultimately permanently geologically stored. The potential synergy benefits of the proposed system include increasing the natural gas field's total producible energy; using the generated geothermal electricity to power some of the operational facilities of the gas field, which increases the overall system efficiency; sharing some of the existing infrastructure (surface facilities, wells, etc.) and jointly utilizing multidisciplinary datasets (on reservoir parameters), thereby

reducing investment costs significantly. The combined system also enables CO_2 Capture and Storage (CCS) by providing energy for, and compensating for the cost of CCS, and/or CO_2-EGR. Furthermore, the useful lifespan of the gas field is extended, thereby postponing the expensive clean-up and abandonment phases of the gas field and reusing otherwise stranded assets.

Our simulations of a coupled reservoir-wellbore-power model show that the average geothermal net electricity generated in our small-scale example model, employing four production wells, is 0.08 MW_e (via an organic Rankine cycle, ORC) over the 26 years of the conventional natural gas recovery (CNGR) stage, 0.19 MW_e over the 1.5 years of the CO_2-EGR stage, and 1.58 MW_e (for the direct CO_2 turbine expansion system) over the 35 years of the CO_2-Plume Geothermal (CPG) stage. We observe a peak geothermal net electricity generation rate of 2.00 MW_e during the CPG stage. This small-scale example model is highly scalable. Hence, the results obtained in this study show that the proposed system is worth considering for real applications, as it can be readily implemented in oil/gas fields with deep natural gas reservoirs to produce additional, significant energy (electric power) and add value to CO_2.

During the CPG stage, our simulations indicate that four times more electric power is generated by directly using the produced CO_2 in the direct (thermosiphon-based) CO_2 turbine expansion system (i.e. a CPG system) than by employing an indirect (ORC-based) system, which utilizes simply the heat from the natural gas. Hence, using the direct CO_2 turbomachinery CPG system results in higher electric power output rates than those of indirect systems, where the latter typically have much smaller thermal efficiencies than direct systems. More net electric power can likely be generated, where much larger reservoir development strategies (number of wells, well placement, production rates) are employed. Further studies will focus on parameter-space optimizations to evaluate the sensitivity of different key parameters on (and optimize for) the power-generation capacity of the combined CO_2-EGR–CPG system.

CO_2-EGR can serve as an important transitional stage for CPG. During the CO_2-EGR stage, CO_2 readily displaces the natural gas and a CO_2 plume is formed quickly in the reservoir to establish a CO_2 connection between the CO_2 injection and production wells. Hence, deep natural gas reservoirs (depleted or partially depleted) can be particularly well-suitable for CPG (pilot or later commercial) system developments.

All the external CO_2 injected and employed during the CO_2-EGR stage is permanently stored in the reservoir. More CO_2 could likely be stored both during the CPG and during a post-CPG stage, depending on the reservoir storage capacity. In our small-scale simulation example, about 16 million tons of CO_2 are eventually permanently stored in the (previous) natural gas reservoir, i.e. most of the natural gas has been replaced by the CO_2. Given that

the natural gas had been safely stored over long geologic times before natural gas extraction commenced, it is likely that the CO_2, that replaced most of the natural gas, is thereafter safely stored over long (i.e. geologic) times.

Acknowledgments

Nomenclature

Dimensionless parameters and constants

λ_p parasitic load fraction (kW$_e$/kW$_{th}$)

μ_α dynamic viscosity of the α phase (liquid or gas phase)

η_{th} thermal efficiency of an organic Rankine cycle (kW$_e$/kW$_{th}$)

η_{ie} isentropic expansion of the turbine (kW$_e$/kW$_{th}$)

$k_{r\alpha}$ relative permeability of the α phase (liquid or gas phase)

M_g mobility of gas phase

M_l mobility of liquid phase

n number of elements considered for the wellbore model

Q mass vapor quality at prevailing temperature and pressure

S_g saturation of gas phase in the reservoir

S_{gr} irreducible saturation of gas phase

S_g^{well} saturation of gas phase in the well

S_l saturation of liquid phase in the reservoir

S_{lr} irreducible saturation of liquid phase

S_l^{well} saturation of liquid phase in the well

X_{CH4} mass fraction of methane in gas phase

X_{CO2} mass fraction of CO_2 in gas phase

Variables

λ_{dry} formation thermal conductivity under fully gas-saturated conditions (W/m^{o}C)

λ_{wet} formation thermal conductivity under fully water-saturated conditions (W/m^{o}C)

D_w well diameter (m)

dz interval length step between two elements (m)

h specific enthalpy (J/kg)

h_{in} enthalpy of the fluid at the inlet of the turbine (direct system) (J/kg)

$h_{in,c}$ enthalpy of CO_2 at the inlet of the condenser/cooling unit (J/kg)

h_{in_ind} enthalpy of the Rankine fluid entering the turbine (indirect system) (J/kg)

h_{out} outlet enthalpy of the fluid at the turbine considering the given turbine's isentropic efficiency (J/kg)

$h_{out,c}$ enthalpy of CO_2 at the outlet of the condenser/cooling unit (J/kg)

$h_{out,s}$ outlet enthalpy of the fluid leaving the condenser considering a perfect turbine (J/kg)

h_{out_ind} enthalpy of the Rankine fluid leaving the turbine to the condenser (indirect system) (J/kg)

$\dot{m}$ mass flowrate (kg/s)

P_0 bottom-hole pressure (Pa)

P_{co} parasitic power used by the cooling unit/condenser (W$_e$)

P_{cond} pressure of the fluid leaving the condenser (Pa)

P_{net} net power generated by the direct system (W$_e$)

P_{pump} parasitic power used by the pump (W$_e$)

$P_{t,dir}$ turbine (gross) power generated by the indirect system (W$_e$)

$P_{t,ind}$ net power generated by the indirect system (W$_e$)

P_{wh} production wellhead pressure (Pa)

Q_{ex} amount of heat extracted by the indirect system (W$_{th}$)

S_{in} entropy of the fluid at the inlet of the turbine (J/kg^{o}C)

T_0 bottom-hole temperature (^{o}C)

T_{out} outlet temperature of the primary fluid passing the ORC (^{o}C)

T_{out_cond} temperature of the cooled and condensed CO_2 leaving the condenser (^{o}C)

T_{sur} surface ambient temperature (^{o}C)

T_{wh} production wellhead temperature (^{o}C)

3

Numerical analysis and optimization of the performance of CO_2-Plume Geothermal (CPG) production wells and implications for electric power generation[*]

Justin Ezekiel[a], Benjamin M. Adams[a], Martin O. Saar[a,b], Anozie Ebigbo[a,c]

[a]*Geothermal Energy and Geofluids Group, Department of Earth Sciences, ETH-Zürich, Sonneggstrasse 5, 8092 Zürich, Switzerland*

[b]*Department of Earth and Environmental Sciences, University of Minnesota, Minneapolis, USA*

[c]*Hydromechanics Group, Helmut Schmidt University, Hamburg, Campus Nord, Friedrich-Ebert-Damm 245, 22159 Hamburg, Germany*

Abstract

CO_2-Plume Geothermal (CPG) power plants can produce heat and/or electric power. One of the most important parameters for the design of a CPG system is the CO_2 mass flowrate. Firstly, the flowrate determines the power generated. Secondly, the flowrate has a significant effect on the fluid pressure drawdown in the geologic reservoir at the production well inlet. This pressure drawdown is important because it can lead to water flow in the reservoir towards, and into, the borehole. Thirdly, the CO_2 flowrate directly affects the two-phase (CO_2 and water/brine) flow regime within the production well. An annular flow regime, dominated by the flow of the CO_2 phase in the well, is favourable to increase CPG efficiency. Thus, flowrate optimizations of CPG systems need to honor all of the above processes. We investigate the effects of various operational parameters (maximum flowrate, admissible reservoir-pressure drawdown, borehole diameter) and reservoir parameters (permeability anisotropy and relative permeability curves) on the CO_2 and water flow regime in the production well and on the power generation of a CPG system. We use a numerical modeling approach that couples the reservoir processes with the well and power plant systems. Our results show that water accumulation in the CPG vertical production well can occur. However, with proper CPG system design, it is possible to prevent such water accumulation in the production well and to maximize CPG electric power output.

Keywords: CO_2-plume geothermal, production well, wellbore flow regimes, numerical modeling, power generation, CO_2 capture utilization and storage (CCUS).

3.1 Introduction

In this era of global energy transition to clean and sustainable energy and to tackle the challenges posed by global climate change, carbon dioxide (CO_2) capture and storage (CCS) in deep saline aquifers and depleted oil and gas reservoirs is widely considered as a significant means to reduce CO_2 emissions to the atmosphere (Bert et al., 2005). One of the promising technologies that supports shifting the world's energy production to renewables, in this case geothermal energy, while at the same time ensuring a safe removal and storage of captured CO_2 in the subsurface, is the concept of CO_2-plume geothermal (CPG).

CPG involves the injection of (supercritical) CO_2 from an emitter into existing, naturally porous and permeable geologic formations for geothermal energy recovery and eventually permanent geologic storage of most of the originally injected CO_2, constituting a CO_2 capture, utilization and storage (CCUS) technology. The naturally porous and permeable formations required for CPG are common throughout the world and are seen to exist where economically favorable storage sites have been identified (Bert et al., 2005; Coleman, J.L., Jr., and Cahan, 2012; Eccles and Pratson, 2014; Procesi et al., 2013).

During the CPG approach, the injected CO_2 is geothermally heated as it circulates in the reservoir. Some of the heated CO_2 is produced at the surface and can be used for direct heat utilization and/or electric power generation in a direct CPG turbomachinery power plant. The benefits associated with using CO_2 instead of water as the subsurface working fluid for geothermal energy extraction, while simultaneously storing CO_2, have been discussed in detail in different CO_2-based geothermal literature (e.g. Adams et al., 2015; Ezekiel et al., 2020; Pruess, 2008; Randolph and Saar, 2011).

Previous CPG analyses (Randolph and Saar, 2011; Adams et al., 2014, 2015; Garapati et al., 2015), as well as many CO_2-based EGS studies (e.g. Brown, 2000; Pruess, 2006, 2008; Atrens et al., 2009), focused on subsurface heat transfer or surface components of the system without accounting for the effect of water entering the production well on the CO_2 thermosiphon and on the heat extraction and power generation rates. The pre-test modeling of the first field-scale experiment of a CO_2-thermosiphon (to test the concept of supercritical CO_2 heat extraction from the subsurface) conducted at the South Eastern Regional Partnership for Carbon Sequestration (SECARB) Cranfield Site (USA) initially predicted a sustainable thermosiphon should be possible at the site. However, this particular field test showed that its thermosiphon (initiated by venting the production well) decayed quickly and could not be sustained (Freifeld et al., 2016, Pan et al., 2015, Pan et al., 2018). They postulated that liquid water entering the production well could be one of the important factors damping the CO_2 thermosiphon flowrate.

Most gas production wells have liquid (water) entering the well. If the gas velocities are not high enough, the water accumulates, forming slugs. Such slug formation may cause the overall fluid density to increase in the production well. The higher density may increase the bulk weight of fluids in the well, resulting in decreased flow (velocity) for a given pressure gradient. This transient process, called liquid loading, continues until the well is filled with water. To remove the liquid water in a gas production well, the oil and gas industries apply artificial lift and/or pumping (Lea et al., 2008). Also, they usually use small-diameter production pipes for gas production, which reduces the probability of slug or churn flow in the well. In contrast, for conventional geothermal energy extraction (using water as the subsurface working fluid), large-diameter wells are preferred in order to ensure large mass flowrates and minimize heat loss. In both greenfield or brownfield CPG systems, brine and CO_2 are typically present in the partially saturated reservoir around the injection and production well regions with varying ratios of water–CO_2 saturation. Under such conditions, complicated CO_2-water-rock interactions prevail in the reservoir (Pruess, 2006), so that the produced fluid may contain a mixture of water (brine) and CO_2. However, large amounts of water in the CPG production well can be detrimental to the performance of the well and the power plant, which may

ultimately reduce the efficiency of the CO_2-based geothermal energy system (Freifeld et al., 2016; Pan et al., 2018).

In addition, water influx into the well poses a problem, as the produced water must be disposed of at the land surface, or reinjected elsewhere, and the mass flowrate of CO_2 produced at the surface may be significantly reduced. Therefore, for successful CPG deployments, it is important to investigate the optimal fluid pressure drawdown, flowrate, and production well pipe diameter (in the reservoir) to reduce the tendency of water entering the production well, to avoid slug/churn flow and liquid loading in the production well, and to minimize heat and pressure losses as the fluid moves up to the wellhead, which optimizes the system power output.

The CO_2 flowrate (or CO_2 velocity) in the production well is an important factor, as it determines (i) how much water is drawn into the production well (water upconing), (ii) whether the water entering the well can accumulate in the well, and (iii) the power output that can be achieved. In previous CPG studies, the production mass flowrate has either been chosen arbitrarily (Garapati et al., 2015b; Randolph and Saar, 2011a) or chosen based on a power-flowrate analysis to maximize net power generation (Adams et al., 2015). However, minimizing the amount of water in the production well is an additional constraint that should probably be considered when determining the optimal CO_2 circulation flowrate of CPG systems.

Hence, the objective of this study is to investigate the fluid-flow performance of the CPG production well for different reservoir and operational conditions. In that regard, we employ a coupled flow (reservoir and production well) and power-generation model to determine possible factors that may influence the flow regimes, potential water accumulation (liquid loading) in the CPG production well and the power generation performance of such a CPG system. In this study, we also present an insight on why the Cranfield (USA) CO_2 thermosiphon field test failed due to liquid water in the production well.

3.2 Numerical modeling concept

The CPG system is modeled here using a system of numerical models coupled sequentially to each other by passing relevant model output from one component to the next, as shown in Figure 3.1. The subsurface flow model describes the two-phase flow of CO_2 and brine in the reservoir. The production well model determines how the conditions in the well change as the fluid moves upwards. The power-system model calculates the electric power output. In the following sections, each model and the interfaces between the models are described.
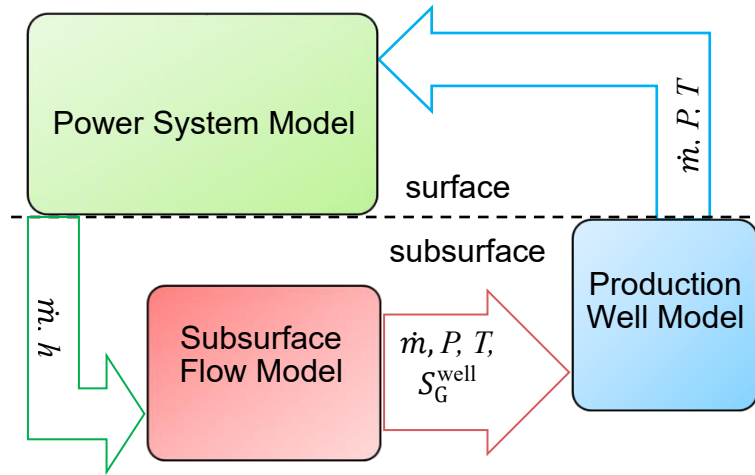
Figure 3.1: Numerical modeling concept. The boxes represent separate models, while the arrows represent the information that is passed between the models (pressure, P, temperature, T [°C], volume fraction of CO_2 in the borehole, S_G^{well}, CO_2 mass flowrate, $\dot{m}$, and CO_2 enthalpy, h [J/kg]. No injection well model is required, as pure CO_2 is injected, which can be analytically represented.

3.2.1 Influx of fluids into the borehole

Most gas production wells produce at least some liquid water. When liquid water enters the well with the flowing gas, the gas can carry the water up the well if the velocity of the gas is high enough. If the gas velocity is below the critical minimum velocity required to drag the water droplets out of the production well, then water will accumulate in the production well and liquid loading may eventually occur, which may reduce the productivity and the lifetime of the well. Liquid loading will also increase the pressure drop in the wellbore due to hydrostatic pressure contributions of the flowing fluids (weight of the gas and the accumulated liquid in the wellbore).

In order to assess the relative amounts of CO_2 versus water entering the inlet of the production well, consider Figure 3.2, which shows the top view of the screened interval of the production well. From Darcy's law, there is a fluid flux, q_α [m/s], of Phase α from the reservoir into the borehole due to the radial pressure gradient near the borehole. If one neglects capillary pressure, i.e. assumes $P_L \approx P_G$, then the relative water flux into the well can be approximated by

$$\frac{q_L}{q_L + q_G} \approx \frac{\lambda_L}{\lambda_L + \lambda_G} . \tag{3.1}$$

Where the mobility of Phase α is given by $\lambda_\alpha = \frac{k_{r\alpha}}{\mu_\alpha}$. Here, $k_{r\alpha}$ and μ_α are relative permeability [-] and dynamic viscosity [Pa·s] of Phase α, respectively. Phase α can either be liquid water (L) or supercritical/gaseous CO_2 (G). Note that this assumption may lead to inaccuracies for low liquid water saturations in the reservoir.
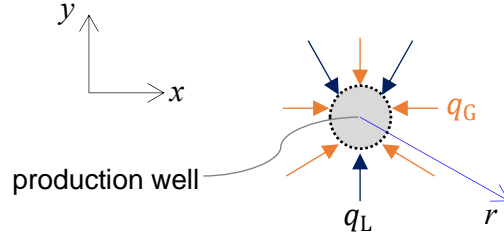
Figure 3.2: Top view of the reservoir– well interface. The fluxes of liquid water, q_L, and supercritical/gaseous CO_2, q_G, into the well depend on the mobility of each phase, the horizontal reservoir permeability and the fluid pressure gradient.

Given the relative fluxes into the well, one can estimate the volume fraction of liquid water at the bottom of the well, S_L^{well},

$$S_L^{\text{well}} = \frac{q_L}{q_L + q_G},$$ (3.2)

$$S_L^{\text{well}} \approx \frac{\lambda_L}{\lambda_L + \lambda_G} \text{ and } S_G^{\text{well}} \approx \frac{\lambda_G}{\lambda_L + \lambda_G}.$$ (3.3)

As shown in Equation (3.1), the mobilities of the phases, and consequently S_α^{well}, depend on the relative permeabilities and the viscosities of the phases. The relative permeabilities are functions of the phase saturations in the reservoir rock surrounding the well. To convert the volume fraction to mass fraction, we define the mass fraction of the fluid entering the well, represented by M_α, as the ratio of the mass flowrate of each phase, $\dot{m}_\alpha$ [kg/s], entering the well to the total mass flowrate, $\dot{m}_{\text{total}}$ [kg/s], of the two phases,

$$M_\alpha = \frac{\dot{m}_\alpha}{\dot{m}_{\text{total}}},$$ (3.4)

where

$$\dot{m}_{\text{total}} = \dot{m}_L + \dot{m}_G.$$ (3.5)

Therefore, the liquid and the gas mass fractions can be calculated by

$$M_L = \frac{\dot{m}_L}{\dot{m}_{\text{total}}} = \frac{S_L^{\text{well}} \varrho_L}{S_L^{\text{well}} \varrho_L + S_G^{\text{well}} \varrho_G}$$ (3.6)

and

$$M_G = \frac{\dot{m}_G}{\dot{m}_{\text{total}}} = \frac{S_G^{\text{well}} \varrho_G}{S_L^{\text{well}} \varrho_L + S_G^{\text{well}} \varrho_G}$$ (3.7)

respectively, where, $\varrho_L \text{ and } \varrho_G$ are the densities [kg/m³] of the liquid and gas phases, respectively. For the evaluation of flow conditions in the borehole, the superficial velocities of the fluid phases, $U_{S,\alpha}$ [m/s], are required. These can be calculated from the information regarding the fluid influx into the well,

$$U_{S,\alpha} = \frac{Q_\alpha}{A} = \frac{\dot{m}_\alpha}{\varrho_\alpha A}, \tag{3.8}$$

where Q_α [m³/s] is the volumetric flowrate of Phase α and A [m²] is the cross-sectional area.

3.2.2 **Determining the two-phase flow regimes in the production well**

The specific two-phase (CO_2 and water) flow regime in a vertical CPG production well is determined by the velocity and the relative amounts of the fluid phases in the production well. The four basic flow regimes in a vertical well (Figure 3.3) occur in a progression displaying an increasing gas flow rate for any fixed rate of liquid flow. For *bubble flow*, the well is almost completely filled with liquid. The free gas phase is more or less uniformly distributed as discrete small bubbles within the continuous liquid phase. The flow transitions to a *slug flow* regime when these small gas bubbles coalesce into larger bubbles that eventually fill the entire pipe cross-section. Slugs of liquid that contain smaller bubbles of entrained gas also form between the large gas bubbles (Sun et al., 2002). As the gas mass flowrate increases, the larger gas bubbles become unstable and collapse, which results in a highly turbulent *churn flow* pattern (Lea et al., 2008). *Annular flow* occurs at high gas flowrate (velocity). The gas flows upward in the center of the well as a continuous phase, and any liquid in the well is carried upwards, entrained in the gas as liquid droplets or a mist. If the gas flowrate is not high enough, the droplets fall, accumulate at the bottom of the well, and the flow regime transitions to a slug/churn flow pattern. Aside from pure gas flow (no liquid is present), annular flow is the desired flow regime for CPG, since it means that the volume fraction (saturation) of CO_2 in the production well is high and the pressure gradient in the production well is relatively low.

We adopt the models of Taitel et al. (Taitel et al., 1980) for determining the steady-state two-phase upward flow regimes in vertical pipes for our CO_2-water system of fluids. Tatei's model gives distinctive flow-pattern transitions for the four flow regimes that can exist in a vertical pipe. The two-phase flow regime of the CO_2 and water in the production well depends on the flowrates, the fluid properties, and the cross-sectional area of the well. We plot the transition boundaries between three basic CO_2-water flow regimes, i.e. bubble, slug/churn, and annular flow in Figure 3.4.
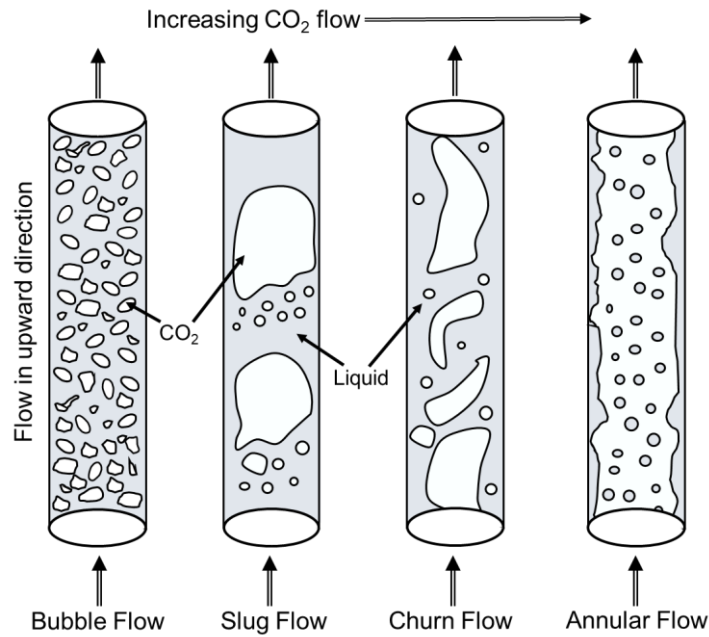
Figure 3.3: Two-phase (gas, approximated by supercritical CO_2, and liquid, represented by water or brine here) flow regimes in a vertical production well (modified from Yadigaroglu et al., 2018).
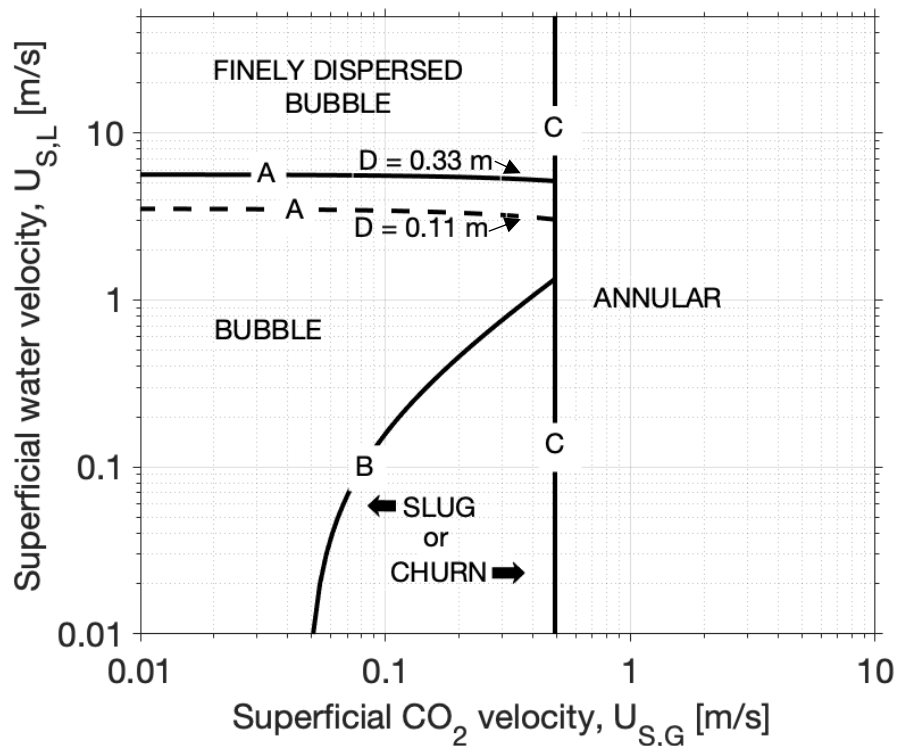
Figure 3.4: Flow pattern regimes for vertical production well examples with 0.11 m and 0.33 m pipe diameters, Dw, for the fluid (brine and CO2) properties, given by our base-case reservoir conditions of 100 °C, 25 MPa, and 0.15 salinity. Note that only the transition boundary between "finely dispersed bubbles" to "bubbles" depends on the production well pipe diameter.

Figure 3.5 is a semi-log plot of total mass flowrate against the CO_2 mass fraction. The figure shows the flow-pattern transitions for this study's base-case fluid properties (see Table 3.1) and a relatively large well pipe diameter of 0.33 m. The calculations are carried out using the conditions near the inlet of the production well. We consider this to be the area with the highest

amount of water by volume because, as the fluids rise in the well, the fluid pressure decreases, leading to a significantly greater expansion of the supercritical/gaseous CO_2 than the liquid water and hence a reduction of the volume fraction of water. Hence, we expect the bottom of the well to have the highest volume fraction of free-phase liquid water that originally entered through the well screen. The exsolution of water from CO_2 can take place during the ascent of CO_2, that originally contained dissolved water, towards the production wellhead (Fleming et al., 2020), however, we ignore this likely minor addition of free-phase liquid water here.
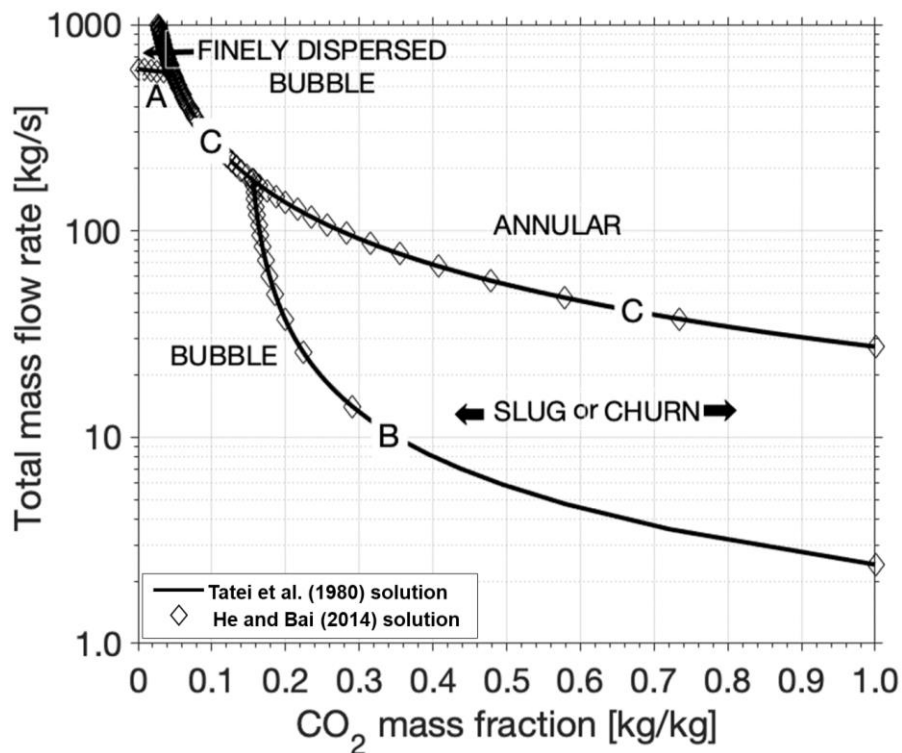
Figure 3.5: Flow pattern regimes, denoted by total mass flowrate (of CO_2 and brine with 0.15 salinity) and the mass fraction of CO_2 under our base case conditions of 100 °C and 25 MPa, with a production well pipe diameter of 0.33 m.

In Figure 3.5, the solid curves are results obtained by using the flow pattern transition equations from Taitel et al. (Taitel et al., 1980), while the diamond points are the results obtained by using the equations from He and Bai (He and Bai, 2014). The interfacial tension between CO_2 and brine is calculated to be approximately 0.033 mN/m (Bachu and Brant Bennion, 2009). The transition curves change significantly with the well pipe diameter. The smaller the well pipe diameter, the lower the minimum flowrate required to achieve annular flow. When the pipe diameter is reduced from 0.33 m (Figure 3.5) to 0.11 m the minimum CO_2 flowrate (at 99.9% CO_2 mass fraction), required to achieve annular flow, significantly decreases from 25 kg/s to 3 kg/s. For the case of 100% (pure) CO_2 (in practice, there is almost always some amount of water), there should be a discontinuity in the plots as pure CO_2 does not have a minimum flowrate.

3.2.3 **Subsurface flow model**

We set up a generic three-dimensional, homogeneous, axisymmetric geothermal reservoir model comprising a brine-saturated aquifer formation with an anticlinal (dome-shaped) structure (Figure 3.6). The model's geometry and well configuration is similar to the one used in a previous study (Ezekiel et al., 2020). The aquifer formation is bounded by impermeable bedrock and caprock formations. The properties of the geothermal reservoir model are given in Table 3.1. This reservoir model serves as an initial, conceptual, small-scale system (which is scalable) having only 4 production wells.
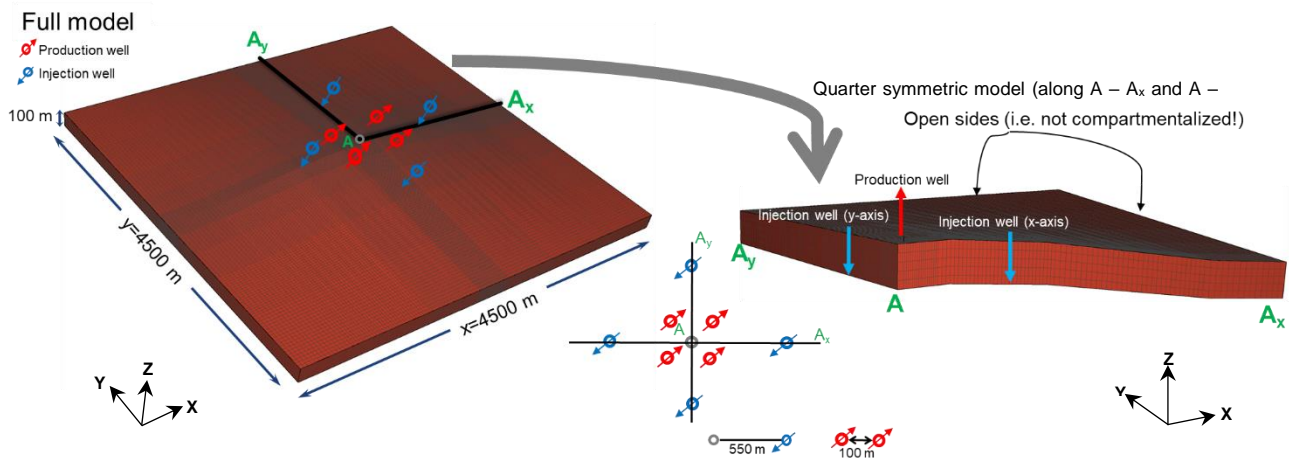
Figure 3.6: The full model (left) and the symmetric quarter model (right), showing the location of the production and injection wells. Note that the overlying, impermeable caprock is not shown. For the base case model, all the sides of the model are open (i.e. the reservoir is not compartmentalized). The injection (blue) to production (red) well distance is 500 m.

The numerical reservoir simulator employed in this study is TOUGH2 (Pruess et al., 2012) with the fluid property module "ECO2N" to provide fluid properties for water and sub/supercritical CO_2 (Pruess and Spycher, 2007). The pressure at the bottom of the well (screened interval), which is a function of the wellbore flowrate, is determined using the Thiem approximation (Coats, 1977; Pruess et al., 2012).

In this study, the numerical simulation consists of two stages. The first stage is called the CO_2 plume establishment (PE) stage. During this first stage, CO_2 is injected into the reservoir, displaces brine and develops the CO_2 plume. This stage is crucial since a sufficient amount of CO_2 in the reservoir is necessary to minimize water upconing at the production well once production commences. During the PE stage, the production wells are shut in and CO_2 is injected at a fixed rate of 30 kg/s/well. Based on a semi-analytical model to estimate power output as a function of flowrate (shown in Figure A.1 in the Appendix), this flowrate is close to the optimum in terms of power. For the base case model, the PE stage is complete when the CO_2 plume (at the production well region) has achieved a pore-space CO_2 saturation of 55%.

Table 3.1: Parameters for the base case reservoir model

Parameter	Value
Reservoir size (km x km x km)	4.5 x 4.5 x 0.1
Depth (km)	2.5
Porosity (-)	0.20
Horizontal permeability, k_h (m^2)	10^{-13} (100 mD)
Thickness (m)	100
Reservoir initial pressure (Pa)	Hydrostatic (25 MPa at the top of the reservoir)
Reservoir initial temperature (°C)	100
Initial CO_2 mass fraction	0.025 (dissolved in brine)
Residual CO_2 saturation (-)	0.10
Residual brine saturation (-)	0.25
van Genuchten parameters α (Pa), m (-)	3×10^3, 0.77
Native brine NaCl saturation (ppm)	150,000
Mol. diffusivity in gas; in water (m^2/s)	10^{-5}; 10^{-10}
Rock grain density (kg/m^3)	2650
Thermal conductivity λ_{wet}, λ_{dry} (W/m/°C) *	2.51, 1.6
Rock specific heat capacity (J/kg/°C)	1000
Geothermal gradient (°C/km)	34
Rock compressibility (1/Pa)	10^{-10}
CO_2 injection enthalpy (J/kg) **	2.4×10^5
Injection-production well distance (m)	~500
Lateral boundary conditions of the reservoir	Hydrostatic pressure; 100°C (Dirichlet boundary conditions).
Top and bottom boundary conditions of the reservoir	No fluid flow and no heat flux.
Initial conditions	Hydrostatic equilibrium, no heat flow, pore space entirely occupied by brine.

*λ_{wet} and λ_{dry} are formation heat conductivity under fully water-saturated and fully gas-saturated conditions, respectively. Here, Somerton's interpolation formula for heat conductivity, λ, as a function of water saturation, S_L, is used, i.e. $\lambda(S_L) = \lambda_{dry} + \left(S_L^{0.5}\left[\lambda_{wet} - \lambda_{dry}\right]\right)$ (Somerton, 1992).

**Given the average pressure and temperature of CO_2 at the injection wellhead, determined from the power plant model in Section 3.2.5 (15 °C, 5.6 MPa), the CO_2 enthalpy at the bottom-hole is estimated using the wellbore model described in Section 3.2.4.

Once the CO_2 saturation around the production well reaches 55%, the CPG stage begins. During this stage, the production wells are open, and a maximum fluid extraction rate at the production well is set. However, the pressure decrease (at the production well downhole element), due to production, is not allowed to fall below 7 MPa, as compared to the initial reservoir fluid pressure. This results in flowrates that are initially low, but gradually increase over several days until the maximum is attained. To determine the base case model maximum or optimal flowrate to set, we use a simplified power-mass-flowrate model, without heat loss considerations (Adams et al., 2015), described in the Appendix B.1. The peak of the total production mass flowrate for power generation is estimated to be 130 kg/s (using 4 injection-production well pairs with the base-case well pipe diameters of 0.21 m) for the reservoir model

considered in this study. Considering heat loss, we assume that the optimal power output will decrease, which will in turn, decrease the optimal (peak) total production mass flowrate. Hence, the chosen value for the base case model is 120 kg/s (i.e. 30 kg/s/well). This value will be varied in Section 3.3.3.1. For this study, the simulation of the CPG stage is set to run for about 40 years in total, which is within the lifespan of power plants. Here, the geothermally heated CO_2 (and potentially some liquid water or brine) is produced. At the land surface the geothermally heated CO_2 (and possibly some water/brine if not yet removed) is run through a turbine to generate electric power. Thereafter, the CO_2 is cooled/condensed and reinjected into the original reservoir. Any produced water/brine is removed, using a water-CO_2 separator, before the cooled CO_2 is reinjected into the reservoir.

3.2.4 Wellbore heat-transfer model

In this study, we implement a simple one-dimensional (1D) vertical wellbore model to determine the final temperature and pressure of the produced fluid at the production wellhead. The bottom-hole boundary conditions are defined as the reservoir pressure, temperature, total mass flowrate of the fluid at any given time during fluid production. The pressure, temperature, total mass flowrate of the fluids, and the CO_2 volume fraction of the produced fluid, as it enters the production well through the well screen, are the input values for the wellbore model calculation as presented in Figure 3.1. Brine property values are determined from the relationships provided by Haas et al. (Haas, 1976) and Phillips et al. (Phillips et al., 1981) for density and viscosity calculations, respectively.
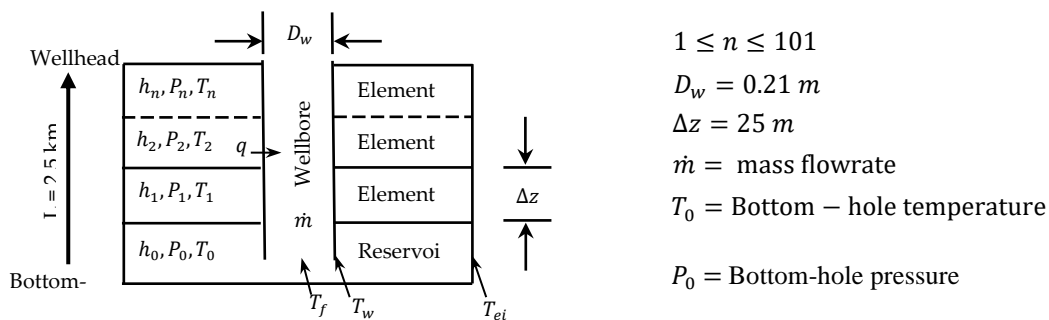
Figure 3.7: Schematic of the one-dimensional well model (not to scale), where h, P, and T are the enthalpy, pressure, and temperature, respectively, at each of the 25m-long elements (for the base-case model) and q is the heat transfer function of the wellbore model.

We set up a vertical production well (2500 m long), which is divided into 100 equal elements (Figure 3.7). We develop the model in MATLAB using the CoolProp-MATLAB wrapper (Bell et al., 2014) for the iterative calculation of the thermodynamic properties of the fluid components, using the standard equations of state (Bell et al., 2014; Bell and Jäger, 2016). Conservation of mass equations, as presented in Equations (3.9) to (3.12) (Adams et al., 2015;

Atrens et al., 2009) are used to numerically calculate the fluid state in the production well across each 25m-long vertical well element (Δz), as the fluid flows up inside the well as shown in Figure 3.7. The subscript i denotes the element number, which goes from 0 to n (n in this case is 101) as shown in Figure 3.7. The well segments are considered adiabatic but not isenthalpic (Adams et al., 2015; Randolph et al., 2012). This results in

$$h_{i-1} + \frac{U_{S,G_{i-1}}^2}{2} + g\Delta z_{i-1} = h_i + \frac{U_{S,G_i}^2}{2} + g\Delta z_i \,, \tag{3.9}$$

$$P_{i-1} + \frac{\varrho_{i-1} U_{S,G_{i-1}}^2}{2} + \varrho_{i-1} g\Delta z_{i-1} = P_i + \frac{\varrho_i U_{S,G_i}^2}{2} + \varrho_i g\Delta z_i - \Delta P_{loss} \,, \tag{3.10}$$

where

$$\Delta P_{loss} = f \frac{\varrho U_{S,G}^2 \Delta z}{2 D_w} = f \frac{8 \dot{m}^2 \Delta z}{\pi^2 \varrho D_w^5} \tag{3.11}$$

and

$$\dot{m} = \varrho_{i-1} A U_{S,G_{i-1}} = \varrho_i A U_{S,G_i} \,. \tag{3.12}$$

The frictional factor, f, employed in the well model, is calculated using the Moody Chart and is dependent on the inner pipe diameter of the well, the pipe surface roughness and the velocity of the fluid, through the Reynolds Number (Moody and Princeton, 1944). In this study, we assume that the production well is made of stainless steel pipes, such as Bare CR13 well piping (used in corrosive environments), with a surface roughness of 55×10^{-6} m (Adams et al., 2015; Farshad and Rieke, 2006).

Usually, the fluid in the well gains heat through fluid convection and loses or gains heat to the surroundings through conduction. Heat loss to, or gain from, the surroundings by the wellbore fluid depends on the formation temperature distribution around the wellbore and the differences between the temperature of the wall of the wellbore (i.e. the wellbore/formation interface) and the formation temperature. The conductive heat exchange between the wellbore and the surrounding formation is calculated using the method proposed by Zhang et al. (Zhang et al., 2011). To keep our wellbore heat-transfer calculations simple, we make the following assumptions: (i) the thermal resistances between the cased well and the formation is negligible because of the high conductivity of casing metals, and (ii) vertical conductive heat flow within the formation is negligible (Zhang et al., 2011). The convective heat transfer function for each well element is determined using the Nusselt Number. We neglect convective heat transfer outside the wellbore because of the relatively low-permeability, overlying caprocks (Randolph et al., 2012). The effects of heat advection by groundwater in permeable overburden units on the heat transfer coefficient is not included here. Therefore, to include

conservation of energy in the wellbore model, using the heat transfer functions, the enthalpy at the end of the element becomes

$$h_i + \frac{U_{S,G_i}^2}{2} + g\Delta z_i = h_{i-1} + \frac{U_{S,G_{i-1}}^2}{2} + g\Delta z_{i-1} - \left[(\pi\Delta z D_w)\,{}^q\!/_{\dot{m}}\right]. \tag{3.13}$$

To account for the decrease in enthalpy as the fluid moves up inside the production well, the energy conservation equation, as shown in Equation (3.13), is applied to the wellbore model. For simplicity, we calculate the enthalpy for only the CO_2 phase, while assuming the liquid phase has negligible influence. However, a simplified method of averaging the enthalpies of CO_2 and water to calculate the enthalpy of a two-phase CO_2/water mixture in the production well has been presented by Fleming et al. (Fleming et al., 2020).

Table 3.2: Parameters for wellbore and power plant models.

Parameters	Base case values
Well length (m)	2500
Well pipe diameter (m)	0.21
Wellbore flowing bottom-hole pressure (MPa)*	18
Productivity index (m³/s/Pas)**	3.89×10^{-12}
Fluid components	CO_2 and Brine
Mean formation thermal conductivity (W/m°C)	2.51
Mean formation density (kg/m³)	2650
Mean formation specific heat capacity (J/kg °C)	1000
Well pipe material and surface roughness, (m)	Bare CR13; 55 x 10^{-6} (Adams et al., 2015; Farshad and Rieke, 2006)
Power systems	Direct CO_2 system – no pumping requirement; fluid – >90% CO_2 mass fraction Direct CO_2 system – pumping required when <90% CO_2 mass fraction
Direct turbine isentropic efficiency	0.78
Condensing or cooling tower approach temperature (°C)	7
CO_2 injection temperature at surface (°C)	22

* The wellbore flowing bottom-hole pressure, P_{wb}, is fixed at 18 MPa (for the base case) and the flowrate increases according to the set productivity index. At the maximum flowrate (fixed at 30 kg/s/well for the base case), P_{wb} varies and is calculated by $q_\alpha = \frac{k_{r\alpha}}{\mu_\alpha}\rho_\alpha \cdot PI \cdot (P_\alpha - P_{wb})$ (Pruess et al., 2012).

** The productivity index (PI) is calculated as $PI = \frac{2\pi k dz}{\ln(r_e/r_w)-1/2}$ (Pruess et al., 2012). The perforation layer thickness is 20 m, the well radius, r_w, is 0.105 m, the grid block area is 100 m² and the skin influence is neglected.

The wellbore model provides the approximate values of the temperature and pressure of the produced fluid (in this case, only the CO_2 phase) as it reaches the wellhead, which also serve as the input values for calculating the enthalpy of the produced CO_2 phase, used for power

generation calculations. The wellbore and power plant model parameters used for this study are presented in Table 3.2.

3.2.5 **Power system model**

The direct-CO_2 CPG system can be modeled in at least two ways: as a direct-CO_2 thermosiphon-only or as a direct-CO_2 pumped cycle (Figure 3.8), where the latter may yield somewhat more net power, however, this effect is typically not pronounced (Adams et al., 2015, 2014). Therefore, we model the simpler direct-CO_2 thermosiphon-only CPG system, employing the analysis presented in Adams et al. (Adams et al., 2015). As no pump or compressor is used in a thermosiphon-only CPG system, the flow of CO_2 is entirely generated by the CO_2 density difference between the injection and production wells (Adams et al., 2014).
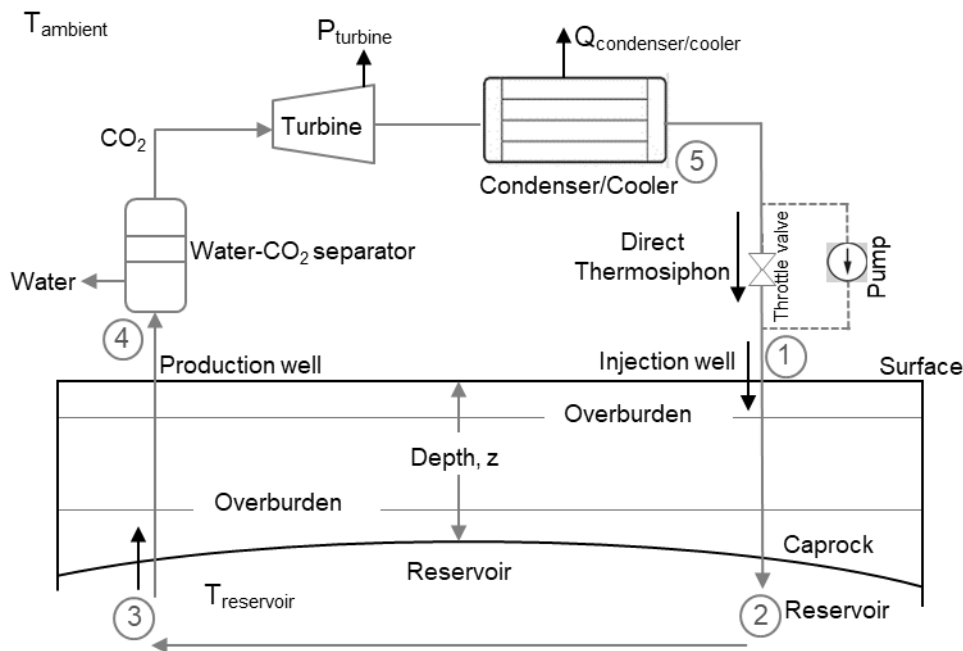
Figure 3.8: An illustration of a possible implementation of a simplified direct-CO_2 CPG system (Adams et al., 2015), showing the thermosiphon and/or pumped (with throttle valve) systems in an anticlinal reservoir CPG system in a deep saline aquifer.

An illustration of the implementation of the direct CO_2 thermosiphon power system is shown in Figure 3.8**.** The numbers (1-5) represent the CO_2 state points as the CO_2 moves through the reservoir, the wellbores and the power plant. At State 1, liquid CO_2 is injected into the reservoir, flowing down inside the injection well to State 2, transitioning to a supercritical fluid along the way. The injected CO_2 heats up to the reservoir temperature as it moves through the reservoir from State 2 to State 3. The CO_2 is under hydrostatic pressure when it reaches the production well at State 3. The heated CO_2 rises through the production well to State 4 (at the land surface), losing some heat and pressure (enthalpy) due to frictional losses, pressure losses and heat lost to the surrounding rock formation, as discussed in Section 3.2.4. Once the CO_2 reaches the land

surface, the supercritical/gaseous CO_2 component of the produced fluid is separated from the liquid water (or brine) in a water-CO_2 separator (this separation may alternatively occur after the turbine to maintain high mass flowrates through the turbine (Fleming et al., 2020). The separated CO_2 is expanded and cooled through a two-phase turbine and further cooled and condensed isobarically through the cooling and condensing towers at the land surface, reaching State 5. The CO_2 then returns to State 1, completing the heat engine power cycle.

The power output of the turbine, P_t [W$_e$], for the direct-CO_2 system, is calculated as the product of the CO_2 mass flowrate, $X_{CO2} \cdot \dot{m}$, and the difference between the turbine inlet, h_{in}, and outlet, h_{out}, enthalpies of the fluid (Equation 3.14), where the outlet enthalpy is calculated using an isentropic turbine efficiency of $\eta_{ie} = 78\%$ (Ezekiel et al., 2020),

$$P_t = X_{CO2} \cdot \dot{m} \cdot (h_{in} - h_{out}).$$
(3.14)

The net power, P_{net} [W$_e$], generated by the direct system is then defined by

$$P_{net} = P_t - P_{co} - P_{pump} \, ,$$
(3.15)

where P_{co} and P_{pump} are the parasitic cooling/condensing power and pump power, respectively, required to operate the power plant, where $P_{pump} = 0$ for the thermosiphon-only CPG system considered here. The heat extraction rates of the cooling/condensing towers are equal to the products of the CO_2 mass flowrate and the difference between the fluid enthalpies at the inlet, $h_{in,c}$, and outlet, $h_{out,c}$, of the condenser. Equation (3.16) provides the parasitic power requirements of the cooling/condensing towers, where the parasitic load fraction, i.e. the ratio of the parasitic energy load [kW$_e$] to the heat-rejection energy [kW$_{th}$], is set to $\lambda_p = 0.03$ (details are provided in Section 2 of the Supplemental Information in Adams et al. (Adams et al., 2015)),

$$P_{co} = X_{CO2} \cdot \dot{m} \cdot \left(h_{in,c} - h_{out,c} \right) \cdot \lambda_p.$$
(3.16)

As part of the base case parameters used in this study, the temperature and pressure of the cooled and condensed CO_2 at the CO_2 reinjection wellhead is considered to be 22 °C (i.e. an approach temperature of 7 °C + an ambient temperature of 15 °C) and 5.6 MPa, respectively. The subsurface conditions at which the CO_2 is reinjected into the reservoir are $P = 25$ MPa, $T = 100$ °C. These conditions are accounted for by a mass- and enthalpy-flux boundary condition in the subsurface fluid flow model.

3.3 Results

3.3.1 Calculating the CO₂ saturation in the well

Determining the CO_2 saturation (i.e. volume fraction) in the well is important for the characterization of the fluid flow regime existing at the bottom of the production well at any given time. Figure 3.9 shows the results of the CO_2 saturation in the well for the base case model (Table 3.3) used for this study and five different models of published CO_2-based geothermal energy extraction and/or CO_2 storage studies in deep aquifer systems. Their respective reservoir and fluid parameters are shown in Table 3.3. The complete equations for calculating the density and dynamic viscosity of the brine solutions, using the respective Haas (Haas, 1976) and Phillips et al. (Phillips et al., 1981) correlations.

One can see from that, owing to its low viscosity, compared to brine, at typical CPG reservoir conditions, the flux of CO_2 into the well is significantly higher than that of water when the CO_2 saturation in the reservoir pore space, surrounding the production well inlet, is greater than about 0.30 for all cases. For example, for our base case, a CO_2 reservoir pore space saturation of about 55% yields a CO_2 saturation of >98.0% in the production well.

The differences between the various cases shown in stem primarily from differences in the relative permeability–saturation constitutive relationships used in each case (van Genuchten or Brooks-Corey parameters in Table 3.3) and the residual water saturation values. Hence, the higher the residual water saturation and the more homogenous the pore-size distribution in the reservoir pore space, the greater is the CO_2 volume fraction (and mass fraction) in the well. The effect of temperature, pressure, and salinity also contribute to this effect, but to a lesser degree.

Table 3.3: Reservoir parameters of selected CO_2-based geothermal and/or CO_2 storage models. Here, S is the water salinity, S_r is residual saturation, m is the van Genuchten parameter, k_r is relative permeability, and n is the Brooks-Corey pore-size-distribution index for the gas (G) and the liquid (L) phases. (Garapati et al., 2015; Guyant et al., 2015; Levy et al., 2018; Zhang et al., 2016; Delshad et al., 2013).

Model	T (°C)	P (MPa)	S (-)	S_{Lr}	S_{Gr}	van-Genuchten m	Brooks-Corey k_{rG} max	k_{rL} max	n_L	n_G
Garapati et al. (2015)	100	25	0.2000	0.30	0.05	0.46				
Aquistore model (Guyant et al (2015))	100	35	0.2500	0.40	0.10	0.70				
Levy et al. (2018)	225	22.5	0.0001	0.05	0.01	0.65				
Zhang et al. (2016)	150	35	0.1015	0.30	0.05		1.0	0.35	6.0	2.0
Cranfield model (Delshad et al. (2013))	125	32	0.1500	0.40	0.05		0.8	1.00	4.2	2.6
Base case	100	25	0.1500	0.25	0.10	0.77				
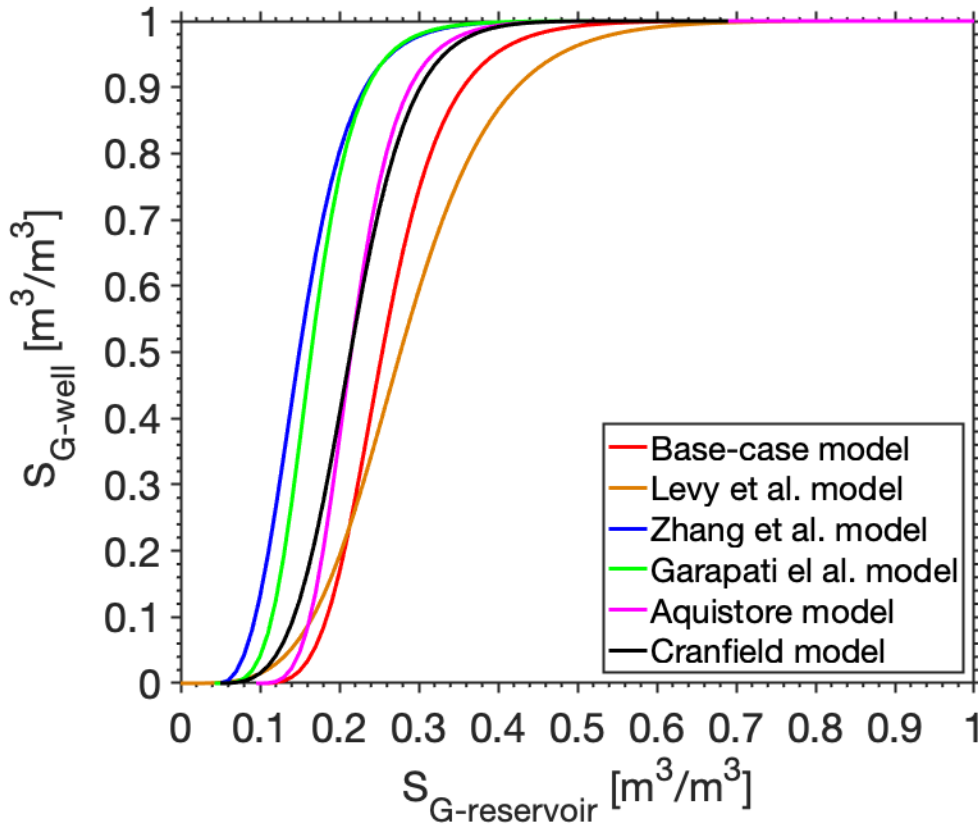
Figure 3.9:The calculated CO_2 volume saturation in the production well for a given CO_2 reservoir saturation in the pore space surrounding the production well for different published reservoir models, i.e. the base-case model (this paper), Levy et al. model (Levy et al., 2018), Zhang et al. model (Zhang et al., 2016), Garapati et al. model (Garapati et al., 2015), Aquistore model (Guyant et al., 2015), and Cranfield model (Delshad et al., 2013).

3.3.2 **Base-case simulation results**

Using the base case parameters, listed in Table 3.1 (representing a typical CPG reservoir initially filled with brine), where the injection-to-production well distance in the reservoir is, with 500 m, quite large, the CO_2 plume establishment stage (i.e. until a saturation of $S_G = 55.0\%$ exists in the pore space around the production well inlet) requires about 4 years and requires a total of 15.5 Mtons of CO_2 injected through the four injection wells. Figure 3.10a shows the CO_2 gas saturation in the reservoir at the end of the CO_2 plume establishment stage (just before the start of the CPG stage).

Figure 3.11a shows that when the production well is opened (at time $= t_0$), the CO_2 saturation around the production well decreases from 55.0% to the lowest value of 32.0% because of the water upconing effect (see Section 3.2.1). This time of lowest CO_2 saturation in the reservoir's pore space around the inlet of the production wells is referred to in this study as the critical time, t_{crit}. Afterwards, the pore-space CO_2 saturations around the production well inlets begin to increase. After 40 years of fluid production (i.e. the end of the CPG stage which is represented by t_{end}), the pore-space CO_2 saturations around the production well inlets reach 47.5%. The CO_2 saturation in the reservoir at the end of the 40 years (CPG stage) is shown in
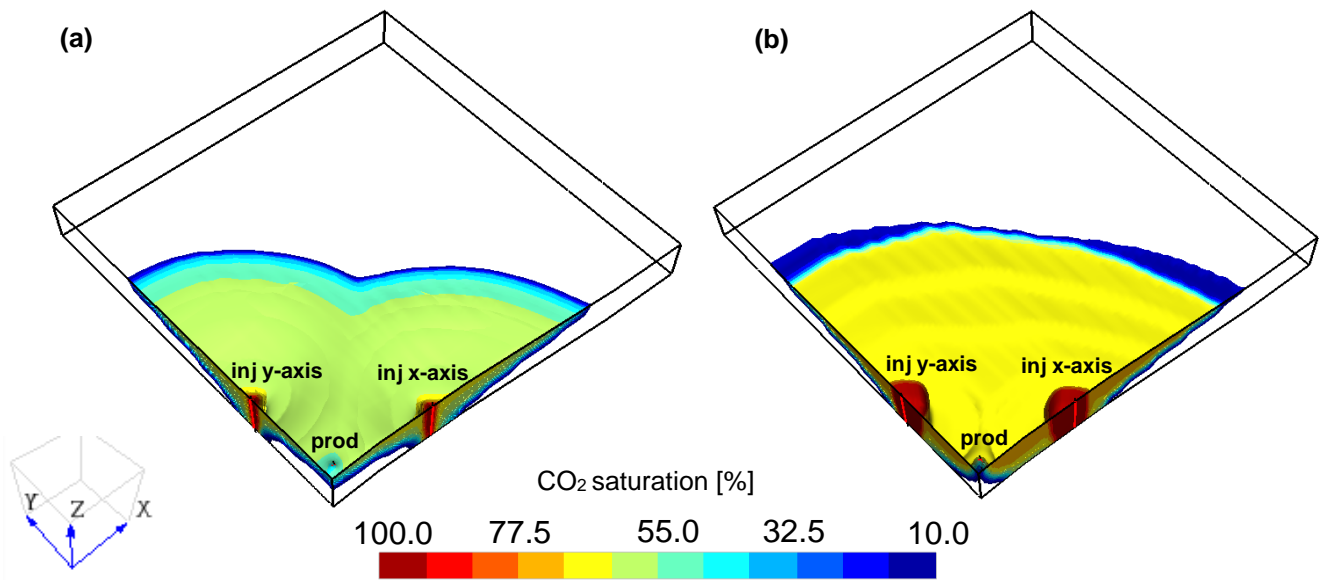
Figure 3.10: Quarter (base case) model showing the CO_2 saturation in the pore space before (a) and after (b) the CPG stage. Note that the part of the models with CO_2 saturations less than $S_{Gr} = 0.1$ has been blanked.

Figure 3.10b. Figure 11a also shows that the flowrate reaches the maximum flowrate of 30 kg/s/well after 5.5 years of CO_2 production. Figure 3.11b shows that the mass fraction of CO_2 entering the production well decreases from 0.99 to 0.61. This lowest value of 0.61 corresponds to the time t_{crit}, and the CO_2 saturation around the production well is at the lowest value. The mass fraction of CO_2 and the production mass flowrate at t_{crit} is represented as X_{crit} and $\dot{m}_{crit}$, respectively. It can be observed (Figure 3.11b) that the conditions in the wellbore never reach the slug/churn transition line. Hence, the fluid flows in the (desired) annular flow regime throughout the simulated 40 years. At the end of the CPG stage, the cool CO_2 front arrived at the location of the production well (Figure 3.12).

The total net power generated for the base case decreases from 0.40 MW_e at the start of fluid production and circulation during the CPG stage to about 0.30 MW_e at t_{crit}. The net power then increases to a peak value of 0.80 MW_e after 10 years. After this time, thermal breakthrough (large drop in the reservoir temperature) occurs at the production well (Figure 3.12), leading to a steady power decrease down to about 0.40 MW_e at the end of fluid production. The average net power generated is 0.58 MW_e (0.202 GW_e-h in 40 years) for this small-scale example problem (employing only 4 production wells).

Hence, for this base case example, we see in Figure 3.11a that although water enters the well (maximum water saturation at t_{crit}), the flow regime is expected to remain annular all through the simulated period (Figure 3.11b). Reservoir heat depletion starts after 10 years; however, the reservoir continues to provide more than 70% of the average net power generated over the entire period considered.
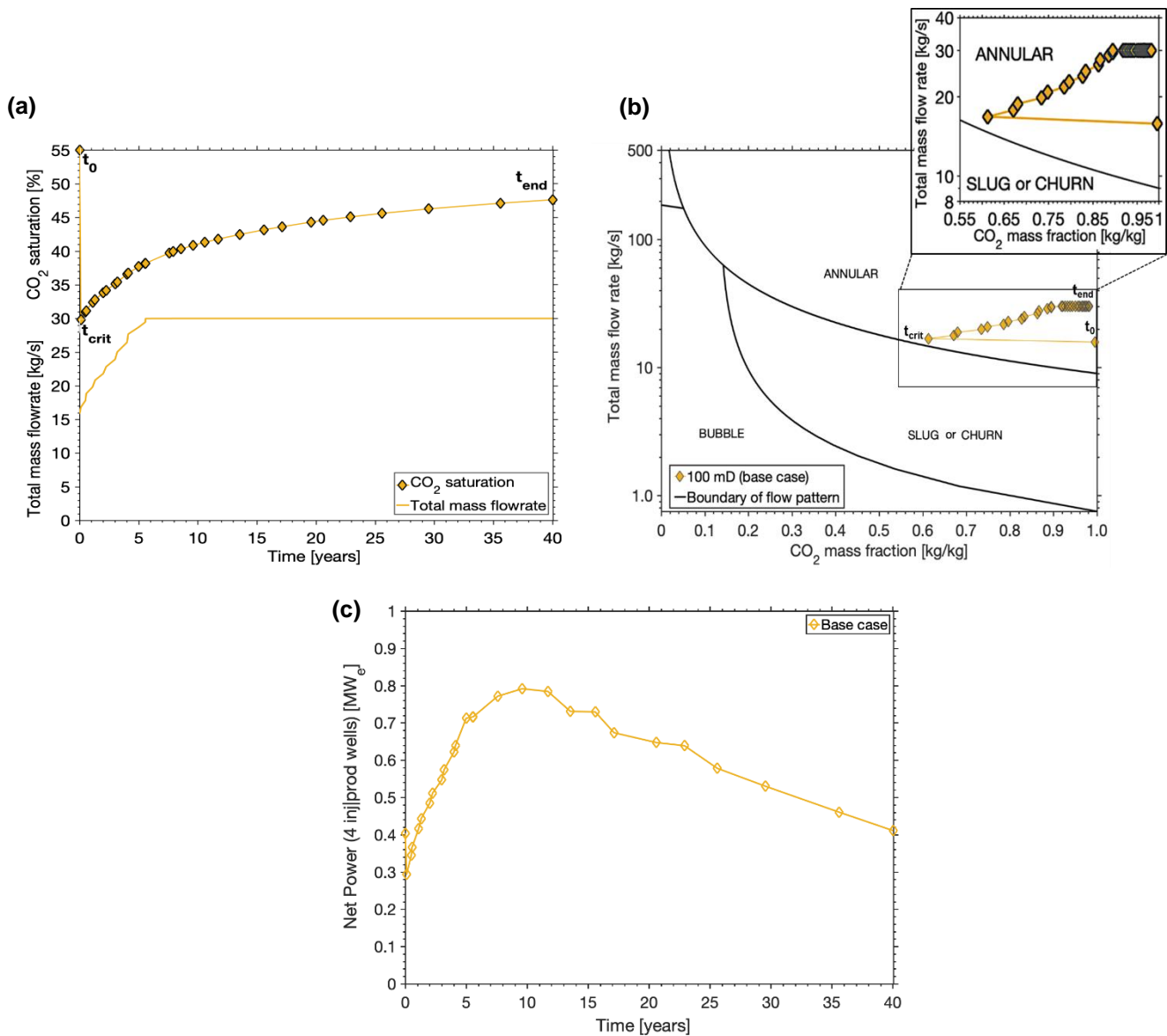
Figure 3.11: CPG simulation results for the base case. (a) Time series of the total fluid mass flowrate and changes in CO_2 saturation in the pore space surrounding the production well inlet, (b) Bottom wellbore flow regimes, determined by the total fluid mass flowrate and CO_2 mass fraction in the production well. The inset figure shows an enlarged region of the plot. (c) Time series of net electric power generation, employing the 4 injection-production well pairs.

3.3.3 Variation of operational parameters

To optimize the overall performance of the system, or minimizing the amount of water entering the production well and maximizing power output, we investigate how the system responds to changes in three operational parameters that must be chosen by the geothermal power plant operator, and compare these results to those of the base case. The three operational parameters are:

  i.   Maximum fluid production rate.
 ii.   Admissible reservoir fluid pressure reduction.
iii.   Production well pipe diameter.

For all cases, the amount of CO_2 injected and the duration of the CO_2 plume-establishment (PE) stage is the same as that for the base case.
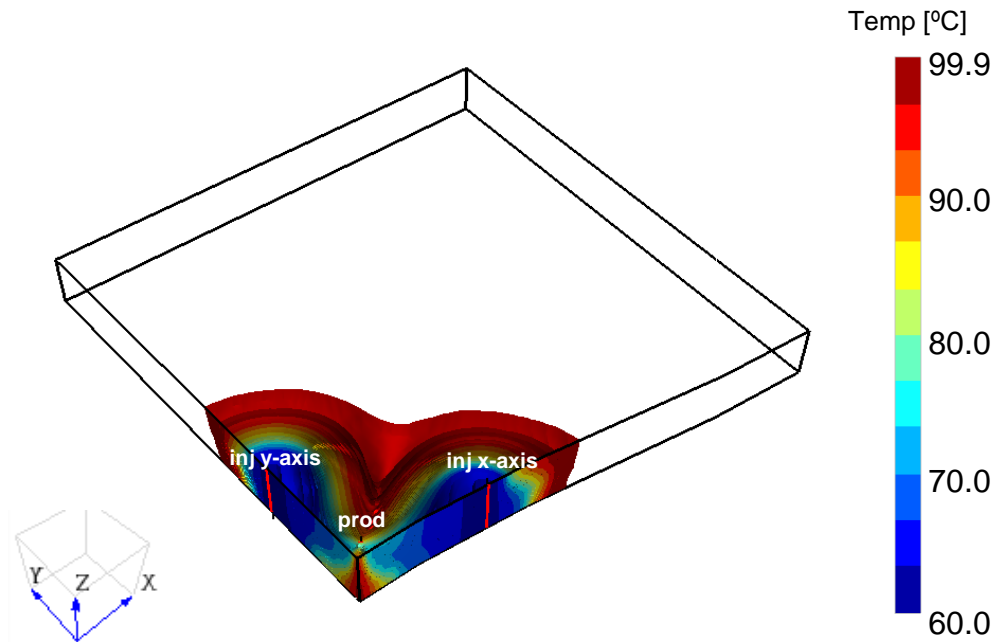
Figure 3.12: Quarter (base case) model, showing the temperature distribution in the reservoir at the end of the CPG stage. Note that the part of the model with the temperature equal to, or greater than, the initial temperature of 100 °C has been blanked.

3.3.3.1 *Maximum fluid production flowrate*

For the first permutation of this sensitivity analysis, the maximum circulation flowrate is varied: 20 kg/s/well, 25 kg/s/well, 30 kg/s/well (base case), 35 kg/s/well, and 40 kg/s/well. In all cases, the respective CO_2 injection rate is held identical to the maximum fluid production flowrate considered. Using the simplified power-mass-flowrate model (Figure B.1 in the Appendix), these maximum circulation flowrates are chosen such that their corresponding power output do not surpass the achievable optimum power output when relatively large well diameters are used. The power-mass-flowrate model (using the largest well diameter of 0.33 m) indicates that below a maximum circulation flowrate of 40 kg/s/well, i.e. equivalent to 160 kg/s, the power output increases with mass flowrate and decreases if the maximum circulation flowrate exceeds 40 kg/s/well.

Figure 3.13a shows that the time required for the system to reach the prescribed maximum fluid production rate increases as the required production flowrate increases. The case with a 20 kg/s/well flowrate takes about 1.27 years, while that with a 40 kg/s/well flowrate takes up to 10.5 years to reach the required flowrate. Also, Figure 3.13a shows an equal decrease in the original CO_2 saturation in the pore space surrounding the production well inlet of 55% to about 30% at the critical time, t_{crit}, for all flowrate cases since they all have the same pressure

drawdown at the start of fluid production. Afterwards, the CO_2 saturation increases with time with the highest flowrate (40 kg/s/well) having the highest CO_2 saturation at the production well at the end of the simulation, t_{end}. This is because the CO_2 saturation in the reservoir increases as the CO_2 injection rate increases.

Note that for the sake of clarity, in Figure 3.13b, we only show the results starting from the critical time, t_{crit}, to the end time, t_{end}, and do not show the results from t_0, as we did for the base case (Figure 3.11b). This is because it is at t_{crit} that we observe the lowest CO_2 mass fraction inside the well, representing the "least favorable" fluid state with the highest likelihood of the fluid flow in the well being in the slug/churn flow regime, most likely to cause liquid loading. Figure 3.13b shows that, for all flowrates considered, and at the prescribed admissible pressure drawdown (7 MPa), annular flow can be maintained inside the well, i.e. liquid loading should not occur.
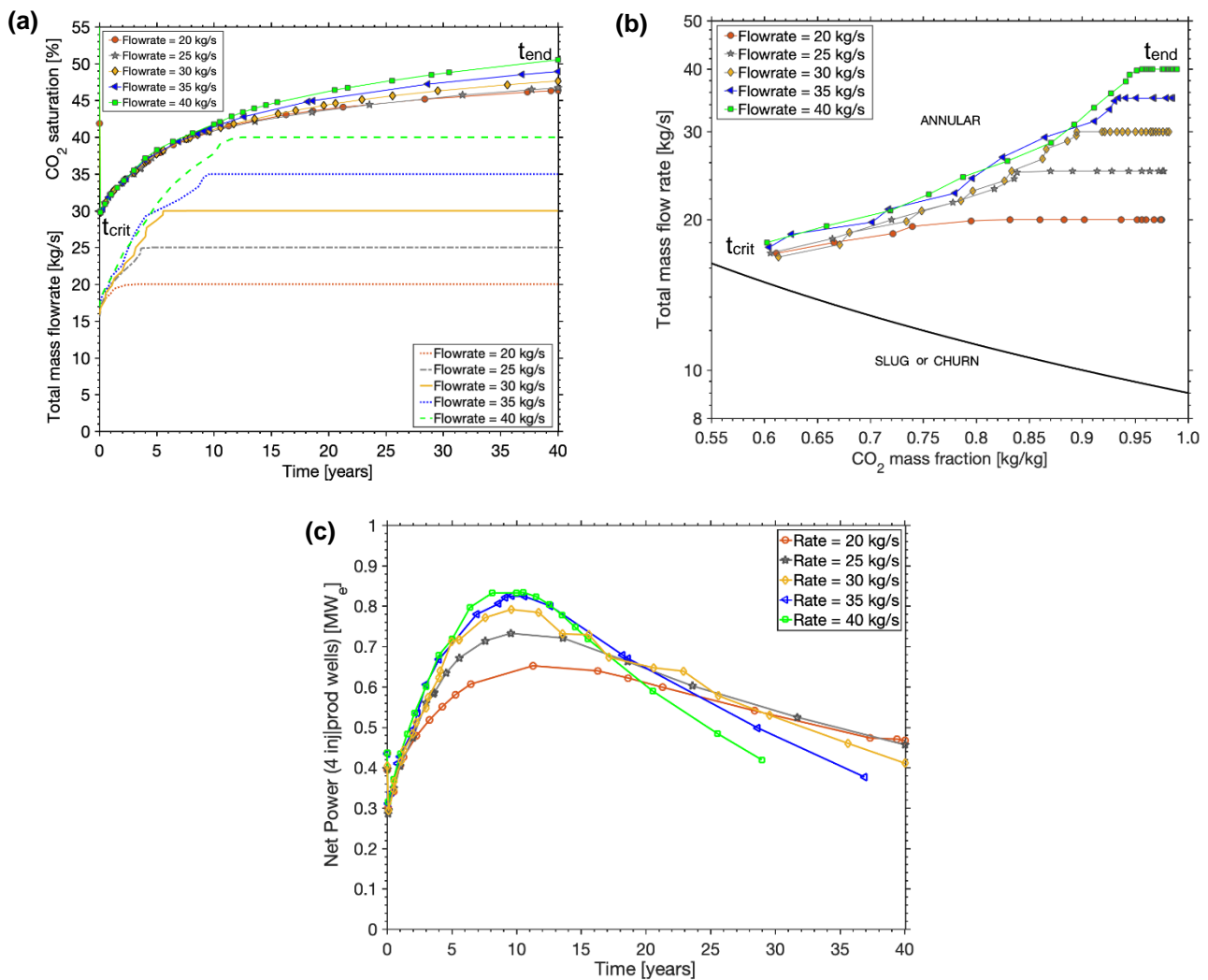
Figure 3.13: CPG simulation results for different maximum fluid production rates per well, showing (a) the time series plot of the total fluid mass flowrate and changes in CO_2 saturation in the pore space around the production well inlet, (b) the bottom wellbore flow regime, and (c) the time series of net electric power generation.

The power generated with time is shown in Figure 13c. We observe that the peak net power generated increases with increasing flowrate. However, after the peak is reached, there is a steeper decline in net power with increasing flowrate. This indicates that the heat depletion rate increases as the flowrate increases. Table 3.4 shows that, for the simulation period considered, the average net power generated increases with the flowrate, regardless of the increasing heat depletion rate. However, due to the high pressure (frictional) loss associated with high flowrates in relatively low-diameter well pipes (in this case 0.21 m), there is a large pressure and temperature drop of the produced CO_2 in the wellbore. At some point in time, the saturation vapor pressure of CO_2 is reached (which the wellbore model cannot handle), causing the wellbore simulation to stop. At this point we assume that CO_2 can no longer be favorably produced. This is observed for the higher flowrates of 35 and 40 kg/s/well as the simulation did not reach the desired 40 years end time (Table 3.4). Hence, even though these two flowrates generated higher average net power than the base case, the average net energy generated is less. This indicates that there is an upper bound to the maximum flowrate when the reservoir is depleted too rapidly. An additional constraint to the optimal flowrate comes from the maximum power that can be generated (Figure B.1). The upper-bound maximum flowrate, using the simple power-mass-flowrate model for a 0.21 m well pipe diameter, is calculated to be 32.5 kg/s/well (i.e. 130 kg/s for all 4 wells).

3.3.3.2 *Admissible reservoir-pressure reduction*

The admissible reduction in reservoir fluid pressure is varied as: 3, 5, 7 (base case), and 9 MPa pressure difference, ΔP, between the lowest pressure in the reservoir and the initial pressure. In a real-field application, this value will have to be chosen so as not to damage the caprock. Acceptable values depend on the structural setting and the caprock type. Figure 3.14a shows that the total fluid (CO_2 and water) mass flowrate increases faster as the pressure difference increases. The case of 9 MPa pressure difference achieves the maximum flowrate of 30 kg/s/well in 2.8 years, compared to the base case pressure difference (7 MPa) example, which takes 5.5 years. For a pressure difference of 3 MPa, the total fluid mass flowrate of 30 kg/s/well is not reached in 40 years.

The CO_2 saturation in the pore space around the production well inlet decreases more strongly with increasing fluid pressure difference (Figure 3.14a). Therefore, care must be taken that the achieved flowrate does not cause significant water upconing and related water flow into the production well that could lead to slug/churn flow in the production well. For a fluid pressure difference of 3 MPa, the maximum fluid mass flowrate is not reached. This implies that CO_2 additions are required during CO_2 injection throughout the 40-year CPG operation in this case.

There are two opposing effects here: lower admissible reservoir pressure reductions lead to less water production but also lead to low initial flowrates in the production well (decreasing

the likelihood for annular flow to occur). The flowrates achieved in the well at early times (t_{crit}) for both the 3 MPa and 5 MPa cases are lower than the critical flowrate needed to maintain annular flow (Figure 3.14b). In those cases, a pump (at the CO_2 injection wellhead – see below) may be necessary to produce the CO_2 during the time the production well is in the slug/churn flow regime. Greater admissible reservoir pressure reductions tend to draw in more water into the production well (which is undesirable), but also result in high flowrates in the production well, necessary to transport the water droplets up and out of the well (Figure 3.14b). This tradeoff should be accounted for when determining the optimal flowrate for a CPG system. It is possible that the chosen flowrate leads to a period of time (especially at early times) during which the flow regime is slug/churn flow. Thus, a pump would be required to maintain the desired flowrate. To note, such a pump or compressor can be installed at the injection well head for pure-CO_2 injection, as discussed at the end of Section 3.4.
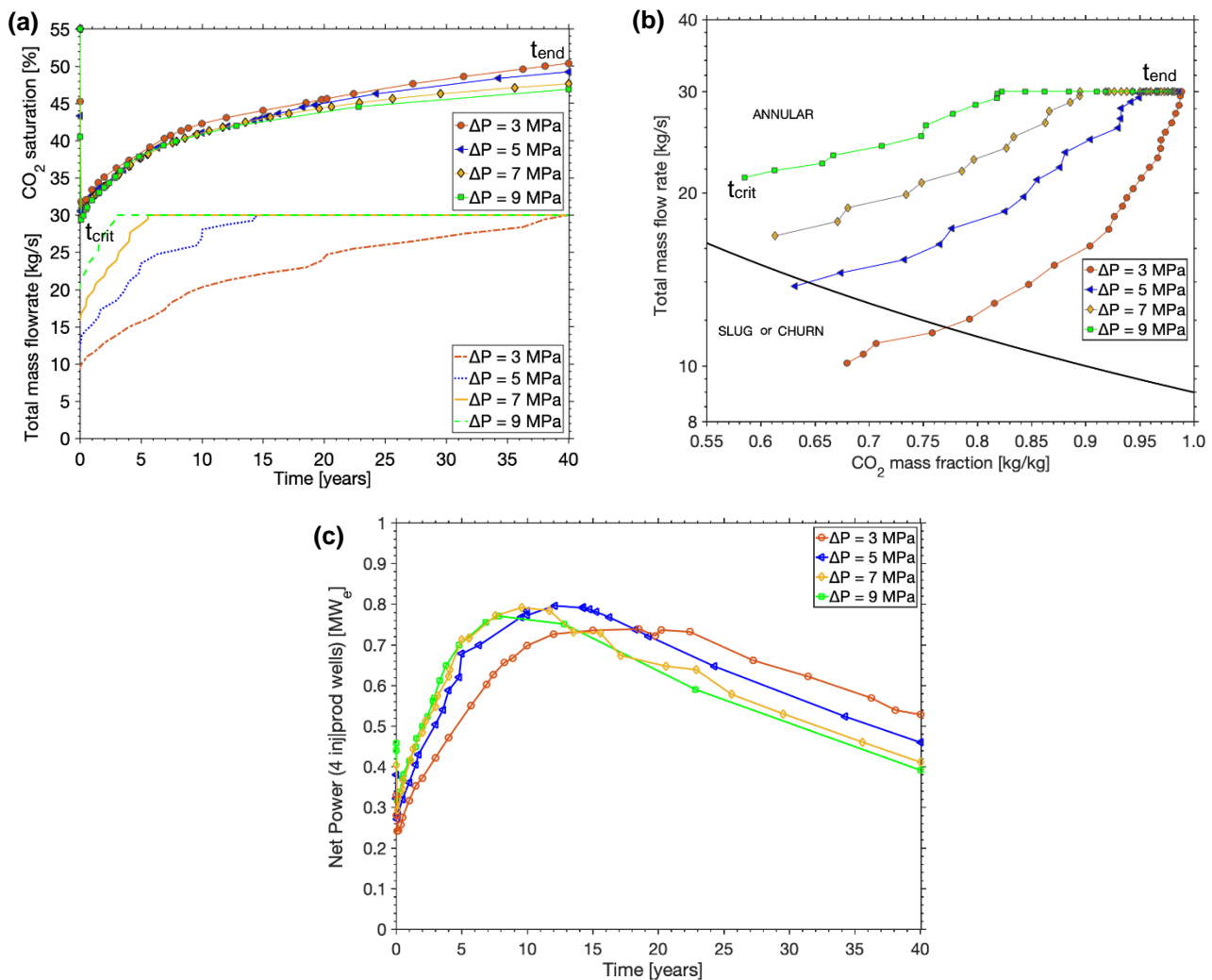
Figure 3.14: CPG simulation results for different admissible pressure differences (drawdowns), showing (a) the time series plot of the total total fluid mass flowrate and changes in CO_2 saturation in the pore space around the production well inlet, (b) the bottom wellbore flow regime, and (c) the time series of the net electric power generation.

The power generation results in Figure 3.14c show that the heat depletion rate increases with ΔP. Note that the parasitic pumping power, which may be required for the two lower ΔP cases, is not accounted for in this study. Thus, the average net power for these two lower ΔP cases may be lower than what is reported in Table 3.4. For the two cases that achieved annular flow all through the 40-year simulations, Table 3.4 shows that the average net power output (and energy generated) for the base case $\Delta P = 7$ MPa is higher than that for $\Delta P = 9$ MPa. Hence, in selecting an optimal ΔP that satisfies all criteria of wellbore flow performance and power generation, the base case $\Delta P = 7$ MPa appears to be the optimal pressure difference for this particular CPG system. Furthermore, an upper limit of the admissible reservoir pressure reduction typically exists, which results from considerations concerning caprock integrity (Vialle et al., 2019).

3.3.3.3 *Production well pipe diameter*

Large production well pipe diameters ensure high fluid flowrates and low heat losses to the surrounding rock formation during fluid ascent. However, small pipe diameters result in higher CO_2 superficial velocities for a given flowrate, necessary to avoid the slug/churn flow regime in the production well. The production well pipe diameter is therefore an important optimization parameter for CPG systems. Hence, we vary the production well pipe diameter, taking on the values of 0.11 m, 0.21 m (base case), 0.33 m, and 0.41 m, which closely match the well pipe diameter values used in Adams et al., 2015. The power-flowrate model described in Appendix B.1, used to acquire the maximum power output of the base case considered in this study, also sampled these values of well pipe diameters.

The achieved wellbore flowrate slightly increases with increasing well pipe diameter (Figure 3.15a). The well diameter of 0.11 m takes about an additional 3.5 years to reach the 30 kg/s/well flowrate, compared to the well diameter of 0.41 m. The CO_2 saturation profile over time is almost the same for all cases considered. The larger well pipe diameters (0.33 m and 0.41 m) cause flow that is partially or fully in the slug/churn flow regime (Figure 3.15b). Note that in Figure 3.15b, as opposed to the previous cases, the total mass flux, G (i.e. the total mass flowrate divided by the wellbore cross-sectional area), is plotted as a function of CO_2 mass fraction. The flow pattern transition lines change with varying diameters (as described in Section 3.2.2), and to maintain a unique boundary transition line, the total mass flux is used here. Figure 3.15b shows that G needs to be above about 500 kg/s/m^2 to start and stay in the annular flow regime. In large-diameter production wells, it is important to ensure that the gas flowrate is high and above the critical flowrate needed to lift the liquid to the land surface. Figure 15b also shows that, as the total mass flowrate increases, the plot for the well pipe diameter of 0.33 m moves from the slug/churn flow regime into the annular flow regime, right before it reaches the 30 kg/s/well flowrate (i.e. equivalent to $G=350.75$ kg/m^2/s total mass flux per well). However, throughout the 40 years of CPG simulation time, the largest well pipe diameter case does not

reach the critical flowrate needed to achieve annular flow even at the maximum total mass flowrate (30 kg/s/well).
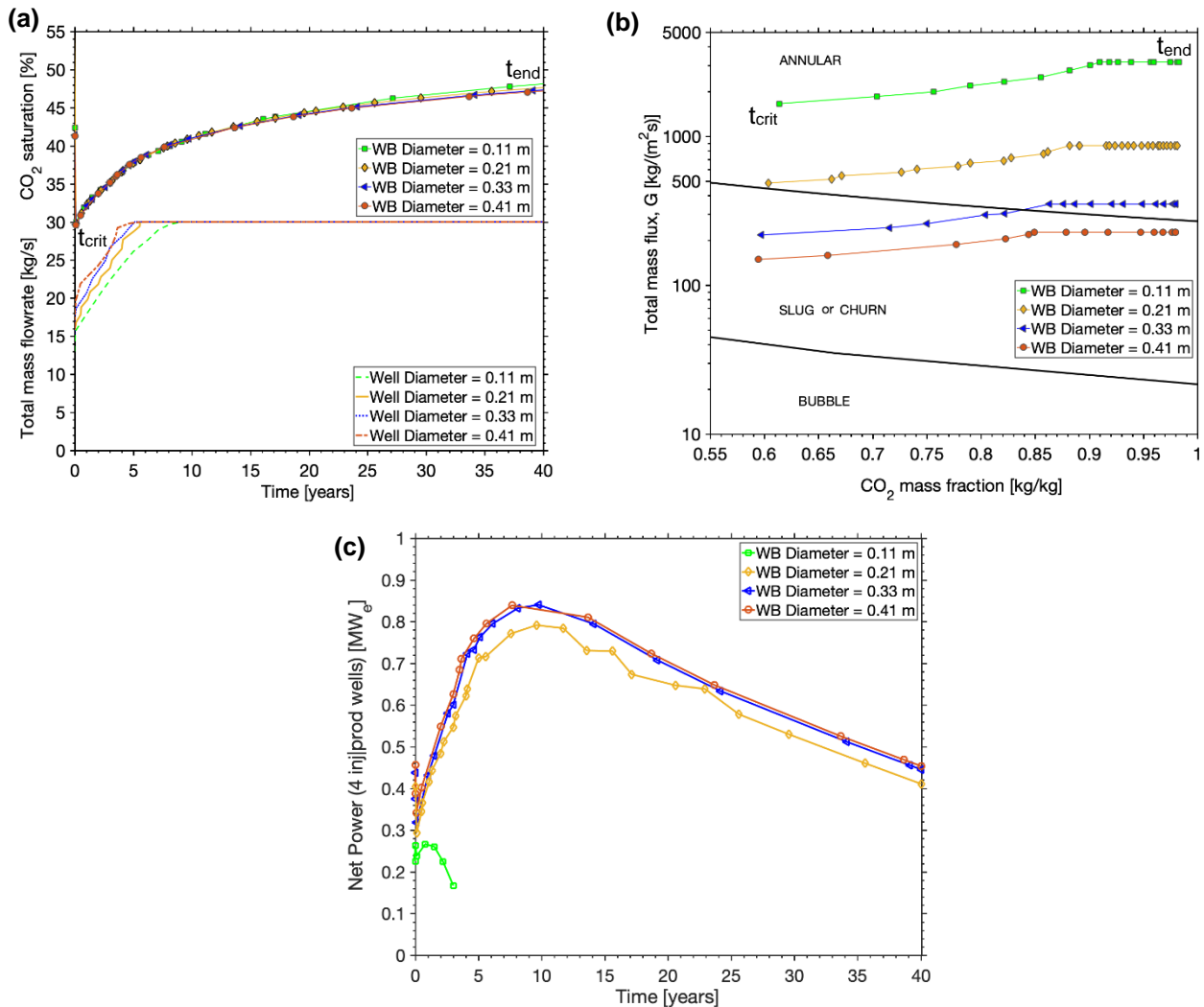
Figure 3.15: Simulation results for different production well (WB) pipe diameters, showing (a) the time series plot of the total fluid mass flowrate and changes in pore-space CO_2 saturation around the production well inlet, (b) the bottom wellbore flow regime, determined by the total mass flux (G) and the CO_2 mass fraction in the production well, (c) the time series of net electric power generation.

Figure 3.15c shows that the power generated by the smallest well pipe diameter of 0.11 m decreases drastically from 0.26 MW_e until the simulation terminates at 0.17 MW_e after only 3 years. This is because of the high pressure (frictional) and heat losses encountered in the small-diameter production well, with relatively high flowrates. Due to this large pressure and temperature drop of the produced CO_2, the saturation vapor pressure of CO_2 is reached (and out of range for the wellbore model thermophysical properties). However, a lower flowrate (associated with the larger well pipe diameters) allows lower pressure and heat losses and could likely delay the time the saturation vapor pressure of CO_2 is reached, hence more power is generated. In this example, the 0.21 m well pipe diameter is optimal. With the given base case 7 MPa admissible reservoir pressure reduction and the resulting initial flowrates, the 0.21

m well diameter maintains an annular wellbore flow regime (Figure 3.15b), and from Table 3.4, the average net electric power generated is lower but very close (with a difference of 0.028 MW_e) to the average net power generated by the two larger 0.33 m and 0.41 m well pipe diameters (that had slug/churn flow during most of the simulation times). These results highlight the importance of considering the well pipe diameter when designing and optimizing CPG systems, as also observed by Adams et al. (in prep. 2020).

3.3.4 Variation of reservoir parameters

In this section, we carry out numerical simulations to investigate the influence of two key reservoir parameters (permeability anisotropy and relative permeability) on the flow regime in the production well and on electric power generation. For all simulations, except for the respective parameters considered, the reservoir and fluid parameters are the same as in the base case (Table 3.1).

Varying these reservoir characteristics changes the amount of time needed to complete the CO_2 plume establishment (PE) stage. Hence, for the PE stage, we present the various simulation results in terms of the duration of the PE stage and the mass of CO_2 injected. The results serve as the initial conditions for the simulation of the CPG stage for the different cases described in this chapter.

3.3.4.1 *Reservoir-permeability anisotropy*

Permeability anisotropy is implemented here by reducing the value of the vertical permeability, k_v, while keeping the horizontal permeability, k_h, constant at 100 mD. This way, we stay as close as possible to the base case, and the variations here focus on the importance of vertical flow. As shown in Figure 3.16a, the duration of the PE stage and the mass of injected CO_2, required to reach a CO_2 saturation of 55% in the pore space around the production well inlet increase as the anisotropy of the reservoir permeability increases. Figure 3.16b shows that the drop in the CO_2 saturation around the production well (due to fluid pressure drawdown) decreases with increasing permeability anisotropy (for $k_v < k_h$). This is mainly because, due to the lower vertical permeability, water upconing to the well perforation (at the top of the reservoir) is reduced. Accordingly, the maximum flowrate is more readily achieved at higher CO_2 saturations. These factors favor an annular flow regime (Figure 3.16c). However, from a power generation perspective, higher permeability anisotropies lead to higher heat depletion rates, lower peaks in power generation, and a sharp decrease in power generation with time (Figure 3.16d), requiring re-optimizing the flowrate.
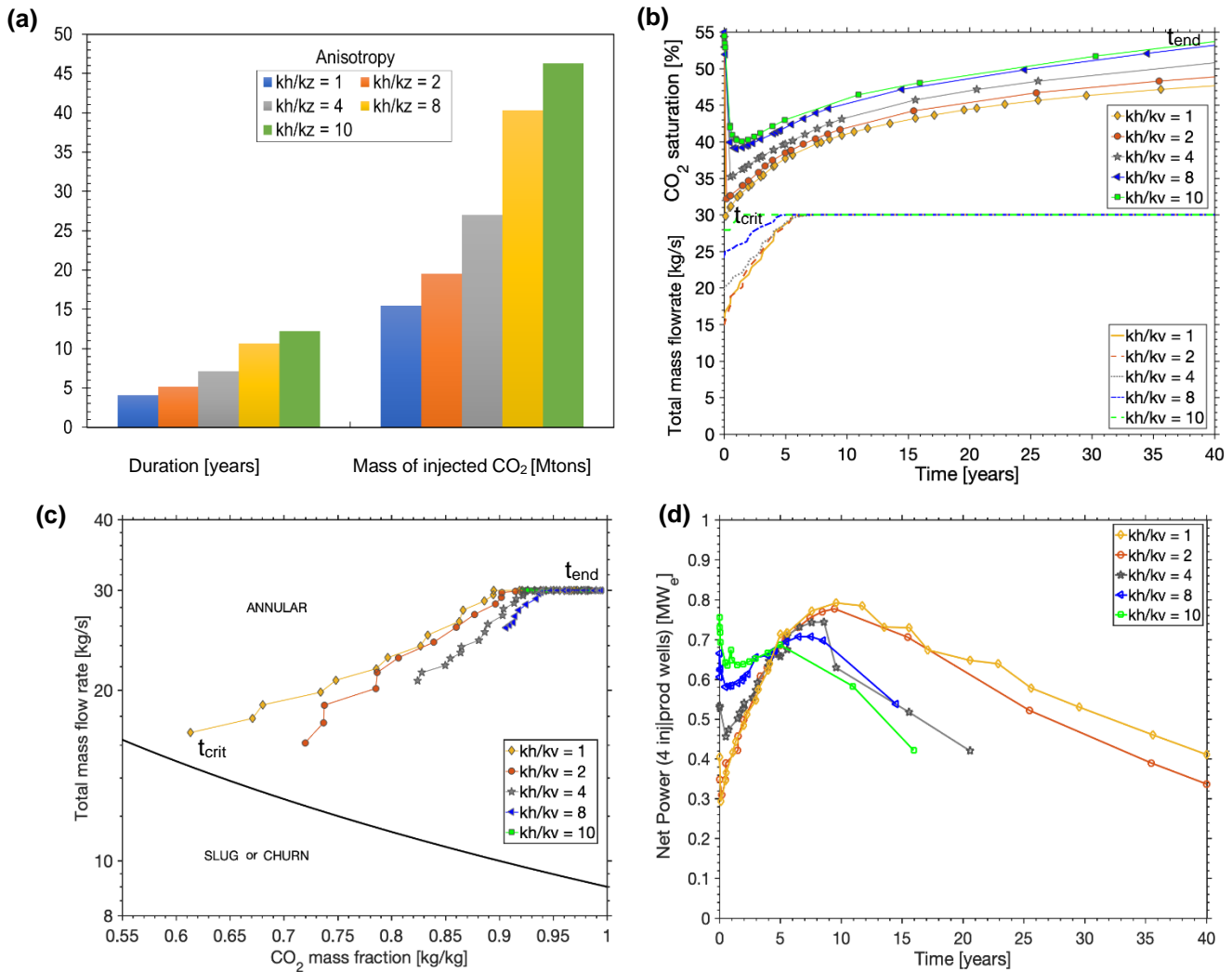
Figure 3.16: CPG simulation results for different reservoir anisotropies of horizontal, k_h, to vertical, k_v, permeability, showing (a) the duration and mass of CO_2 injection during the CO_2-plume establishment (PE) stage, (b) time series plot of the total fluid mass flowrate and changes in CO_2 saturation in the pore space around the production well inlet, (c) the bottom wellbore flow regime, and (d) time series of net electric power generation.

3.3.4.2 *Relative permeability*

Here, we vary the van Genuchten (VG) parameter, *m*, between 0.65 and 0.97. This corresponds to mildly heterogeneous (0.65) to highly homogeneous (0.97) pore-size distributions (compare with values in (Ghezzehei et al., 2007). For comparison, Barea sandstone, which is regarded as a very homogeneous rock, has a van Genuchten parameter of 0.89, as reported in Ghezzehei et al., 2007. Figure 3.17 shows relative permeability versus water saturation curves for the different VG parameters considered in this study. The CO_2 relative permeability remains the same for all values of *m*. The water relative permeability increases as *m* increases and the slope of the water relative permeability becomes steeper as *m* increases. The VG parameter describes the pore-size distribution of the reservoir. A low value indicates that the pore sizes are homogenously distributed and a high value points to a less homogenous (i.e. heterogenous) pore size distribution.
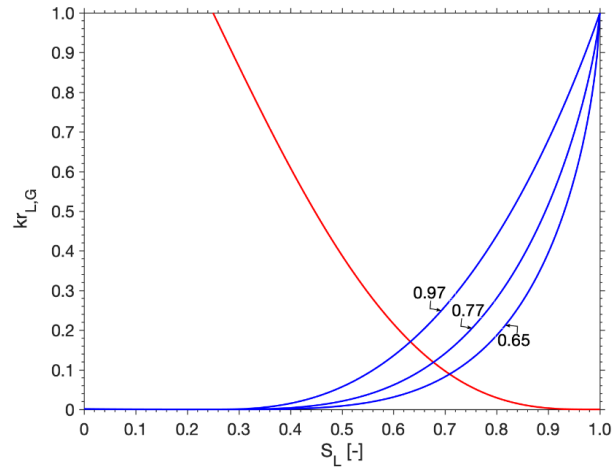
Figure 3.17: Relative permeability-liquid saturation curves for different van Genuchten (VG) parameters. The supercritical/gaseous CO_2 relative permeability curve (red line) is the same for all VG parameters.
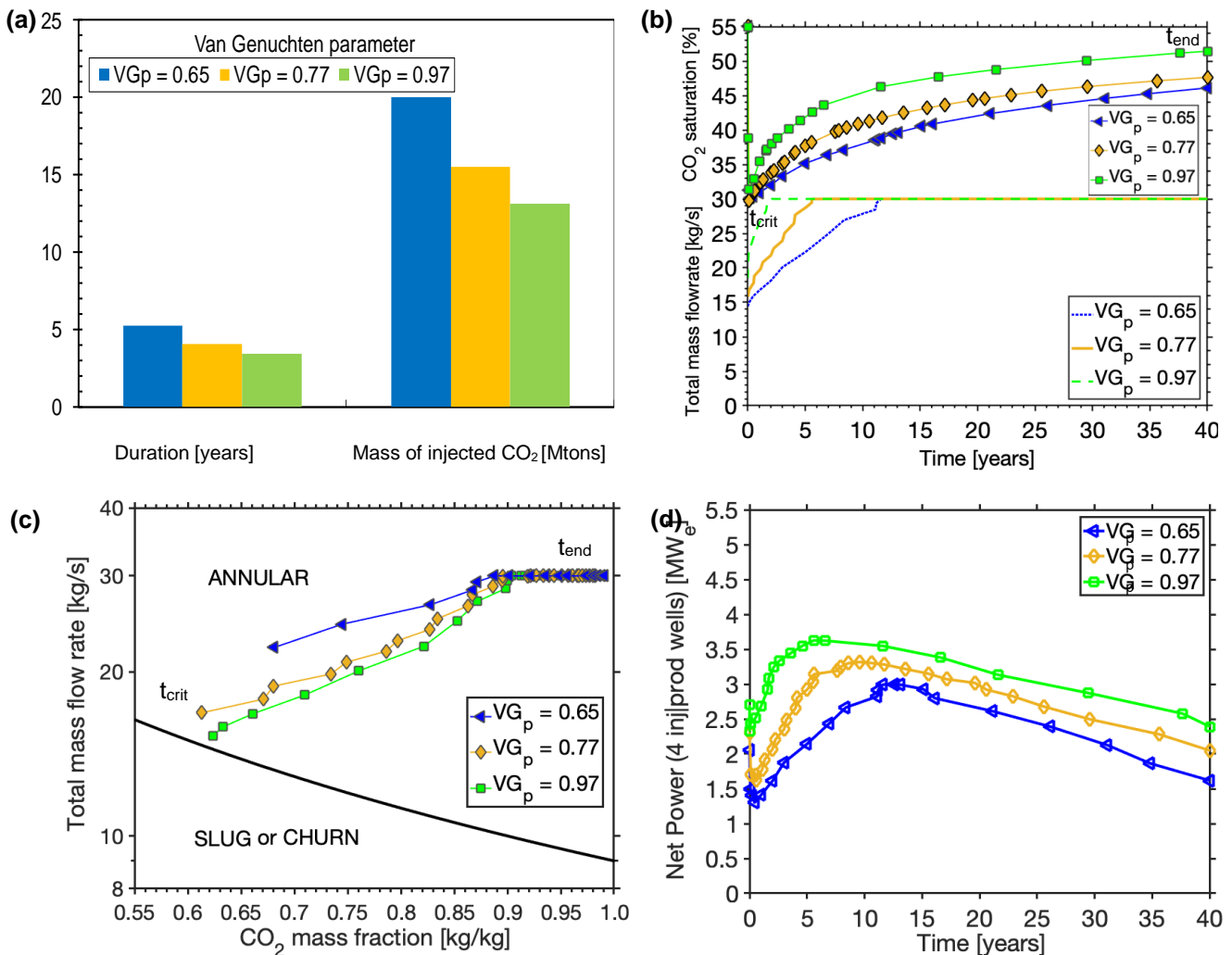
Figure 3.18: CPG simulation results for different van Genuchten relative permeability parameters, showing (a) the duration and mass of CO_2 injected during the CO_2-plume establishment (PE) stage, (b) time series plot of the total mass flowrate and changes in CO_2 saturation in the pore space around the production well inlet, (c) bottom wellbore flow regime, and (d) time series of net electric power generation.

Table 3.4: CPG simulation results, for the different operational and reservoir parameters, showing the average net electric power generated (in MW_e), average net electrical energy generated (in GW_e-h), the wellbore simulation end time, t_{end} (in years, where the check symbol, $\sqrt{}$, means that the simulation completed all 40 years), the CO_2 saturation entering the production well, S_{Gwell}, at t_{crit}, when S_{Gwell} is at its lowest value, the CO_2 mass fraction, XCO_2, at t_{crit}, and the mass flowrate of CO_2, $\dot{m}CO_2$ (in kg/s/well), at t_{crit}.

	Average net power	Average net energy	End time	$S_{G\text{-well}}$	XCO_2	$\dot{m}CO_2$
Flowrate						
20 kg/s	0.500	0.175	$\sqrt{}$	0.761	0.611	10.002
25 kg/s	0.536	0.188	$\sqrt{}$	0.757	0.606	10.139
30 kg/s	0.575	0.202	$\sqrt{}$	0.754	0.604	10.156
35 kg/s	0.595	0.193	37.00	0.755	0.605	10.643
40 kg/s	0.630	0.160	29.00	0.753	0.603	10.758
ΔP						
3 MPa	0.524	0.184	$\sqrt{}$	0.802	0.680	6.832
5 MPa	0.590	0.207	$\sqrt{}$	0.771	0.632	8.701
7 MPa	0.575	0.202	$\sqrt{}$	0.754	0.604	10.156
9 MPa	0.526	0.184	$\sqrt{}$	0.746	0.585	12.423
Well diameter						
0.11 m	0.235	0.006	3.00	0.760	0.614	9.667
0.21 m	0.575	0.202	$\sqrt{}$	0.754	0.604	10.156
0.33 m	0.603	0.211	$\sqrt{}$	0.751	0.597	11.101
0.41 m	0.599	0.210	$\sqrt{}$	0.750	0.594	11.684
Anisotropy						
kh/kv = 1	0.575	0.202	$\sqrt{}$	0.754	0.604	10.156
kh/kv = 2	0.554	0.194	$\sqrt{}$	0.838	0.720	11.577
kh/kv = 4	0.589	0.106	20.60	0.905	0.824	17.127
kh/kv = 8	0.635	0.081	14.50	0.952	0.906	23.293
kh/kv = 10	0.651	0.091	16.00	0.961	0.922	27.664
VG parameter						
VG_p = 0.65	0.490	0.172	$\sqrt{}$	0.768	0.624	9.571
VG_p = 0.77	0.575	0.202	$\sqrt{}$	0.754	0.604	10.156
VG_p = 0.97	0.706	0.248	$\sqrt{}$	0.815	0.728	15.596

Figure 3.18a shows that it takes longer, and that a larger mass of injected CO_2 is required, for low values of the VG parameter (0.65) to reach a CO_2 saturation of 55% in the pore space around the production well inlet. Figure 3.18b shows that the decrease in CO_2 saturation (due

to fluid pressure drawdown at the start of production) is similar for all cases. At lower m, the water relative permeability is very low (for a CO_2 saturation of 55%), as shown in Figure 3.17, and the water phase is almost immobile, which means that the water hardly flows into production well. Figure 3.18c shows that all cases achieved annular flow conditions in the production well, with the case of $m = 0.97$ having the highest CO_2 mass fraction and flowrate at t_{crit}.

The net power generation results presented in Figure 3.18d show that the net power peaks at an earlier time (Figure 3.18d) and the average net power output (Table 3.4) increases as the value of the VG parameter increases. Afterward, the power output declines at a constant rate. Hence, higher values of the VG parameter (more heterogeneous pore size distributions) result in favorable production well fluid flow and CPG power-generating performances.

3.3.5 **Minimum superficial CO_2 velocity as a design parameter**

To design a CPG system which avoids water accumulation, and thus maintains annular flow, in the production well, the velocity of CO_2 in the production well must be higher than the minimum superficial CO_2 velocity, calculated with Turner's model (Turner et al., 1969). To determine how this minimum value changes with depth, for a CPG system, we plot the minimum superficial CO_2 velocity with depth (800 – 3250 m) in Figure 3.19a. We apply an approximately standard continental-crust geothermal temperature gradient of 34 °C/km and assume a constant salt mass fraction of 0.15 in the water at all depths, which can be used to calculate the density of brine (Haas, 1976) and the fluid pressure gradient at the various depths considered. For the range of pressures and temperatures considered at these depths, the interfacial tension for the CO_2-water system is determined using the empirical exponential equation described by Bachu et al. (Bachu and Brant Bennion, 2009), decreasing from 0.037 to 0.032 mN/m as depth increases from 800 m to 3200 m. Figure 20 shows that the minimum superficial CO_2 velocity, for the described CPG system, is around 0.43 – 0.45 m/s if the depth is greater than 1500 m and between 0.45 and 0.70 m/s for depths between 1500 m and 800 m.

A more practical design parameter than the superficial CO_2 velocity is the bulk (total) velocity of the fluid in the well (i.e. the sum of the superficial velocities of water and CO_2). The minimum bulk velocity necessary to maintain annular CO_2 flow in the borehole depends on the composition of the fluids in the borehole. For a given volume fraction (saturation) of CO_2 in the well, the minimum bulk velocity, U_{total}, can be calculated from the minimum CO_2 superficial velocity by

$$U_{total} = U_{S,G} \Big/ S_{G\text{-well}} . \tag{3.17}$$
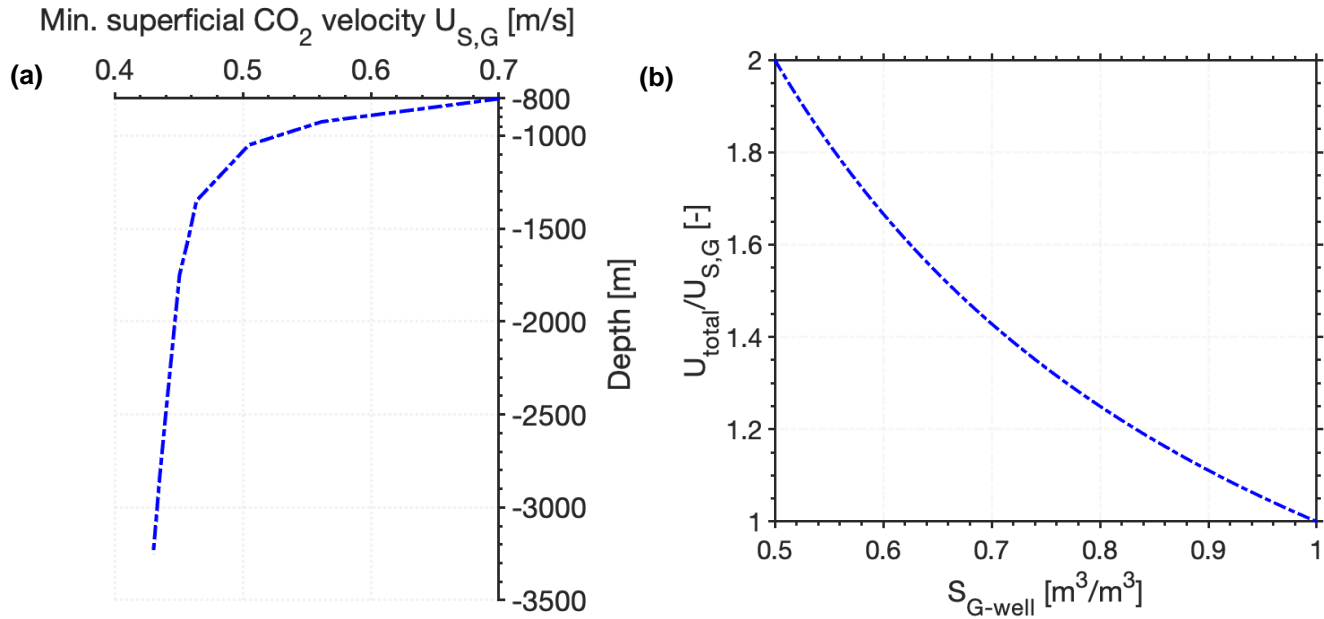
Figure 3.19: (a) Variation of the minimum superficial CO_2 velocity with depth for a CPG system with a geothermal temperature gradient of 34 °C/km and a dissolved salt mass fraction in the water phase of 0.15. (b) Variation of the ratio of total (bulk) velocity, U_{total}, to the superficial CO_2 velocity, $U_{S,G}$, as a function of the CO_2 saturation in the production well, S_{G-well}.

Figure 3.19b shows the ratio of total (bulk) velocity, U_{total}, to the superficial CO_2 velocity, $U_{S,G}$, for CO_2 saturations in the production well, S_{G-well}, ranging from 0.5 to 1. For example, when S_{G-well} = 0.5, the figure indicates that the minimum bulk velocity, required in the borehole to maintain annular fluid flow, is 0.9 m/s for depths greater than 1500 m and between 0.9 m/s and 1.4 m/s for shallower depths, ranging from 1500 m to 800 m.

3.3.6 Application to Cranfield CO_2-based geothermal field experiment

We can apply the findings of this study to gain some insights into the problems with liquid water in the production well, postulated as one of the factors that led to the failure of the Cranfield (USA) CO_2 thermosiphon field test (see Introduction section 3.1). Apart from the factors discussed by Pan et al. (Pan et al., 2018) that could potentially sustain the thermosiphon flowrate at the Cranfield field test, it is also important to optimize the flowrate initiated by venting the production well. During the field test, the maximum flowrate achieved by venting the production well was 2.1 kg/s during Venting #3 (Freifeld et al., 2016). However, using Cranfield's reservoir and fluid properties (presented in Table 3.3) and the production wellbore diameter of 0.14 m used at the Cranfield site (see Freifeld et al., 2016 and Pan et al., 2018 for more details), we calculated that a minimum mass flowrate of 3.95 kg/s (i.e. with a minimum superficial CO_2 velocity of 0.43 m/s and a minimum bulk (water and CO_2) velocity of 0.48 m/s (at 0.3 CO_2 saturation in the pore space surrounding the production well inlet, which corresponds to 0.9 CO_2 saturation in the production well); cf. and Section 3.3.5) is required to achieve annular flow in the wellbore that could sustain a thermosiphon (Figure 3.20).
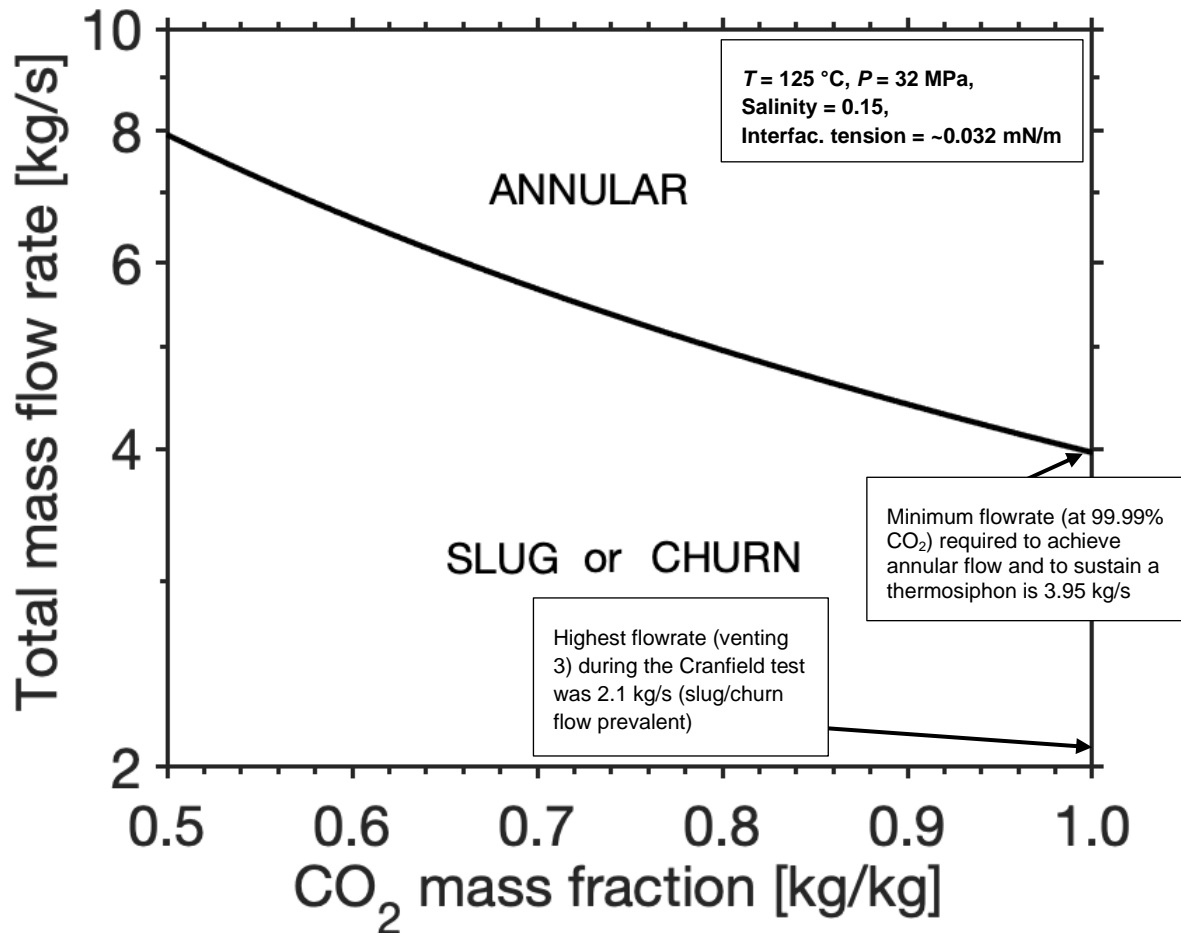
Figure 3.20: The production well flow regime for the Cranfield CO_2 circulation test in the US, as a function of total fluid mass flowrate and CO_2 mass fraction. The minimum flowrate required to achieve annular flow in the wellbore that could sustain a thermosiphon, i.e. without requiring pumping, is 3.95 kg/s. The highest total mass flowrate actually achieved during the Cranfield CO_2 circulation test was only 2.1 kg/s (Freifeld et al., 2016).

The minimum mass flow rate required to achieve annular flow increases as the mass fraction of water in the well increases (Figure 3.20). From this point of view, the low mass flowrate achieved (i.e. a maximum of 2.1 kg/s) during the Cranfield test is not enough to prevent water accumulation in the production well over time (liquid loading). Almost twice that maximum flowrate of 2.1 kg/s would have been necessary to ensure any entrained water is lifted out of the production well, achieving annular flow and supporting the CO_2 thermosiphon that was being tested at the Cranfield site.

3.4 Discussion

The coupling of the reservoir, production wellbore, and power systems makes it possible to optimize the production flowrate in such a way as to ensure annular flow in the production well without unduly compromising CPG power output. The base-case results show that the largest water production occurs immediately, once the CPG stage starts, and may lead to slug/churn flow at this early time. Slug/churn flow in the production well causes pressure

fluctuations, undermines CO_2 circulation and the thermosiphon, and leads to a higher fluid density in the production well. Thus, a typically small, pure-CO_2 pump or compressor at the CO_2 injection wellhead may be necessary to maintain the required production well fluid flowrate, if the flow regime in the production well is that of slug/churn flow at the beginning of CPG operations. The operational parameters should be optimized for the given reservoir characteristics to achieve an annular-regime flowrate and maximize a combination of power output and lifetime of the geothermal system. From the cases studied here, the following inferences can be drawn:

a. For a fixed fluid mass flowrate or downhole pressure difference, CO_2 velocities decrease with increasing well pipe diameter. This can lead to slug/churn flow in the production well. However, small well pipe diameters yield high fluid pressure and heat losses, which results in lower power generation. Hence, to optimize the system, a production well pipe diameter that can achieve annular flow, while minimizing fluid pressure and heat losses in the production well, is sought. In our study, a production well pipe diameter of 0.21 m results in an optimal fluid flowrate, compared to pipe diameters of 0.11 m, 0.33 m, and 0.41 m. Optimizing CPG well pipe diameters and CPG injection-to-production well spacings is also considered from a somewhat different perspective in Adams et al. (Adams et al., in prep. 2020) should also be considered when designing CPG systems.

b. When varying admissible reservoir fluid pressure reductions, our results show that there is a tradeoff between high fluid flowrates and water entering the production well. Relatively high reservoir fluid pressure reductions lead to high flowrates and hence higher amounts of water entering the production well. However, high total fluid flowrates (associated with high CO_2 velocities) could be high enough to carry the water out of the well. In addition, higher flowrates lead to faster rates of heat depletion of the reservoir (Adams et al., in prep. 2020). Finally, the reservoir can only support flowrates that do not cause reservoir pressure drawdowns that could compromise the structural integrity of the caprock.

c. Our reservoir parameter sensitivity analysis shows that lower vertical permeabilities (i.e. higher permeability anisotropies) lead to a reduced water upconing effect, meaning that less water is drawn into the production well through its screen. Higher permeability anisotropies also enable higher fluid flowrates in the reservoir, increasing system power output but also decreasing the CPG power plant lifetime. The reservoir-parameter sensitivity analysis also shows that the shapes of the relative permeability curves considerably affect the relative amounts of CO_2 and water entering the production well. Therefore, precise measurements of relative permeability curves for the specific reservoir formation to be employed during CPG operations, are particularly

important to improve predictions of CPG performance, particularly at the very beginning of the operation, when the system is most prone to water entering the production well.

It should again be noted that in this study, we only consider free-phase liquid water entering the production well through the well screen, and its effect on the flow regime in the production well and associated well lifetime. In another paper (Fleming et al., 2020), we have investigated the exothermic exsolution of water from originally water-saturated CO_2 and its effect on CPG power generation. Such exsolved and then free-phase liquid water, even though likely minor in amount and thus effect on the flow regime in the production well, should ideally also be considered (in addition to the free-phase liquid water or brine entering through the production well screen considered in the current study) when analyzing what fluid flow regime prevails in the CPG production well. Furthermore, any produced water needs to be removed from the produced CO_2 stream before CO_2 reinjection into the CPG reservoir, as otherwise the CO_2 injectivity into the geologic reservoir is likely significantly compromised (Garapati et al., 2015b). Finally, it should be noted that a CO_2 pump or compressor, that may be installed to ensure annular flow in the CPG production well, would be installed at the (pure-CO_2) injection wellhead at the land surface and is likely small in power (Adams et al., 2015). Such a small, CO_2 injection wellhead pump is thus not a considerable complication in CPG system development and maintenance, particularly when compared to deeply submersed water pumps in hydrothermal system production wells. If additional CO_2 is continually supplied, then the large-scale CO_2 injection pumps or compressors may be used for this purpose as well.

3.5 Conclusions

This study highlights the importance of properly designing CO_2-Plume Geothermal (CPG) systems by optimizing the fluid production flowrate to minimize the amount of water entering the production well and maintain annular flow in the production well and preventing liquid loading in the well, while maximizing power generation. We present a flow pattern transition method to determine the flow regime in a CPG production well for a CO_2-brine system for different total fluid mass flowrates and corresponding CO_2 mass fractions. Our findings are as follows:

1) The minimum total mass flowrate, required to achieve annular flow in the production well, decreases as the CO_2 mass fraction increases and as the well pipe diameter decreases. For the base case considered in this study, this minimum CO_2 flowrate significantly reduces from 25 kg/s to 3 kg/s as the well pipe diameter decrease from 0.33 m to 0.11 m.

2) In order to achieve annular flow in the production well, at 50% $S_{G\text{-well}}$ for example, the required minimum superficial CO_2 velocity is approximately 0.45 m/s if the reservoir

depth is greater than about 1500 m and between 0.45 and 0.70 m/s for shallower reservoir depths between 1500 m and 800 m. Hence, using these values for a given reservoir depth and mass or volume fraction of water in the CPG production well, the minimum flowrate, necessary to achieve annular flow, can generally be determined.

3) We provide insights into one of the reasons why the CO_2 thermosiphon test at the Cranfield site (USA) was unsuccessful. Using the reservoir properties and well pipe diameter at the Cranfield site, our results show that the minimum CO_2 flowrate, required to achieve annular flow in the production well, is about twice as high as the actual maximum flowrate achieved during the venting stages of the Cranfield test.

4) The results of the operational parameter sensitivity study show that the admissible reservoir fluid pressure drawdown is an important limiting factor for achieving the fluid flowrate in the CPG production well necessary to avoid water accumulation. In addition, the well diameter can be optimized so as to obtain a high CO_2 velocity but low heat and pressure losses in the well.

5) The results of the reservoir parameter sensitivity study highlight that higher permeability anisotropies enable higher fluid flowrates in the reservoir, which increases the CPG system power output but also decreases the power plant lifetime. Also, the correct measurements or estimations of relative permeability is important for any reservoir associated with CPG operations to improve predictions of CPG production well and power generation performances.

Acknowledgments

4

Sensitivity study of reservoir and operational parameters on the energy-extraction and CO_2-storage performance of the combined CO_2-EGR–CPG system[*]

_____

Justin Ezekiel[a], Diya Kumbhat[a], Anozie Ebigbo[a,b], Benjamin M. Adams[a], Martin O. Saar[a,c]

[a]*Geothermal Energy and Geofluids Group, Department of Earth Sciences, ETH-Zürich, Sonneggstrasse 5, 8092 Zürich, Switzerland*

[b]*Hydromechanics Group, Helmut Schmidt University, Hamburg, Campus Nord, Friedrich-Ebert-Damm 245, 22159 Hamburg, Germany*

[c]*Department of Earth and Environmental Sciences, University of Minnesota, Minneapolis, USA*

_____

[*] In preparation.

Abstract

Utilizing CO_2 for combined enhanced gas recovery (EGR) and geothermal energy extraction in sedimentary reservoirs (CPG) has shown potential for maximizing energy generation from natural gas reservoirs. The combined CO_2-EGR–CPG system has been introduced as a feasible approach that constitutes a CO_2 capture double utilization and storage (CCUUS) system. In this study, we carry out reservoir simulations, using TOUGH2, to evaluate the sensitivity of different key reservoir and operational parameters on the natural gas recovery, geothermal-energy (electricity) generation and CO_2-storage performances of the combined system. The reservoir parameters include horizontal permeability, permeability anisotropy, reservoir temperature, and relative permeability; while the operational parameters include well pipe diameters and ambient surface temperature. Using example of depleted and partially depleted natural gas reservoir models, we also investigated the effects of carrying out CO_2-plume establishment stage (only CO_2 injection with no production for 1.5 years) on the performance metrics and on the fluid flow regime in the production. The simulation results show that partially depleted reservoirs, associated with CO_2 plume establishment stage, achieve the best overall energy (natural gas and geothermal) recovery performance and the quickest transition to CPG stage. Reservoir temperature is the most significant parameter that influences the energy recovery and CO_2 storage performance of the combined CO_2-EGR–CPG system. The results of this study pave the way for future power-generation optimization studies to enhance the appeal of combining CO_2-EGR and CPG projects and to help launch this technology at commercial scales.

4.1 Introduction

We have presented, in Ezekiel et al. (2020), the potential for extracting heat from produced natural gas and utilizing supercritical carbon dioxide (CO_2) as a working fluid for the dual purpose of enhancing gas recovery (CO_2-EGR) and extracting geothermal energy (CPG) from deep natural gas reservoirs for electric power generation, while ultimately storing all of the subsurface-injected CO_2. This approach, termed combined CO_2-EGR–CPG system, constitutes a CO_2 capture double utilization and storage (CCUUS) system. The advantages associated with this combined system have been discussed in detail in Ezekiel et al. (2020) and Zhang et al. (2017). Some of these main advantages include: (i) the combined system contains less pore-water influence (due to the presence of unrecoverable residual natural gas), which could make it possible for the CO_2 to flow as a single phase in the reservoir. This also reduces the complicated CO_2-rock-water interactions to reservoir properties and makes the system more attractive and efficient for CO_2-based geothermal energy extraction than other (mostly water-bearing) sedimentary geothermal reservoirs; (ii) additional natural gas and geothermal energy is extracted for power generation, which leads to an increase in the

gas field's total amount of producible energy; (iii) economic (cost-saving) benefits are achieved by using/sharing already-existing multidisciplinary datasets (on reservoir parameters), infrastructure (surface facilities, wells etc.). Hence, investment costs are significantly reduced; (iv) the combined system facilitates CCUS, providing energy (electricity, heat) to, and compensating for the cost of, both CCS and gas-field operations; (v) extends the useful lifetime of the gas reservoir; recover otherwise stranded assets such as wells, offshore platforms, etc.; and postponing of the expensive plugging of the wells and abandonment stages of the gas field.

Different stages have been identified for energy (and power) generation from the combined system. These includes the conventional natural gas recovery (CNGR) stage, where natural gas is produced by the primary recovery drive and at the surface, the associated heat is extracted and converted to power using an Organic Rankine cycle (ORC) or a CO_2-based Rankine cycle (CRC). The CNGR stage is followed by the CO_2-EGR stage when the fluid pressure or natural gas has been depleted and the remaining natural gas cannot be economically recovered by just the natural primary drive. Hence, CO_2 is injected into the reservoir to recover the remaining natural gas and reduce the residual methane content in the reservoir. During the CO_2-EGR stage, CO_2 breakthrough occurs in the production well (typically when the CO_2 mass fraction in gas phase is about 10%). Hence, the installation of a CH_4-CO_2 separator is required at the surface. A transition period exists at this stage before the CPG stage begins. During this transition period, the heat in the separated methane is extracted, and converted to power. However, the separation process of CO_2 and CH_4 is cost and energy intensive, requiring higher energy input than the geothermal power generated during the CO_2-EGR stage. Also, the separated CO_2 is not used for energy extraction and is simply reinjected into the reservoir (Ezekiel et al., 2020). In this study, we classify the transition period under the CO_2-EGR stage. The separation of the produced mixed fluid continues till about 90% mass fraction of the produced fluid is CO_2. At this point, the CPG stage commences and all the produced fluid (mostly CO_2) is sent directly to the direct CO_2 turbine for power generation. Reservoir simulation results (for the CPG stage) show that, using a scalable reservoir model example, a CO_2-circulation mass flowrate of 110 kg/s results in a maximum power output of 2 MW_e for the combined system (Ezekiel et al., 2020). The CO_2 leaving the turbine is further cooled and reinjected into the reservoir. When the reservoir heat is depleted, the injection and production wells are shut down and the injected CO_2 is permanently stored in the natural gas reservoir.

In this chapter, we use a similar, but improved, anticlinal natural gas reservoir model described in Ezekiel et al. (2020), to carry out reservoir simulations (in TOUGH2), aimed at expanding the existing study on the combined CO_2-EGR–CPG system to:

(i) accommodate lessons learned on the influence of bottom-hole production flowrate on water entering the production well and the subsequent flow regime(s) established. This will also validate, for different residual CH_4 content, the favorable configuration of the combined system that achieves less water inflow into the production well during the CPG stage (associated with high production mass flowrate) and ensures the establishment of an annular flow regime in the bottom-hole region of the production well;

(ii) investigate the effect of residual CH_4 content, the effect of CO_2-plume establishment stage, and the effects of different reservoir and operational (non-reservoir) parameters on both the natural gas recovery, the electric power generation, and CO_2 storage capability performances of the combined system;

This study focuses on varying, within a defined range, and determining how sensitive some of the key reservoir and operational parameters can influence the key performance metrics (mentioned in the above points (i) and (ii)) of the combined system. This study also provides a preliminary guide for identifying the favorable factors that are essential in selecting suitable natural gas reservoirs, and the most effective implementation strategy, for the proposed combined CO_2-EGR–CPG system.

4.2 Methodology

In this section, we describe the natural gas model, numerical simulation and performance metrics adapted for this study. We highlight the improvements and changes we have made to the original natural gas reservoir model (presented in Ezekiel et al., 2020) and the implementation strategy/concept of the combined system for effective natural gas and geothermal energy extraction from the natural gas reservoir. We use the numerical model to simulate the three main stages (CNGR, CO_2-EGR+TP and CPG stages) associated with the combined system, for investigating (1) the effect of including the CO_2-plume establishment stage (as described in Ezekiel et al., 2020) on reducing the chances of water entering the production well, using examples of depleted and partially depleted gas reservoir models, during the CO_2-EGR stage (including the transition period before the start of the CPG stage), and (2) the effects of different reservoir and operational parameters on the natural gas and geothermal energy recovery, and CO_2-storage, performances of the combined system.

4.2.1 Reservoir modeling and simulation

4.2.1.1 *Modified reservoir model (after Ezekiel et al., 2020)*

Using some of the reservoir properties of some examples of hot/deep natural gas fields in the world, we set up a similar natural gas reservoir to that of our previous study (see Figure

2.2 of Ezekiel et al. (2020)), in terms of model geometry, well configuration, boundary conditions, and relative permeability functions. However, the fluid properties of the current model are updated, such that the salt concentration changes from zero in the previous model to 150,000 ppm in the current model. Furthermore, the y-axis dimension of the full model is extended from previously 3 km to now 4.5 km, so that the updated model has equal dimensions on all sides. We also introduce a horizontal to vertical permeability anisotropy of $k_h/k_v = 2$ in the base-case model. We carry out our simulation using the same reservoir simulator, TOUGH2 with the EOS7C module (Oldenburg et al., 2004) developed for simulating gas and brine flow, as well as heat transport, in the natural gas reservoir. The rock and fluid properties of the new model, as well as the initial conditions, are summarized in Table 4.1.

Table 4.1: Parameters for the base-case reservoir model

Parameter	Value
Reservoir size, x (km), y (km), z (km)	4.5 x 4.5 x 0.1
Depth (km)	3.0
Porosity (-)	0.20
Horizontal permeability, kh (m²)	10^{-13} (100 mD)
Anisotropy k_h/k_v (-)	2.0
Thickness (m)	100
Reservoir initial pressure	Hydrostatic (30 MPa at the top of the reservoir)
Reservoir initial temperature (°C)	120
Initial CO_2 mass fraction	0.025 (dissolved in brine)
Residual gas saturation (-)	0.05
Residual brine saturation (-)	0.25
van Genuchten parameters α (Pa), m (-)	3×10^3, 0.77
Native brine NaCl saturation (ppm)	150,000
Mol. diffusivity in gas; in water (m²/s)	10^{-5}; 10^{-10}
Rock grain density (kg/m³)	2650
Thermal conductivity λ_{wet}, λ_{dry} (W/m°C)	2.51, 1.6
Rock specific heat capacity (J/kg°C)	1000
Geothermal gradient (°C/km)	35
Rock compressibility (1/Pa)	10^{-10}
CO_2 injection enthalpy (J/kg)	2.8×10^5
Well diameter (m)	0.14
Lateral boundary conditions of the reservoir	Hydrostatic pressure; 120°C (Dirichlet boundary conditions).
Top and bottom boundary conditions of the reservoir	No fluid flow and no heat flux. flux (as background heat flux is typically negligible).
Initial conditions	Hydrostatic equilibrium, no heat flow, pore space entirely occupied by brine.

4.2.1.2 *Reservoir simulation schemes*

Based on the new model of the proposed combined CO_2-EGR-CPG described above, the numerical simulation is carried out in three main stages:

a) the CNGR stage with a base-case duration of 25 years at a production flowrate of 4 kg/s/well.

b) the CO_2-EGR stage with all simulated cases lasting for 1 year with a high injection-production flowrate ratio (Ezekiel et al., 2020; Zhang et al., 2017) (i.e. injection flowrate of 30 kg/s/well and production flowrate of 4 kg/s/well). The high injection-production flowrate ratio is beneficial for achieving a good CO_2-EGR performance as well as a short duration for establishing an adequate CO_2-plume reservoir (Zhang et al., 2017). After the 1-year period of high injection-production flowrate ratio, the production rate is increased to 30 kg/s/well (equal to the injection flowrate). The CO_2-EGR stage ends when the mass fraction of CO_2 (XCO_2) at the production well region has reached 90%. Thus, the CO_2-EGR stage is associated with the mixed-fluid production and their separation at the surface. In this study, the period between 10% to 90% CO_2 mass fraction in the production well is referred to as the transition period. The longer this "transition period", the longer the time, and the higher the parasitic power, required to separate the mixed fluid at the surface. The cases that are associated with 1.5 years of CO_2-plume establishment (PE) stage, after the CO_2-EGR stage (of 1 year), are also considered. This implies that, in the current study, we carry out the CO_2-EGR stage before the PE stage.

c) the CPG stage starts, after the transition period, when the CO_2 mass fraction at the production well region has reached 90%. The base-case CPG-stage duration is for 30 years at a circulation flowrate of 30 kg/s/well.

4.2.2 **Performance metrics**

In this section, we present how we calculate the metrics used to measure the energy and CO_2-storage performance for the different cases considered in this study. These metrics include:

(a) the CO_2 saturation (in the reservoir and in the well), and the corresponding flow regime established (at the bottom-hole section of the production well) at the time of highest water saturation around the production well inlet region of the reservoir (ref. Ezekiel et al. 2020). This performance metric is only applicable for the reservoir parameters and it can be used to determine the importance of the PE stage for the combined system to achieve an annular flow regime (dominant CO_2 flow) in the production well. The method to calculate this metric, using the gas saturation in the well and flowrate can be found in Chapter 3 and Appendix B.4.

(b) the natural gas recovery performance (NGRP), which incorporates the amount of natural gas recovered (in terms of natural gas recovery factor) and the duration of the CNGR and CO_2-EGR stages (including the "expensive" transition period). The natural gas recovery factor during the CNGR and CO_2-EGR stages can be measured as a percentage of the original gas in place (OGIP). These respective factors are calculated as

$$\text{CNGR factor, } F_{\text{CNGR}} \text{ (\%)} = \frac{V_{g-\text{CNGR}}}{\text{OGIP}} \cdot 100, \tag{4.1}$$

where $V_{g-\text{CNGR}}$ is the volume of gas produced during the CNGR stage, OGIP is the volume of gas initially in place,

$$\text{EGR factor, } F_{\text{EGR}} \text{ (\%)} = \frac{V_{g-\text{EGR}}}{\text{OGIP}} \cdot 100, \tag{4.2}$$

where $V_{g-\text{EGR}}$ is the volume of gas produced during the CO_2-EGR stage, and

$$\text{Ultimate recovery factor, } F_{\text{UR}} \text{ (\%)} = F_{\text{CNGR}} + F_{\text{EGR}} . \tag{4.3}$$

The volumes of the produced gas during the CNGR and CO_2-EGR stages, respectively, can be obtained from the TOUGH2 simulation output files.

The natural gas recovery performance is measured using an average project annual index factor (cumulative) value, RI, which is calculated as the ultimate recovery factor [%] divided by the durations of the CNGR and CO_2-EGR+TP stages, t_{EGR} [year] (Equation 4.4).

$$\text{RI (\%/year)} = \left. F_{\text{UR}} \text{ (\%)} \middle/ (t_{\text{CNGR}} + t_{\text{EGR+TP}}) \text{ (year)} \right. . \tag{4.4}$$

The recovery index provides a way to select the best reservoir parameters (independent of non-reservoir parameters) and strategies that favour natural gas recovery and less duration (saving costs) for the CO_2-CH_4 separation process during the CO_2-EGR stage. The separation process of CO_2 and CH_4 is an expensive operation and the separated CO_2 is not used for energy extraction and is simply reinjected into the reservoir (Ezekiel et al., 2020). Hence, the lower this transition period (or duration of the CO_2-EGR+TP stage), the higher the energy efficiency of the combined system. Hence, a high value of RI_{AE} is favorable and implies that the difference between the energy recovered and the energy (and duration) used for separation is potentially large.

(c) the average net geothermal electricity (measured in Gigawatt-hour [GW_eh]) generated using the produced fluid – natural gas (via the organic/CO_2-based Rankine cycle) during CNGR, Q_{CNGR}, and EGR, Q_{EGR}, stages and from the produced CO_2 (via the direct CO_2 turbomachinery) only during CPG stage, Q_{CPG} The average net power generated are calculated using the output wellhead temperature and pressure results gotten from the

wellbore heat transfer model described in Ezekiel et al. (2020). The power system models, applied in this study, for the indirect (ORC) and direct CO_2 turbomachinery power systems have also been extensively described in Ezekiel et al. (2020).

(d) the amount of CO_2 stored (in tons) is calculated by subtracting the mass of CO_2 present in the reservoir at the start of the CNGR stage from the mass of CO_2 present in the reservoir after the CPG stage. These values can be obtained from the output file of the TOUGH2 simulation. The mass in kilogram [kg] is converted to megatons [Mtons].

4.2.3 Parameter-space sensitivity analysis of the performance metrics

4.2.3.1 *Residual methane content and CO2-plume establishment stage*

In our simulations, the residual CH_4 content is accounted for in the simulations using two main cases: Case 1 (base case) and Case 2, which consider the CNGR stage for 25 years and 26 years, respectively. This implies that Case 2 would have a lesser residual CH_4 content than Case 1, and that the gas saturation around the production well has started to reduce, leading to the termination of the CNGR stage. Case 2 is equivalent to the example case presented in Ezekiel et al. (2020). This case (Case 2) is an example of a depleted reservoir, while Case 1 is an example of a partially depleted natural gas reservoir because it has a higher proportion of the residual CH_4 in the reservoir after the CNGR stage. These two main cases are further classified into 4 sub-cases to represent cases with and without the 1.5 years of the CO_2-plume establishment (PE) stage. Cases 1-A and 2-A consider the 1.5 years of the PE stage, whereas Cases 1-B and 2-B do not consider the PE stage. This implies that, for the "B" cases, there is no waiting time (that involves only CO_2 injection and no fluid production) after the 1-year CO_2-EGR stage to prime the reservoir with CO_2 and establish a substantial CO_2 connection between the injection and the production wells. This allows us to investigate if the PE stage is important for the combined system in terms of reducing the amount water entering the production well, ensuring annular flow in the production wells, and in reducing the "expensive" transition period. The corresponding effects of these 4 different sub-cases on the minimum CO_2 saturation in the well, natural gas recovery (during the CNGR and CO_2-EGR stages – including the transition period), the geothermal energy generation (during the 3 stages) and CO_2-storage (after the CPG stage) performance metrics are evaluated and discussed in this study (in Section 4.3).

4.2.3.2 *Reservoir and operational parameters*

Furthermore, we vary some key reservoir and operational (non-reservoir) parameters, in a fixed range of 5%, from the upper and lower bounds of the base case conditions (presented in Table 4.1) to investigate the sensitivity of these parameters on the following performance metrics of the combined system described in the next section. The reservoir parameters (and

their respective base case values) that have been studied include, permeability (100 [mD]), anisotropy k_h/k_v (2.0 [-]), relative permeability (van Genuchten parameter of 0.77 [-]), and initial temperature (120 [°C]). The operational parameters (and their respective base case values) that have been studied include well diameter (0.14 [m]), average ambient surface temperature [15 °C], and CO_2 injection enthalpy (2.8×10^5 [J/kg]).

The simulations for each of the parameter spaces (reservoir and operational) considered in this study are run for a duration of 25 years for the CNGR stage and without considering the PE stage. The simulation results (high and low bounds) of the performance metrics for each respective parameter spaces, considered in this study, are compared to the simulation results of the base case example presented as Case 1-B (i.e. non-depleted natural gas reservoir without the PE stage). The comparison indicates the sensitivity on the performance metrics (m) for a 5% change (both high and low) in the value of the parameter space (X) from the base case value considered in this study. Mathematically, we represent this sensitivity value, σ, as

$$\sigma = \frac{\left(m_{\text{high}} - m_{\text{low}}\right)/m_0}{\left(X_{\text{high}} - X_{\text{low}}\right)/X_0} \tag{4.5}$$

m_0 and X_0 are the performance metric result and parameter for the base case. We chose $\left(X_{\text{high}} - X_{\text{low}}\right)/X_0$ = 10% (i.e. 5% both ways from the base case). This implies that Equation (4.5) becomes,

$$\sigma = 10 \cdot \frac{m_{\text{high}} - m_{\text{low}}}{m_0} \tag{4.6}$$

It should be noted that the non-reservoir parameters will have no effect on the natural gas recovery performance because this performance metric is only dependent on the reservoir conditions. Also, the sensitivity values obtained for the minimum CO_2 saturation in the well and CO_2-storage performance metrics do not show any significant changes with the 5% variation in parameter space. We, therefore, do not include the results for these two performance-metrics in our sensitivity analysis carried out in this study.

4.3 Results and discussions

4.3.1 Effects of residual CH$_4$ content and CO$_2$-plume establishment stage on the performance metrics

4.3.1.1 *CO$_2$ saturation and flow regime in the production well*

Here, we present the simulation results for the two main cases of a partially depleted (Case 1-A, B) and a depleted (Case 2-A, B) natural gas reservoir, which are represented by Figures

4.1a and b, respectively. At the time when we have the highest water saturation around the production well inlet, we consider whether the PE stage is critical to ensure annular flow in the bottom-hole region of the production wells. Recall that "A" denotes that the PE stage exists, whereas "B" denotes that the PE stage does not exist. Figure 4.3a shows that at the time of highest water saturation at the bottom-hole, the partially depleted NG reservoir cases show higher CO_2 saturation in the r reservoir and in the well than the depleted NG reservoir cases. Case 1-A has the highest CO_2 saturation in the reservoir and in the well. This is due to ease of gas connection between the production and injection wells in the case where there is higher residual methane and less water around the region of the wells. The PE stage also assists in ensuring that more CO_2 is the bottom-hole before the high flowrate is applied (after the CO_2-EGR stage) that leads to pressure drawdown sucking more water close to the production well region, which causes the CO_2 saturation in this region to reduce the minimum value (i.e. highest water saturation). The results in Figure 4.3a show that Case 2-B (depleted reservoir with no PE stage considered) has the highest water saturation (>70% in the reservoir and about 21% in the well) during this high flowrate-induced pressure drawdown. Furthermore, the simulation results (Figure 4.2) show that, at a fixed total production rate of 30 kg/s/well, Case 2-B, followed by 2-A, has the lowest mass fractions of gas (X_{g-well}) at the bottom of the production well. The lower the residual CH_4 content, after the CNGR stage (depleted reservoir), the higher is the probability that the production well experiences slug/churn flow. However, for relatively low diameter production wells (14 cm and 21 cm), annular flow is guaranteed even when the residual CH_4 content is very low (Case 2-A) and there is no PE stage (Case 2-B). As the production well diameter increases to 33 cm, Case 2-B (depleted reservoir with no plume establishment option) exhibits slug/churn flow at the bottom of the production well due to the low gas mass fraction (high water saturation) and low gas velocity in these large-diameter production wells, especially early on, when increasing the production mass flowrate to 30 kg/s/well. Hence, if the diameter of the production wells is relatively large (which is sometimes the case, in order to reduce production pressure losses), the CO_2 plume establishment stage is necessary/critical to include for depleted natural gas reservoirs. Alternatively, as discussed in Chapter 3, an optimal well size needs to be determined that will achieve and sustain the required minimum gas velocity, needed to carry the liquid water in the well to the land surface (achieving annular flow regime), while resulting in minimal pressure (and heat) losses in the well. However, our results show that partially depleted gas reservoirs quickly achieve a gas connection between the injection and the production wells, causing less water to enter the production well and maintaining annular flow for most applicable well sizes.
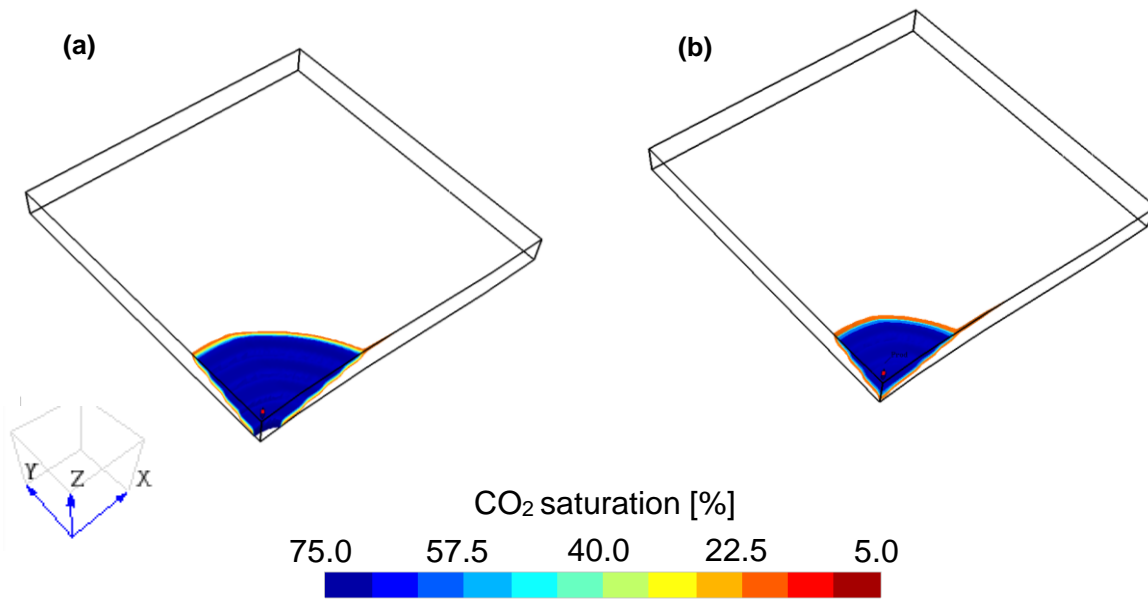
Figure 4.1: Quarter model showing the CO₂ saturation (after the CNGR stage) for the partially depleted (a) and depleted (b) natural gas reservoir model. Note that the part of the models with CO2 saturation less than 15% has been blanked. The simulation for the depleted gas reservoir is stopped when the liquid saturation at the production well region started to increase, whereas the simulation for the partially depleted gas reservoir is stopped (after 25 years of CNGR) when the production well region has not experienced any increase in the liquid saturation.
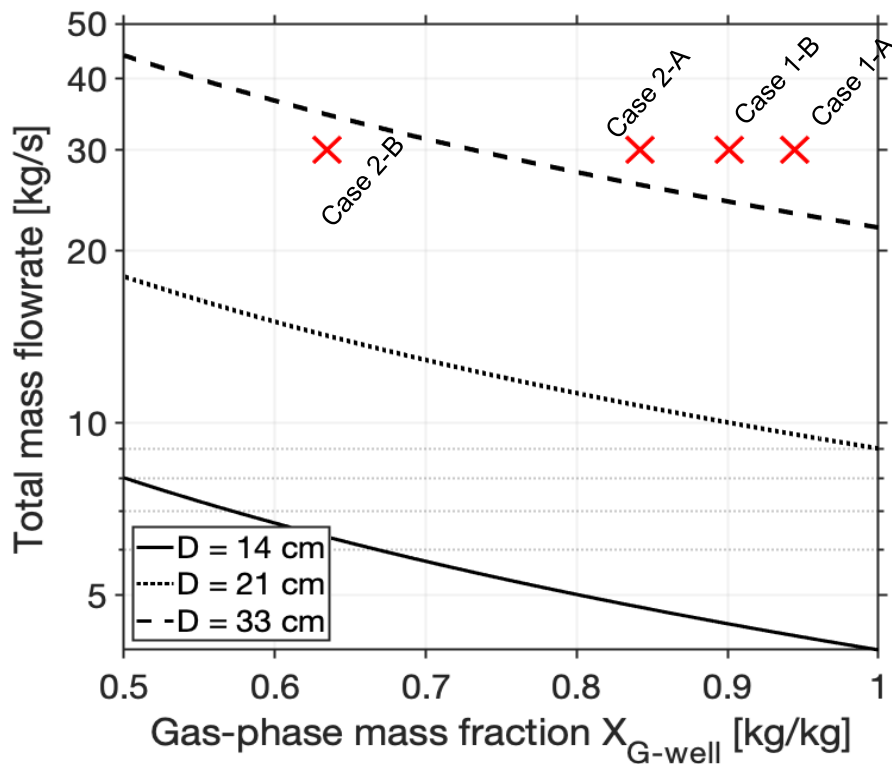
Figure 4.2: Flow regime plot showing the lowest gas-phase mass fraction points of the four cases. The lines indicate the minimum flowrate (at corrresponding gas-phase mass fractions) needed to achieve an annular flow regime for different well sizes. The right (top) side of the lines indicate the annular flow regime and the left (down) side indicates the slug/churn flow regime.

4.3.1.2 *Natural gas recovery performance (NGRP)*

In this study, natural gas recovery performance (NGRP) mainly refers to the natural gas produced during the CNGR stage and the CO_2-EGR stage (including the transition period (TP), i.e. the period before the CO_2 mass fraction (in gas phase) of the produced fluids reaches 90%), at a minimal (optimal) duration for the stages. This duration of natural gas recovery also includes the time of CH_4-CO_2 separation at the land surface. Here, we investigate the effect of residual CH_4 content (in terms of partially depleted or depleted natural gas – with and without CO_2-plume establishment) on the natural gas recovery performance.

Table 4.2: Simulation results of the percentages of the original gas in place (OGIP) that are recovered during the CNGR and CO_2-EGR+TP stages, and their associated natural gas recovery index (RI). The RI is calculated to assess the natural gas recovery performance of the 4 cases considered in this study.

Cases	%OGIP recovered at CNGR stage	%OGIP recovered at EGR+TP stage	Total %OGIP recovered, F_{UR}	Duration of CO_2-EGR+TP stage (year)	Total duration of NG recovery (year)	RI (%/year)
Case 1-A: 25 years w/PE	83.51	3.48	86.99	1.50	28.50	3.28
Case 1-B: 25 years no PE	83.51	7.43	90.94	3.82	28.82	3.16
Case 2-A: 26 years w/PE	86.85	0.63	87.48	2.00	28.00	3.12
Case 2-B: 26 years no PE	86.85	2.84	89.69	2.97	28.97	3.10
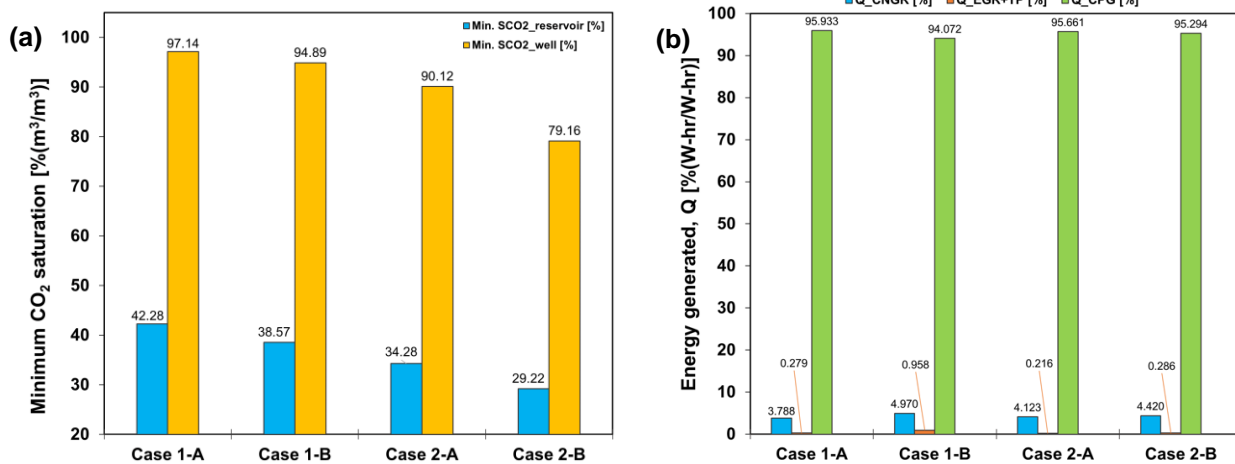
Figure 4.3: Simulation results, for the four cases representing different residual CH_4 content with/without CO_2-plume establishment, showing (a) the minimum CO_2 satiration in the reservoir and in the well at the time high pressure drawdown and maximum water saturation are observed at the production well (borrom-hole), b) the precentage of the total net geothermal electricity generated during the three main stages of the project.

The simulation results show that natural gas recovered during the CNGR is greater for the depleted reservoir scenario (Table 4.2). Case 2 achieves a CNGR factor of 86.44%, which is higher than that of Case 1 (82.97%). This indicates that the residual CH_4 content for Case 1

is higher than Case 2 by approximately 3.50%. The gas recovery during the CO_2-EGR stage is higher for the cases without CO_2-plume establishment (Case 1-B and Case 2-B). This is because of the relatively higher CO_2-CH_4 mixing rate that is associated with the CO_2-plume establishment stage, which may slightly reduce natural gas recovery during the CO_2-EGR stage. This implies that, the combined system that is not associated with the PE stage yields better ultimate natural gas recovery than when the PE stage is planned for the combined system.

Table 4.3: Simulation results of the net geothermal electricity generation and CO_2 storage performance metrics, at the different stages of the combined system, calculated for the 4 different cases (considering residual methane content and CO_2-plume establishment). Note that the average net power for each stage (calculated using the power model described in Ezekiel et al., 2020) and the durations of the different stages are used to calculate the average net electricity generated (in GW_eh).

Cases	Net electricity generated at CNGR stage [GWeh]	Net electricity generated at CO_2-EGR+TP stage [GWeh]*	Net electricity generated at CPG stage [GWeh]**	Total net electricity generated during the project [GWeh]	Amount of CO_2 stored [Mtons]
Case 1-A: 25 years w/PE	9.163	0.676	232.048	241.887	5.85
Case 1-B: 25 years no PE	9.163	1.767	173.443	184.373	5.10
Case 2-A: 26 years w/PE	9.246	0.484	214.514	224.244	6.30
Case 2-B: 26 years no PE	9.246	0.599	199.342	209.184	5.43

* the duration of the respective CO_2-EGR+TP stage, for each of the 4 cases, is given in Table 4.2.

** the duration of the respective CPG stage, for each of the 4 cases, is calculated as: the end year – the durations of the CNGR and CO_2-EGR+TP stages.

Furthermore, the average annual recovery index (RI), which is used to assess the natural gas recovery performance of the combined system, is important because it accounts for the duration of CO_2-CH_4 separation. A higher value of RI indicates a less duration of CO_2-CH_4 separation and a faster build-up of the CO_2 plume in the natural gas reservoir (such as observed in Case 1-A). From Table 4.2, for both the depleted and non-depleted NG reservoir, when the PE stage is considered, we observe a decrease in the number of years for the expensive separation period in the CO_2-EGR+TP stage, but it has a lower natural gas recovery factor. However, when the recovery index is calculated we see that the cases with PE has the higher recovery index. For the non-depleted reservoir, the index shows that the expensive separation duration was reduces from 3.82 years to 1.50 years (although there is 1.5 years of only CO_2 injection) when the PE stage is considered, and this leads to a better performance for the Case 1-B than Case 1-A (without PE stage) with a difference of 0.12 in the average annual recovery index (i.e. ΔRI). For the depleted reservoir, there is a slight increase in NG production performance with a 0.02 change in the ΔRI. Hence, the simulation results show that the partially depleted reservoir, with the PE stage considered (Case 1-A),

will achieve the most favorable natural gas recovery performance out of the 4 cases considered in this study.

The implication of planning the CPG (with the PE stage) before the natural gas is depleted can be favorable. It can result in a significant higher natural gas production performance (including lower expenses and parasitic power losses needed in the CH_4-CO_2 separation phase), even though a slight decrease in ultimate natural gas production is observed. When the gas reservoir is gas depleted, there is no clear improvement in the NG performance if the PE stage is included. Hence, the PE stage may not necessary for deep depleted natural gas reservoirs with respect to the proposed combined system.

4.3.1.3 *Geothermal energy (electricity) generation and CO_2-storage performance*

The simulation results, in Table 4.3, show that the average total net geothermal energy (in GW_eh), from the combined system, decreases as the reservoir becomes depleted of natural gas (i.e. from Case 1-A to 2-A and from Case 1-B to 2-B), independent of whether a CO_2-plume establishment stage exists. It has been reported (in Zhang et al., 2017) that the residual CH_4 content may reduce the geothermal energy extraction performance of supercritical CO_2 in a natural gas reservoir. However, in this study, the most of the residual CH_4 is removed from the reservoir (during the CO_2-EGR stage, till 90% XCO_2 is reached at the production well), which would lead to an increase in the volume of natural gas recovered. The average net geothermal energy (during the CO_2-EGR stage), generated by extracting the heat contained in the produced (or separated) natural gas, will increase because of the increased volume of natural gas recovered. Hence, the energy generated during the CNGR and CO_2-EGR+TP stages is dependent on the volume of the OGIP recovered during these stages.

During the CNGR stage, the amount of natural gas produced and the duration of the CNGR stage for the depleted reservoir cases is greater than the partially depleted NG reservoir cases by 3.35% (Table 4.2). This leads to a higher energy generated for the depleted reservoir cases than the partially depleted reservoir cases, as shown in Table 4.3 and Figure 4.3b.

During the CO_2-EGR+TP stage, the cases with the PE stage has lesser duration and thus lesser energy generated than the cases without the PE stage (Table 4.2 and Table 4.3). However, the lesser duration is favorable to minimize the parasitic power losses associated with longer duration of CO_2-EGR+TP stage where the CH_4-CO_2 mixture needs to be separated at the land surface. The depleted NG reservoir generated lesser energy than the partially depleted NG reservoirs because of the higher natural gas %OGIP observed for the latter (see Table 4.2). In the CO_2-EGR+TP stage, Case 1-A (partially depleted with no PE stage) has the highest energy generated (due to longer duration of the CO_2-EGR+TP stage) compared to the other cases considered in this study, with an average net power and average net energy generated of 52.82 kW_e and 1.77 GW_eh (for 3.82 years) respectively.

Table 4.2 and Table 4.3 show that Case 1-A, with the lowest duration of the CO_2-EGR+TP stage (1.50 years), has the highest value of the geothermal energy generated (243 GW_eh for 28 years) during the CPG stage. This is as a result of the shorter the duration of the CO_2-EGR+TP stage, which ensures an earlier start of the CPG stage. This leads to a longer duration for the CPG stage and, hence, better electric energy generation performance (Figure 4.3b).

Table 4.3 also shows that depleting the NG reservoir and then carrying out CO_2-plume establishment, as seen in Case 2-A, increases the amount of CO_2 that is ultimately stored in the reservoir. This case achieves the highest amount of CO_2 stored (6.30 Mtons) and we obtain a difference of about 0.45 Mtons of CO_2 stored when compared to the partially depleted reservoir with CO_2-plume establishment (Case 1-A).

Of all four cases considered, the combined CO_2-EGR–CPG system, in a partially depleted reservoir, including a PE stage, yields the best results in terms of: (i) the annular flow regime in the production well, (ii) the natural gas recovery performance (including having the least duration of the CO_2-EGR+TP stage), (iii) the average total net electricity generation performance, and (iv) second to the highest amount of CO_2 stored during the entire project duration. Hence, planning the combined CO_2-EGR–CPG system (associated with the PE stage) to commence before the natural gas reservoir is completely gas-depleted could be the most favorable and optimal scenario for the future development of the combined system.

4.3.2 Effects of reservoir and operational parameters on the performance metrics

4.3.2.1 *Natural gas recovery performance*

Recall that this performance metric is only dependent on the changes in the reservoir parameter spaces and it is not influenced by the other non-reservoir parameters. Figure 4.4 shows the sensitivity of the reservoir parameters considered in this study on the natural gas recovery performance for the durations of the CNGR and CO_2-EGR+TP stages (when natural gas is being produced and methane is separated from CO_2). The parameters plotted on the upper part of the horizontal logarithmic axis (Figure 4.4) indicate those with a positive sensitive value (σ), and those parameters that are plotted on the lower part of the axis have a negative σ. A positive (+) value of σ shows that there is an increase in the NGRP when the value of the parameter space increases and vice versa. A negative (−) value of σ indicates that there is a decrease in the NGRP when the value of the parameter space increases and vice versa.

The sensitivity results, plotted in Figure 4.4, show that permeability anisotropy and reservoir temperature are the most sensitive parameters (~ 0.2) with respect to the NGRP, with both having different signs for their sensitivity values. We observe that as permeability

anisotropy increases, the NGRP significantly decreases (i.e. negative σ value). However, an increase in reservoir temperature would lead to a significant increase in the NGRP. The horizontal permeability parameter is the least sensitive parameter, for the NGRP, and its sensitivity value (+) significantly varies from the most sensitive parameters (permeability anisotropy and reservoir temperature) by 2 orders of magnitude.
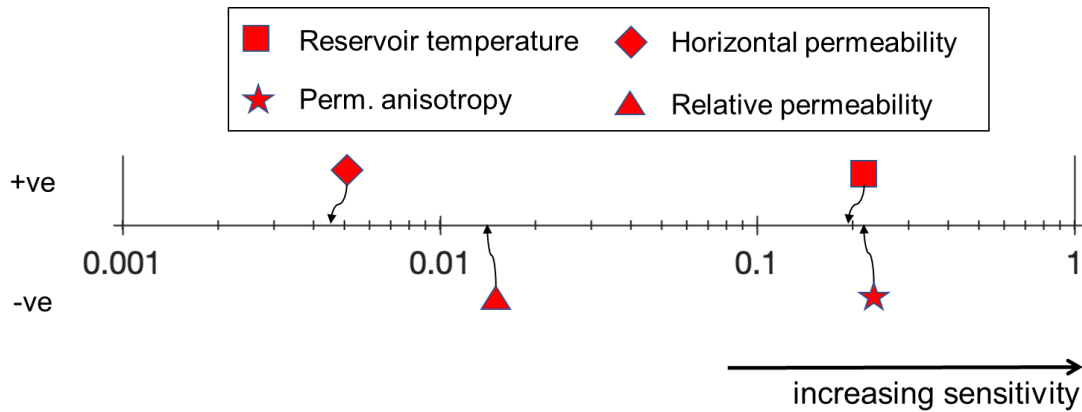
Figure 4.4: Sensitivity values (plotted on a logarithmic axis) of the natural gas recovery performance metric for the reservoir parameter-spaces considered in this study. This is only calculated during the CNGR and CO2-EGR+TP stages, when natural gas (mostly methane) is produced and methane is separated from the produced mixed CH_4-CO_2 fluid. The positive (upper) part signifies parameters when being increased by 10% will result in an increase in their performance metric values, and the negative (lower) part identifies parameters when being increased by 10% will result in a decrease in their performance metric values when they increase.

4.3.2.2 *Geothermal-energy (electricity) generation performance*

During the CNGR stage, the average net power and electricity generated by the base case are 0.042 MW_e and 9.16 GW_eh for 25 years. The time series plots of the simulation results showing the net power generated can be found in Appendix C. Figure 4.5 shows that the most sensitive parameter that influence the net electrical geothermal energy generated in this stage is the reservoir temperature (σ = +5.0), followed by the mean surface ambient temperature. We observe that the net energy generated increases with increase in reservoir temperature (positive σ) but decreases with an increase in the mean surface ambient temperature (negative σ). The permeability anisotropy parameter is the least sensitive parameter to this performance metric during the CNGR stage. The sensitivity value (+0.0015) varies by 3 orders of magnitude from that of the reservoir temperature parameter. Figure 4.5 also shows that during the CNGR stage, changes in the other parameters considered in this study will have lesser effects on the geothermal energy generation performance, with their $\sigma < \pm 0.1$.
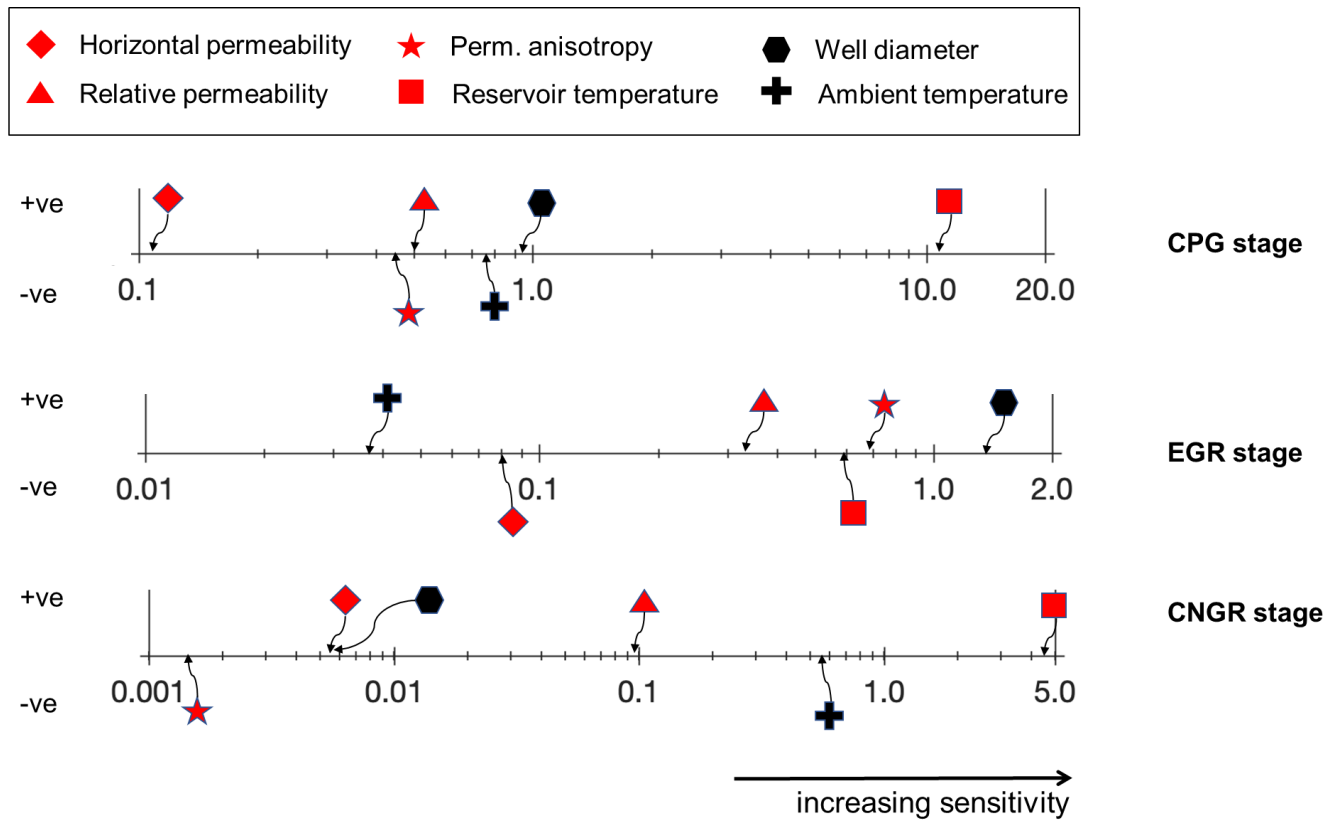
Figure 4.5: Sensitivity values (plotted on a logarithmic axis) of the geothermal-energy generation performance metric for the reservoir and operational parameter-spaces considered in this study. This is calculated for the three main stages of the combined system. The positive (upper) part signifies parameters when being increased by 10% will result in an increase in their performance metric values, and the negative (lower) part identifies parameters when being increased by 10% will result in a decrease in their performance metric values when they increase.

During the CO_2-EGR+TP stage, the average net power and the electricity generated are 0.053 MW_e and 1.78 GW_eh (for 3.82 years). From Figure 4.5, we observe that the most sensitive parameter, for the CO_2-EGR+TP stage, is the wellbore diameter, with σ = +1.50. This is because in the stage, the CO_2 mass fraction increases, leading to a higher density of the fluid flowing in the well, causing higher pressure (frictional) loss as the well diameter decreases. This significantly decreases the energy extractable from the produced/separated methane. The least sensitive parameter is the mean ambient surface temperature, with σ = +0.028. From Figure 4.4, we observe that anisotropy and temperature have the highest sensitivity on NGRP, and this directly influences the high sensitivity results of the energy generated achieved by these two parameters during the CO_2-EGR+TP stage, because the energy generated (at this stage) is proportional to the volume of natural gas produced and the duration of the CO_2-EGR+TP stage.

During the CPG stage (when the CO_2 mass fraction is >90% and only the direct CO_2-thermosiphon power system model is used), the average net power and the geothermal energy generated for the base case (i.e. Case 1-B described in Section 4.3.1.3) are 0.739 MW_e

and 173.44 GW$_e$h (for 27.18 years). This is about 14.0 – 17.5 times higher than the average net power generated during the CNGR and CO_2-EGR+TP stages, respectively. This is due to the use of the direct power system and the increase in production mass flowrate from 4 kg/s to 30 kg/s applied during this stage. Note that the energy generated by the other cases (Cases 1-A, 2-A and B) considered in this study (in Section 4.3.1.3) are greater than the base case (Case 1-B) used for parameter space sensitivity study.

The most sensitive parameter for this stage is reservoir temperature, with a sensitivity value $\sigma > +10.0$. Wellbore diameter and the mean surface ambient temperature also show high sensitivity values, during the CPG stage, because as the wellbore diameter increases (at relatively high flowrate) the pressure and heat losses decrease, while lower mean surface ambient temperature favors higher net energy extraction and power generation at the turbine. The least sensitive parameter, in this stage, is the horizontal permeability with about 2 orders of magnitude lower sensitive than the reservoir temperature parameter. In this study, we can observe that reservoir temperature is the most important parameter for the combined system, especially during the CNGR and CPG stages. It is also important to point out that these two parameters, wellbore diameter and relative permeability, have positive sensitivity values of the geothermal electricity generation performance metric for all the 3 stages considered in this study.

4.4 Conclusions

We have presented a reservoir simulation study to investigate the effects of residual CH_4 content and the CO_2-plume establishment (PE) stage on sustaining annular flow regime, when a relatively high production mass flowrate is used in a combined CO_2 enhanced gas recovery (EGR) – CO_2 plume geothermal (CPG) system. In addition, the sensitivity of some key reservoir and operational parameters on the natural gas recovery, geothermal energy generation and CO_2 storage performances of the combined system have been investigated. Our key results and findings are:

Minimum CO_2 saturation and flow regime in the production well (bottom-hole):

The simulation results show that partially depleted natural gas reservoir case (with the PE stage considered) achieves the highest CO_2 saturation (in the reservoir and in the well) at the time of high-pressure drawdown caused by increase in the production flowrate. Furthermore, at a relatively high production mass flowrate (about 30 kg/s/well) and large well diameters (from 33 cm), the depleted natural gas reservoir case (without the CO_2-plume establishment option) experiences slug/churn flow near the bottom of the production well, due to the low gas mass fraction and low gas velocity. However, the partially depleted natural gas reservoir case quickly achieves a gas connection between the injection and the

production wells, leading to less water entering the well, maintaining the desired annular flow regime in the production well for most applicable well sizes.

Natural gas recovery performance:

The simulation results show that, the partially methane-depleted reservoir case, with the PE stage considered, achieves the most favorable natural gas recovery performance (during the entire project duration), because it has the highest recovery index due to relatively high ultimate recovery factor and the shortest duration of the required CO_2-CH_4 separation.

The simulation results also show that, out of the 4 reservoir parameters considered in this study, permeability anisotropy and reservoir temperature are the most sensitive parameters that any changes in their values lead to significant change in the NGRP of the combined system. The horizontal permeability parameter is observed as the least sensitive parameter, for the NGRP, and its sensitivity value significantly varies from the most sensitive parameters (permeability anisotropy and reservoir temperature) by 2 orders of magnitude.

Geothermal electric power generation and CO_2 storage performances:

The higher the natural gas recovery, during the CNGR stage, the better is the geothermal energy extraction performance during this stage. Recovering and separating the residual CH_4, up to 90% CO_2 mass fraction, leads to an increase in the volume of natural gas recovered and, hence, the average extractable geothermal energy (to be converted to electric power), during the CO_2-EGR+TP stage, increases. However, the natural gas reservoir model cases, with no PE stage, have longer durations of the CO_2-EGR+TP stage than those that include a PE stage, causing a delay in the start of, and ultimately a decrease in the geothermal energy generation performance, of the CPG stage. This indicates that a shorter duration of the CO_2-EGR+TP stage, achieved by including a PE stage, serves as an important transitional stage for later CPG operations, due to the quick increase in the reservoir's CO_2 saturation and fast establishment of a CO_2 connection between the injection and the production wells. A gas-depleted reservoir (i.e. lower residual CH_4 content after the CNGR stage), associated with the PE stage, has the most favorable effect on the amount of CO_2 stored (CO_2 storage performance) in the reservoir.

Evaluating the sensitivity of the key reservoir and operational parameters, considered in this study, with respect to the geothermal energy generation performance, we observe that:

(a) during the CNGR stage, the most sensitive parameter is the reservoir temperature followed by the mean surface ambient temperature. The reservoir anisotropy parameter is the least sensitive parameter.

(b) during the CO_2-EGR+TP stage, the most sensitive parameter is the wellbore diameter, while the least sensitive parameter is the mean ambient surface temperature.

(c) for the CPG stage, shorter CO_2-EGR+TP stage duration ensures an increase in the CPG stage duration, yielding better geothermal energy generation of the combined system during this stage. The most sensitive parameter for the CPG stage is the reservoir temperature, with wellbore diameter and the mean surface ambient temperature also showing relatively high sensitivity values. The least sensitive parameter, in this stage, is the horizontal permeability.

In summary, the simulation results obtained in this study has revealed that the PE stage is very important for the combined system because it enables the natural gas reservoir to achieve a higher value for the minimum CO_2 saturation at the time of high pressure drawdown and an annular flow regime for all applicable wells sizes. Also, when the PE stage is applied to the partially depleted natural gas reservoir case, we achieve the most effective implementation strategy, for the combined CO_2-EGR–CPG system. Considering PE stage for a methane-depleted natural reservoir case leads to the best CO_2 storage performance of the combined system. These preliminary results also reveal that the most sensitive parameter that leads to a change in the performance metrics (natural gas recovery and geothermal power generation performances) is the reservoir temperature.

<div align="right">

5

</div>

Conclusions and Outlook

_____

5.1 Conclusions

In this thesis, we presented the novel combined CO_2-EGR–CPG system as a technology that can simultaneously extract natural gas and geothermal energy, for power generation, from a deep, high-temperature natural gas reservoir. Also, CO_2 is simultaneously stored in this natural gas reservoir. We carried out a feasibility study of the combined system, using the defined implementation process and identified the potential benefits associated with the combined system. The natural gas recovery and power-generation potentials of the combined system have been investigated using a coupled reservoir, wellbore and power-plant model. We also developed a method to define the design criteria for the production wells of the CPG system (a component of the combined system) to ensure higher productivity of the heated CO_2. A parameter-space optimization study has also been carried out to identify the key reservoir (uncontrollable) and operational (controllable) parameters and their effects on the overall performance of the combined system.

In the first study of this thesis, we presented an overview of the combined system, listing the potential synergies associated with the combined system. The potential synergy benefits of the proposed system could include: (i) increasing the natural gas field's total producible energy; (ii) using the generated geothermal electricity to power some of the operational facilities of the gas field, which increases the overall system efficiency; (iii) sharing some of the existing infrastructure (surface facilities, wells, etc.) and jointly utilizing multidisciplinary datasets (on reservoir parameters), (iv) thereby reducing investment costs significantly. The combined system also enables CO_2 Capture and Storage (CCS) by providing energy for, and compensating for the cost of CCS, and/or CO_2-EGR. Furthermore, the useful lifespan of the gas field is extended, thereby postponing the expensive clean-up, plugging of wells, and abandonment phases of the gas field and reusing otherwise stranded assets. A coupled reservoir, wellbore and power-plant model enabled us to present an optimized example of the combined system (which is scalable) and simulations were carried out to assess the technical feasibility of the proposed system in co-producing natural gas

and geothermal energy for power generation. We also established that the combined system can easily be adapted and optimized for real application in an existing gas field. The main takeaway from the results of the first study include:

- The results show that combined system can potentially contribute to the concept of valorization of CO_2. We have shown that the combined system enables the use of CO_2 for the application in Enhanced Gas Recovery (EGR) (over 1.5 years) and (predominantly, over 35 years) CO_2-based geothermal power generation, and subsequent geologic storage of the CO_2 in deep natural gas reservoirs. Hence, the combined system constitutes a Carbon Capture double-Utilization and Storage (CCUUS) system, where 100% of the underground-injected CO_2 is ultimately permanently geologically stored.

- The simulation results show that the CO_2-EGR can serve as an important transitional stage for CPG. This is because of the displacement of the remaining natural gas, and a quick establishment a CO_2 connection between the CO_2 injection and production wells is observed. Hence, this further informs us that deep natural gas reservoirs (depleted or partially depleted) can be particularly well-suitable for CPG (pilot or later commercial) system developments.

- Our simulations of a coupled reservoir-wellbore-power model show that the average geothermal net electricity generated, by the 4 production wells, is highest during the CPG stage (1.58 MW_e over 35 years). A peak geothermal net electricity generation rate of 2.00 MW_e during the CPG stage was achieved.

- The simulations showed that, during the CPG stage, four times more electric power is generated using the direct (thermosiphon-based) CO_2 turbine expansion system than when the indirect (ORC-based) system is used. Hence, this corroborates the findings of some existing studies that the direct CO_2 turbomachinery generates higher electric power output than those of indirect systems.

- The simulation results also show that all the external CO_2 injected during the CO_2-EGR stage is permanently stored in the reservoir. More CO_2 could likely be stored both during the CPG and during a post-CPG stage, depending on the reservoir storage capacity. About 16 million tons of CO_2 are eventually permanently stored in our example natural-gas reservoir model. Given that the natural gas had been safely stored over long geologic times before natural gas extraction commenced, it is likely that the integrity of the caprock and the safety of the stored CO_2 is assured for millions of years.

- The example-model employed in this study, is highly scalable, which indicates that the proposed system should be considered for real applications, as it can be readily implemented in oil/gas fields with deep natural gas reservoirs to produce additional, significant energy (electric power). Furthermore, more net electric power can likely

be generated, where larger and optimized reservoir development strategies (e.g. number of wells, well placement, production rates, etc.) are employed.

Following the first study, we carried out a numerical investigation into the importance of designing the CPG-component of the combined system by optimizing the production flowrate, to (i) minimize the amount of water entering the production well, (ii) maintain annular flow in the production well, and (iii) maximize the power generated. The key results of this study include:

- A flow-pattern transition method used to determine the flow regime for a CO_2-water system in a vertical production well, at different total mass flowrates and CO_2 mass fractions, was presented.

- The results show that the minimum total mass flowrate required to achieve annular flow in the production well decreases with increase in the CO_2 mass fraction and decrease in wellbore size. For the base-case example considered in this study, the minimum CO_2 flowrate required to achieve an annular flow regime shows a significant decrease (from 25 kg/s to 3 kg/s) with decreasing wellbore diameter (from 0.33 m to 0.11 m).

- We estimated that for a CPG production well to achieve annular flow, the minimum superficial CO_2 velocity should be equal to or greater than 0.45 m/s for reservoir depths greater than about 1500 m, and between 0.45 and 0.70 m/s. for shallower reservoir depths between 1500 m and 800 m. When the CO_2 saturation (in the production well) is 50%, the minimum bulk velocity is calculated to be twice the values of the corresponding minimum superficial CO_2 velocity, and they are equal when the CO_2 saturation is 100%. Hence, we can easily determine the minimum (bulk or CO_2) flowrate necessary to achieve annular flow using these values at any given depth and mass/volume fraction of water/ CO_2 in the CPG production well.

- Using the reservoir properties and well size at the Cranfield site, we were able to provide an insight into one of the reasons why the CO_2 thermosiphon test for the Cranfield site failed. We estimated that the minimum CO_2 flowrate required to achieve annular flow in Cranfield's production well is about 2 kg/s higher than the maximum flowrate achieved in the field test during the venting stages, and thus, not enough to maintain the expected annular flow in the production well.

- The base-case simulation results, using a coupled reservoir-wellbore-power model, show that slug/churn flow may occurs at the start of the CPG stage due to the highest water production associated with this time. The slug/churn flow in the production well causes pressure fluctuations, undermines the thermosiphon, and leads to a

higher fluid density in the borehole and lower pressure at the land surface. Hence, this may result in a decrease in the power output of the direct CPG power system. Installing a pump may be necessary to maintain the required flowrate. If the flowrate is maintained, the amount of water entering the well goes down with time.

- The simulation results show that the controllable (operational) parameters should be optimized for any given reservoir characteristics to achieve an annular-regime flowrate and maximize a combination of power output and lifetime (heat-depletion rate) of the geothermal system.

- At fixed mass flowrate (or downhole pressure difference), the CO_2 velocity is seen to decrease with increasing well diameter, which could lead to slug/churn flow in the production well. However, small well diameters yield high fluid pressure and heat losses, which results in lower power generation. Hence, to optimize the CPG system, a production-well diameter that can achieve annular flow, while minimizing pressure and heat losses in the production well is sought. In our study, the production-well diameter of 0.21 m resulted in an optimal fluid flowrate.

- Varying the admissible reservoir-pressure reduction in the system, our simulation results show that there is a tradeoff between high flowrate and water entering the well. The higher the reservoir-pressure reduction, the higher the achieved flowrate, which may draw higher amount of water entering the well. However, the high flowrate (associated with a high CO_2 velocity) could be high enough to carry the water out of the well. In addition, higher flowrates lead to higher heat depletion rates of the reservoir and lowers the power plant lifetime.

- Finally, for this study, the simulation results for the reservoir-parameter (uncontrollable) sensitivity analyses show that lower vertical permeabilities (i.e. stronger anisotropy) lead to a reduced water-upconing effect. This allows for higher flowrates, but the power plant lifetime decreases. The shapes of the relative permeability curves influence the relative amounts of CO_2 and water entering the well. Hence, good measurements of these relative permeability curves for any specific rock are important for predicting the success of the CPG system.

The third study involves a reservoir simulation (sensitivity) study to investigate the effect of different reservoir and operational parameters on the natural gas recovery, geothermal energy (electricity) generation and CO_2-storage performances of the combined CO_2-EGR–CPG system. The natural gas recovery performance is measured by the recovery index (RI), which is amount of gas recovered divided by the duration of the project life cycle (before the start of the CPG stage). Also, we investigated the the effects of residual CH_4 content and

the CO_2-plume establishment (PE) stage on sustaining annular flow, and on the above-mentioned performance metrics, when a relatively high production (base-case) mass flowrate of 30 kg/s/well is used. The key findings of this study include:

- At the base-case mass flowrate of 30 kg/s/well, the depleted natural gas reservoir model example (i.e. lower residual CH_4 content) without carrying out the PE stage will experiences a slug/churn flow at the start of the CPG stage when the well diameter increased to 0.33 m. The reason for this has been reported in the point #2 of the second study (described above) that the minimum total mass flowrate (and superficial CO_2 and bulk velocities) required to achieve annular flow increases as the wellbore size increases. However, the simulation results also show that, when the PE stage is carried out first before the CPG stage commences, the depleted reservoir model example will achieve annular flow (for all well sizes).

- The partially depleted reservoir model example achieves annular flow in the production well for all the cases of all applicable wellbore sizes, with or without carrying out the PE stage. This is because the high residual CH_4 content and the CO_2-EGR process quickly enables a quick gas connection between the production and injection wells and lowers the water saturation around and in the production well.

- Carrying out the PE stage leads to a decrease in the duration of the mixed CO_2-CH_4 production and separation. Thus, an increase the overall natural gas recovery performance (NGRP) of the combined system is achieved for both the partially methane-depleted and partially depleted reservoir model examples. the partially methane-depleted reservoir case, with the PE stage considered, achieves the most favorable NGRP.

- The simulation results show out of the 4 reservoir parameters considered in this study, permeability anisotropy and reservoir temperature are the most sensitive parameters to NGRP of the combined system. The horizontal permeability parameter is observed as the least sensitive reservoir parameter.

- The simulation results show that the natural gas reservoir model cases, with no PE stage, have longer durations of the CO_2-EGR+TP stage than those that include a PE stage. This causes a delay in the start of the CPG stage and ultimately a decrease in the geothermal energy generation performance for these two cases that do not consider the PE stage. This implies that, for the combined system, the PE stage is important to achieve higher energy generation performance.

- The simulation results also show that natural gas reservoir example cases that considered the PE stage have the best CO_2-storage performance when compared to the reservoir examples cases that do not consider the PE stage.

- With respect to geothermal energy generation performance, the sensitivity simulation results of the key reservoir and operational parameters show that reservoir temperature is the most sensitive parameter during the CNGR and CPG stages. The reservoir anisotropy and the horizontal permeability parameters are the least sensitive parameters for the CNGR and CPG stages respectively. During the CO_2-EGR+TP stage, the most sensitive parameter is the wellbore diameter, while the least sensitive parameter is the mean ambient surface temperature.

5.2 Outlook

To further enhance the applicability and optimization of the combined system, the following future studies are recommended:

- More studies are needed to completely understand these complicated CO_2/CH_4-water-rock interactions, and ways to reduce the associated negative effects, especially during CO_2 injection into a depleted or partially depleted natural gas reservoir. Several studies have investigated the influence of complicated interactions between CO_2, formation water, and host rock and their effects on the reservoir properties, CO_2 injectivity and storage capacity for CO_2-based EGR, CPG and carbon storage processes in saline aquifers and partially depleted and depleted natural gas reservoirs (Cui et al., 2015, 2017b, 2017a; Kim et al., 2012; Xu et al., 2014). The general conclusion is that the fluid-rock interactions during geothermal exploitation could cause severe reservoir damage and limit the heat-mining performance of the injected CO_2. Specifically, the backflow of the formation water towards the injection well, caused by rapid evaporation of formation water and the resulting high capillary-pressure gradient, can lead to salt precipitation and reduced permeability in the area close to the injection well (Cui et al., 2016, 2015).
- Monitoring and verifying any environmental safety concerns associated with the combined system is very important for the success of this proposed technology. CO_2 may leak to the surface or to a freshwater aquifer through faults or abandoned wells (Nogues et al., 2011; Jung et al., 2013). During CO_2 injection, regular measurements, for example, reservoir temperature and pressure changes, are necessary to monitor the migration process of CO_2, reservoir overpressure that could affect caprock integrity, fault reactivation etc. (Xu et al., 2014; Liu et al., 2016; Zbinden et al., 2017). The caprock integrity and safety of the injected CO_2 into the natural gas reservoir need to be investigated at the end of the CPG stage of the combined system. Hence post-CPG (hydromechanical) simulations are necessary to assess the caprock integrity and ensure the permanent safe storage of the injected CO_2.

- Numerical simulations for a parameter-space sensitivity study, with an improved coupled reservoir-wellbore-power model, is essential to determine the power-generation potential of the combined system. Coupled with the results of this thesis, these can serve as a preliminary guideline for screening and selecting natural gas reservoirs and optimal operational parameters suitable for the higher natural gas recovery, power generation and CO_2 storage capacity.

- Using commercial (coupled) reservoir and wellbore simulators, real-field high-temperature natural gas reservoirs (models) could be used as case studies, which also incorporates reservoir heterogeneities, complexities and uncertainties, to further assess the performance of the combined system.

- Planning of the combined CO_2-EGR–CPG system, at the early stages of the natural gas-reservoir development, could be very useful for maximizing the output of the system. The best development schemes can be identified for the given reservoir types and conditions at the early stage of the natural gas reservoir's life, and the facilities installed in the field can be adequately adapted, at the early stage, at less overall cost and risks. Hence, the most favourable development strategies, using a real-field natural gas reservoir as a case study, should be investigated.

- Techno-economic assessment of the combined system is important before an actual field implementation. The energy gained and the saved investments costs, carbon credits, including the increased useful lifetime of the gas field, needs to be weighed against the costs of running the combined system. This assessment can also help to identify areas where energy losses in the combined system's loop can be eliminated and to develop scenarios to further optimize the energy and economic benefits of the combined CO_2-EGR–CPG system.

Appendix to Chapter 2

_____

A.1 Power-flowrate analysis

Adams et al. (Adams et al., 2015) showed that the power generated by a CPG system varies substantially, depending on the circulating CO_2 mass flowrate. Depending on the mass flowrate, the power can be substantially reduced from the optimum or even become negative. Thus, the mass flowrate of a CPG system should be the result of an optimization study and not merely selected.
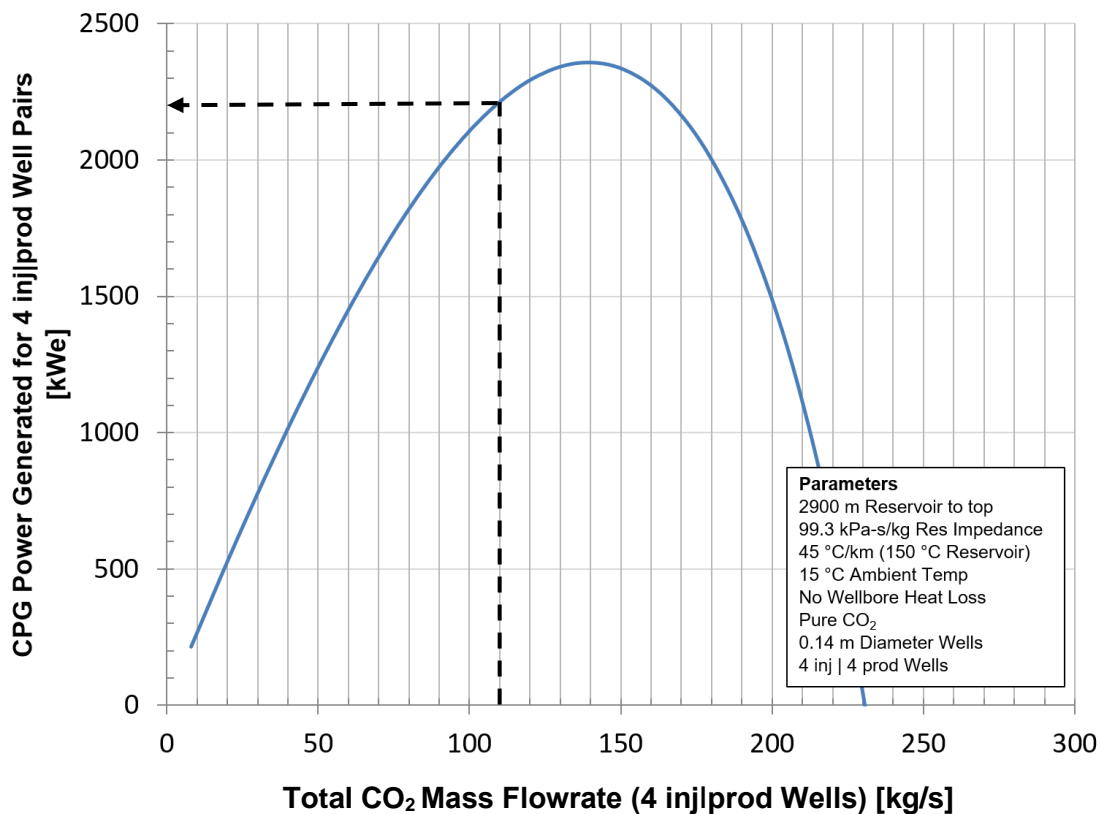
Figure A.1: CPG power generated for 4 injection-production well pairs versus total CO_2 mass flowrate without considering heat transfer in the wellbore. The dotted black line indicates the total production rate (110 kg/s) used in the study, which gives a CPG power of 2.20 MWe.

For instance, Figure A.1 shows the CPG power generated versus CO₂ mass flowrate for a system that is similar to that examined here, with a 2.9 km deep reservoir, 45 °C/km geologic temperature gradient, 0.14 m well diameter, and a 99 kPa-s/kg reservoir impedance. The result of this simplified simulation is a CPG power generation of 2.40 MWₑ at an optimum mass flowrate of 140 kg/s. Thus, in the numerical simulation example considered in this study, a CPG circulation rate of 27.5 kg/s is selected, equivalent to 110 kg/s for all four injection and production wells. Wellbore heat transfer is not considered in this example CPG power generation calculation (Figure A.1).

A.2 Examples of wellbore heat loss for different CO₂ versus methane mass fractions

Figure A.2 shows an example plot of production wellhead temperature and pressure for different mass fractions of CO₂, ranging from 0 to 1 (i.e. from all methane to all CO₂). The initial reservoir conditions (bottom-hole), at a depth of 3 km, are set at 150 °C and 30 MPa.
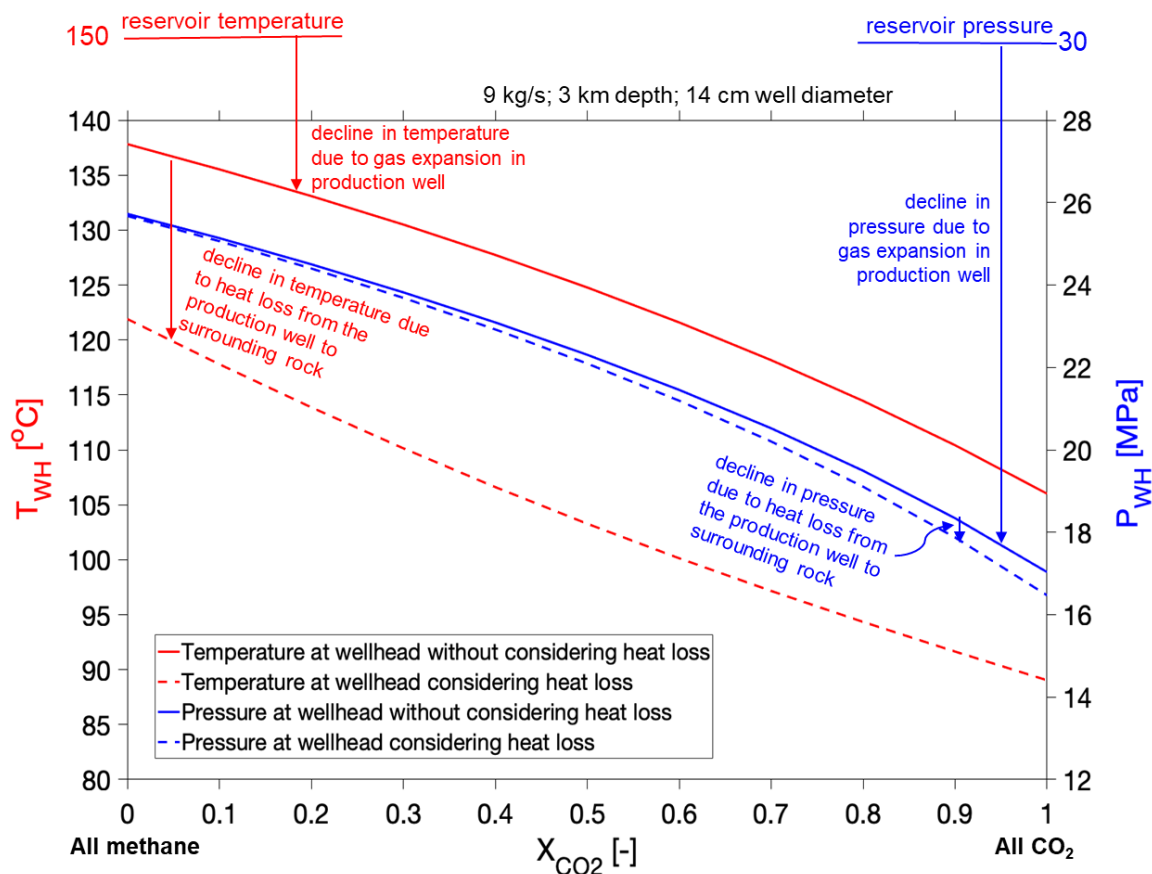
Figure A.2: An annotated example of wellhead temperature and pressure for different mass fractions of CO₂ (*X*CO₂) versus methane.

The thick lines, in Figure A.2, indicate wellbore calculations that do not consider heat loss from the production well to the surrounding rocks (i.e. adiabatic conditions), whereas the dashed lines indicate that heat loss is accounted for in the calculations. Without heat loss, the observed decline in temperature and pressure of the produced fluid, as it rises to the

wellhead, is caused by gas expansion in the production well. The temperature of methane decreases by 12 °C and that of CO_2 by 42 °C during the rise, and corresponding expansion, from the reservoir to the surface. When we consider heat loss, as the fluid rises to the wellhead, there is a further decline in the produced fluid's wellhead temperature (by 15 °C) and a slight pressure drop (~0.5 MPa, when it is only CO_2). Our wellbore model (with heat transfer consideration) shows that, during fluid rise in the production well, both temperature and pressure decrease with increasing CO_2 mass fraction in the produced fluid.
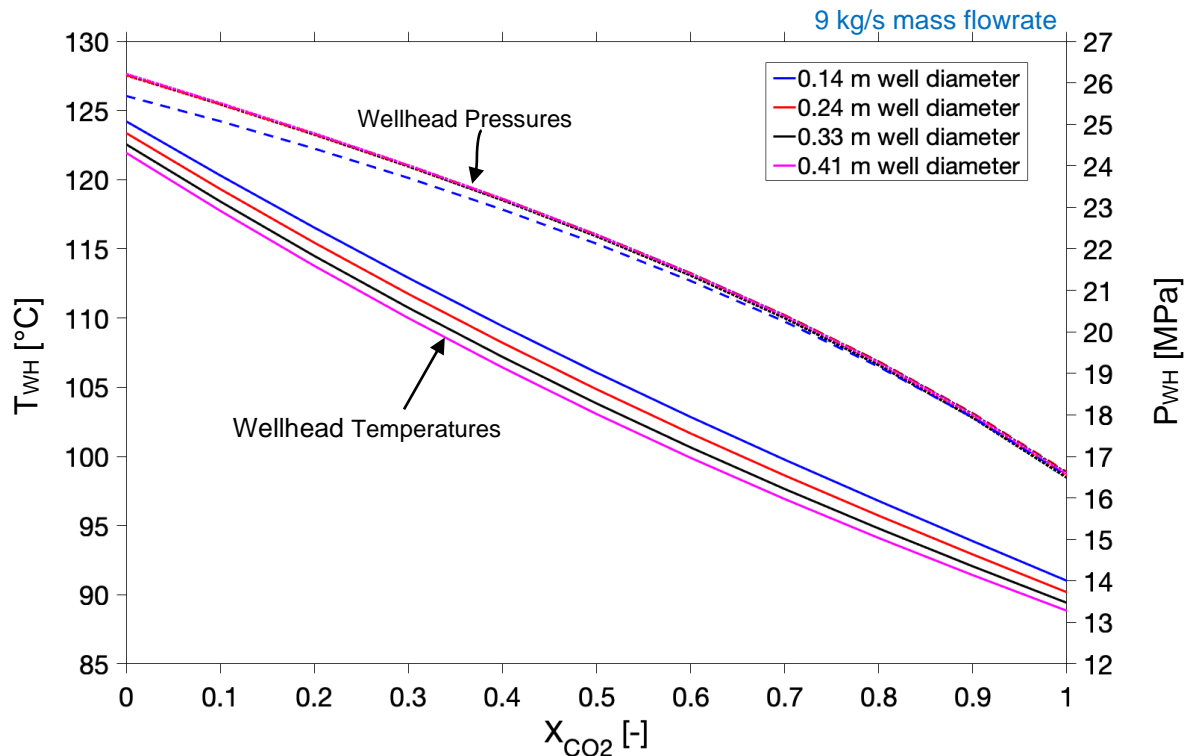

Figure A.3: Wellhead temperatures and pressures for various mass fractions of CO_2 versus methane for various wellbore diameters, using a common fluid mass flowrate of 9 kg/s.

Furthermore, using a constant mass flowrate, and increasing the diameter of the production well, the wellhead temperature of the produced fluid (different mass fractions of CO_2) tends to decrease, with a small (negligible) increase in wellhead pressure (Figure A.3). Higher heat loss rates result from larger wellbore diameters, as larger wellbore diameters increase the surface area of the wellbore through which the heat is transferred from the wellbore to the surrounding rock. However, if there is a corresponding increase in the fluid mass flowrate, as the wellbore diameter is increased, the wellhead temperature (and pressure) will increase, because heat loss from the fluid to the surrounding formation decreases (Figure A.4). Thus, wellbore heat loss is primarily a function of fluid mass flowrate (Ramey Jr., 1962). It has also been reported by Randolph et al (Randolph et al., 2012) that in large-diameter CPG production wells (with high flowrates), less than a 1 °C reduction in wellhead temperature is expected. Hence, high fluid flowrates (in a large wellbore diameter) will give

higher wellhead temperatures and pressures, maximizing the power output of the combined CO_2-EGR–CPG system.
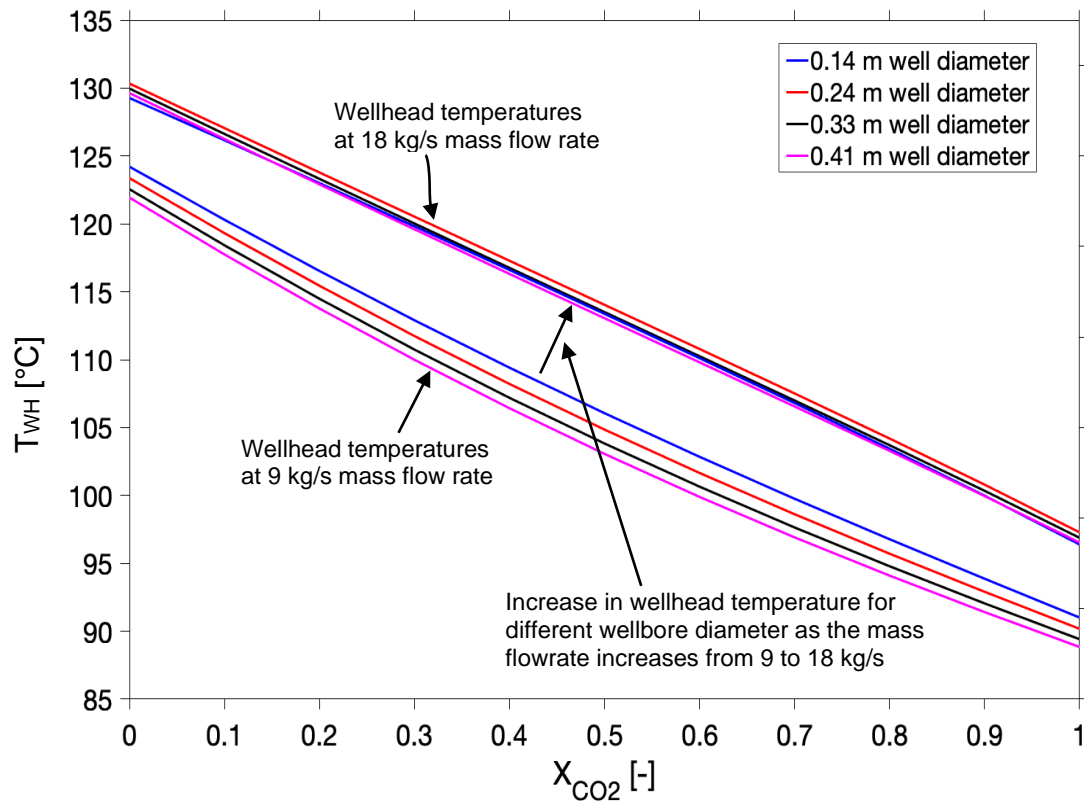

Figure A.4: Wellhead temperatures for various fluid mass fractions of CO_2 versus methane for various wellbore diameters when considering two different mass flowrates (9kg/s and 18 kg/s).

A.3 Thermal efficiency and outlet temperature plots for an indirect (R245fa) Rankine cycle

The same R245fa Organic Rankine Cycle (ORC) simulation of Adams et al. (Adams et al., 2015) is used here. As the thermal efficiency of an ORC is only dependent on the temperature being supplied to it, the simulation results of Adams et al. (Adams et al., 2015) can be directly applied here. The relationship for thermal efficiency is shown in Figure A.5. The thermal efficiency is the electric power generated, divided by the available heat at the production wellhead. The available heat is the difference between the enthalpy of the fluid at the production wellhead and the enthalpy at the same pressure and ambient temperature.

Figure A.6 shows the temperature of the fluid exiting the ORC as a function of the fluid entering the ORC. The subcritical ORC cannot extract all available heat from the fluid, due to pinch point constraints within the R245fa evaporator and preheater. Thus, the injection temperature of the produced fluid is found from this relationship so that an accurate simulation of reservoir heat depletion is made.

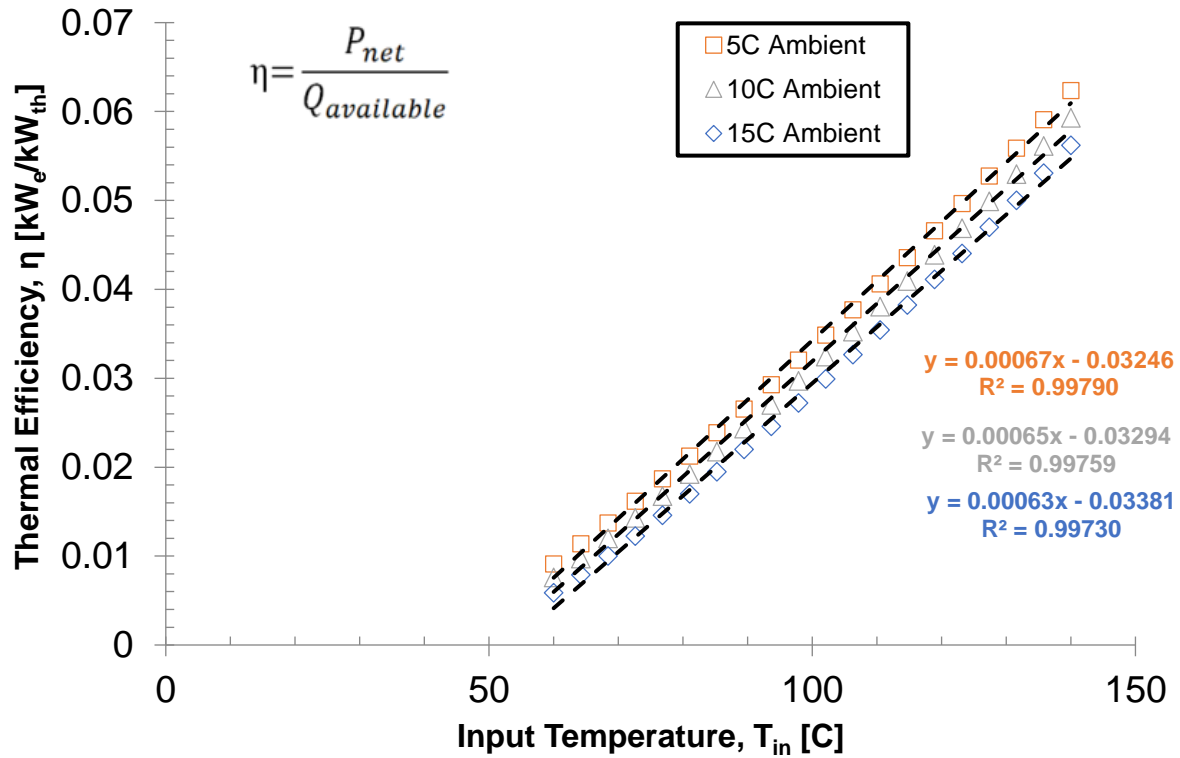Figure A.5: Correlation plot of the thermal efficiency of the R245fa Rankine cycle, using the inlet temperature of the primary (produced) fluid and the ambient temperature at the Earth surface.
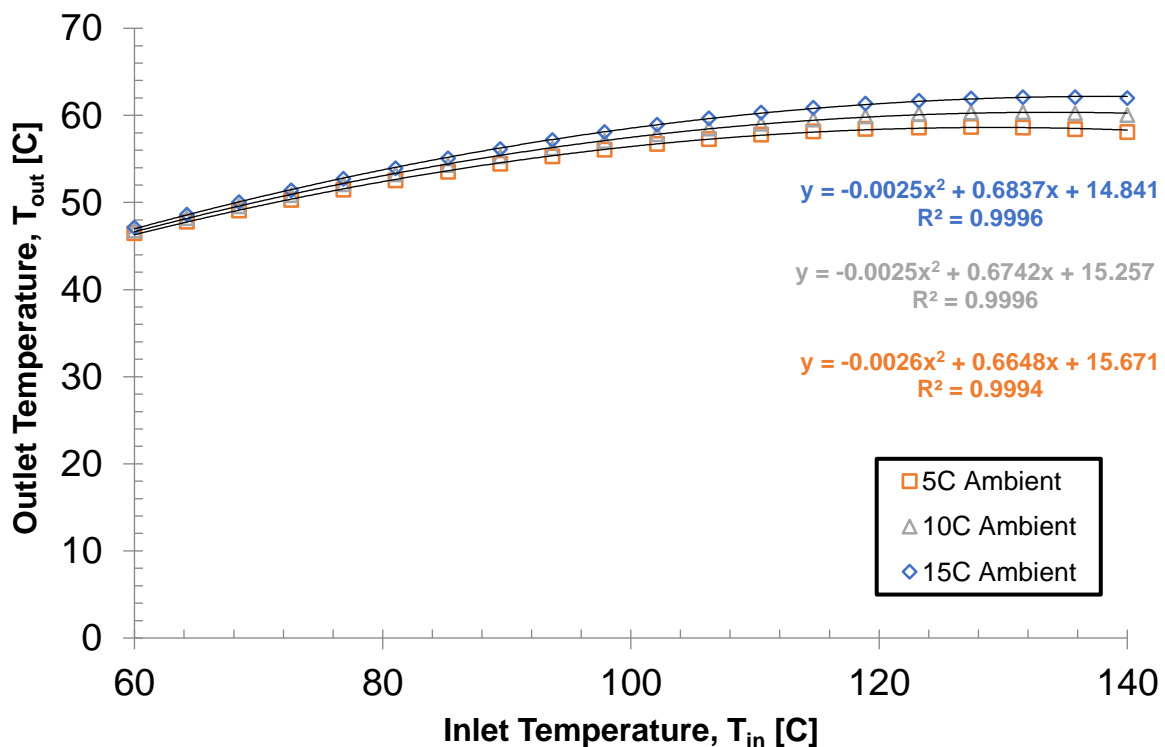

Figure A.6: Correlation plot of the outlet temperature of the primary (produced) fluid in the R245fa Rankine cycle, using the inlet temperature of the primary fluid and the ambient temperature at the Earth surface.

B

Appendix to Chapter 3

_____

B.1 Power-mass-flowrate model

Depending on the mass flowrate, the power generated by a CPG system varies significantly. It can reduce from the optimum or even become negative. Thus, the mass flowrate of a CPG system should not be merely selected but should be the result of an optimization study with respect to the reservoir and operational properties of the CPG system. For example, Figure A1 the power generated, using well diameters of 0.11 m, 0.21 m (base case) and 0.33 m, as total CO_2 circulating mass flowrate increases. The parameters used for the power calculation are the base-case parameters described in this study (Table 4.1) and a reservoir impedance of 104.2 kPa-s/kg determined using the base-case permeability, CO_2 flowrate and distance between the wells (i.e. 500 m).. The wellbore heat transfer is not considered in this semi-analytic example CPG power generation calculation. The result of this simplified simulation shows that power generated increases as the total mass flowrate increases till about 130 kg/s with 0.716 MW_e power generated and from this point declines as the flowrate increases. The figure also shows that as wellbore diameter decrease to 0.11 m, optimal power output starts to decrease at very small total mass flowrate (58 kg/s). The case of well diameter of 0.33 m, generated a peak power output of 0.774 MW_e at 150kg/s, which is very close to the results of the case of 0.21 m wellbore diameter. Hence, a base case of a CPG circulation flowrate of 30 kg/s/well is selected, which is equivalent to 120 kg/s for the total four injection and production wells used in the numerical simulation examples considered in this study.
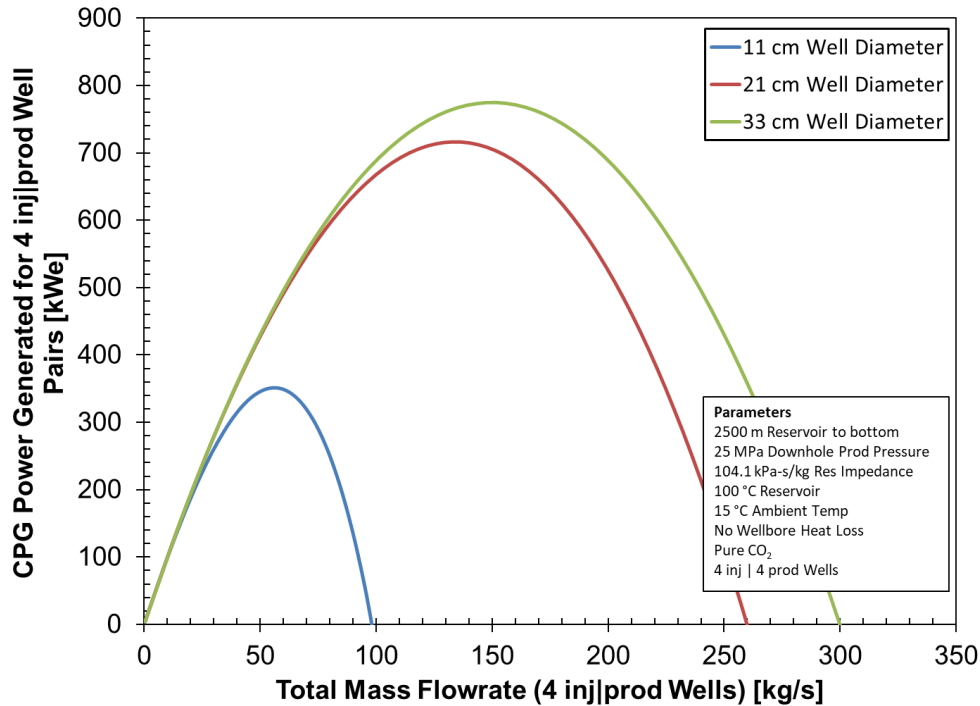
Figure B.1: An example illustrating the CPG power generated by 4 injection-production well pairs at varying total mass flowrates for 3 different wellbore diameters. Heat loss in the wellbore is not considered in this example.

Supporting Documents

B.2 Determining the density and viscosity of brine

To calculate the density and viscosity of the brine at temperature T (in Kelvin), with the known mass fraction of the salt X_{NaCl} (in fraction), we use the correlation models used for TOUGH2 ECO2N, i.e. Haas (Haas, 1976) for brine density and Philips et al. (Phillips et al., 1981) for brine dynamic viscosity calculations;

The correlation presented by Haas (Haas, 1976; Pruess et al., 2012) To calculate the density of brine (solution of water and NaCl) is valid for brine concentrations between 0 mol NaCl/kgH_2O and halite saturation at temperatures between 80 °C and 325 °C.

First, we calculate the molality of the salt, b (in mol$_{NaCl}$/kg$_{H2O}$);

$$b = \frac{1000 X_{NaCl}}{1 - X_{NaCl} M_{NaCl}}$$

M_{NaCl} is the molecular weight of NaCl = 0.058443 kg/mol;

The brine density ρ_b is calculated as:

$$\rho_b = \left[\frac{1000\big(1000 + (bM_{NaCl})\big)}{\big(1000v_0 + (\varphi M_{NaCl})\big)}\right]$$

where

v_0 (in cm³/g) is the is the vapor-saturated specific volume of liquid H₂O at the fluid temperature T,

$$v_0$$
$$= \frac{\left[3.1975 + \left(-0.315154 \cdot \theta^{\frac{1}{3}}\right) + (-1.203374 \times 10^{-3} \cdot \theta) + (7.48908 \times 10^{-13} \cdot \theta^4)\right]}{\left[1 + \left(0.1342489 \cdot \theta^{\frac{1}{3}}\right) + (-3.946263 \times 10^{-3} \cdot \theta)\right]}$$

$$\theta = 647.27 - T$$

φ is the apparent molal volume of NaCl in the solution (in cm³/mol);

$$\varphi = -167.219 + 448.55v_0 + (-274.07v_0)^2 + (kb^{0.5})$$

$$k = (-13.644 + 13.97v_0) \times (v_0/(3.1975 - v_0))^2$$

We apply the correlation of Phillips et al. (Phillips et al., 1981) to calculate the viscosity of brine, which is valid for brine concentrations ≤ 420,000 ppm at temperatures between 10° and 350° C (Adams and Bachu, 2002). The viscosity of the brine μ_b is calculated using the expression:

$$\mu_b = \mu_w\left[1 + 0.0816b - 0.0122b^2 + 0.000128b^3\right.$$
$$\left. + \left(0.000629T\big(1 - e^{(-0.7b)}\big)\right)\right]$$

where μ_w is the dynamic viscosity of pure water,

$$\mu_w = f(T,P)_{H_2O}$$

B.3 Relative permeability and capillary pressure correlation models

The van Genuchten (1980) model (Genuchten, 1980; Pruess et al., 2012) is used to predict the relative liquid permeability k_{rL} and gas k_{rG} permeability(Pruess et al., 2012):

$$k_{rL} = \begin{cases} \sqrt{S^*}\left\{1 - \left(1 - [S^*]^{1/m}\right)^m\right\}^2 & : S_L < S_{Ls} \\ 1 & : S_L \geq S_{Ls} \end{cases}$$

$$k_{rG} = \begin{cases} (1 - S_\#)^2\left(1 - S_\#^2\right) & : S_{Gr} > 0 \\ 1 - k_{rL} & : S_{Gr} = 0 \end{cases}$$

where

$$S_\# = \left.(S_L - S_{Lr})\middle/(1 - S_{Lr} - S_{Gr})\right.$$

From the equations above, it can be deduced that as the m-value increases (the formation becoming less homogeneous), liquid relative permeability will increase while the gas relative permeability will decrease.

Some numerical studies use the earlier Brooks-Corey (1964) model (Mahabadi et al., 2016; R. H. Brooks and A. T. Corey, 1964):

$$k_{rL} = k_{rLmax} \times S_\#{}^{n_L},$$

$$k_{rG} = k_{rGmax} \times S_\alpha{}^{n_G},$$

where

$$S_\alpha = \left.(S_G - S_{Gr})\middle/(1 - S_{Lr} - S_{Gr})\right.$$

k_{rlmax} and k_{rgmax} are the maximum relative permeabilities of the liquid and gas respectively. n_L and n_G are Brooks-Corey's fitting parameters for liquid and gas permeability respectively. The lower the values of n_L and n_G, the higher the relative permeabilities of the liquid and gas and vice-versa (Mahabadi et al., 2016)).

Analytical expression commonly used to capture the capillarity and water saturation relation (P_c-S_L), typically known as water retention curve is the van Genuchten (1980) model (Genuchten, 1980; Mahabadi et al., 2016):

$$P_c = P_0 \left[(S^*)^{-\frac{1}{m}} - 1 \right]^{1-m}$$

where

$$S^* = \left.(S_L - S_{Lr})\middle/(S_{Ls} - S_{Lr})\right.$$

where P_0 is the gas entry pressure, S_L is the liquid (water or brine) saturation, S_{Ls} is the liquid saturation at which gas permeability starts to occur, S_{Lr} and S_{Gr} are the residual liquid and gas saturation, respectively, m is the van Genuchten fitting parameter which relates to the distribution of pore spaces. Lower values of m show steeper P_c-S_L curve (Mahabadi et al., 2016), which is typical for sediments with wider pore size distribution. Higher values of m relate to highly heterogeneous sediments.

B.4 Characterizing the wellbore fluid flow transition pattern map

(I) Taitel et al. model

Taitel et al. (Taitel et al., 1980) developed models for calculating and predicting the gas-water flow pattern transition boundaries in a vertical well. Their models are based on physical mechanisms that are suggested for each flow-pattern transition. They include the following:

Bubble to fine-bubble transition

An increase in the liquid rate would lead to the turbulent breakup of the existing bubbles. If this breakup is consistent and there is no recoalescence, then the dispersed (fine) bubble flow pattern will be formed or maintained (if it was already existing). The dispersed, or fine, bubble flow pattern exists once the bubbles can break into a small critical size, with the bubble diameter calculated as:

$$d_c = \left[\frac{0.4\sigma}{\Delta\varrho g}\right]^2$$

Where $\Delta\varrho = \varrho_L - \varrho_G$; σ is the interfacial tension calculated using the correlations from (Bachu and Brant Bennion, 2009).

Here, liquid is the solution of water and salt (NaCl)). The transition for the bubble to finely dispersed bubble flow pattern can be found using the dimensionless expression in Equation (B.1), which relates the flowrates, well sizes and fluid properties,

$$U_{S,L} + U_{S,G} = 4\left\{\frac{D^{0.429}(\sigma/\varrho_L)^{0.089}}{(\mu_L/\varrho_L)^{0.072}}\left[\frac{\Delta\varrho g}{\varrho_L}\right]^{0.446}\right\} \tag{B.1}$$

Bubble to slug/churn transition

The transition from bubbly to slug flow exists when the dispersive forces are not dominant. This can also be characterized using the bubble void fraction (Taitel et al., 1980). At low liquid rates when turbulent bubble breakup is low, the bubble to slug flow transition exists when the void fraction reaches 0.25 (Griffith and Wallis, 1961). Therefore, if the fluid properties are known, the values of $U_{S,L}$ and $U_{S,G}$ can be calculated using Equation (B.2) and it is independent of the wellbore diameter.

$$3U_{S,G} - U_{S,L} = 1.15\left[\frac{\sigma\Delta\varrho g}{\varrho_L^2}\right]^{0.25} \tag{B.2}$$

Annular flow transition

The Turner's entrained drop model can be used to calculate the minimum gas velocity required to suspend a drop and prevent a slug/churn flow (i.e. sustain an annular flow). As shown in Equation (B.3), the minimum gas velocity can be determined from the balance between the entrained drop drag forces (first term) and the gravitational forces (second term).

$$U_G = \left[\left(\frac{4We_{crit}}{3C_d} \right) \frac{\sigma \Delta \varrho g}{\varrho_G^2} \right]^{0.25}$$ (B.3)

We_{crit} is the Weber number (i.e. maximum diameter of liquid drops).

C_d is the Drag coefficient for a sphere.

Turner et al. (Turner et al., 1969) suggested that $We_{crit} = 30$ and $C_d = 0.44$. Therefore, Equation (B.3) becomes

$$U_G = 3.1 \left[\frac{\sigma \Delta \varrho g}{\varrho_G^2} \right]^{0.25}$$ (B.4)

For annular flow, the liquid film thickness even when relatively high liquid flowrates exist. This implies that the gas superficial velocity $U_{S,G}$ can replace the true gas velocity U_G in Equation (B.3). Hence, the final annular transition boundary can be calculated using Equation (B.4).

(II) Alternative method to characterize the wellbore flow transition pattern

To verify the solutions obtained using the equations from Taitel et al. (Taitel et al., 1980) for the different flow pattern transition boundaries, we adopt a new approach proposed by He et al. (He and Bai, 2014) for wet gas flowrate measurement with Venturi meter based on a two-phase mass flow coefficient. They investigated the relationships of the two-phase mass flow coefficient, K with these three important fluid-flow parameters: the Lockhart–Martinelli parameter X_{LM}, the gas-to-liquid density ratio ϱ_R and the gas densiometric Froude number Fr_G.

Using the K-X_{LM} model developed by He et al. . (He and Bai, 2014) for the Venturi meter, K and X_{LM} are defined as follows:

$$K = \frac{\dot{m}_L + \dot{m}_G}{\dot{m}_{G,app}} = \frac{\dot{m}_{total}}{\dot{m}_{G,app}}$$

$\dot{m}_{G,app}$, termed 'apparent' gas mass flowrate, is the uncorrected gas mass flowrate produced by the higher gas-liquid density ratio when a Venturi meter is used in a wet gas flow. It can be mathematically calculated as,

$$\dot{m}_G = \frac{\dot{m}_{G,app} \times K}{1 + X_{LM} \Big/ \left(\frac{\varrho_G}{\varrho_L}\right)^{0.5}}$$

which implies that

$$\dot{m}_{G,app} = \frac{\dot{m}_G}{K}\left[1 + \frac{X_{LM}}{\left(\frac{\varrho_G}{\varrho_L}\right)^{0.5}}\right]$$

X_{LM} is a dimensionless parameter commonly used to characterize a wet gas. A wet gas can be considered as a subset of two-phase flow, and is a condition described as a relatively small amount of liquid in a flow that is predominantly gas by volume. A fluid with $X_{LM} <$ 0.3 can be said to be a wet gas. It is mathematically defined as,

$$X_{LM} = \frac{\dot{m}_L}{\dot{m}_G}\left(\frac{\varrho_G}{\varrho_L}\right)^{0.5}$$

The relationship between K and X_{LM} is expressed as

$$K = bX_{LM} + c$$

Where b is the slope and c is the intercept. When we have a dry gas (i.e. there is no liquid in the wet gas), $\dot{m}_L$ and X_{LM} are equal to zero, $\dot{m}_{G,app}$ will become equal to $\dot{m}_G$, and K reduces to 1, i.e.

$$K = \frac{\dot{m}_L + \dot{m}_G}{\dot{m}_{G,app}} = 1$$

This implies that for the dry gas, K becomes

$$K = 1 = c$$

Hence, for the wet gas, K is

$$K = bX_{LM} + 1$$

The slope b can be determined in terms of the gas-to-liquid density ratio ϱ_R and the gas densiometric Froude number Fr_G.

$$b = \frac{0.5681}{\left(\varrho_G/\varrho_L\right)^{0.5}} - 0.1444 Fr_G - 0.1494$$

Hence,

$$K = X_{LM}\left[\frac{0.5681}{\left(\varrho_G/\varrho_L\right)^{0.5}} - 0.1444 Fr_G - 0.1494\right] + 1$$

where

$$Fr_G = \frac{U_{S,G}}{(gD)^{0.5}}\left(\frac{\varrho_G}{\Delta\varrho}\right)^{0.5}$$

If $\dot{m}_G$ is known, $\dot{m}_{total}$ can be found by using K to find $\dot{m}_{G,app}$,

Therefore,

$$\dot{m}_{total} = K \times \dot{m}_{G,app}$$

If $\dot{m}_{total}$ is known, $\dot{m}_G$ can be found by K (calculated for wet gas) to find $\dot{m}_{G,app}$. Then, calculate for $\dot{m}_G$.

Therefore, we use these relationships to calculate $\dot{m}_{total}$ or $\dot{m}_G$, which can be used to validate the initial solution of $\dot{m}_{total}$ presented in Equation (3.7)

As shown in Figure 3.7 and Figure B.1 (for 0.33 m and 0.11 m wellbore diameters respectively), using the base-case fluid properties, the model of He et al. (He and Bai, 2014) perfectly matches that of Taitel et al. (Taitel et al., 1980) when both are used to calculate the flow transition pattern for CO_2-brine mixture.
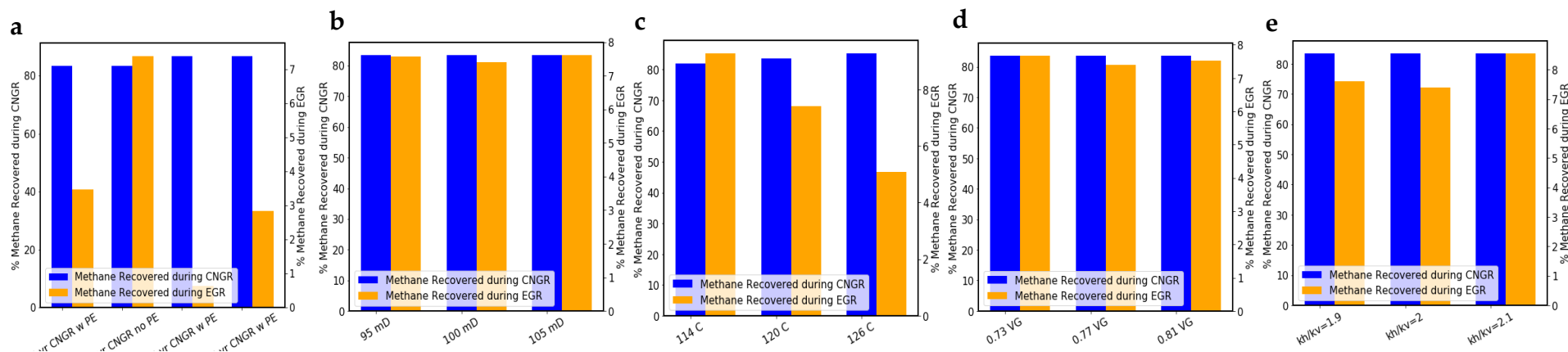
Appendix to Chapter 4

Figure C.1: Percentage of original gas in place (OGIP) recovered during the CNGR and EGR stages for the 4 reservoir model example cases (a) and the 4 reservoir parameters [permeability (b), temperature (c), relative permeability (d), and permeability anisotropy (e)].

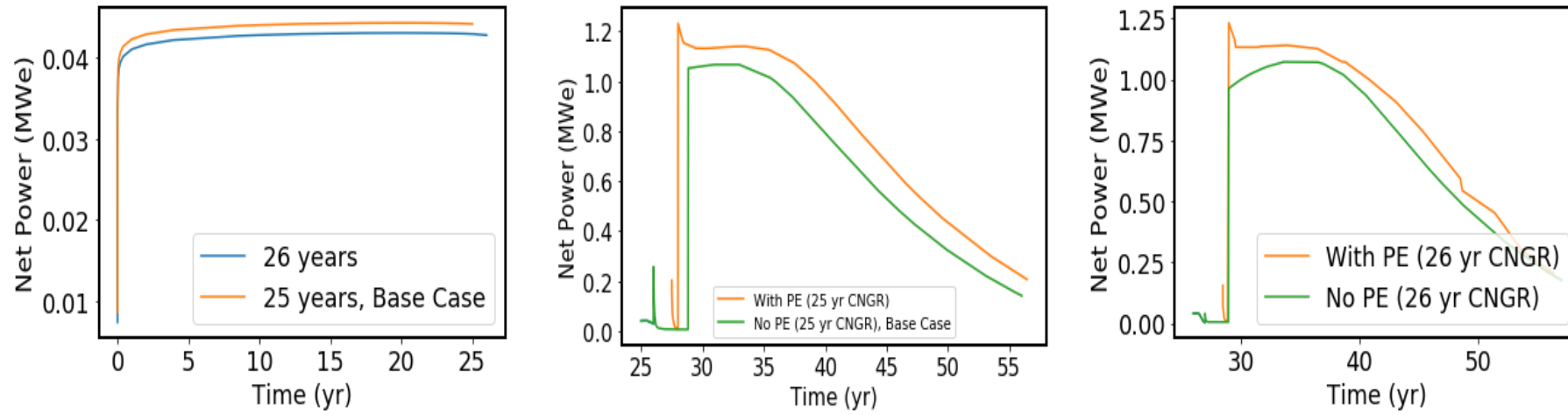Figure C.2: Simulation results (time-series plot) for the 4 reservoir model example cases showing the net geothermal power generated during CNGR stage (0 – 25/26 years) and EGR-CPG stages (25/26 – 55/56 years).

Figure C.3: Simulation results for the reservoir permeability parameter showing the geothermal net power generated during CNGR stage (0 – 25 years) and EGR-CPG stages (25 – 55 years).

Figure C.5.4: Simulation results for the reservoir temperature parameter showing the geothermal net power generated during CNGR stage (0 – 25 years) and EGR-CPG stages (25 – 55 years).

Figure C.5: Simulation results for the relative permeability (van Genuchten) parameter showing the geothermal net power generated during CNGR stage (0 – 25 years) and EGR-CPG stages (25 – 55 years).
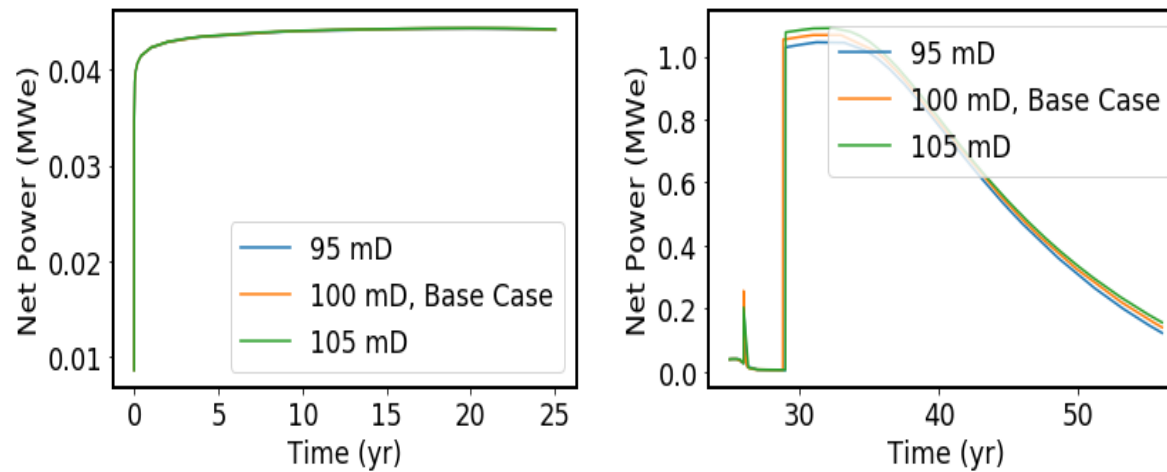
Figure C.6: Simulation results for the reservoir permeability anisotropy parameter showing the geothermal net power generated during CNGR stage (0 – 25 years) and EGR-CPG stages (25 – 55 years).

Figure C.7: Simulation results for the mean ambient surface temperature parameter showing the geothermal net power generated during CNGR stage (0 – 25 years) and EGR-CPG stages (25 – 55 years).

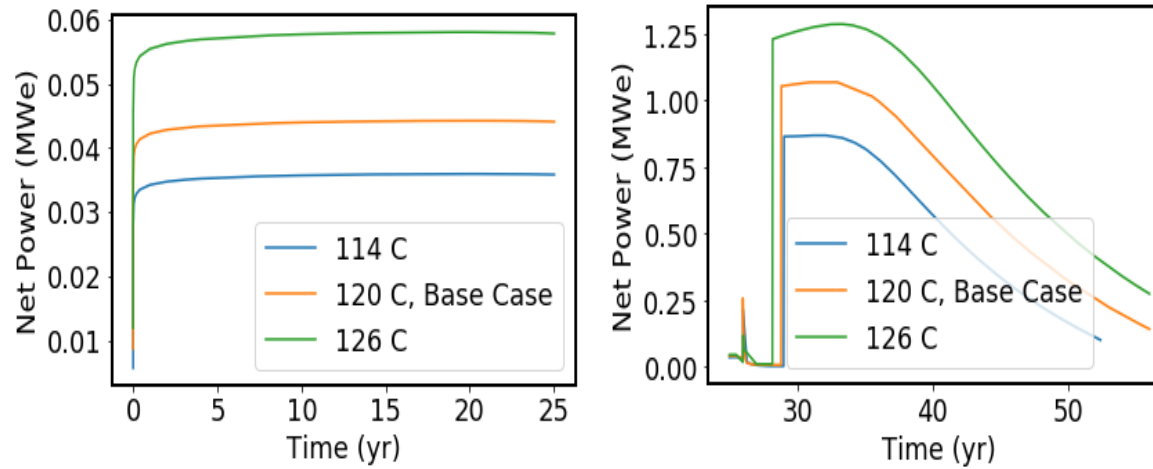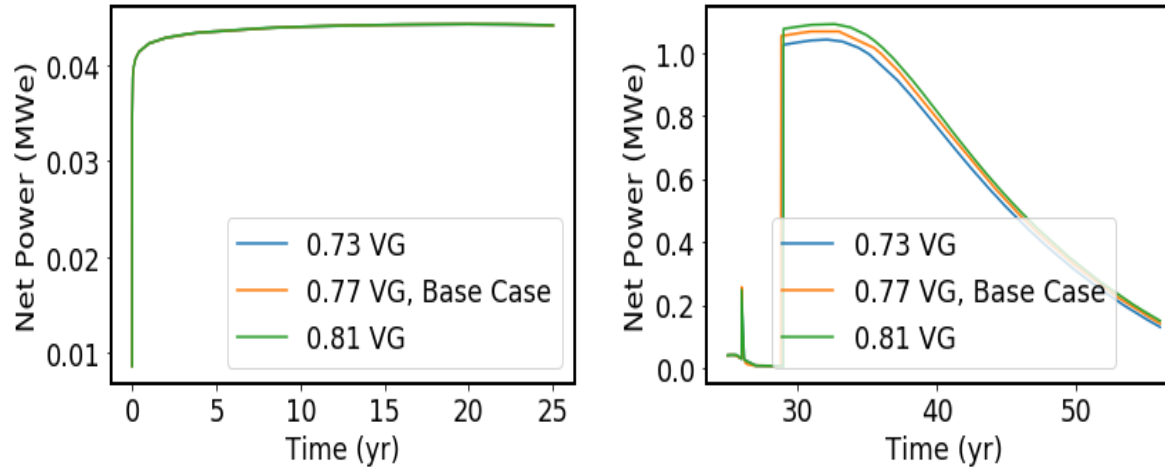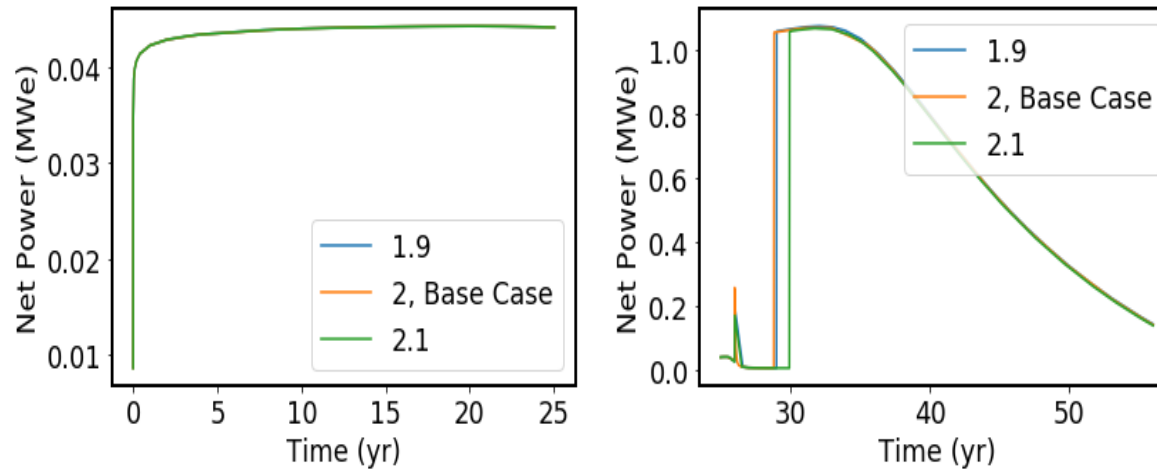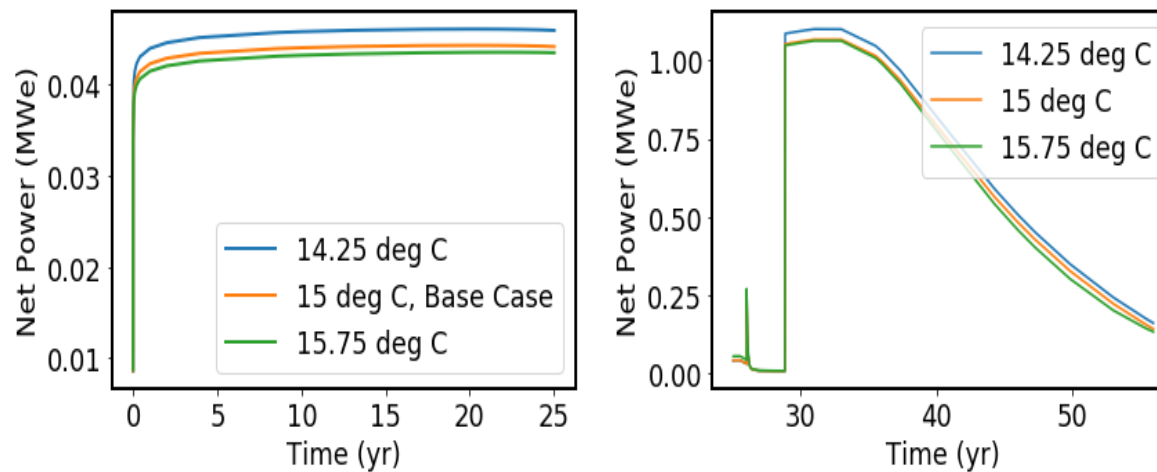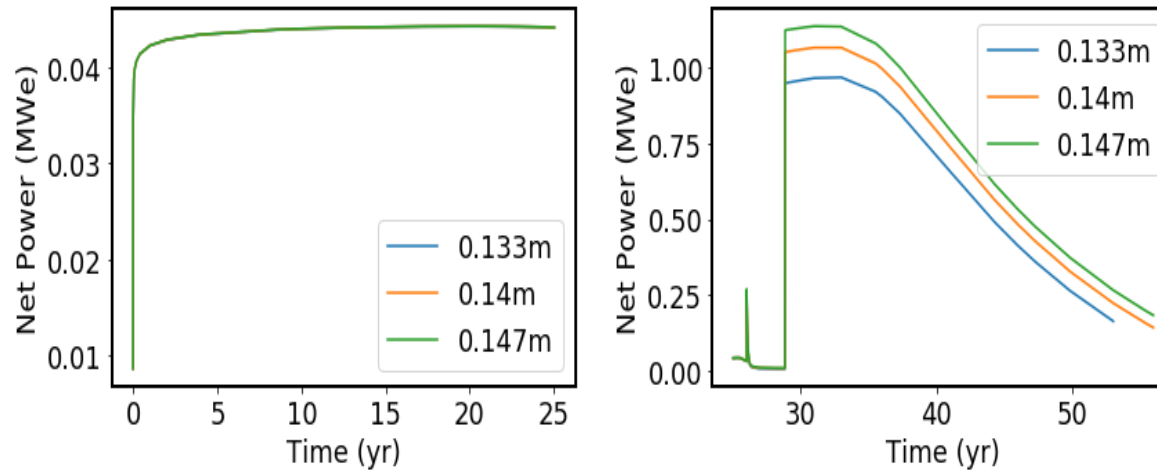Figure C.8: Simulation results for the well pipe diameter showing the geothermal net power generated during CNGR stage (0 – 25 years) and EGR-CPG stages (25 – 55 years).

Bibliography

_____

Abi-Aad Naji, 1998. Natural gas reserves, development & production in Qatar.

Adams, B.M., Kuehn, T.H., Bielicki, J.M., Randolph, J.B., Saar, M.O., 2015. A comparison of electric power output of CO_2 Plume Geothermal (CPG) and brine geothermal systems for varying reservoir conditions. Appl. Energy 140, 365–377. https://doi.org/10.1016/J.APENERGY.2014.11.043

Adams, B.M., Kuehn, T.H., Bielicki, J.M., Randolph, J.B., Saar, M.O., 2014. On the importance of the thermosiphon effect in CPG (CO_2 plume geothermal) power systems. Energy 69, 409–418. https://doi.org/10.1016/j.energy.2014.03.032

Adams, B.M., Vogler, D., Kuehn, T.H., Bielicki, J.M., Garapati, N., Saar, M.O., 2020. A Characterization of Temperature Depletion in a Sedimentary Basin and its Effect on the Electric Power Output of CO2 Plume Geothermal (CPG) Power Systems. (in Prep.

Adams, J.J., Bachu, S., 2002. Equations of state for basin geofluids: algorithm review and intercomparison for brines. Geofluids 2, 257–271. https://doi.org/10.1046/j.1468-8123.2002.00041.x

Adaro, J.A., Galimberti, P.D., Lema, A.I., Fasulo, A., Barral, J.R., 1999. Geothermal contribution to greenhouse heating. Appl. Energy 64, 241–249. https://doi.org/10.1016/S0306-2619(99)00049-5

Ahn, J.H., Jeong, J.H., Choi, B.S., Kim, T.S., 2019. Influence of various carbon capture technologies on the performance of natural gas-fired combined cycle power plants. J. Mech. Sci. Technol. 33, 1431–1440. https://doi.org/10.1007/s12206-019-0245-x

Al-Hasami, A., Ren, S., Tohidi, B., 2005. CO_2 injection for enhanced gas recovery and geo-storage: Reservoir simulation and economics, in: SPE Europec/EAGE Annual Conference. https://doi.org/10.2118/94129-MS

Al-Siddiqi, A., Dawe, R.A., 1999. Qatar's oil and gasfields: A review. J. Pet. Geol. 22, 417–436. https://doi.org/10.1111/j.1747-5457.1999.tb00477.x

Atrens, A., Gurgenci, H., Rudolph, V., 2009. Exergy analysis of a CO_2 thermosiphon, in: Proceedings of the Thirty-Fourth Workshop on Geothermal Reservoir Engineering. Stanford, California, pp. 1–6.

Axelsson, G., Stefánsson, V., Björnsson, G., Liu, J., 2005. Sustainable management of geothermal resources and utilization for 100-300 years, in: Proceedings World Geothermal Congress, International Geothermal Association, Antalya, Turkey, 24-29 April. pp. 1–8.

Bachu, S., 2003. Screening and ranking of sedimentary basins for sequestration of CO_2 in geological media in response to climate change. Environ. Geol. 44, 277–289. https://doi.org/10.1007/s00254-003-0762-9

Bachu, S., Brant Bennion, D., 2009. Interfacial Tension between CO_2, Freshwater, and Brine in the Range of Pressure from (2 to 27) MPa, Temperature from (20 to 125) °C, and Water Salinity from (0 to 334 000) mg·L−1. J. Chem. & Eng. Data 54, 765–775. https://doi.org/10.1021/je800529x

Bakos, G.C., Fidanidis, D., Tsagas, N.F., 1999. Greenhouse heating using geothermal energy. Geothermics 28, 759–765. https://doi.org/10.1016/S0375-6505(99)00041-3

Bazyrov, I., Glazyrina, A., Lukin, S., Alchibaev, D., Salishchev, M., Ovcharenko, Y., 2017. Time-dependent hydro-geomechanical reservoir simulation of field production. Procedia Struct. Integr. 6, 228–235. https://doi.org/10.1016/J.PROSTR.2017.11.035

Beck, L., Temple-Smith, L., 2020. Is CCS expensive?: Decarbonisation costs in the net-zero contect.

Bell, I.H., Jäger, A., 2016. Helmholtz energy transformations of common cubic equations of state for use with pure Fluids and mixtures. J. Res. Natl. Inst. Stand. Technol. 121, 26. https://doi.org/10.6028/jres.121.011

Bell, I.H., Wronski, J., Quoilin, S., Lemort, V., 2014. Pure and pseudo-pure fluid thermophysical property evaluation and the open-source thermophysical property library CoolProp. Ind. Eng. Chem. Res. 53, 2498–2508. https://doi.org/10.1021/ie4033999

Bert, M., Davidson, O., Coninck, H. de, Loos, M., Meyer, L., 2005. IPCC special report on carbon dioxide capture and storage.

Bielicki, J.M., Peters, C.A., Fitts, J.P., Wilson, E.J., 2015. An examination of geologic carbon sequestration policies in the context of leakage potential. Int. J. Greenh. Gas Control 37, 61–75. https://doi.org/10.1016/J.IJGGC.2015.02.023

Bjørlykke, K., 1989. Sedimentology and petroleum geology. Springer-Verlag.

BP, 2018. BP statistical review of world energy 2018: Natural gas.

Brindley, A.W., Mohammad, A.J., Al-Dulaimi, A.A., 1984. Dukhan Khuff gas reservoir performance, in: Proceedings of 8th Doha Tech. Symp. Doha, Qatar. pp. 111–116.

Brown, D.W., 2000. A hot dry rock geothermal energy concept utilizing supercritical CO_2 instead of water, in: Proceedings of the Twenty-Fifth Workshop on Geothermal Reservoir Engineering. Stanford, California, pp. 1–6.

Brunetti, A., Scura, F., Barbieri, G., Drioli, E., 2010. Membrane technologies for CO_2 separation. J. Memb. Sci. 359, 115–125. https://doi.org/https://doi.org/10.1016/j.memsci.2009.11.040

Buckley, S.E., Leverett, M.C., 1942. Mechanism of Fluid Displacement in Sands. Trans. AIME 146, 107–116. https://doi.org/10.2118/942107-G

Burke, L., 2011. Natural gas production and anomalous geothermal gradients of the deep Tuscaloosa Formation, in: American Association of Petroleum Geologists, Annual Convention and Exhibition, Houston, Texas.

Burke, L., 2010. Temperature trends and preservation rates in the deep Tuscaloosa

Formation, Judge Digby Field, Louisiana, in: Gulf Coast Association of Geological Societies Transactions. pp. 77–86.

Burke, L., 2009. Temperature, overpressure, and accumulation size: deep Tuscaloosa Formation, Judge Digby field, Louisiana, in: USGS Geologic Review of Gulf Coast, Nov. 3 – 6.

Carlo, C., Martin, K.G., 1979. The Lower Tuscaloosa trend of South-Central Louisiana: "You ain't seen nothing till you've seen the Tuscaloosa" 29, 37–41.

Chu, Y., He, X., 2018. Process Simulation and Cost Evaluation of Carbon Membranes for CO_2 Removal from High-Pressure Natural Gas. Membranes (Basel). 8, 1–9. https://doi.org/10.3390/membranes8040118

Clemens, T., Secklehner, S., Mantatzis, K., Jacobs, B., 2010. Enhanced gas recovery, challenges shown at the example of three gas fields, in: SPE EUROPEC/EAGE Annual Conference and Exhibition Held in Barcelona, Spain, 14– 17 June. pp. 1–17. https://doi.org/https://doi.org/10.2118/130151-MS

Coats, K.H., 1977. Geothermal Reservoir Modelling, in: SPE Annual Fall Technical Conference and Exhibition. Society of Petroleum Engineers, Denver, Colorado, p. 33. https://doi.org/10.2118/6892-MS

Coleman, J.L., Jr., and Cahan, S.M., 2012. Preliminary catalog of the sedimentary basins of the United States: U.S. geological survey open-file report.

Cui, G., Ren, S., Rui, Z., Ezekiel, J., Zhang, L., Wang, H., 2017a. The influence of complicated fluid-rock interactions on the geothermal exploitation in the CO_2 plume geothermal system. Appl. Energy. https://doi.org/10.1016/j.apenergy.2017.10.114

Cui, G., Zhang, L., Ren, B., Enechukwu, C., Liu, Y., Ren, S., 2016. Geothermal exploitation from depleted high temperature gas reservoirs via recycling supercritical CO_2: Heat mining rate and salt precipitation effects. Appl. Energy 183, 837–852. https://doi.org/10.1016/J.APENERGY.2016.09.029

Cui, G., Zhang, L., Ren, B., Zhuang, Y., Li, X., Ren, S., Wang, X., 2015. Geothermal exploitation with considering CO_2 mineral sequestration in high temperature depleted gas reservoir by CO_2 injection, in: Carbon Management Technology Conference. pp. 1–9. https://doi.org/10.7122/439516-MS

Cui, G., Zhang, L., Tan, C., Ren, S., Zhuang, Y., Enechukwu, C., 2017b. Injection of supercritical CO_2 for geothermal exploitation from sandstone and carbonate reservoirs: CO_2-water-rock interactions and their effects. J. CO_2 Util. 20, 113–128. https://doi.org/10.1016/j.jcou.2017.05.006

De Ruiter, J., van der Laan, G., & Udink, H.G., 1967. Development of the North Netherlands gas discovery in Groningen, in: 7th World Petroleum Congress. Mexico, pp. 221–229.

Delshad, M., Kong, X., Tavakoli, R., Hosseini, S.A., Wheeler, M.F., 2013. Modeling and simulation of carbon sequestration at Cranfield incorporating new physical models. Int. J. Greenh. Gas Control 18, 463–473. https://doi.org/10.1016/j.ijggc.2013.03.019

Denney, D., 2006. Technical and economic challenge of mature gas fields: The Giant Altmark Field, Germany. J. Pet. Technol. 58, 38–39. https://doi.org/10.2118/0106-0038-JPT

Dijksman, N.C., Steenbrink, J., 2009. Managing a Giant: 50 years of Groningen Gas, in: 2009 SPE Offshore Europe Oil & Gas Conference & Exhibition. Aberdeen, UK, pp. 1–17. https://doi.org/10.2118/123931-MS

Dutcher, B., Fan, M., Russell, A.G., 2015. Amine-based CO_2 capture technology development from the beginning of 2013 — A review. ACS Appl. Mater. Interfaces 7, 2137–2148. https://doi.org/10.1021/am507465f

Eccles, J.K., Pratson, L., 2014. A "carbonshed" assessment of small- vs. large-scale CCS deployment in the continental US. Appl. Energy 113, 352–361. https://doi.org/https://doi.org/10.1016/j.apenergy.2013.07.002

Ezekiel, J., Ebigbo, A., Adams, B.M., Saar, M.O., 2020. Combining natural gas recovery and CO_2-based geothermal energy extraction for electric power generation. Appl. Energy 269, 1–21. https://doi.org/https://doi.org/10.1016/j.apenergy.2020.115012

Ezekiel, J., Ebigbo, A., Adams, B.M., Saar, M.O., 2019. On the use of supercritical carbon dioxide to exploit the geothermal potential of deep natural gas reservoirs for power generation, in: Proceedings of the European Geothermal Congress Held At Den Haag, The Netherlands,.

Farshad, F.F., Rieke, H.H., 2006. Surface roughness design values for modern pipes. SPE Drill. Complet. 21, 212–215. https://doi.org/10.2118/89040-PA

Feather, B., Archer, R.A., 2010. Enhanced natural gas recovery by carbon dioxide injection for storage purposes, in: 17th Australas Fluid Mechanics Conference, Auckland, New Zealand. Auckland, New Zealand, pp. 1–4.

Fleming, M.R., Adams, B.M., Kuehn, T.H., Bielicki, J.M., Saar, M.O., 2020. Increased Power Generation due to Exothermic Water Exsolution in CO_2 Plume Geothermal (CPG) Power Plants. Geothermics 88, 101865. https://doi.org/https://doi.org/10.1016/j.geothermics.2020.101865

Freifeld, B.M., Pan, L., Doughty, C., Zakem, S., Hart, K., Hostler, S., 2016. Demonstration of Geothermal Energy Production Using Carbon Dioxide as a Working Fluid at the SECARB Cranfield Site, Cranfield, Mississippi, in: Proceedings, 41st Workshop on Geothermal Reservoir Engineering. pp. 1–14.

Ganjdanesh, R., Bryant, S.L., Orbach, R.L., Pope, G.A., Sepehrnoori, K., 2014. Coupled carbon dioxide sequestration and energy production from geopressured/geothermal aquifers. SPE J. 19, 239–248. https://doi.org/10.2118/163141-PA

Ganjdanesh, R., Bryant, S.L., Pope, G.A., Sepehrnoori, K., 2013. Making CCS pay for itself: Storage strategies in geopressured-geothermal aquifers, in: Energy Procedia. Elsevier B.V., pp. 2495–2504. https://doi.org/10.1016/j.egypro.2013.06.131

Ganjdanesh, R., Pope, G.A., Sepehrnoori, K., 2015. Production of energy from saline aquifers: A method to offset the energy cost of carbon capture and storage. Int. J.

Greenh. Gas Control 34, 97–105. https://doi.org/10.1016/j.ijggc.2015.01.004

Garapati, N., Randolph, J.B., Saar, M.O., 2015a. Brine displacement by CO_2, energy extraction rates, and lifespan of a CO_2-limited CO_2-Plume Geothermal (CPG) system with a horizontal production well. Geothermics 55, 182–194. https://doi.org/10.1016/j.geothermics.2015.02.005

Garapati, N., Randolph, J.B., Saar, M.O., 2015b. Brine displacement by CO_2, energy extraction rates, and lifespan of a CO_2-limited CO_2-Plume Geothermal (CPG) system with a horizontal production well. Geothermics 55, 182–194. https://doi.org/10.1016/j.geothermics.2015.02.005

Garapati, N., Randolph, J.B., Valencia, J.L., Saar, M.O., 2014. CO_2-Plume Geothermal (CPG) heat extraction in multi-layered geologic reservoirs, in: Energy Procedia. Elsevier, pp. 7631–7643. https://doi.org/https://doi.org/10.1016/j.egypro.2014.11.797

Garcia, B., Billiot, J.H., Rouchon, V., Mouronval, G., Lescanne, M., Lachet, V., Aimard, N., 2012. A geochemical approach for monitoring a CO_2 pilot site: Rousse, France. A major gases, CO_2-carbon Isotopes and noble gases combined approach. Oil Gas Sci. Technol. - Rev. IFP Energies Nouv. 67, 341–353. https://doi.org/10.2516/ogst/2011154

Genuchten, V.M., 1980. A closed-form equation for predicting the hydraulic conductivity of unsaturated soils. Soil Sci. Soc. Am. J. 44, 892–898.

Geoscience Australia and Bureau of Resources and Energy Economics (BREE), 2014. Australian energy resource assessment. 2nd ed. Chapter 4: Gas. Canberra ACT 2601.

Ghezzehei, T.A., Kneafsey, T.J., Su, G.W., 2007. Correspondence of the Gardner and van Genuchten–Mualem relative permeability function parameters. Water Resour. Res. 43. https://doi.org/10.1029/2006WR005339

Global CCS Institute, 2019. Global status of CCS: Targeting climate change. https://doi.org/10.1007/springerreference_15392

Gou, Y., Hou, Z., Li, M., Feng, W., Liu, H., 2016. Coupled thermo–hydro–mechanical simulation of CO_2 enhanced gas recovery with an extended equation of state module for TOUGH2MP-FLAC3D. J. Rock Mech. Geotech. Eng. 8, 904–920. https://doi.org/10.1016/j.jrmge.2016.08.002

Gou, Y., Hou, Z., Liu, H., Zhou, L., Were, P., 2014. Numerical simulation of carbon dioxide injection for enhanced gas recovery (CO_2-EGR) in Altmark natural gas field. Acta Geotech. 9, 49–58. https://doi.org/10.1007/s11440-013-0221-z

Griffith, P., Wallis, G.B., 1961. Two-Phase Slug Flow. J. Heat Transfer 83, 307–318. https://doi.org/10.1115/1.3682268

Guloren, T., 2020. CCS: Applications and Opportunities for the Oil and Gas Industry.

Gurevich, A.E., Chilingarian, G. V., 1993. Subsidence over producing oil and gas fields, and gas leakage to the surface. J. Pet. Sci. Eng. 9, 239–250. https://doi.org/10.1016/0920-4105(93)90017-9

Guyant, E., Han, W.S., Kim, K.Y., Park, M.H., Kim, B.Y., 2015. Salt precipitation and

CO2/brine flow distribution under different injection well completions. Int. J. Greenh. Gas Control 37, 299–310. https://doi.org/10.1016/j.ijggc.2015.03.020

Haas, J.L., 1976. Thermodynamic properties of the coexisting phases and the thermochemical properties of the NaCl compo- nent in boiling NaCl solutions. Geol. Surv. Bull. 1421-B, B1– B70.

Hannis, S., Lu, J., Chadwick, A., Hovorka, S., Kirk, K., Romanak, K., Pearce, J., 2017. CO_2 storage in depleted or depleting oil and gas fields: What can we learn from existing projects?, in: Energy Procedia. pp. 5680–5690. https://doi.org/https://doi.org/10.1016/j.egypro.2017.03.1707

He, D., Bai, B., 2014. A new correlation for wet gas flow rate measurement with Venturi meter based on two-phase mass flow coefficient. Meas. J. Int. Meas. Confed. https://doi.org/10.1016/j.measurement.2014.08.014

Hou, Z., Gou, Y., Taron, J., Gorke, U.J., Kolditz, O., 2012. Thermo-hydro-mechanical modeling of carbon dioxide injection for enhanced gas-recovery (CO_2-EGR): a benchmarking study for code comparison. Environ. Earth Sci. 67, 549–561. https://doi.org/10.1007/s12665-012-1703-2

IEAGHG, 2017. Case studies of CO_2 storage in depleted oil and gas fields.

IEAGHG R&D Programme, 2009. CO_2 storage in depleted gas fields.

IEAGHG R&D Programme, 2000. Barriers to overcome in implementation of CO_2 capture and storage (1) - Storage in disused oil and gas fields.

International Energy Agency, 2018. World Energy Outlook 2018 661. https://doi.org/10.1787/weo-2018-2-en

International Standards Organization, 1996. ISO 13443:1996 - Natural gas - Standard reference conditions.

Janke, B., Kuehn, T., 2011. Geothermal power cycle analysis for commercial applicability using sequestered supercritical CO_2 as a heat transfer or working fluid, in: ASME 5th International Conference on Energy Sustainability, Parts A, B, and C. Washington, DC, USA, pp. 1237–1244. https://doi.org/10.1115/ES2011-54397

Jewell, S., Senior, B., n.d. CO_2 Storage Liabilities in the North Sea: An Assessment of Risks and Financial Consequences.

Jikich, S.A., Smith, D.H., Sams, W.N., Bromhal, G.S., 2003. Enhanced gas recovery (EGR) with carbon dioxide sequestration: A simulation study of effects of injection strategy and operational parameters, in: SPE Eastern Regional Meeting. Society of Petroleum Engineers, Pittsburgh, Pennsylvania, pp. 1–9. https://doi.org/10.2118/84813-MS

Jung, Y., Zhou, Q., Birkholzer, J.T., 2013. Early detection of brine and CO_2, leakage through abandoned wells using pressure and surface-deformation monitoring data: Concept and demonstration. Adv. Water Resour. 62, 555–569. https://doi.org/https://doi.org/10.1016/j.advwatres.2013.06.008

Khan, C., Amin, R., Madden, G., 2013. Carbon dioxide injection for enhanced gas recovery

and storage (reservoir simulation). Egypt. J. Pet. 22, 225–240. https://doi.org/10.1016/j.ejpe.2013.06.002

Kim, K.Y., Han, W.S., Oh, J., Kim, T., Kim, J.-C., 2012. Characteristics of salt-precipitation and the associated pressure build-up during CO_2 storage in saline aquifers. Transp. Porous Media 92, 397–418. https://doi.org/10.1007/s11242-011-9909-4

Koide, H., Tazaki, Y., Noguchi, Y., Iijima, M., Ito, K., Shindo, Y., 1993. Underground storage of carbon dioxide in depleted natural gas reservoirs and in useless aquifers. Eng. Geol. 34, 175–179. https://doi.org/10.1016/0013-7952(93)90086-R

Kühn, M., Förster, A., Großmann, J., Meyer, R., Reinicke, K., Schäfer, D., Wendel, H., 2011. CLEAN: Preparing for a CO_2-based enhanced gas recovery in a depleted gas field in Germany, in: Energy Procedia. Elsevier, pp. 5520–5526. https://doi.org/10.1016/J.EGYPRO.2011.02.538

Kühn, M., Tesmer, M., Pilz, P., Meyer, R., Reinicke, K., Förster, A., Kolditz, O., Schäfer, D., CLEAN Partners, 2012. CLEAN: project overview on CO_2 large-scale enhanced gas recovery in the Altmark natural gas field (Germany). Environ. Earth Sci. 67, 311–321. https://doi.org/10.1007/s12665-012-1714-z

Lea, J.F., Nickens, H. V, Wells, M.R., 2008. CHAPTER 1 - INTRODUCTION, in: Lea, J.F., Nickens, H. V, Wells, M.R.B.T.-G.W.D. (Second E. (Eds.), Gas Well Deliquification. Gulf Professional Publishing, Burlington, pp. 1–11. https://doi.org/https://doi.org/10.1016/B978-075068280-0.50002-0

Leeuwenburgh, O., Neele, F., Hofstee, C., Weijermans, P.-J., de Boer, H., Oosthoek, P., Lefebvre, A., Godderij, R., Gutierrez-Neri, M., 2014. Enhanced Gas Recovery – a Potential 'U' for CCUS in The Netherlands, in: Energy Procedia. Elsevier, pp. 7809–7820. https://doi.org/10.1016/J.EGYPRO.2014.11.815

Levy, E.K., Wang, X., Pan, C., Romero, C.E., Maya, C.R., 2018. Use of hot supercritical CO_2 produced from a geothermal reservoir to generate electric power in a gas turbine power generation system. J. CO2 Util. 23, 20–28. https://doi.org/10.1016/J.JCOU.2017.11.001

Lindeberg, E., 2011. Modelling pressure and temperature profile in a CO_2 injection well, in: Energy Procedia. Elsevier, pp. 3935–3941. https://doi.org/10.1016/J.EGYPRO.2011.02.332

Liu, H., Hou, Z., Were, P., Gou, Y., Sun, X., 2016. Numerical investigation of the formation displacement and caprock integrity in the Ordos Basin (China) during CO_2 injection operation. J. Pet. Sci. Eng. 147, 168–180. https://doi.org/https://doi.org/10.1016/j.petrol.2016.04.041

Logan, J., Heath, G., Macknick, J., Paranhos, E., Boyd, W., Carlson, K., 2013. Natural gas and the transformation of the U.S. energy sector: Electricity.

Loutan, C., 2015. Briefing on the duck curve and current system conditions [WWW Document].

Lund, J.W., Boyd, T.L., 2016. Direct utilization of geothermal energy 2015 worldwide

review. Geothermics 60, 66–93. https://doi.org/10.1016/J.GEOTHERMICS.2015.11.004

Mahabadi, N., Dai, S., Seol, Y., Sup Yun, T., Jang, J., 2016. The water retention curve and relative permeability for gas production from hydrate-bearing sediments: pore-network model simulation. Geochemistry, Geophys. Geosystems 17, 3099–3110. https://doi.org/10.1002/2016GC006372

Meer, B.L.G.H. Van der, Arts, R.J., Geel, C.R., Hofstee, C., Winthaegen, P., Hartman, J., D'Hoore, D., 2009. K12-B: Carbon Dioxide Injection in a Nearly Depleted Gas Field Offshore the Netherlands, in: Grobe, M., Pashin, J.C., Dodge, R.L. (Eds.), Carbon Dioxide Sequestration in Geological Media — State of the Science. American Association of Petroleum Geologists, p. 0. https://doi.org/10.1306/13171250St593387

Moeck, I.S., 2014. Catalog of geothermal play types based on geologic controls. Renew. Sustain. Energy Rev. 37, 867–882. https://doi.org/10.1016/J.RSER.2014.05.032

Moody, L.F., 1944. Friction factors for pipe flow. Trans. A.S.M.E. 66, 671–684.

Moody, L.F., Princeton, N.J., 1944. Friction factors for pipe flow. Trans ASME 671–84.

Mualem, Y., 1976. A new model for predicting the hydraulic conductivity of unsaturated porous media. Water Resour. Res. 12, 513–522. https://doi.org/10.1029/WR012i003p00513

Nogues, J.P., Nordbotten, J.M., Celia, M.A., 2011. Detecting leakage of brine or CO_2 through abandoned wells in a geological sequestration operation using pressure monitoring wells, in: Energy Procedia. pp. 3620–3627. https://doi.org/https://doi.org/10.1016/j.egypro.2011.02.292

Oldenburg, C.., Stevens, S.., Benson, S.., 2004. Economic feasibility of carbon sequestration with enhanced gas recovery (CSEGR). Energy 29, 1413–1422. https://doi.org/https://doi.org/10.1016/j.energy.2004.03.075

Oldenburg, C.M., 2003. Carbon sequestration in natural gas reservoirs: Enhanced gas recovery and natural gas storage, in: Proceedings, TOUGH Symposium 2003, LBNL California May 12–14.

Oldenburg, C.M., Benson, S.M., 2002. CO_2 injection for enhanced gas production and carbon sequestration, in: SPE International Petroleum Conference and Exhibition in Mexico. Society of Petroleum Engineers, Villahermosa, Mexico, pp. 1–10.

Oldenburg, C.M., Moridis, G.J., Spycher, N., Pruess, K., 2004. EOS7C Version 1.0: TOUGH2 Module for cambon dioxide or nitrogen in natural gas (methane) reservoirs, Earth Sciences Division, Lawrence Berkeley National Laboratory, University of California.

Oldenburg, C.M., Pruess, K., Benson, S.M., 2001. Process modeling of CO_2 injection into natural gas reservoirs for carbon sequestration and enhanced gas recovery. Energy & Fuels 15, 293–298. https://doi.org/Doi 10.1021/Ef000247h

Pan, L., Doughty, C., Freifeld, B., 2018. How to sustain a CO_2-thermosiphon in a partially saturated geothermal reservoir: Lessons learned from field experiment and numerical modeling. Geothermics 71, 274–293. https://doi.org/10.1016/j.geothermics.2017.10.004

Papay, J., 1999a. Improved recovery of conventional natural gas. Part I: Theortical discussion of recovery methods. Erdoel, Erdgas, Kohle 6, 302–308.

Papay, J., 1999b. Improved recovery of conventional natural gas. Part II: Results of a pilot test. Erdoel Erdgas Kohle 115, 354–356.

Patel, M.J., May, E.F., Johns, M.L., 2016. High-fidelity reservoir simulations of enhanced gas recovery with supercritical CO_2. Energy. https://doi.org/10.1016/j.energy.2016.04.120

Pathak, P., Fidra, Y., Avida, H., Kahar, Z., Agnew, M., Hidayat, D., 2004. The Arun gas field in Indonesia: Resource management of a mature field, in: SPE Asia Pacific Conference on Integrated Modelling for Asset Management, Kuala Lumpur, Malaysia, March 29-30. pp. 1–22. https://doi.org/10.2118/87042-MS

Phillips, S., Igbene, A., Fair, J., Ozbek, H., Tarvana, M., 1981. A Technical Databook for Geothermal Energy Utilization. Lawrence Berkeley Laboratory Report 12810.

Polak, S., Grimstad, A.A., 2009. Reservoir simulation study of CO_2 storage and CO_2-EGR in the Atzbach–Schwanenstadt gas field in Austria, in: Energy Procedia. pp. 2961–2968. https://doi.org/https://doi.org/10.1016/j.egypro.2009.02.072

Polak, S., Zweigel, J., Lindeberg, E., Pannetier-Lescoffit, S., Schulz, H.-M., Faber, E., Teschner, M., Poggenburg, J., May, F., Krooss, B., Alles, S., Kunaver, D., 2006. The Atzbach-Schwanenstadt gas field - A potential site for onshore CO_2 storage and EGR. Geophysics 25.

Procesi, M., Cantucci, B., Buttinelli, M., Armezzani, G., Quattrocchi, F., Boschi, E., 2013. Strategic use of the underground in an energy mix plan: Synergies among CO_2, methane geological storage and geothermal energy. Latium Region case study (Central Italy). Appl. Energy 110, 104–131. https://doi.org/10.1016/J.APENERGY.2013.03.071

Pruess, K., 2008. On production behavior of enhanced geothermal systems with CO_2 as working fluid. Energy Convers. Manag. 49, 1446–1454. https://doi.org/https://doi.org/10.1016/j.enconman.2007.12.029

Pruess, K., 2006. Enhanced geothermal systems (EGS) using CO_2 as working fluid-A novel approach for generating renewable energy with simultaneous sequestration of carbon. Geothermics 35, 351–367. https://doi.org/10.1016/j.geothermics.2006.08.002

Pruess, K., Oldenburg, C., Moridis, G., 2012. TOUGH2 user's guide, version 2 (revised).

Pruess, K., Spycher, N., 2007. ECO2N – A fluid property module for the TOUGH2 code for studies of CO_2 storage in saline aquifers. Energy Convers. Manag. 48, 1761–1767. https://doi.org/https://doi.org/10.1016/j.enconman.2007.01.016

Qatar, D., 1991. Dukhan Field - Qatar Arabian Platform. TR Struct. Traps V 103–120.

R. H. Brooks and A. T. Corey, 1964. Hydraulic Properties of Porous Media and Their Relation to Drainage Design. Trans. ASAE 7, 0026–0028. https://doi.org/10.13031/2013.40684

Ramey Jr., H.J., 1962. Wellbore heat transmission. J. Pet. Technol. 14, 427–435. https://doi.org/10.2118/96-PA

Randolph, J.B., Adams, B., Kuehn, T.H., Saar, M.O., 2012. Wellbore heat transfer in CO_2-based geothermal systems. Geotherm Resour Counc. Trans.

Randolph, J.B., Saar, M.O., 2011a. Combining geothermal energy capture with geologic carbon dioxide sequestration. Geophys. Res. Lett. 38, 1–7. https://doi.org/10.1029/2011GL047265

Randolph, J.B., Saar, M.O., 2011b. Coupling carbon dioxide sequestration with geothermal energy capture in naturally permeable, porous geologic formations: Implications for CO_2 sequestration, in: Energy Procedia. Elsevier, pp. 2206–2213. https://doi.org/10.1016/j.egypro.2011.02.108

Regan, M.L.M., 2010. A Numerical Investigation into the Potential to Enhance Natural Gas Recovery in Water-drive Gas Reservoirs through the Injection of CO_2. The University of Adelaide.

RockWare, 2017. PetraSim User Manual.

Romero, C.E., Pan, C., Ramírez Mendez, L.P., Levy, E.K., Aguilar Corona, A., Chávez López, O.A., Rubio Maya, C., 2015. Assessment of the use of CO_2 injection for heat mining in geothermal reservoirs in Mexico, in: International Pittsburgh Coal Conference Pittsburgh. pp. 1–17.

Rubin, E.S., Zhai, H., 2012. The cost of carbon capture and storage for natural gas combined cycle power plants. Environ. Sci. Technol. 46, 3076–3084. https://doi.org/10.1021/es204514f

Rückheim, J., Voigtlaender, G., Stein-Khokhlov, M., 2005. The technical and economic challenge of "mature gas fields": The Giant Altmark Field, a German example, in: SPE Europec/EAGE Annual Conference. Society of Petroleum Engineers, Madrid, Spain, pp. 1–4. https://doi.org/10.2118/94406-MS

Rybach, L., 2003. Geothermal energy: sustainability and the environment. Geothermics 32, 463–470. https://doi.org/10.1016/S0375-6505(03)00057-9

Sahuquet, B.C., Ferrier, J.J., 1982. Steam-drive pilot in a fractured carbonated reservoir: Lacq Superieur Field. J. Pet. Technol. 34, 873–880. https://doi.org/10.2118/9453-PA

Shi, Y., Jia, Y., Pan, W., Huang, L., Yan, J., Zheng, R., 2017. Potential evaluation on CO_2-EGR in tight and low-permeability reservoirs. Nat. Gas Ind. B 4, 311–318. https://doi.org/10.1016/J.NGIB.2017.08.013

Somerton, W.H., 1992. Thermal properties and temperature-related behavior of rock/fluid systems, 1st ed. Elsevier Science.

Spath, P.L., Mann, M.K., 2000. Life cycle assessment of a natural gas combined-cycle power generation system. NREL Life Cycle Assess. 1–56. https://doi.org/10.2172/776930

Suckale, J., 2009. Induced seismicity in hydrocarbon fields. Adv. Geophys. 51, 55–106. https://doi.org/10.1016/S0065-2687(09)05107-3

Sun, B., Wang, R., Zhao, X., Yan, D., 2002. The mechanism for the formation of slug flow in vertical gas–liquid two-phase flow. Solid. State. Electron. 46, 2323–2329.

https://doi.org/https://doi.org/10.1016/S0038-1101(02)00243-5

Surindra, D.M., Caesarendra, W., Prasetyo, T., Mahlia, M.T., Taufik, 2019. Comparison of the Utilization of 110 °C and 120 °C Heat Sources in a Geothermal Energy System Using Organic Rankine Cycle (ORC) with R245fa, R123, and Mixed-Ratio Fluids as Working Fluids. Processes 7. https://doi.org/10.3390/pr7020113

Taitel, Y., Bornea, D., Dukler, A.E., 1980. Modelling flow pattern transitions for steady upward gas-liquid flow in vertical tubes. AIChE J. 26, 345–354. https://doi.org/10.1002/aic.690260304

Tissot, B.P., Welte, D.H., 1984. Petroleum formation and occurrence. Springer-Verlag.

Townsend, A., Raji, N., Zapantis, A., 2020. The value of carbon capture and storage (CCS), Thought Leadership.

Turner, R.G., Hubbard, M.G., Dukler, A.E., 1969. Analysis and Prediction of Minimum Flow Rate for the Continuous Removal of Liquids from Gas Wells. J. Pet. Technol. 21, 1475–1482. https://doi.org/10.2118/2198-PA

U.S. Energy Information Administration, 2020. Price Data - U.S. Natural Gas Electric Power Prices [WWW Document].

van Beek, F., Troost, J.P.., 1979. The Groningen Gas Field: A case history of the development of a giant gas field. J. Pet. Technol. 31, 815–820. https://doi.org/doi:10.2118/7423-PA

van der Burgt, M.J., Cantle, J., Boutkan, V.K., 1992. Carbon dioxide disposal from coal-based IGCC's in depleted gas fields. Energy Convers. Manag. 33, 603–610. https://doi.org/10.1016/0196-8904(92)90062-2

Van Der Meer, L.G., Kreft, E., Geel, C., Hartman, J., 2005. K12-B A Test site for CO_2 storage and enhanced gas recovery, in: SPE Europec/EAGE Annual Conference and Exhibition, Madrid, Spain, 13-16 June. pp. 1–9. https://doi.org/https://doi.org/10.2118/94128-MS

Vialle, S., Ajo-Franklin, J., Carey, J.W., 2019. Geological Carbon Storage: Subsurface Seals and Caprock Integrity. American Geophysical Union and John Wiley & Sons, Inc.

Vos, L.L., 2003. Groningen field review; Volume 5: Dynamic modeling and technical ultimate recovery factor.

Xie, H., Li, X., Fang, Z., Wang, Y., Li, Q., Shi, L., Bai, B., Wei, N., Hou, Z., 2014. Carbon geological utilization and storage in China: current status and perspectives. Acta Geotech. 9, 7–27. https://doi.org/10.1007/s11440-013-0277-9

Xu, C., Dowd, P., Li, Q., 2016. Carbon sequestration potential of the Habanero reservoir when carbon dioxide is used as the heat exchange fluid. J. Rock Mech. Geotech. Eng. 8, 50–59. https://doi.org/https://doi.org/10.1016/j.jrmge.2015.05.003

Xu, T., Feng, G., Shi, Y., 2014. On fluid-rock chemical interaction in CO_2-based geothermal systems. J. Geochemical Explor. 144, 179–193. https://doi.org/10.1016/j.gexplo.2014.02.002

Yadigaroglu, G., Hetsroni, G., Hewitt, G.F., 2018. Flow Regimes, in: Yadigaroglu, G., Banerjee, S., Hewitt, G.F. (Eds.), Introduction to Multiphase Flow: Basic Concepts, Applications and Modelling. pp. 95–140. https://doi.org/10.1007/978-3-319-58718-9

Yamamoto, H., 2008. PetraSim: A graphical user Interface for the TOUGH2 Family of multiphase flow and transport codes. Groundwater 46, 525–528. https://doi.org/10.1111/j.1745-6584.2008.00462.x

Zbinden, D., Rinaldi, A.P., Urpi, L., Wiemer, S., 2017. On the physics-based processes behind production-induced seismicity in natural gas fields. J. Geophys. Res. Solid Earth 122, 3792–3812. https://doi.org/10.1002/2017JB014003

Zhai, H., Rubin, E.S., 2013. Comparative performance and cost assessments of coal- and natural-gas-fired power plants under a CO_2 emission performance standard regulation. Energy & Fuels 27, 4290–4301. https://doi.org/10.1021/ef302018v

Zhang, L., Cui, G., Zhang, Y., Ren, B., Ren, S., Wang, X., 2016. Influence of pore water on the heat mining performance of supercritical CO_2 injected for geothermal development. J. CO2 Util. 16, 287–300. https://doi.org/10.1016/j.jcou.2016.08.008

Zhang, L., Ezekiel, J., Li, D., Pei, J., Ren, S., 2014. Potential assessment of CO_2 injection for heat mining and geological storage in geothermal reservoirs of China. Appl. Energy 122, 237–246. https://doi.org/10.1016/j.apenergy.2014.02.027

Zhang, L., Li, X., Zhang, Y., Cui, G., Tan, C., Ren, S., 2017. CO_2 injection for geothermal development associated with EGR and geological storage in depleted high-temperature gas reservoirs. Energy 123, 139–148. https://doi.org/10.1016/j.energy.2017.01.135

Zhang, Y., Pan, L., Pruess, K., Finsterle, S., 2011. A time-convolution approach for modeling heat exchange between a wellbore and surrounding formation. Geothermics 40, 261–266. https://doi.org/10.1016/J.GEOTHERMICS.2011.08.003

Ziabakhsh-Ganji, Z., Nick, H.M., Donselaar, M.E., Bruhn, D.F., 2018. Synergy potential for oil and geothermal energy exploitation. Appl. Energy 212, 1433–1447. https://doi.org/10.1016/J.APENERGY.2017.12.113

Curriculum Vitae: EZEKIEL, JUSTIN CHIMA

Seestrasse 77c
8610, Uster (Zürich)
Switzerland
Phone: (+41) 77 979 75 68
cezekiel@ethz.ch, justinezzy@gmail.com
LinkedIn; Personal Homepage

Nationality: Nigerian
Date of birth: 02.06.1986

EDUCATION

09.2016 – present	**ETH Zürich**, Ph.D. in Earth Sciences (Geophysics) Thesis: *"Assessment and optimization of combined geological carbon storage and energy production from deep natural gas reservoirs"* Thesis Defense: July 2020
09.2012 – 12.2014	**China University of Petroleum (East China)**, Master of Science in Oil and Gas Field Development Engineering Final grade: 4.0/4.0 Thesis: *"Screening of gas injection techniques for IOR in low permeability reservoirs: Case Study of Q131 block in Liaohe Oilfield, China"*
09.2003 – 12.2008	**Federal University of Technology, Owerri**, Bachelor of Technology in Geology Specialization: Geophysics, Final grade: 4.6/5.0 (First Class Honors) Thesis: *"A gravity study to map the subsurface structures in some parts of the Njaba River sub-basin, Southeastern Nigeria: An implication to petroleum potential"*
06.2002	**Federal Government College, Okposi**, High School Science and sport program

RESEARCH EXPERIENCE

09.2016 – present	**ETH Zürich**, Geothermal Energy and Geofluids Group, Switzerland, Research assistant – Numerical modeling of multi-phase fluid flow and heat transport (coupling reservoir, wellbore and power-plant systems) during deep geothermal projects and natural gas exploitation – Supervision of Master's students' theses research work (including semester projects). – Publication of research results, attend and present research results at conferences and workshops.

12.2012 – 12.2014   – **China University of Petroleum (East China)**, China, Laboratory of Gas injection for enhanced oil (and gas) recovery
                    – Conducted two research projects on:
                        – screening different gas injection techniques for enhanced oil recovery in the Q131(low permeability) oil block
                        – numerical modeling to assess the potential of CO_2-based heat mining and carbon storage in various geothermal systems of China
                    – Publication of research results, attended conferences and workshops.

05.2011 – present   **Federal University of Technology,** Owerri, Nigeria, Lecturer
                    – Tenure track teaching and research position
                    – Teaching core geology and geophysics courses, including hydrogeology, applied geophysics, geophysical exploration techniques, etc.
                    – Supervision of Master's degree students' theses (including field work) and the final semester projects of undergraduate students
                    – Participation in independent and collaborative research projects with other faculty members
                    – Training and mentoring students for international and national competitions, such as the Society of Exploration Geophysicists (SEG) Challenge Bowl, AAPG Imperial Barrel Award competition, etc.
                    – Managing the super-computing lab of the department (2011 - 2016)
                    – Publication of research results, attended conferences and training workshops.

04.2010 – 03.2011   **Shell Petroleum Development Company (SPDC-West),** Warri, Nigeria Internship
                    – Training on the use of ArcGIS, Workbench, Surfer for Shell's infrastructure mapping projects
                    – Writing of geotechnical reports.

03.2009 – 02.2010   **National Youth Service Corps,** Abuja, Nigeria, Corps Member
                    – One-year mandatory paramilitary and social-service exercise undertaken by all Nigerian graduates
                    – Teaching Mathematics and Physics to High School students
                    – Participation in various (voluntary) societal development projects.

SELECTED PUBLICATIONS

Justin Ezekiel, Anozie Ebigbo, Benjamin M. Adams, Martin O. Saar. "Combining natural gas recovery and CO_2-based geothermal energy extraction for electric power generation." *Applied Energy* (2020).

Guodong Cui, Shaoran Ren, Zhenhua Rui, **Justin Ezekiel**, Liang Zhang, Hongsheng Wang. "The influence of complicated fluid-rock interactions on the geothermal exploitation in the CO_2 plume geothermal system." *Applied Energy* (2018).

Justin Ezekiel; Shaoran Ren; Liang Zhang; Yuting Wang; Yanmin Liu; Junyu Deng; Guibin Wang. "Displacement mechanisms of air injection for IOR in low permeability light oil reservoirs." *International Journal of Oil Gas and Coal Technology (*2017).

Liang Zhang, Dexiang Li, **Justin Ezekiel**, Weidong Zhang, Honggang Mi, Shaoran Ren. "CO_2 geological storage into a lateral aquifer of an offshore gas field in the South China Sea: storage safety and project design." *Frontiers of Earth Science* (2015).

Liang Zhang, **Justin Ezekiel**, Dexiang Li, Jingjing Pei, Shaoran Ren. "Potential assessment of CO_2 injection for heat mining and geological storage in geothermal reservoirs of China." *Applied Energy* (2014).

Jianhua Ren, Liang Zhang, **Justin Ezekiel**, Shaoran Ren, Shangzhi Meng. "Reservoir characteristics and productivity analysis of tight sand gas in Upper Paleozoic Ordos Basin China." *Journal of Natural Gas Science and Engineering* (2014).

AWARDS AND HONORS

09.2016 – 08.2019	Swiss Government Excellence Scholarships for Foreign Scholars and Artists, ETH Zürich, Switzerland
09.2012 – 12.2014	Joint Post-Graduate Scholarship Award by the Federal Scholarship Board (FSB) Nigeria and Chinese Scholarship Council (CSC) China
12.2008	University Award, Best Graduating Student in the University, Federal University of Technology Owerri
12.2008	Dean's Award, Best Graduating Student in the School of Science, Federal University of Technology Owerri

COMPUTER SKILLS

Operating Systems	*Mac, Windows* and *Linux*
Programming	*Python, SQL (Basic), R (Basic)*
Software	*MATLAB, TOUGH2/TOUGH3*, *Petrasim*, *PFLOTRAN*, *Petrel, CMG, Eclipse*, *Microsoft Office Package* (*Word*, *Excel*, *PowerPoint, etc.*), *ArcGIS*, *LaTeX*, *Paraview* and *Adobe Illustrator*

LANGUAGES

Igbo	Mother tongue
English	Proficient
Chinese	Basic knowledge (HSK 4)
German	Basic knowledge

PROFESSIONAL CREDENTIALS

− Member, American Association of Petroleum Geologists (AAPG)
− Member, Nigerian Association of Petroleum Explorationists (NAPE)
− Student Member, Society of Petroleum Engineers (SPE)
− Student Member, Society of Exploration Geophysicists (SEG)
− PRINCE2 Project Management Certification (Foundation)

HOBBIES

Traveling, soccer, listening to music, hiking, reading technical and financial reports.